UNIVERSIDAD COMPLUTENSE DE MADRID

FACULTAD DE FARMACIA

TESIS DOCTORAL

Mesoporous Silica Nanoparticles for the Potential Treatment of Osteoporosis

Nanopartículas Mesoporosas de Sílice para el Tratamiento Potencial de la Osteoporosis

MEMORIA PARA OPTAR AL GRADO DE DOCTOR CON MENCIÓN INTERNACIONAL

PRESENTADA POR

Patricia Mora Raimundo

Directores

Miguel Manzano García

Federico Gilberto Hawkins Carranza

Madrid

Mesoporous Silica Nanoparticles for the Potential Treatment of Osteoporosis

Nanopartículas Mesoporosas de Sílice para el Tratamiento Potencial de la Osteoporosis

Patricia Mora Raimundo

Memoria para optar al grado de Doctor por la Universidad Complutense de Madrid

Departamento de Química en Ciencias Farmacéuticas
Facultad de Farmacia, UCM
Madrid 2020

Directores:
Miguel Manzano García
Federico Gilberto Hawkins Carranza

Departamento de Química en Ciencias Farmacéuticas

Facultad de Farmacia

UNIVERSIDAD
COMPLUTENSE
MADRID

Mesoporous Silica Nanoparticles for the Potential Treatment of Osteoporosis

Nanopartículas Mesoporosas de Sílice para el Tratamiento Potencial de la Osteoporosis

MEMORIA PRESENTADA POR

Patricia Mora Raimundo

Directores

Miguel Manzano García

Federico Gilberto Hawkins Carranza

Para optar al grado de Doctor con Mención Internacional por la

Universidad Complutense de Madrid

Madrid 2020

Creo que de todo este gran libro lo más importante para mí son estas primeras páginas, lo que más me va a costar escribir sentimental y emocionalmente hablando. Lo creáis o no voy a esforzarme mucho por primero, no llorar mientras escribo estas líneas, y segundo tratar de ser concisa, que los que me conocéis sabréis que lo de ir al grano yo no lo trabajo mucho.

Desde que empecé la carrera de farmacia supe que lo que me gustaba y apasionaba era el "cacharrear" en el laboratorio, aportar ese pequeño granito de arena al desarrollo, cultivar mi conocimiento enriqueciéndome principalmente de la gente brillante que me rodea. Fue en primero de carrera, en la clase de Química Inorgánica, donde un gran profesor, Jesús Román, nos animó a colaborar en algún departamento de la facultad, y así tener una primera toma de contacto con la ciencia. Como no podía ser de otra manera, mi espíritu de chica polvorilla me llevó a enfrascarme en la locura de sumarme a este gran grupo de investigación. Fui a hablar con Jesús y Miguel Manzano para mostrarles mis ganas y entusiasmo de colaborar con ellos en el trabajo que me ofreciesen, acabando finalmente en manos de Miguel, y desde ahí hasta el día de hoy. No voy a mentiros, cuando llegué al laboratorio pensé que me iban a tener limpiando pipetas, y no solo me equivocaba, sino que las pipetas eran de un solo uso, es decir no iba a tener que limpiarlas para mi sorpresa. Así empecé trabajando con Miguel en el mundo de las nanopartículas. Desde ahí estuve en contacto con el grupo de investigación durante mis 4 años restantes de carrera aprendiendo lo que era ser una pequeña científica. Cuando se fue acercando el final de mi carrera de farmacia, un día 17 de marzo, (lo recuerdo a la perfección porque era el día de mi santo), Miguel como regalo de santo me anunció la posibilidad de ser contratada por un proyecto otorgado a la Profesora María Vallet que me permitiría llevar a cabo una tesis doctoral. Me lancé a la piscina y por supuesto agradecí infinitamente la confianza depositada en mí. Ahí empezaron 4 años de retos, de aprendizajes, de mucho trabajo, pero a la vez de conocer gente excepcional, de crecimiento personal y disfrute. Y es que al final en todo este tipo de cosas lo que verdaderamente importa son todas aquellas personas que te acompañan en el camino, no el destino como tal (que también…). Y de ahí que esta sección se encuentre al principio de este libro de grosor considerable, ya que está principalmente dedicada a lo más importante, agradecer a todos aquellos que de una u otra manera me han acompañado durante estos años de investigación.

A la Profesora María Vallet Regí, Marita, por confiar en mi y brindarme la oportunidad de unirme a tu gran grupo de investigación, y así poder dar mis primeros pasos en la carrera científica en un grupo de gran renombre.

A la European Research Council (ERC), por la financiación proporcionada a través del proyecto europeo VERDI, que me ha permitido llevar a cabo mi tesis doctoral. Al Centro de Investigación Biomédica en Red (CIBER-BBN), por las ayudas económicas que me permitieron realizar una estancia predoctoral en Israel.

A Juan Carlos Doadrio, actual Vicerrector de Relaciones Institucionales de la Universidad Complutense, pero antiguo director del departamento, por haberme ayudado siempre en todo lo que estaba en tu mano, por tus buenos días mañaneros y por todas esas conversaciones sobre nuevos restaurantes madrileños que tanto disfrutamos.

A Federico Gilberto Hawkins por acogerme como doctoranda y siempre darme tu punto de vista clínico sobre mi investigación.

A Miguel Manzano, mi director de Tesis y poco a poco mi director de vida profesional. Tengo muchas cosas que agradecerte. Primeramente, el haberte lanzado a la locura de elegirme como doctoranda, que como bien has sufrido en tus venas, no es tarea fácil. Por aguantar mis

discusiones, mis ciertos problemas con la informática, mis días buenos y mis días no tan buenos. Gracias por preocuparte por mi desde el día uno, por querer transmitirme tu entusiasmo por la vida y por no solo no cortarme las alas sino lanzarme hacia todo aquello que me proponga. Gracias por la infinidad de conversaciones en momentos críticos en los que siempre has sido capaz de hacerme ver el lado positivo, porque si hay una palabra que te pueda definir de la manera más precisa es optimista. Gracias por animarme a llevar a cabo la estancia científica en un país que en un principio no me parecía ni de lejos la mejor de las opciones, y que gracias a tus ánimos he podido descubrir todo el potencial que tenía tanto en lo profesional como en lo personal. En definitiva, gracias por estos 4, más bien 8, años que hemos compartido.

Al llegar a este laboratorio he tenido la oportunidad de cruzarme con una gran cantidad de personas que en mayor o menor medida han pasado a formar parte de mi día a día. Gracias a Antonio, Blanca, Sandra, Isabel, Montse, África y María Teresa por recibirme siempre con una sonrisa y echarme una mano cuando he necesitado. A Pili y Lidia por, entre risas, ayudarme con cualquier problema logístico, a Jose por siempre estar para arreglar todos mis desastres informáticos, y eliminar mis epidemias de viruses por todo el laboratorio. A Dani Arcos por nuestras conversaciones sobre la vida junto a nuestra fruta de media mañana en el despacho. A Jose, Perla, Javi, Mary, Sara.. por todos esos viernes y por siempre recibirme con una sonrisa en la cafetería y preocuparos por mi bienestar siempre que me veíais con peor cara, ver vuestra energía en momentos de desconexión contagia y hace más fácil un día duro. Al personal de limpieza, y en especial a María, que ha sido la que nos ha acompañado estos últimos años, por hacer de nuestro laboratorio un lugar algo más higiénico.

Y como bien os he dicho, en este laboratorio he tenido la oportunidad de compartir muchos momentos con gente excepcional, desde todos aquellos estudiantes que han pasado más o menos tiempo por el laboratorio hasta aquellos que han pasado a convertirse en personas imprescindibles. Empezando por Rebeca, por todas nuestras risas en el TG y por hacerme participe de uno de los días más bonitos de tu vida. A Sandra titi, por llegar siempre con una sonrisa desde las tierras lejanas de Químicas. A Irene, por querer aprender lo poco que podía enseñarte, se que el camino que decidiste te hará enormemente feliz. A Anna, por de una u otra manera transmitir siempre una sensación de tranquilidad y amabilidad. A Clara, por todas nuestras conversaciones, por todas las recetas y restaurantes más chics del momento. A Elena, primero por todas las risas que nos acompañaron, por tu energía y tu tesón, se que al final todo lo que te propongas saldrá adelante. A Javi, por sacarme siempre una carcajada con tu naturalidad en estado puro. A Manuel, por tener una palabra amable y una sonrisa preparada en el mejor momento. A Carla y Guille nuevas incorporaciones, por aportar sangre nueva al laboratorio. Jeremy, merci beaucoup pour tout, pour offre moi l'opportunité de t'accompagne dans mon future professionnel. A Noemí, mi chica pelirroja, por siempre haber estado dispuesta a escucharme y ayudarme tanto en lo personal como en lo profesional, siempre con la palabra y el consejo perfecto. A Edu Guisasola, por tus conversaciones en las cuales me animaste siempre a seguir y confiar en que todo, al final, con más o menos tesón saldría, y efectivamente, tenías razón. A Marina, mi niña de tierras murcianas, porque los años que hemos compartido has sido siempre energía en estado puro y felicidad personificada, y créeme eso se agradece y mucho, estos últimos años te hemos echado mucho en falta. A Víctor, por ser mi compañero de laboratorio, de festivales, de fiesta, de viajes, por ser el mayor hater de la ciudad y aun así conseguir hacerme olvidar cualquier mal trago que tenga encima.

A Juan y Jesús, por a pesar de meteros constantemente conmigo preocuparos siempre de mi bienestar. A Jesús, por desde un principio haber sido la razón que me impulsó a embarcarme en

todo lo que posteriormente leeréis. A Juan, por de una u otra manera haber sido un apoyo fundamental a lo largo de esta tesis doctoral. A Vicky y Ana Fontecha, por haber estado siempre para escucharme, en todo momento, sin importar la razón. A Vicky, por haberme sabido guiar siempre a tomar las mejores decisiones profesionales y personales. A Ana, por haberme sabido tranquilizar, y siempre defenderme frente a las constantes críticas en los momentos del té. Chicos, no sabéis cuan importantes habéis sido los cuatro durante estos cuatro años.

A mis italianas, Mónica y Barbara, gracie per arrivare al momento justo, per tanti momento insieme, per tutte li sera con un espresso. Sono secura che questo non finirá qui. Molte gracie italiani.

A nuestros vecinos del piso de arriba, mis orgánicos por excelencia, Marta, Ángel, Marco, Jose, Olmo, Jorge, Cris, gracias por tantos ratos juntos, tantas risas y esas cañas de viernes que debemos retomar. En especial a ti Marta, por todos los ratos compartidos, pronto nos reencontraremos en nuestros destinos respectivos. Porque estas aventuras no acaben.

A mis chicos de microbiología, Belén, Yuli, Sonia, Vero, Inés, Raúl y Javier por acogerme en vuestros desayunos como a una más. Especialmente a Luciana, Lulu, por haber llegado y en cuestión de dos meses calar de la manera en la que lo has hecho. Eres una mujer alucinante y sé que el mundo tiene algo muy bueno preparado para nosotras.

A Dani Lozano, por ser de los que más intensamente ha tenido que sufrirme, por ser siempre comprensivo con mis locuras en el laboratorio, por acompañarme en toda mi investigación, enseñarme tanto y tener la paciencia más infinita conmigo.

A Juan Luis, porque desde el día uno fuiste mi inspiración, mi compañero farmacéutico en este mundo de “químicos”, aunque cada vez haya menos químicos. Por haberme enseñado, explicado e inspirado. Por tantas conversaciones donde sentía como poco a poco me empapaba de tu conocimiento. En gran parte ha sido gracias a ti que esta tesis pueda estar hoy escrita. A Rocío, por mostrarme que con constancia y esfuerzo todo acaba saliendo, por ser una fiel compañera de salidas y siempre desprender esa energía que te caracteriza. Prometo no felicitarte en ningún cumpleaños, sino más bien recordarte lo joven que se te ve.

Al Maño, Miguel Gisbert, por todo, por acompañarme estos 5 años, por compartir conmigo risas, juegos, momentos de desesperación en el despacho, por escuchar la palabra de dios conmigo, por siempre estar dispuesto a ayudarme en todo lo que haya estado en tus manos. Gracias.

A Sergio, no sabría ni por dónde empezar, por dejar tu impronta en mí, por darme los mejores consejos, por siempre tener el consuelo perfecto, la palabra perfecta, el abrazo perfecto. Por haber estado siempre, y seguir estando. Te echo de menos.

A Gonzalo, por estar, por seguir, y por saber que estarás. Por ser mi confidente, mi apoyo, por entender mi forma de conducción, por los días de sushi, por el Bingo Roma, por nunca perder tu espíritu. Por ser de las personas más luchadoras que conozco. Por ser un padrazo. Te mereces todo lo mejor.

A Nati, mi apoyo indispensable, mi compañera de conversaciones infinitas, mi ejemplo de mujer. Gracias por aun estando a miles de kilómetros, seguir siempre contagiándome tu felicidad. Gracias por todos estos años que hemos compartido en los que has sido mi apoyo constante.

To Professor Avi Schroeder, for giving me the opportunity of joining his amazing group, for letting me learn about science, about Israel and about these amazing people. To Shivan, Rothem,

Egor, for treating me always really kind. To Omer, Maria, Mor, Gal, Aviram, for taking care of me so much, for making me feel at home being actually really far from my family, for becoming my Israeli family, for teaching me the most useful words in Hebrew. To Mohhamed and Dina for taking me as part of you, for just caring of me, for all the nights and plans. I love you guys. And finally, to Maya, Mayus, thank you so much simply for existing, for teaching me everything you know in the lab, for at least trying to let me be part of one of the most important days of your life, for becoming more than a friend. Schroeder Lab, I miss you so much.

Hay una frase que siempre he tomado como guía, la escuche antes de empezar la carrera, pero se puede aplicar también a estos 4 años de doctorado, "si el día que termines la carrera, solo tienes la carrera, entonces no tendrás nada". Durante estos 4 años de doctorado no solo he aprendido una infinidad sobre ciencia, sobre cómo desarrollar un proyecto, sobre como sobrepasar la frustración, sobre cómo lidiar con el error y modificarlo para transformarlo en acierto. Sino que también he sido capaz de mantener muchos de mis hobbies de siempre, crear nuevos, y formarme en muchos otros aspectos que el académico. Pero, además, y creo que lo más importante, he conocido gente excepcional con la cual he creado lazos muy especiales. Y eso me lo llevo conmigo, como parte de mí.

Muchas otras personas que no han compartido poyata conmigo han sido indispensables para mi durante todo este tiempo, ya que de una u otra forma han hecho de todos estos años, los más bonitos hasta la fecha.

A Javi Arroyo y Nacho Hernando, por siendo farmacéuticos como yo siempre sentir interés por mi proyecto y motivarme a continuar. Por acabar estando siempre en los momentos importantes, ya sea para sacarme una sonrisa o compartir una cerveza.

A Molero y Jaime, por seguir, sin importar el tiempo, lo que se unió hace años, parece que nada va a poder separar.

A Jorge y Carlos, mis compañeros no solo de piso, sino de batalla. Por aguantar días de manta y helado, pero también días de hiperactividad. Por siempre quererme a pesar de mi desastre.

A mis amigas farmacéuticas, Maca, Laura, Irene y Rochis, por siempre haber creído en mí, desde el momento en el que decidí entrar a trabajar en el laboratorio, y siempre haberme animado a darme cuenta de todo lo que era capaz de hacer.

A Albi y Caye, por estar, siempre estar, por confiar en mí, por acompañarme todos estos años y aun siendo complicado, siempre sacar tiempo para compartir un café, una cerveza o una copa y ponernos al día.

A Bachita y Perelló, por siempre estar para hacerme desconectar, por esas escapadas anuales que te cargan de energía para volver a coger la ciencia con ganas.

A Nacho y Mario, adquisiciones de nuevos retos y experiencias, por pasar a ser indispensables para mí, por estar siempre dispuestos a sacarme una carcajada y compartir conmigo los mejores recuerdos que guardo.

A Eli y Fran, por hacerme reír aun sin quererlo, por cuidarme y querer siempre lo mejor para mí. A Ricitos, mi nuevo ángel de la guarda, por estar siempre sin importar el momento ni las consecuencias. A Guille, por siempre mostrarme la verdad, por hacerme mejor persona, y por esas infinitas conversaciones sobre tantos y tantos temas que me han hecho crecer.

A Moni, porque no podía ser de otra manera, por ser ya más que amiga, más que confidente, más que apoyo. Por ser la persona más buena, fuerte e íntegra que conozco. Por compartir conmigo infinidad de pasiones, por ser vía de escape y hacer de estos últimos momentos de tesis una época digna de recordar con infinito cariño.

Y como no, a mis dos pilares, mis siempre presentes Alex y Mariajo, por sin saberlo, ser de las personas más importantes que tengo, por siempre haber creído en mí, impulsarme a hacer todo lo que me he planteado, por estar cuando he necesitado, siempre, sin importar la razón, sin importar el momento, siempre. Os quiero.

And last but not least, to Alon, Babi thanks just for appearing in my life in this crazy moment, I think I don't need to write nothing because you already know everything. Thanks for be there no matter what or when. Toda Raba haim sheli, Ohevet Otraj meod meod super meod.

Y es que siempre dicen que los amigos son la familia que eliges, y tengo la infinita suerte de haber elegido la mejor y conservarla cerca.

Y por último a esa familia que no eliges, pero que, en mi caso, la elegiría mil veces, porque no existe mejor. A todos, empezando por mis tíos, tanto de una familia como de la otra, por quererme apoyarme y mostrarme siempre que soy capaz de todo lo que me proponga. A mis primos, todos ellos, pero especialmente Carlos, Silvia y Cris que siempre han estado para mí, con los oídos bien abiertos para escuchar mis dramas, y con los mejores consejos preparados, por cuidarme siempre. A mi tía Maite, por compartir desayunos en la facultad, y por siempre ver en mí cosas excepcionales. A mi Madrina, por motivarme siempre en perseguir mi sueño, y comprender mi locura cuando compartimos casa, porque madrina "¡Es lunes, Animo Pati que tú puedes!". A mis Abuelos, ambos dos. Ramón por mostrarme siempre que la vida es dura, y que nadie regala nada, que todo hay que ganarlo con esfuerzo y trabajo. A Jorge, por ser impoluto, por ser el mayor ejemplo a seguir, por enseñarme que siempre hay algo nuevo que aprender, "aprendiz de todo, maestro de nada". Por ser mi motor para seguir por el mero hecho de verte orgulloso de mi, y aunque ya no pueda disfrutar de ese momento, sé que desde donde estés, estarás orgulloso de ver a tu nieta doctora. A mis abuelas, ambas dos. Pitusa, por ser energía hecha mujer, por enseñarme que a pesar de las adversidades siempre hay que tener preparada una sonrisa, porque la vida merece demasiado la pena para pasarla apenado. A Carmen, por ser fortaleza, por ser el claro ejemplo de que se puede con todo, porque eres mi mujer de hierro. Me siento afortunada de poder decir que he aprendido tanto de vosotros. A mi hermano, y mi cuñada, Jorge y Cristina, por incluso desde la distancia ser un gran pilar para mí, por desviviros por hacerme participe del crecimiento de vuestros pequeños retoños, por siempre velar por mi bien, y preocuparos por cómo me trata la vida. A mi hermana, Paloma, simplemente por siempre estar, por ver reflejado en tus ojos el orgullo que sientes por mí y que eso sea motor para no decepcionarte. Y finalmente a mis padres, Loreto y Luis, ya que lo mejor siempre se guarda para el final, y el mayor regalo que he podido tener siempre es haber tenido los padres que he tenido, que siempre me han permitido llevar a cabo mis sueños, proporcionándome todo lo necesario. Por haberme cuidado siempre, sin importar el cuándo, el cómo, el dónde ni el porqué. Por haberme inculcado los valores que me han hecho la mujer que soy ahora. Por estar siempre, por sentiros orgullosos de vuestra hija, y transmitírmelo de la mejor manera. Os quiero.

Patricia

A mi abuelo, por algún día conseguir, como TÚ, "salirme de la tabla".

Glossary of Terms

Ago2: argonaute endoribonuclease

ALN: alendronate

ALP: alkaline phosphatase

APTES: 3-aminopropyltriethoxysilane

BMC: bone mineral content

BMD: bone mineral density

BMP-R: bone morphogenetic proteins receptor

BMPs: bone morphogenetic proteins

BPs: bisphosphonates

BRU: bone remodeling units

BS/BV: bone surface fraction

BS: bone surface

BV/TV: bone volume fraction

BV: bone volume

CBDs: collagen binding domains

CFU-M: colony-forming unit macrophage

CTAB: cetyltrimethylammonium bromide

DAPI: 4′,6-diamidino-2-fenilindol

DCC: N,N'-dicyclohexylcarbodiimide

DCM: dichloromethane

Dex/BMP-2@chi-MSNs: mesoporous silica nanoparticles coated with chitosan and co-loaded with dexamethasone and BMP-2

Dex@chi-MSNs: mesoporous silica nanoparticles coated with chitosan and co-loaded with dexamethasone

Dkk-1: dickkopf-1

DLS: dynamic light scattering

DMAP: 4-dimethylaminopyridine

DMEM: Dulbecco’s modified eagle’s medium

DMF: N,N-dimethylformamide

DMSO: dimethyl sulfoxide

EDTA: ethylenediaminetetraacetic acid

ERT: estrogen replacement therapy

FDA: Food and Drug Administration

FITC: fluorescein isothiocyanate

FMSNs: FITC labeled mesoporous silica nanoparticles

FTIR: Fourier-transform infrared

GAPDH: glyceraldehyde 3-phosphate dehydrogenase

HA: hydroxyapatite

HRT: hormone replacement therapy

IGF: insulin-like growth factor

IL: interleukin

LRP5/6: low density lipoprotein receptor-related protein-5/6

M-CSF: macrophage colony-stimulating unit

MEFs: mouse embryonic fibroblast

mRNA: messenger RNA

MSNs: mesoporous silica nanoparticles

MSNs@PEI: poly(ethylenimine) coated mesoporous silica nanoparticles

MSNs@PEI-siCtl: poly(ethylenimine) coated mesoporous silica nanoparticles bound to siRNA negative control

MSNs@PEI-siGLO: poly(ethylenimine) coated mesoporous silica nanoparticles bound to siGLO

MSNs@PEI-siRNA: poly(ethylenimine) coated mesoporous silica nanoparticles bound to siRNA

MSNs-PA: alendronate functionalize PEGylated mesoporous silica nanoparticles

MSNs-PA@PEI: poly(ethylenimine) coated alendronate functionalize PEGylated mesoporous silica nanoparticles

MSNs-PA@PEI-siRNA: poly(ethylenimine) coated alendronate functionalize PEGylated mesoporous silica nanoparticles bound to siRNA

MSNs-PEG: PEGylated mesoporous silica nanoparticles

OPG: osteoprotegerin

OST: osteostatin

OST-MSNs@PEI: osteostatin loaded poly(ethylenimine) coated mesoporous silica nanoparticles

OST-MSNs@PEI-siRNA: osteostatin loaded poly(ethylenimine) coated mesoporous silica nanoparticles bound to siRNA

OST-MSNs-PA@PEI: osteostatin loaded poly(ethylenimine) coated alendronate functionalized PEGylated mesoporous silica nanoparticles bound to siRNA

OVX: ovariectomized mice

PA: alendronate modified poly(ethylenglycol)

PBS: phosphate-buffered saline

PEG: poly(ethylenglycol)

PEI: poly(ethylenimine)

PLGA: poly(lactide-co-glycolide acid)

PosControl: positive control siRNA

PTH: parathyroid hormone

PTHrP: PTH related protein

qRT-PCR: quantitative reverse transcription polymerase chain reaction

RANK: receptor activator of nuclear factor κB

RANKL: receptor activator of nuclear factor κB ligand

RES: reticuloendothelial system

Rh-MSNs@PEI-siGLO: rhodamine B-labeled mesoporous silica nanoparticles coated with PEI and bound with siGLO

RISC: RNA-induced silencing complex

RNAi: RNA interference

sc: subcutaneously

SATES: 3-triethoxysilyl propylsuccinic anhydride

SD: standard deviation

SDS: sodium dodecyl sulfate

SERMs: selective estrogen receptor modulators

SiCtl: negative control siRNA

siGLO: fluorescence siRNA-analog

siRNA: small interfering RNA

Tb.N: trabecular number

Tb.Sp: trabecular separation

Tb.Th: trabecular thickness

TEM: transmission electron microscopy

TEOS: tetraethyl orthosilicate

TFA: trifluoroacetic acid

TGA/DTA: thermogravimetry and differential temperature analyses

TGF: transforming growth factor

Trp: tryptophan

TSPMP: 3-trihydroxysilylpropyl methylphosphonate

TV: tissue volume

UV: ultraviolet

VERDI: polyValent mEsopoRous naosystem for bone DIseases

WHO: World Health Organization

XRD: X-ray diffraction

μCT: micro-computed tomography

Summary

The overall objective of this PhD thesis has been the design of mesoporous nanoparticles for biomedical applications. In particular, this doctoral thesis has comprised the development of a nanocarrier for the potential treatment of bone diseases, more specifically in osteoporosis.

The initial context of this doctoral thesis was the European project "VERDI" ("polyValent mEsopoRous naosystem for bone DIseases"). The proposal involved the use of mesoporous materials to treat three situations of clinical relevance in bone pathology: bone infection, bone cancer (primary tumors and bone metastases) and osteoporosis.

Osteoporosis is considered the most prevalent disease involving bone degeneration. It is a silent disease and due to the aging population is considered one of the major public health problems facing postmenopausal women and aging individuals of both sexes. Although several effective antiosteoporotic treatments have been developed, their side effects limit their further application. Therefore, many efforts have been headed towards the development of other alternatives for osteoporosis treatment reducing their drawbacks for a better long-term use and adherence.

The inhibition of the Wnt/β-catenin pathway has recently gained attention as therapeutic target in bone diseases such as osteoporosis. One of the main inhibitors of this pathway is sclerostin, a protein encoded by SOST gene. Its activity results in a reduction of osteoblast formation and differentiation. Several types of sclerostin monoclonal antibodies have been developed as anabolic drugs to block the activity of sclerostin, increasing osteoblast differentiation for osteoporosis treatment. However, these antibodies can cause an immune response, which limits the use of this treatment.

Silencing SOST gene with a specific small interfering RNA (siRNA) could be an effective approach that could overcome the immune response limitation. Even though siRNAs seem to be promising candidates as therapy agents for bone disorders, their main problem relies on their delivery due to their very short half-life and poor internalization capacity through cell membranes. This is an old problem for nucleic acid therapeutics, in which the delivery challenge has remained the same for the last 40 years. The use of nanoparticles for carrying these molecules has been successfully demonstrated to overcome the problems presented.

Different drugs with anti-osteoporotic activity have been reported, although, the magic bullet remains missing. In this sense, combination therapy has been proposed as a potential alternative to achieve better results in osteoporosis remission. There are several approaches for osteoporosis treatment and therefore larger number of possible combinations to achieve a combined therapy. Then, there is a large field in research to seek for an appropriate strategy to confront the disease. The key point for such therapy is to design a dual delivery system that can transport drugs to

desirable sites controlling the release behavior of several drugs. In this case, nanoparticles could also play an important role, being able to transport and deliver several drugs at the same time.

Since osteoporosis is a systemic disease, the treatment options should be administrated either by subcutaneous or intravenous administration. For this reason, the chosen treatment options should be able to circulate for long periods of time around the circulatory system, and to accumulate in the target tissue, in this case, the bone.

Nanoparticles can enhance colloidal stability and increase tissue specificity by being properly functionalized with for example poly(ethylene glycol) (PEG) and different targeting moieties, conferring an efficient delivery. The nanocarrier would transport the drugs to bone tissue and there release the therapeutic agents. In this sense the nanoparticles would protect the drug from biodegradation, optimizing the dose without scarifying de treatment efficacy and would reduce the exposure to non-target cells, minimizing their potential side effects. In the present doctoral thesis, we selected mesoporous silica nanoparticles (MSNs) as drug nanocarriers due to their physicochemical stability and their textural properties, high surface area and pore volume, which provide a high drug loading capacity. Also, the mesoporous structure of the nanoparticles empowered the system with the possibility of co-load and co-delivering several therapeutic agents to achieve a combination treatment.

The present PhD thesis is divided in three main parts. First, the development and evaluation of the MSNs-based nanocarrier able to transport and deliver siRNAs. Second, the evaluation of a combination therapy with SOST siRNA and osteostatin delivered by MSNs. And third, the last part is focused on the modifications performed for achieving an effective systemic administration and the evaluation of that systemic treatment regarding gene expression modification and bone microarchitecture improvement.

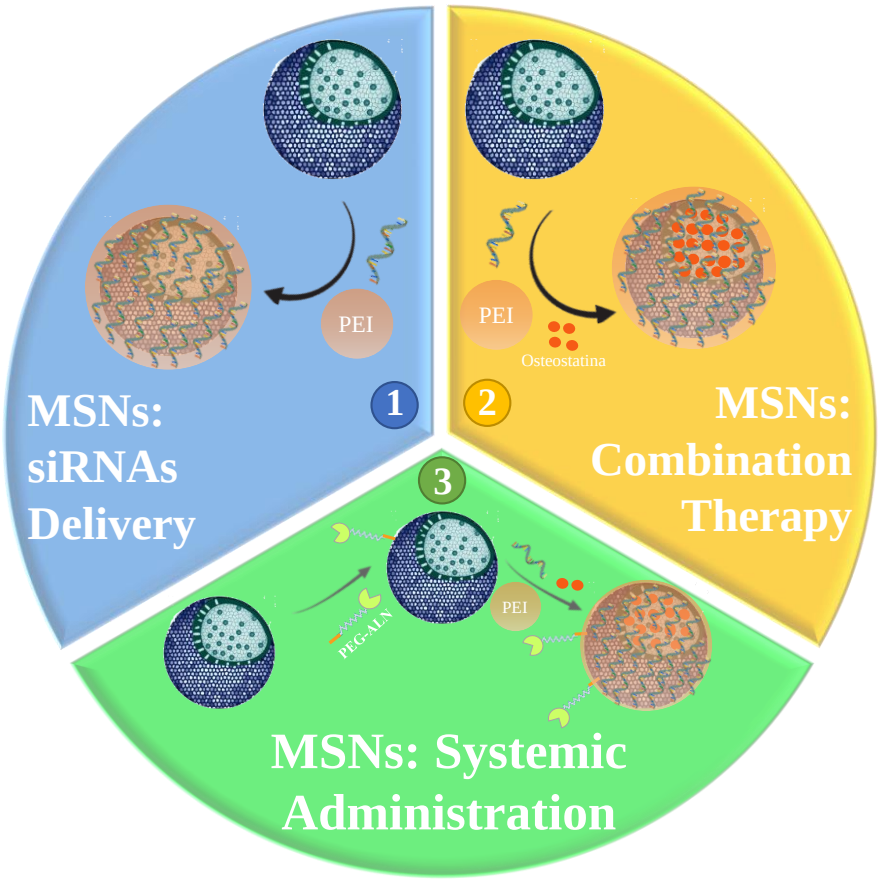

Graphical summary of the parts in which the present doctoral thesis is divided.

The **first part** of this doctoral thesis deals with the development and evaluation of the MSNs-based nanocarrier able to transport and deliver siRNAs. The major bottleneck for siRNA-based treatments is the necessity of a delivery method to transport siRNAs into targeted cells. MSNs could be an appropriated platform to deliver siRNAs. The nanoparticles could load the nucleic acids inside the pores or bound to the surface. The negative nature of nucleic acids, makes necessary the surface modification of MSNs, which is negative, to achieve the desired positive charge in their surface to bind siRNAs. To accomplish this fact, MSNs were functionalized with poly(ethyleneimine) (PEI), a cationic polymer, conferring the positive charge needed. In this stage, different PEI:MSNs ratios and different polymer molecular weights (5 kDa, 8 kDa, 10 kDa) were compared to optimize the system. The election of the ratio and molecular weight was carried out considering the capacity to bind siRNA *versus* the cytotoxicity of the polymer. It is known that, while low molecular weight PEI is not cytotoxic, these polymers are ineffective at transfecting nucleotides. However, high molecular weight PEI has shown cytotoxicity in cells although they are very effective transfecting siRNAs. In this regard, it has been demonstrated that the size, compactness, and chemical modification of PEI affect the efficacy and toxicity of the polymer, and a compromise between both parameters had to be met.

After finding the most appropriated conditions for PEI ratio (1:2) and molecular weight (5 kDa), the nanoparticles were evaluated *in vitro*. It this sense, the capacity to penetrate cells and release the siRNA inside the cytosol was initially evaluated by flow cytometry and confocal laser scanning microscopy. Then, the capacity of knocking down SOST gene and the effect of this silencing in the expression of two osteogenic markers (Runx2 and Alp) was evaluated by real-time quantitative reverse transcription polymerase chain reaction (qRT-PCR).

Since SOST gene is mainly expressed by osteocytes *in vivo*, and osteocyte-like cell line (MLO-Y4 cells) expresses low to undetectable levels of this gene, it was necessary to find a cell line which could express noticeable levels of SOST. This was necessary to demonstrate that the designed system could effectively knockdown the gene *in vitro*. In this sense, mouse embryonic fibroblasts (MEFs) were reported to express high levels of SOST under certain conditions. Thus, we cultured MEFs for 3 weeks observing increased levels of SOST expression detectable after 3 days, which were increased up to 20-fold after 14 days. Therefore, MEFs provided us an *in vitro* system in which SOST was greatly expressed after 2 weeks of incubation without the necessity to expose the cells to any osteogenic inductor.

Therefore, once the cell model was developed, PEI grafted MSNs were loaded with siRNA and delivered to MEF cells, evaluating their silencing capability. We demonstrated that SOST was successfully knocked down by the administrations of siRNA loaded MSNs. Then, the expression of the early osteogenic markers was evaluated and we could confirm that after silencing SOST the expression of those genes considerably increased.

After the *in vitro* validation of the system, the next step was to evaluate the nanoplatform *in vivo* in an osteoporotic scenario. One of the most common osteoporosis in humans is the postmenopausal osteoporosis, which was selected for the animal model here employed. It is well known that estrogen deficiency enhances bone resorption, being the main cause of this type of osteoporosis. Thus, the most popular animal model for postmenopausal osteoporosis is normally generated by ovariectomy, so ovariectomized mice were used for the evaluation of the developed nanosystem in this work. After the injection of a siRNA loaded MSNs suspension inside the femoral bone marrow, the expression of SOST, Alp, and Runx2 was evaluated. The employed nanoparticles were observed to be able to knockdown SOST and enhance the expression of Alp and Runx2, in total agreement with the results previously obtained *in vitro*.

The **second part** of this thesis deals with the evaluation of a combination therapy with SOST siRNA and osteostatin delivered by MSNs for osteoporosis treatment. A combination therapy has been proposed for boosting the potential osteogenic effects of the approach here presented. In this sense, the coadministration of SOST siRNA with other anabolic agent was explored to determine if an additive effect could be achieved.

The already optimized system was loaded with osteostatin and it was evaluated if after coating MSNs with PEI they were able release the peptide while transporting the siRNA. After confirming that PEI was not acting as a polymeric barrier for the release of osteostatin, the efficacy of the complete nanosystem (MSNs loaded with osteostatin and siRNA) was evaluated *in vitro*. The effect of both biomolecules delivered at the same time was greater than the one obtained by the delivery of either the siRNA or the peptide independently. Therefore, a synergistic effect between both biomolecules was confirmed, obtaining better results in silencing SOST and enhancing osteogenic markers expression.

With these promising results the effect of the complete system was evaluated in a low bone mass model: ovariectomized mice. The osteostatin and siRNA loaded nanoparticles were injected inside the femoral bone marrow, and after 5 days the gene expression was evaluated. Mice treated with each biomolecule separately modified the expression of the three genes, (knocking down SOST and increasing the expression of Runx2 and Alp). However, the co-administration of both biomolecules yielded synergistic effects, achieving an effective silencing of SOST and an additive increase of osteogenic markers expression.

The **third part** of this PhD thesis is focused on the modifications performed to the nanoplatform for achieving an effective systemic administration, and the evaluation of the systemic treatment regarding gene expression modification and bone microarchitecture improvement. Considering osteoporosis as a systemic disease, the nanoparticles must present several properties for allowing a systemic administration. The nanoparticles have to be stable in suspension while circulating in the blood. As it has been described in the literature, decorating the nanoparticles with molecules such as PEG would improve the colloidal stability and reduce the opsonization of the nanoparticles. Also, the nanoparticles need to be accumulated in the target tissue to reduce the off-target side-effects. The nanoparticles were decorated with alendronate which have been used as bone-targeting moieties due to their high affinity to HA. In this regard, a conjugate based on PEG and alendronate was synthesized to fulfill both requirements. Alendronate was conjugated via carbodiimide chemistry to the carboxylic acid end of a bifunctional HO_2C-PEG-NH_2, obtaining the desired molecule PEG-ALN (PA). Then, the conjugate was linked to a silane and added to the nanoparticles for the condensation onto the surface. Once the nanoparticles were PEGylated, the PEI grafting was performed obtaining the final system.

The colloidal stability and the targeting capacity of the complete nanocarrier was successfully evaluated. The PEGylated nanoparticles were stable for more than 24 hours, and the nanoparticles functionalized with ALN were accumulated in a HA tablet after 48 hours in contact with fresh PBS.

The PEI:MSNs ratio needed to be optimized after PEGylating the nanoparticles. Regarding siRNA binding capacity and cytotoxicity, 1:2 ratio was found to be optimal. The capability of the nanoparticles to protect the siRNA from the action of the RNases was also evaluated. These enzymes degrade the nucleic acids present in circulation, preventing them to reach their targeted tissue. A RNase stability assay was performed by the evaluation of the intact siRNA presence after reaction with RNase. The nanoparticles were able to protect the siRNA from the RNase activity after 2 hours in contact with the enzyme. This fact was important to be evaluated since the nanoparticles were going to be in circulation for several hours being in contact with RNases.

After the entire optimization of the system, the nanoparticle treatment was evaluated in ovariectomized mice for 2 or 3 weeks. In this case, the injections were performed subcutaneously every two days. After that treatment, the expression of several genes was measured. SOST gene was evaluated, and the results showed that the administration of the nanoparticles decreased the expression of the gene after 2 or 3 weeks of treatment. We also measured the expression of several osteogenic related genes such as, Alp, Runx2, OPG and OSX. The expression of these genes increased after the administration of the nanoparticles in all cases and in both periods of treatment, reaching values of healthy mice. It was also measured the expression of VEGF, a gene related with vascularization, which also increased after nanoparticles treatment.

After the evaluation of the gene expression modification, our next step was to evaluate the effect of this gene fluctuation in the microarchitecture of the bones. The bone quality was evaluated through micro-computed tomography (µCT) after 3 weeks of treatment. We used as positive control the gold standard osteoporosis treatment, the parathyroid hormone (PTH). The results showed that the mice treated with the nanoparticles here developed improved the microarchitecture of the bone regarding several values, such as BMD, BMC, Tr. Th, BV/TV, Tr. Sp and BS/BV, among others. After 3 weeks of treatment the nanoparticle-treated mice reached values close to healthy mice. The results obtained by the administration of the nanoparticles were close and, in some cases, even greater than the values obtained with the PTH treatment. Therefore, the system here proposed could be considered a potential alternative for the osteoporosis remission.

All the results obtained in the present doctoral thesis show the great potential of MSNs to transport and deliver siRNAs as a new alternative for osteoporosis treatment. Also, this system will constitute a promising candidate as a platform for systemic combination therapy against

osteoporosis. The synergistic effect here evaluated between SOST siRNA and osteostatin could be further investigated as possible combination treatment against osteoporosis since it achieved greater results compared with PTH treatment. Taking everything into consideration, the nanosystem here presented would be consider as a promising treatment against osteoporosis disease.

Resumen

El objetivo general de esta tesis ha sido el diseño de nanopartículas mesoporosas para aplicaciones biomédicas. En particular, esta tesis doctoral comprende el desarrollo de un nanotransportador para un potencial tratamiento de enfermedades óseas, más específicamente de la osteoporosis.

El contexto inicial de esta tesis doctoral fue el proyecto europeo VERDI ("*polyValent mEsopoRous naosystem for bone DIseases*"). La propuesta implicaba el uso de materiales mesoporosos para el tratamiento de tres situaciones de relevancia clínica en la enfermedad ósea: infección ósea, cáncer de hueso (tumores primarios y metástasis en hueso) y osteoporosis.

La osteoporosis es la enfermedad ósea más prevalente. Es una enfermedad silenciosa, y debido al envejecimiento de la población, se considera uno de los mayores problemas sanitarios afectando a mujeres postmenopáusicas y a personas mayores de ambos sexos. A pesar de que se han desarrollado diversos tratamientos antiosteoporóticos con alta efectividad, todos ellos presentan sus diversos efectos secundarios que limitan su aplicación. En este sentido, se están dirigiendo muchos esfuerzos hacia el desarrollo de nuevas alternativas para el tratamiento de la osteoporosis en busca de un posible uso a largo plazo y una mayor adherencia por parte del paciente.

La inhibición de la vía Wnt/β-catenina ha llamado la atención como diana terapéutica en enfermedades óseas como la osteoporosis. Uno de los principales inhibidores de esta vía es la esclerostina, proteína codificada por el gen SOST. Su sobreexpresión produce una disminución en la formación y diferenciación de osteoblastos. Existen varios tipos de anticuerpos monoclonales antiesclerostina que se han desarrollado como fármacos anabólicos para bloquear la actividad de esta proteína. De esta manera, al evitar la inhibición de la vía Wnt/β-catenina se permitirá la diferenciación osteoblástica y así poder actuar como un tratamiento de la osteoporosis. Sin embargo, estos anticuerpos pueden causar una respuesta inmune, lo cual limita el uso de este tratamiento. Silenciar el gen SOST con un siRNA especifico puede ser un planteamiento más efectivo para salvar esta limitación de la respuesta inmune. Sin embargo y a pesar de que los siRNAs parecen ser unos candidatos prometedores como agentes terapéuticos en enfermedades óseas, su problema principal reside en su transporte debido a su corta vida media y pobre capacidad de penetración a través de membranas celulares. El uso de nanopartículas para el transporte de estas moléculas puede resolver exitosamente este problema.

Como se ha mencionado previamente, existen diferentes medicamentos con actividad anti-osteoporótica que se encuentran actualmente en el mercado, aunque el tratamiento estrella contra esta enfermedad sigue sin encontrarse. En este sentido, el uso de una terapia combinada puede ser una potencial alternativa para obtener mejores resultados en la remisión de la osteoporosis. Existen diversos planteamientos para el tratamiento de esta enfermedad y, por lo tanto, un mayor numero de combinaciones posibles. Es decir, existe un gran campo de investigación en la

búsqueda de una estrategia apropiada para combatir esta enfermedad. La clave para este tipo de terapia es el diseño de un sistema que permita el co-transporte de fármacos y los pueda liberar en el lugar deseado de manera controlada. En este caso, las nanopartículas pueden jugar un papel crucial, siendo capaces de transportar y liberar varios fármacos al mismo tiempo.

Debido al carácter sistémico de la osteoporosis, el tratamiento debe ser administrado por vía intravenosa o subcutánea. Por esta razón, el tratamiento elegido debe ser capaz de permanecer por largos periodos de tiempo en circulación y acumularse en el tejido diana, en este caso, el hueso. De nuevo, las nanopartículas, gracias a su capacidad de ser modificadas químicamente, pueden incrementar su estabilidad coloidal y su especificad tisular al funcionalizarse con moléculas como PEG o ligandos de vectorización, confiriendo así un transporte eficaz al medicamento cargado. En este sentido, las nanopartículas protegerán el fármaco de la degradación, optimizando la dosis sin sacrificar la eficacia del tratamiento, y reducirán la exposición a células distintas del objetivo, minimizando sus potenciales efectos secundarios.

En la presente tesis doctoral hemos seleccionado las MSNs como nanotransportadores de fármacos debido a su estabilidad fisicoquímica y sus propiedades texturales, elevada superficie especifica y volumen de poro, que las proveen de una gran capacidad de carga. Además, la estructura mesoporosa de las nanopartículas permite la carga de diferentes moléculas terapéuticas, confiriendo así la posibilidad de una terapia combinada.

La tesis doctoral se encuentra dividida en tres partes principales. La primera parte incluye el desarrollo y evaluación de un nanotransportador basado en MSNs capaz de transportar y liberar siRNAs. A continuación, se evaluó un tratamiento combinado de un siRNA contra SOST y osteostatina, transportados por MSNs. La última parte se focaliza en las modificaciones llevadas a cabo en el sistema para conseguir una administración sistémica eficaz y la evaluación del tratamiento sistémico teniendo en cuenta la modificación en la expresión génica y la mejora de la arquitectura ósea.

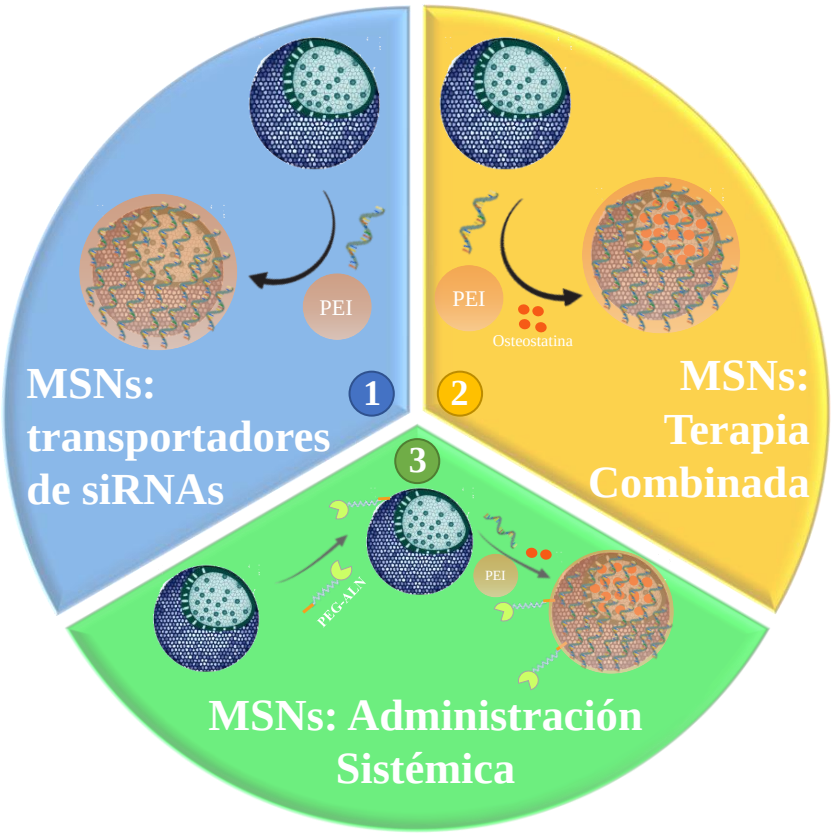

Resumen gráfico de las partes en las cuales se divide la presente tesis doctoral.

La **primera parte** de esta tesis doctoral engloba el desarrollo y evaluación de un nanotransportador basado en MSNs para el transporte y liberación de siRNAs. El cuello de botella de los tratamientos basados en siRNAs es la necesidad de un medio de transporte para llevar los silenciadores génicos al interior de las células diana. Las MSNs pueden ser una plataforma apropiada para transportar siRNAs ya que pueden cargar ácidos nucleicos en el interior de sus poros o anclados a la superficie.

La naturaleza de la carga negativa de los ácidos nucleicos hace necesario que la superficie de las nanopartículas se modifique para obtener así la carga positiva deseada para poder unirse a los siRNAs. Para conseguirlo, las MSNs se funcionalizaron con PEI, un polímero catiónico, obteniendo la carga positiva necesaria. En este paso, se compararon diferentes proporciones de PEI:MSNs y diferentes pesos moleculares del polímero (5 kDa, 8 kDa, 10 kDa) para optimizar el sistema. La elección tanto del ratio como del peso molecular se llevó a cabo teniendo en cuenta la capacidad de unir siRNAs y la posible citotoxicidad del polímero. Mientras PEIs de bajo peso molecular no son citotóxicos, son inefectivos a la hora de transfectar nucleótidos. En cambio, PEIs de elevado peso molecular presentan elevada citotoxicidad en células a pesar de ser altamente eficaces en la transfección de polímeros. En este sentido, se ha demostrado que el

tamaño, la compacidad y las posibles modificaciones químicas como la ramificación del polímero afectan a la eficacia y toxicidad del PEI.

Tras seleccionar la mejor relación PEI:MSNs (1:2) y el peso molecular (5 kDa) apropiados para un carga y liberación eficaz del siRNA, las nanopartículas fueron evaluadas *in vitro*. En un primer lugar, se evaluó la capacidad de penetrar a través de membranas celulares y liberar los siRNAs en el citosol mediante citometría de flujo y microscopía confocal. En segundo lugar, se evaluó la capacidad de silenciamiento de SOST del sistema y el efecto de este silenciamiento en la expresión de dos marcadores osteogénicos (Runx2 and Alp) utilizando qRT-PCR.

Se ha descrito que los fibroblastos embrionarios de ratón (MEFs) pueden expresar niveles de SOST elevados bajo determinadas condiciones. Por ello, cultivamos MEFs durante 3 semanas observando niveles de expresión de SOST crecientes detectables a los 3 día; estos incrementaron hasta 20 veces tras 14 días de cultivo. Por lo que las MEFs nos aportaron un sistema *in vitro* donde SOST se expresaba considerablemente tras 2 semanas de incubación sin necesidad de exponer las células a ningún inductor osteogénico.

Las MSNs recubiertas con PEI se cargaron con siRNA y se aplicaron sobre las MEFs tras 14 días de cultivo para evaluar así su capacidad de silenciamiento. Se demostró que SOST fue silenciado exitosamente con la administración de las MSNs cargadas con siRNA. Posteriormente se evaluó la expresión de marcadores osteogénicos tempranos y se confirmó que tras el silenciamiento de SOST su expresión incrementó de forma considerable.

Tras la validación *in vitro* del sistema, el siguiente paso fue evaluar el sistema *in vivo*. Uno de los tipos de osteoporosis más comunes en los humanos es la osteoporosis postmenopáusica, por ello decidimos centrarnos en esta variante de la enfermedad para nuestro modelo animal. El déficit de estrógenos incrementa la resorción ósea, siendo esta la causa principal de este tipo de osteoporosis, así, el modelo animal más común para osteoporosis postmenopáusica es el obtenido por ovariectomía. Utilizamos ratonas ovariectomizadas para la evaluación de nuestro sistema. Tras inyectar una suspensión de nanopartículas cargadas con siRNA en el interior de la medula ósea femoral, la expresión de SOST, Alp, y Runx2 fue evaluada. Observamos que nuestras nanopartículas eran capaces de silenciar SOST e incrementar la expresión de Alp y Runx2, estando los resultados *in vivo* en concordancia con los obtenidos *in vitro*.

En la **segunda parte** de esta tesis, nos centramos en la evaluación de una terapia combinada compuesta por SOST siRNA y osteostatina liberados por MSNs para el tratamiento de la osteoporosis. Se propuso una terapia combinada para impulsar el potencial efecto osteogénico observado mediante el silenciamiento del gen SOST. Para ello se evaluó la coadministración de SOST siRNA con otro agente anabólico para determinar si se podía obtener un efecto aditivo. El sistema previamente optimizado se cargo con osteostatina y se evaluó si las nanopartículas

recubiertas con PEI eran capaces de liberar el péptido mientras transportaban el siRNA. Tras confirmar que el PEI no actuaba como una barrera polimérica para la liberación de osteostatina, la eficacia del nanosistema completo se evaluó *in vitro*. El efecto de ambas biomoléculas liberadas al mismo tiempo fue considerablemente mayor que el obtenido a través de la liberación de el siRNA o el péptido por separado. Por lo tanto, confirmamos la existencia de un efecto sinérgico entre ambas biomoléculas, obteniendo mejores resultados de silenciamiento de SOST y estimulando en mayor medida la expresión de marcadores osteogénicos. Con estos resultados prometedores, se evaluó el efecto del sistema completo en un modelo de baja masa ósea: ratonas ovariectomizadas. Las nanopartículas cargadas con osteostatina y siRNA se inyectaron en el interior de la medula ósea femoral, y tras 5 días, se evaluó la expresión génica. Las ratonas tratadas con cada una de las moléculas por separado presentaban una variación en la expresión de los 3 genes (silenciamiento de SOST e incremento de Alp y Runx2), pero la coadministración de ambas moléculas conllevó un efecto sinérgico, alcanzando un silenciamiento efectivo de SOST y un incremento de la expresión de marcadores osteogénicos.

La **tercera parte** de esta tesis se está centrada en las modificaciones realizadas sobre el sistema previamente estudiado para conseguir una administración sistémica efectiva y la evaluación del tratamiento sistémico teniendo en cuenta la modificación en la expresión génica y la mejora en la microarquitectura ósea.

Teniendo en cuenta que la osteoporosis es una enfermedad sistémica, las nanopartículas deben presentar varias propiedades para así permitir una administración sistémica del tratamiento. Primero, las nanopartículas necesitan ser estables en suspensión durante su tiempo en circulación sanguínea. Además, deben permanecer el tiempo suficiente en el torrente sanguíneo como para alcanzar los huesos y una vez allí liberar los fármacos previamente cargados. Como ha sido previamente descrito en la literatura, decorar la superficie de las nanopartículas con PEG incrementa el tiempo de circulación de las nanopartículas, aumentando la estabilidad coloidal y reduciendo la opsonización de estas. Otra de las propiedades que requieren las nanopartículas para una administración sistémica eficaz es la capacidad de ser acumuladas en el tejido deseado reduciendo así los efectos adversos. Este fenómeno se conoce como vectorización el cual se basa en la funcionalización de la superficie de las nanopartículas con moléculas que generen una acumulación selectiva en un tejido específico. En este sentido, la matriz ósea mineralizada está compuesta principalmente por hidroxiapatita (HA), por lo que representa una prometedora diana para un transporte selectivo. Los bisfosfonatos, como el alendronato, han sido utilizados como moléculas de vectorización a hueso debido a su elevada afinidad por la HA y su capacidad de unirse a lugares con actividad osteoclástica.

Para alcanzar ambas capacidades se sintetizó un conjugado a base de PEG y alendronato. El alendronato se conjugó a través de química de carbodiimida al acido carboxílico presente en un PEG bifuncional (HO_2C-PEG-NH_2), obteniendo así la molécula de PEG-ALN deseada. Posteriormente, las nanopartículas se recubrieron con el polímero obtenido. El conjugado se unió a un silano y a continuación este se unió a las nanopartículas por condensación en su superficie. Una vez las nanopartículas fueron PEGiladas, el recubrimiento con PEI se llevó a cabo, para dar lugar así al sistema final.

La estabilidad coloidal y la capacidad de vectorización del nanotransportador completo se evaluó de manera exitosa. Las nanopartículas PEGiladas eran estables durante más de 24 horas, y las nanopartículas que se habían funcionalizado con ALN se acumularon sobre una pastilla de HA tras 48 horas en contacto con PBS.

Una vez llevada a cabo la PEGilación de las nanopartículas fue necesario la optimización de las proporciones de PEI:MSNs. Finalmente, el ratio 1:2 se consideró el más apropiado teniendo en cuenta la capacidad de carga de siRNA y la citotoxicidad del polímero.

Otra cuestión a tener en cuenta era la capacidad de la nanopartícula de proteger el siRNA frente la acción de RNasas. Estas enzimas degradan los ácidos nucleicos presentes en circulación evitando así que estos lleguen a su tejido diana. Se llevó a cabo un ensayo de estabilidad frente a RNasas a través de la evaluación del siRNA intacto presente tras una reacción de las nanopartículas cargadas con siRNA frente RNasas. El nanotransportador fue capaz de proteger el siRNA de la acción de las RNasas durante 2 horas en contacto con las enzimas. Este hecho fue de elevada relevancia ya que las nanopartículas se encontrarían en circulación durante varias horas en contacto con RNasas. Por ello, tienen que ser capaces de hacer llegar al siRNA intacto a su tejido diana, en este caso, el hueso.

Finalmente, se comprobó que la nueva funcionalización con PEG-ALN y posterior recubrimiento con PEI permitía la liberación de una carga de osteostatina en los poros. Las nanopartículas PEGiladas se cargaron con osteostatina y posteriormente se recubrieron con PEI. Tras esto, se evaluó la liberación de la osteostatina por parte de las nanopartículas verificando así que la adición del PEG permitía la liberación del péptido.

Tras la optimización completa del sistema, el tratamiento con nanopartículas cargadas con el silenciador y la osteostatina se evaluó sobre ratonas ovariectomizadas durante 2 y 3 semanas. En este caso, las inyecciones se llevaron a cabo de forma subcutánea cada 2 días, consiguiendo así la administración sistémica buscada. Una vez finalizado el tratamiento, se midió la expresión de determinados genes y los resultados mostraron que la administración de las nanopartículas disminuyó la expresión del gen SOST tras 2 y 3 semanas de tratamiento. En segundo lugar, se midió la expresión de varios genes osteogénicos como Alp, Runx2, OPG y OSX. La expresión de

estos genes tras la administración de las nanopartículas ya fuese durante 2 o 3 semanas incrementó en todos los casos, alcanzando valores próximos a los obtenidos en ratonas sanas. Es decir, se consiguió revertir una situación osteoporótica hacia una situación normal.

Tras la evaluación de la expresión génica, el siguiente paso consistió en la evaluación del efecto de esta fluctuación génica sobre la microarquitectura del hueso. Se evaluó la calidad del hueso a través de μCT tras 3 semanas de tratamiento. Se utilizó como control positivo uno de los tratamientos estrella contra la osteoporosis, la PTH. Los resultados obtenidos mostraron que las ratonas tratadas con las nanopartículas diseñadas en la presente tesis doctoral mejoraron su microarquitectura ósea teniendo en cuenta valores como BMD, BMC, Tr.Th, BV/TV, Tr.Sp y BS/BV, entre otros. Tras 3 semanas de tratamiento, las ratonas tratadas con las nanopartículas alcanzaron valores próximos a ratonas sanas. Los resultados obtenidos con la administración de las nanopartículas estaban cercanos a aquellos obtenidos con la administración de PTH y hasta en ciertos casos superaban la acción observada por la hormona. De esta forma, las nanopartículas diseñadas a lo largo de esta tesis suponen una potencial alternativa a los tratamientos presentes contra la osteoporosis.

Todos los resultados obtenidos en esta tesis doctoral muestran el gran potencial de las MSNs de transportar y liberar siRNAs como nueva alternativa para el tratamiento de la osteoporosis. Este sistema se considera un candidato prometedor como plataforma para una terapia sistémica combinada contra la osteoporosis. La combinación de SOST siRNA y osteostatina estudiada a lo largo de esta investigación demuestra la existencia de un efecto sinérgico entre estas dos moléculas. El sistema propuesto en esta tesis doctoral puede fomentar el desarrollo de posibles tratamientos combinados como alternativas contra la osteoporosis. De esta manera, el uso de esta terapia combinada a través de la administración de nanopartículas cargadas, puede considerarse una prometedora alternativa para la posible remisión de la enfermedad.

Chapter I:
General Introduction

Investigar es ver lo que todo el mundo ha visto,
y pensar lo que nadie más ha pensado
Albert Szent-Györgyi
(Fisiólogo Húngaro, Premio Nobel de Medicina 1937)

1. General Introduction

In the last few decades, the mean life expectancy has increased, which has consequently boosted the impact of skeletal diseases. In healthy adults, bone is being continuously renewed by a process known as bone remodeling. Old bone is replaced by new bone in a coordinated sequence of events where bone resorption is always followed by bone formation. In the young adult skeleton, the resorbed bone is quantitatively similar to the formed bone.[1] However, when bone resorption exceeds bone formation, typically in elderly people and postmenopausal women, the bone mass decreases and the bone microarchitecture deteriorates, leading to osteoporosis.[2,3] The frequency of these imbalances turns osteoporosis in the most common systemic skeletal disease. Taking into account the aging population, the medical and socioeconomic impact of osteoporosis is expected to increase in the near future.[4]

1.1 Bone Biology

The human adult bone is constituted by cortical and trabecular (known also as cancellous) bone, being present in different proportions depending on the specific bone. Long bones normally present more cortical bone. Instead, in the vertebrae predominates trabecular bone. Bone is composed by (A) osteoid or bone matrix, which is mainly constituted by an organic phase (collagen type I, proteins and lipids), an inorganic phase of hydroxyapatite, and water and (B) different cells, such as osteoblasts, derived from mesenchymal stem cells, which are considered the bone-forming cells; osteoclasts, derived from hematopoietic stem cells, considered the bone-resorbing cells; osteocytes, located within the bone matrix, and descended from mesenchymal stem cells through osteoblast terminal differentiation; vascular and perivascular cells, responsible of bone tissue vascularization, and immune cells such as macrophages (Figure 1.1).[5,6]

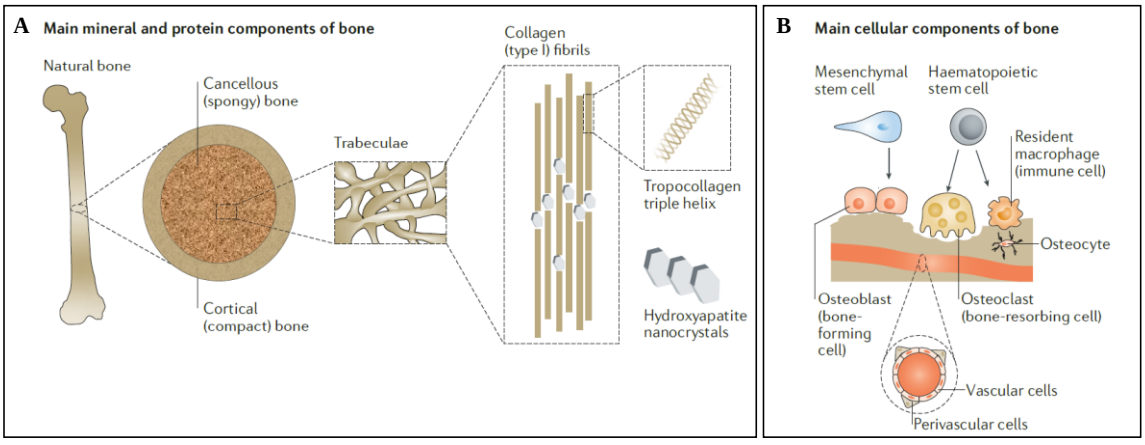

Figure 1.1 Bone physiology (A). Cellular bone components (B). Adapted from Ref 6 with the permission of Nature.

Bone is an active tissue that is constantly being remodeled in response to mechanical stress and hormonal changes.[7] Two different processes take place in bone, bone modelling and bone remodeling. Bone modeling sculpts the bones during skeletal development defining their shape and structure by the independent action of osteoblasts and osteoclasts, but their activities are not necessarily coupled anatomically or temporally. On the contrary, bone remodeling is a process where osteoclasts and osteoblasts work sequentially in the same bone remodeling unit (BRU) to renew bone, maintaining bone strength and preserving mineral homeostasis.[8] The purposes of remodeling include, among others, the replacement of old and damaged bone with new bone to maintain the mechanical strength of bone, calcium and phosphate homeostasis (long term), the maintenance of acid/base balance, and the release of growth factors embedded in bone. It has been estimated that 3–4 million BRUs are initiated each year and 1 million BRUs are actively engaged in adult bone turnover at any time.[8]

Remodeling is a process characterized by four phases, as it can be observed in Figure 1.2. First, the osteoclasts are recruited and activated, this is followed by a bone resorption phase for several weeks where the activated osteoclasts resorb bone. Then, the reversal phase starts, bone resorption stops leading to an extended period of bone formation. The osteoclasts suffer apoptosis and osteoblasts are recruited. Afterwards, the formation phase begins, and osteoblasts generate new organic bone matrix.[9]

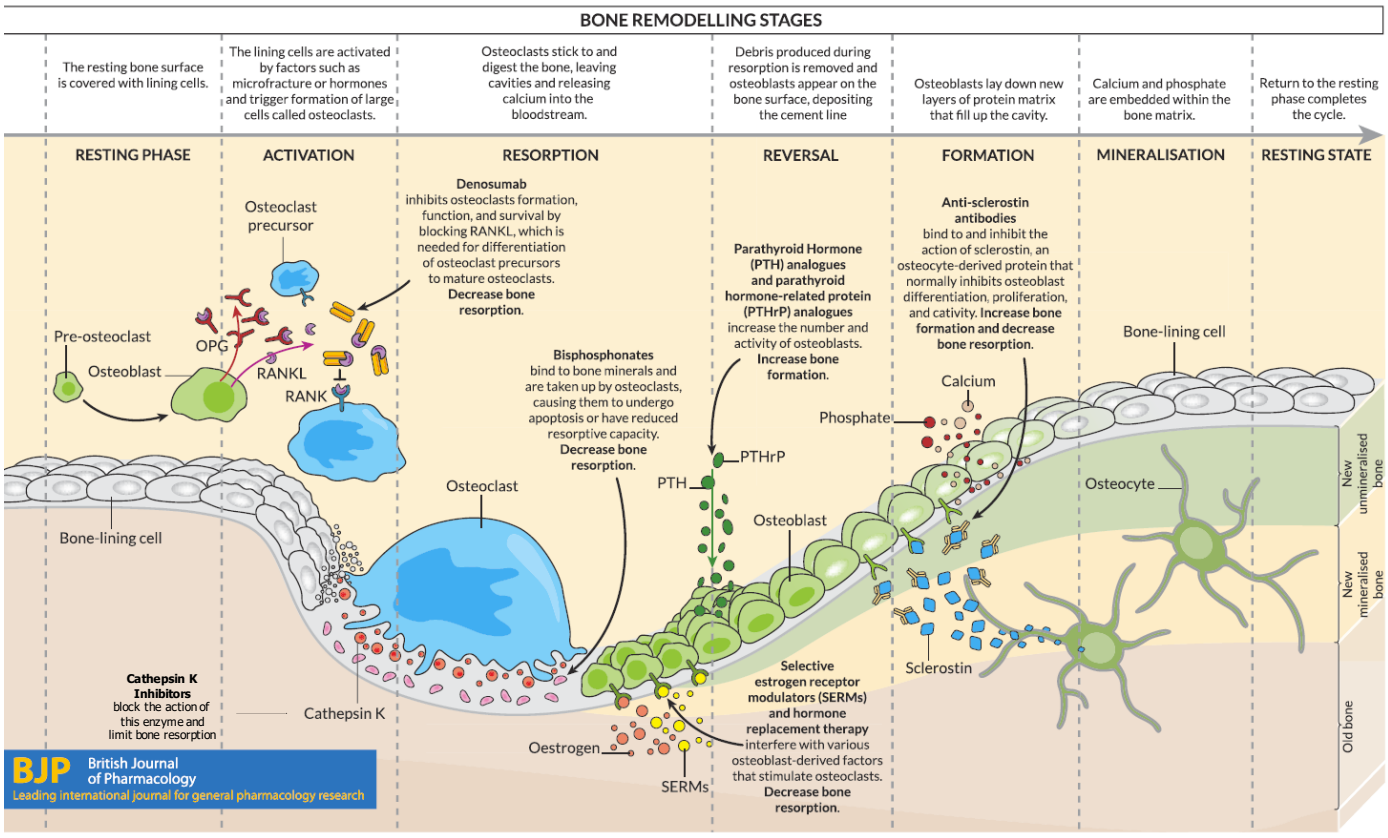

Figure 1.2. Schematic representation of the different phases of bone remodeling and how the different treatments affect bone remodeling. Adapted from Ref 21 with permission from Wiley.

Osteoclasts are myeloid cells derived from mononuclear precursor cells of the monocyte–macrophage lineage in bone marrow.[10,11] They are terminally differentiated and specialized to eliminate mineralized bone matrix. There are specific cytokines that control their formation, maturation, and activity. Their differentiation is mainly regulated by the receptor activator of nuclear factor κB ligand (RANKL) and osteoprotegerin (OPG). The ratio between these two molecules (RANKL:OPG) would determine the osteoclast differentiation. Also, the exposure of preosteoclasts to interleukin (IL)-1 and IL-6, macrophage colony stimulating factor, parathyroid hormone (PTH), 1,25-dihydroxyvitamin D, and calcitonin would affect the osteoclast maturity process.[9] Activated osteoclasts secrete H^+ into the resorption pits beneath them, lowering the pH to 4.5, which helps to solubilize bone mineral, the inorganic fraction of bone. They also secrete cathepsin K, tartrate-resistant acid phosphatase, matrix metalloproteinase-9, and gelatinase from cytoplasmic lysosomes to digest organic matrix, the organic fraction of bone (Figure 1.3).[12] This process results in formation of saucer-shaped Howship's lacunae on the surface of trabecular bone and resorption tunnels or Haversian canals in cortical bone.

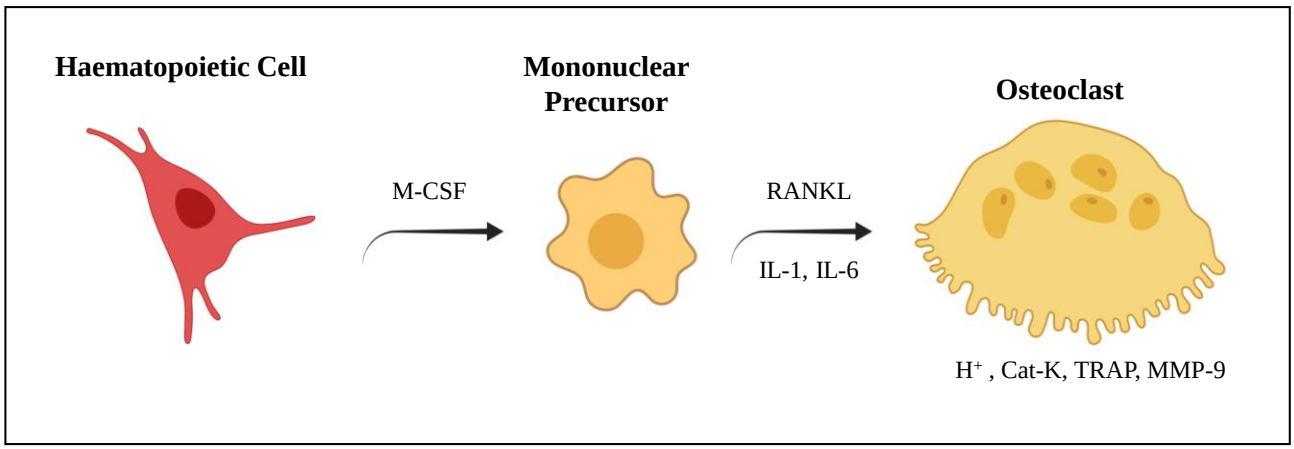

Figure 1.3 Osteoclast differentiation process and molecule secretion.

After the resorption phase, osteoclasts stop functioning and undergo apoptosis, and the matrix debris is removed by macrophage-like cells. This fact is related with the transforming growth factor (TGF)-β which plays a key role in the evolution from resorption phase to bone formation phase. It inhibits RANKL production by osteoblast, decreasing osteoclast bone resorption activity. This leads to the reversal phase, where bone resorption switchs to bone formation.[10] There are several coupling signals that are engaged in the reversal phase such us, insulin-like growth factor (IGF)-1, IGF-2, bone morphogenetic proteins (BMPs), platelet derived growth factors and fibroblast growth factors, among others. These signals would produce the recruitment of several cells to the resorption cavities. Therefore, osteocytes from resorbed bone matrix, and pre-osteoblast recruited for the next phase could be found.

The next step after the reversal phase is the bone formation, which typically takes between 4–6 months to be completed. As it has been mentioned before, osteoblasts are the bone-forming specialized cells. They are developed from pluripotent mesenchymal stem cells and their differentiation and activation is controlled by several factors and signaling pathways. Among them, the wnt/β-catenin pathway has a lot of impact in the differentiation, maturation and activation of osteoblasts.[13] The differentiation from mesenchymal stem cells to the osteoblast lineage requires activity of the canonical wnt/β-catenin pathway and the associated proteins.[14] Additionally, mechanical stimulation and the endocrine signal of the PTH can promote bone formation signals *via* osteocytes. Under resting conditions, osteocytes express sclerostin, protein encoded by SOST gene, that binds to low density lipoprotein receptor-related protein-5/6 (LRP5/6) inhibiting the activation of wnt/β-catenin pathway.[15] On the other hand, mechanical strain on bone and PTH signaling *via* PTH receptors on osteocytes, inhibit osteocyte expression of sclerostin, therefore, wnt proteins could activate the pathway *via* their receptor and coreceptor, LRP5/6, and then promote bone formation. This anabolic wnt signaling pathway is critical in establishing basal bone mineral density.[9,16]

During formation phase, osteoblasts will synthesize new collagenous organic matrix and regulate mineralization of the matrix by releasing small matrix vesicles with calcium and phosphate. At the completion of bone formation, about 50–70% of osteoblasts suffer apoptosis, while the remaining osteoblasts undergo terminal differentiation and immerse in the unmineralized osteoid becoming osteocytes or bone lining cells.[10] Finally, osteoblasts would also regulate the end of the bone formation phase by the expression of osteoclastogenic factors such as RANKL.[17]

Bone remodeling would play a key role in bone health and strength being crucial the perfect balance between the actions of osteoblast and osteoclast. The duration and effectiveness of both resorption and formation phases would determine the appropriate healthiness of the bone tissue.

1.2 Bone Pathology: Osteoporosis

Bone is an active tissue that is constantly being remodeled in response to mechanical stress and hormonal changes. As mentioned above, this bone remodeling is regulated by numerous cytokines, hormones and factors, leading to the sequential and coordinated activity of osteoclasts and osteoblasts to remove old-damaged bone and replace it with new bone matrix. An imbalance in any of these factors that might result in a higher bone resorption than formation would lead to a bone pathology known as osteoporosis. Osteoporosis is defined by the World Health Organization as a “progressive systemic skeletal disease characterized by low bone mass and microarchitectural deterioration of bone tissue, with a consequent increase in bone fragility and susceptibility to fracture”.[18] Taking into account that the mean life expectancy has increased in the last few decades, the impact of skeletal diseases such as osteoporosis has increased.

The World Health Organization has selected a diagnostic criterion using standard deviation of BMD (T-score). BMD is measure using X-rays, dual-energy X-ray absorptiometry (DEXA or DXA), or a special computed tomography scan that uses computer software to determine bone mineral density. The BMD T-score is a value which relates the BMD of the patient with the bone mineral density of a healthy young (premenopausal) adult woman. A T-score of 0 would mean that the BMD is equal to the average of healthy young women. Instead, the differences between the BMD of the patient and that of the average healthy young women are measured in units called standard deviations (SDs). The more SD below 0, the lower BMD and the higher risk of fracture (Table 1.1). Osteoporosis is defined as a BMD that lies 2.5 SDs or more below the average value for young healthy women (a T-score of < -2.5 SD). Instead, the state previous to osteoporosis know as osteopenia is defined as a BMD T-score between –1 and –2.5 SD.[19]

Table 1.1 World Health Organization (WHO) definitions based on bone density levels. Bone Mineral Density (BMD), Standard Deviation (SD)

WHO definitions based on BMD T-scores	
Level	**Definition**
Normal	BMD ±1 SD of the young adult mean.
Osteopenia (Low Bone Mass)	BMD between -1 and -2.5 SD of the young adult mean.
Osteoporosis	BMD < -2.5 SD of the young adult mean.
Severe Osteoporosis	BMD < -2.5 SD of young adult mean, and there have been one or more osteoporotic fractures.

1.2.1 Bone Fractures

Nowadays, osteoporosis affects up to 50% of postmenopausal women and 20% of men older than 50 years leading to a high healthcare costs spent on treating this disease and the associated fractures.[20] Osteoporosis is therefore a major fundamental cause of fractures in individuals over the age of 50 years, with potentially serious and complex sequelae of comorbidities, both physical and psychological. Fractures are often associated with increased morbidity and mortality, dramatically decreasing quality of life. Fractures in elderly patients, depending on localization, morphology, comorbidities and healing potential, can lead to lasting disability and death.[21]

Approximately 1/3 of postmenopausal women suffer osteoporosis worldwide and at least half of them will experience a fracture due to the fragility caused by osteoporosis during their lifetime.[18] Fractures are often associated with increased morbidity and mortality, dramatically decreasing quality of life. The most common fracture sites appear to be the vertebral bodies of the thoracolumbar spine, the distal forearm and the hip, proving the systemic affection of the disease.

The hip fractures are one of the most serious outcomes of the disease, affecting worldwide with high incidence mainly in Europe and United Estates. In Figure 1.4 it can be appreciated the incidence of hip fracture in different countries.

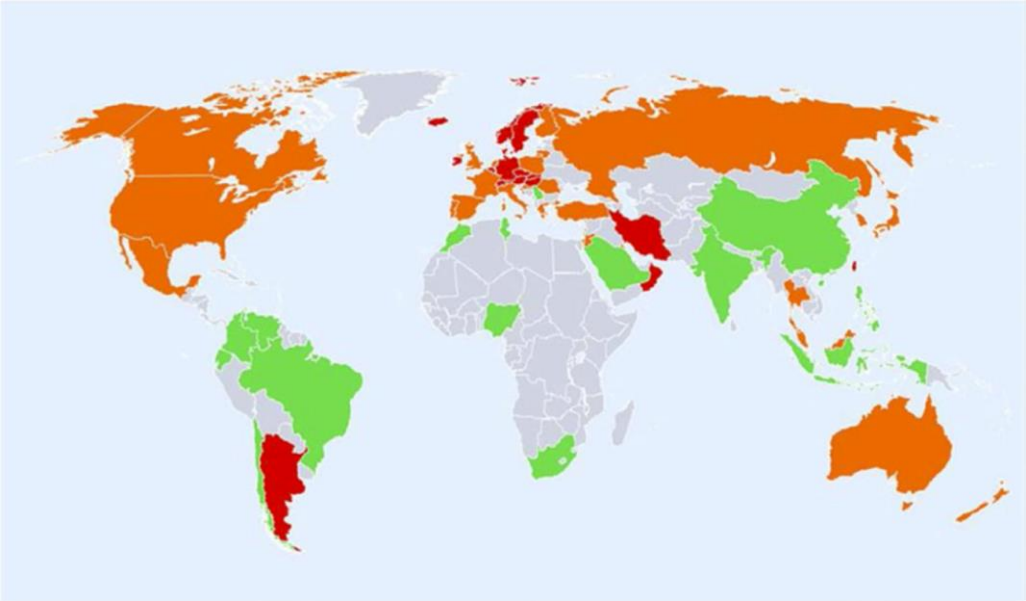

Figure 1.4 Hip fracture rates for men and women combined in different countries of the world categorized by risk; countries are colored red (annual incidence > 250/100,000), orange (150–250/100,000), or green (< 150/100,000) where estimates are available. Reproduced from Ref 18 with permission from Springer.

In order to decrease the affection of fractures, screen the patients to diagnose the disease would be of relevant importance. The screening would include the measurement of BMD and the assessment of risk factors to fracture prediction. They include, advanced age, previous fractures, long-term glucocorticoid therapy, low body weight (less than 58 kg), family history of hip fracture, smoking and excess of alcohol intake.[7]

Therefore, the clinical need to reverse bone loss, to stimulate bone formation and to stimulate bone regeneration to reduce bone fractures is increasing and has become a crucial challenge in health care field.

1.2.2 Osteoporosis Prevention

Within this framework, the approach to osteoporosis, as it is also the case for many other chronic conditions prevalent in older people, should be focused on the prevention not only of the disease but also of the clinical problems associated with frailty and disability, mainly fractures.[22] Despite the various treatments available, the prevention of the disease represents the most important aspect of management. An adequate intake of calcium and vitamin D as well as a healthy lifestyle is the basis for maintaining bone health.[23] Osteoporosis prevention has two phases, primary prevention and secondary prevention. Primary prevention starts during childhood and

adolescence, since this will determine the development of a healthy strong skeleton in the adulthood. Even though genetic factors determine to a great extent the nature of our bones, the promotion of physical activity, adequate nutrition and the avoidance of negative factors for normal bone development such as smoking or alcohol intake, among others, are extremely important. Secondary prevention starts once bone loss or bone fracture has occurred. When osteoporosis is diagnosed, the choice of medications must be individualized considering characteristics of the patient and the risk of fractures. Suffering a fracture is the most potent predictor of new fractures starting a process known as "fracture cascade".[22]

Osteoporosis is commonly diagnosed in advanced stages, usually after fractures have occurred, reducing the quality of life. Clinicians should focus on prevention and early recognition of risk factors leading to osteoporosis, and in this way avoid fracture and ameliorate life style of elderly patients. Taking these facts into consideration, early diagnosis and adequate calcium and vitamin D intake are vital in osteoporosis prevention.[23]

1.3 Osteoporosis Treatments

The bone remodeling process is governed by the action of osteoclasts, which resorb old bone, and osteoblasts, which subsequently stimulate new bone formation. Therefore, these cells are obvious targets for a potential pharmaceutical treatment of osteoporosis. Currently, conventional therapies are limited to two main groups: anti-resorptive drugs, which slow down bone resorption; and anabolic drugs, which stimulate bone formation. Although these conventional drugs are effective in reducing fracture risk and increasing BMD, they present some limitations and side effects which restrict their long-term administration and reduce the treatment adherence as there would be described below. Understanding the osteoporosis signaling pathways have led to the discovery of new agents to treat the disease. These emerging osteoporosis therapeutics have brought the opportunity of improving the available options for osteoporosis treatment.

1.3.1 Antiresorptive Drugs

The main effect of antiresorptive drugs is to inhibit the recruitment, maturation, and/or activity of osteoclasts. Consequently, the administration of these therapeutics would decrease the rate of bone remodeling by reducing the number of BRUs. In fact, antiresorptive agents reduce bone turnover relatively quick by decreasing bone resorption in the initial states. These changes lead to an altered balance between bone resorption and formation that favors an increase in BMD, preserving or strengthening the structure of bone, and reducing the number of fractures.[24] Essentially, antiresorptive therapy preserves existing bone mass and structure and increases the degree of mineralization, but the architecture would not generally be improved. Since osteoclast presence produce the activation of osteoblasts, the reduction of osteoclast number will impair the recruitment of osteoblasts being followed by a reduction in bone formation. Therefore, this

uncoupling of formation and resorption would last for certain time before osteoblast function decreases and accumulation of bone mass lessen. Thus, antiresorptive treatments would increase BMD just to a limited extent.[25] Among the most popular antiresorptive drugs are bisphosphonates, denosumab, estrogen and selective estrogen receptor modulators. Other antiresorptive agent is calcitonin but its use is progressively decreasing being considered a second line therapy.

1.3.1.1 Bisphosphonates

Bisphosphonates (BPs) are the most commonly prescribed agents for osteoporosis therapy, being considered a first-line treatment. Since BPs present high affinity towards hydroxyapatite, they would be accumulated in the bone matrix. In fact, their effect would last for a long time, thanks to their trend to be retained in bone, being possible to administrate them weekly, monthly, yearly or even at longer intervals and they would still suppress bone turnover.[26] There are two main groups of BPs with different mechanisms of action, non-nitrogen containing BPs and nitrogen containing BPs (Table 1.2).

Table 1.2 Chemical structure of bisphosphonates (BPs). Several examples of non-nitrogen containing BPs and nitrogen containing BPs.

BPs	**Non-Nitrogen BPs**		**Nitrogen BPs**	
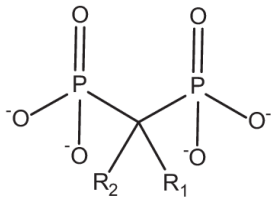	Etidronate	R_1=OH R_2= CH_3	Alendronate	R_1=OH R_2= $(CH_2)_3$-NH_2
	Clodronate	R_1=Cl R_2=Cl	Zoledronate	R_1=OH R_2=CH_2 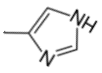
	Oxidronate	R_1=OH R_2=H	Risedronate	R_1=OH R_2= CH_2 

Non-nitrogen containing BPs, such as etidronate, clodronate or oxidronate, are metabolized in osteoclasts to compounds that affect the synthesis of adenosine triphosphate, forming a nonfunctional molecule that competes with it in the cellular energy metabolism. The osteoclasts begin apoptosis and, consequently, the bone resorption rate is reduced.

Nitrogen containing BPs (alendronate, zoledronate and risedronate, among others) block osteoclast function by inhibiting farnesyl pyrophosphate synthase. This enzyme is involved in mevalonate cholesterol synthesis pathway which is critical for membrane protein prenylation (addition of hydrophobic molecules to a protein). They will disrupt osteoclast polarization by preventing formation of the actin ring, breaking into osteoclast cytoskeleton and vesicular trafficking and formation. Osteoclast would be detached from bone, leading to apoptosis and, therefore, a reduction of bone resorption.

Currently, BPs, more precisely nitrogen-containing BPs, are considered first-choice drug for osteoporosis but they still present several side effects. First, they are poorly absorbed from the gastrointestinal tract and, consequently, high doses are required. This leads to gastrointestinal discomfort, arthralgia, and myalgia, which occur in up to 10% of patients. Also, after intravenous bisphosphonate treatment, flu-type symptoms may appear, such as fever, headache and muscle pain. Rare side effects (*e.g.* uveitis, osteonecrosis of the jaw, atypical femoral fractures) are associated with long-term bisphosphonate therapy and despite being rare they have gained more attention among physicians. Due to the presence of these long-term side-effects it has been stated that after 5 years of oral BPs or 3 years of intravenous BPs a reassessment of risk to consider a treatment change should be taken.[26]

1.3.1.2 Denosumab

Denosumab is a human monoclonal antibody (IgG2) that binds and neutralizes RANKL preventing the interaction with its receptor, RANK, present on the surface of osteoclasts and their precursors. Thus, neutralizing RANKL would prevent the recruitment and activation of osteoclasts, decreasing bone resorption in trabecular and cortical bone (Figure 1.5).[27] The half-life denosumab in plasma is 26 days but its effect lasts for around 6 months. This would permit denosumab to be administrated as a subcutaneous injection every 6 months. However, the main drawback of this treatment is the temporally bone formation. Since osteoblast activity and bone formation are dependent on factors released from the osteoclasts and the bone during resorption, the bone formation increased during denosumab treatment will be secondarily reduced at certain point.[26]

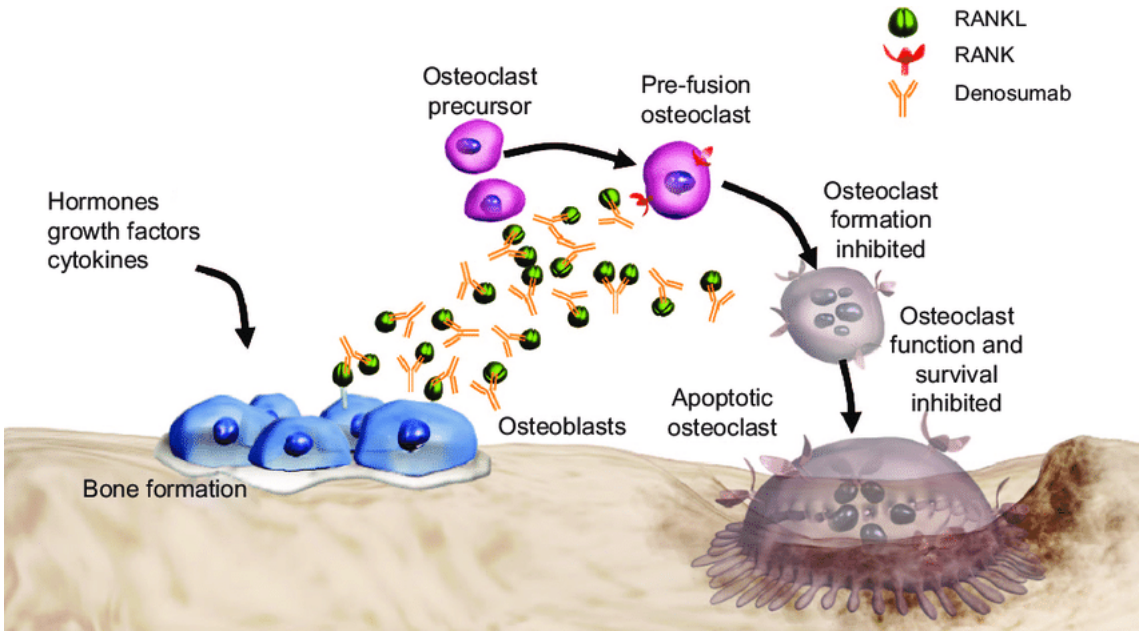

Figure 1.5 Mechanism of action of Denosumab. Reproduced from Ref 27 with the permission from SAGE journals.[27]

The "Fracture REduction Evaluation of Denosumab in Osteoporosis every 6 Months" (FREEDOM) trial showed the efficacy of denosumab on fracture-risk reduction at different skeletal sites among osteoporotic women.[28] This study demonstrated reductions in bone turnover and increases in bone mineral density that were significantly different from placebo. The study continued for 10 years, and bone mineral density continued to increase unlike observed in patients treated with BPs.[29] The effect of the drug is seen within 24 hours of subcutaneous injection and lasts approximately 6 months, hence, the every-6-month dosing schedule. Unlike BPs, the effect of this drug on bone density seems to be progressive for 8 years of use, which suggests that, in addition to antiresorptive qualities, there may be an associated anabolic component.

Denosumab is generally well tolerated, as it has been demonstrated in several trials. The most commonly reported adverse effects are musculoskeletal pain, hypercholesterolemia and cystitis. Similarly to bisphosphates treatment, osteonecrosis of the jaw and atypical femoral fracture are very rare side effects. As a member of the tumor necrosis factor family, RANKL is also expressed in T lymphocytes, B cells and dendritic cells, so its inhibition by denosumab may increase the risk of infection due to an impaired immunity.

1.3.1.3 Estrogen Replacement

Due to the important role of estrogen deficiency on bone loss during menopause, the use of estrogen replacement therapy or estrogen-progestin (hormone) replacement therapy could be effective for prevention of osteoporosis in postmenopausal women.[30] In this sense, the main effect of estrogen on bone tissue is reducing bone resorption by inducing osteoclast apoptosis. However, an anabolic effect has also been shown in estrogen replacement therapy and hormone replacement therapy, with an increased bone density in both the spine and hip.[31] In addition, they reduce the risk of hip, spine and other fractures and also relieve menopausal symptoms in postmenopausal women.[32] However, treatment of osteoporotic women with estrogen replacement therapy to prevent fracture has been controversial, since several side effects have been reported. The Women's Health Initiative trial on estrogen replacement therapy was the first large-scale, randomized, controlled study of healthy women aged 50-79 years. The results of this study showed that there was 34% risk reduction for hip and vertebral fractures and also by the end of the study the incidence of osteoporotic fractures was reduced by 24%. However, estrogen therapy has long-term side-effects including vascular events and breast cancer which limit its widespread use.[33]

1.3.1.4 Selective Estrogen receptor modulators

Due to the adverse effects of estrogen in extra-skeletal organs, such as breast cancer or vascular affections, selective estrogen receptor modulators (SERMs) have been considered for treating osteoporosis avoiding this off-target effects. SERMs contain nonsteroidal synthetic compounds

with similar effects of estrogen on bone and cardiovascular system without any adverse effects on breast and endometrium. Therefore, SERMs would selectively agonize (bone and cardiovascular receptors) or antagonize (breast and endometrium receptors) estrogen receptors in a tissue-selective manner. In this sense, raloxifene is a Food and Drug Administration (FDA)-approved second-generation oral SERM that has estrogenic actions on bone and anti-estrogenic actions on the uterus and breast.[3] Raloxifene is useful for reducing vertebral fracture risk because it increases BMD and reduces bone turnover. However, raloxifene presents several side effects including hot flashes and leg cramps that may lead to formation of serious blood clots in the legs, lungs or even eyes (less common). Also, it is important to consider that raloxifene is teratogenic and should not be used during pregnancy.[34] Therefore, the use of raloxifene in the prevention of osteoporosis should be avoided.

1.3.1.5 Calcitonin

Another antiresorptive agent approved for the treatment of osteoporosis is calcitonin. It acts like the endogenous form of the hormone on the calcitonin receptor of osteoclasts decreasing their activity. Among all recombinant or synthetic calcitonin that have been used for medical purposes, the salmon calcitonin preparation is the most widely used.[35] It is considered as a second-line therapy for osteoporosis in cases where first-line drugs have failed to response or in patients which are found intolerable to other first-line drugs. This could be related to its less effectiveness than other agents such as BPs and an increased risk of cancer by its long-term use. The adverse effects include nausea, vomiting, allergic reactions, hypocalcemia, and prostate cancer among others.[36]

1.3.2 Anabolic Drugs

Anti-resorptive therapy cannot fully restore the lost bone mass and structure. Instead, anabolic agents have the capacity to increase bone mass to a greater degree than antiresorptive agents. They significantly stimulate bone formation which leads to an altered balance between bone formation and resorption with a higher rate of bone turnover. Consequently, the administration of anabolic agents leads to an increased BMD, preserving or improving bone structure, rising bone strength and reducing fracture risk. In addition, they ameliorate bone quality by affecting microarchitectural features such as connectivity, density and geometric features. In order to avoid a life treatment for the patient and since stopping the treatment with these agents would lead to rapid bone loss within six months, patients are usually switched to long-acting BPs or other antiresorptive agents to consolidate the BMD gained during treatment.[9] Therefore, a combination or sequential treatment in osteoporosis has been considered.

1.3.2.1 Parathyroid Hormone

The Parathyroid Hormone also called parathormone, is the main responsible hormone for serum calcium concentration. It is a polypeptide formed by 84 amino acids (PTH (1-84)). This hormone

was the first anabolic agent to be approved. PTH related protein (PTHrP) is another hormone from the same family as PTH with similar effects. They stimulate osteoblast function by binding to a specific receptor, PTH/PTHrP type 1 receptor, and activating several signaling pathways, including the canonical Wnt signaling pathway. However, PTH and PTHrP stimulate not only bone formation but also bone resorption.[37]

The response generated by PTH depends on the nature of the stimulation. It is known that sustained activation of the receptor increases bone resorption, whereas intermittent activation primarily increases bone formation.[26] The PTH/PTHrP type 1 receptor has two different conformations termed R_0 and R_G. Ligands that bind efficiently to the R_0 lead to a prolonged duration of the effect, whereas short duration responses are seen with ligands that bind more selectively to the R_G conformation.[37] The activation of bone resorption by PTH and PTHrP has motivated the research of novel analogs exhibiting "pure" bone anabolism.[9] Several amino-terminal fragments of PTH have been evaluated as potential anabolic drugs. Among them, PTH (1-34), named teriparatide, has been widely used for osteoporosis treatment. Also, different N-terminal PTHrP peptides analogues, such as abaloparatide also bind to the PTH/PTHrP type 1 receptor as PTH.[38] Abaloparatide is a 34-amino acid synthetic analog of PTHrP with 20 identical amino acids to the hormone. These differences were intentionally designed to maximize the stability and anabolic activity of abaloparatide.[25] Therefore, whereas continuous exposure to PTH or PTHrP results in increased bone resorption, intermittent administration of PTH (1-34) or analogue PTHrP (1-34) leads to an anabolic window and enhanced bone formation. The C-terminal fragment of PTHrP (107−111) (osteostatin) has been found to be an important osteoclast inhibitor while inducing osteogenic features *in vitro* and bone regeneration *in vivo*.[39–42]

Teriparatide

Teriparatide is a recombinant human PTH analogue corresponding to the first 34 amino acids of the N-terminal PTH (Figure 1.6). When is administrated by daily subcutaneous injections, it promotes bone anabolism. It is considered a powerful bone forming drug since its action is mainly focused on osteoblast activations and differentiation. Teriparatide increases cancellous and cortical bone formation mainly at sites undergoing active bone remodeling.[26]

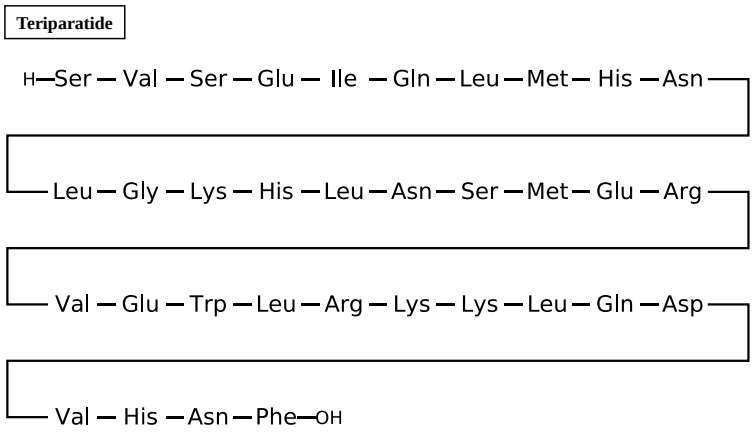

Figure 1.6 Teriparatide amino acid sequence.

Teriparatide should be used as second-line treatment because of certain side-effects below described. Consequently, its major indication is for use in postmenopausal women and men with osteoporosis only at a high risk of fracture. Specifically, it should be used in patients with multiple risk factors for fracture (such as age, previous fractures, glucocorticoid therapy, smoking and alcohol intake, among others), those with very low bone density (T-scores lower than -3.0) or for patients to whom other therapies have failed or are intolerant to other available osteoporosis therapy.[43]

Some side effects of teriparatide include headache, nausea, limb pain and it should be avoided in patients that have increased risks of osteosarcoma. Furthermore, it presents several contraindications including primary and tertiary hyperparathyroidism, pregnancy, lactation, end-organ failure and metastatic skeletal malignancy.[3]

Abaloparatide

Abaloparatide is a 34-amino acid synthetic analogue of PTHrP, which is different to PTHrP in 20 amino acids (Figure 1.7). It is an anabolic treatment that increases BMD at both cortical and trabecular sites and seems to be superior to teriparatide in preventing fracture, although it has been approved only by the FDA.

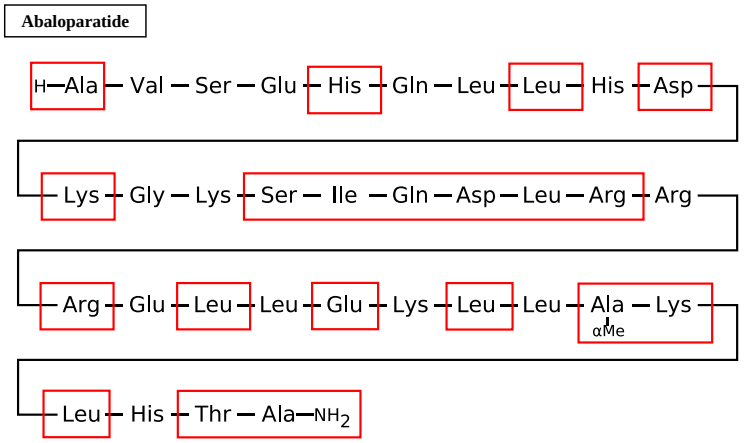

Figure 1.7 Abaloparatide amino acid sequence. Red squares indicate different amino acids compared to Teriparatide.

Abaloparatide has been observed to induce bone formation with a less stimulation of bone resorption than teriparatide. This effect may be due to a higher affinity for the R_G conformation and thus a short activation period.[26] The effect of abaloparatide in comparison with teriparatide and placebo was investigated in postmenopausal women with osteoporosis in the Abaloparatide Comparator Trial In Vertebral Endpoints (ACTIVE) trial.[44] Abaloparatide increased BMD more than placebo at all sites and it conferred a greater increase in BMD at the total hip and femoral neck when compared to teriparatide. Treatment with abaloparatide also reduced the risk of vertebral and non-vertebral fractures, and the incidence of hypercalcemia was lower in women treated with abaloparatide than in women treated with teriparatide.

Side effects of abaloparatide includes nausea, dizziness, headache and palpitations, which were observed more frequently in women treated with abaloparatide than teriparatide.[44] Similarly to teriparatide, there is a dose-dependent increased incidence of osteosarcoma in abaloparatide treated rats. Thus, lifetime treatment with abaloparatide is limited to 18–24 months.[45]

1.3.2.2 Bone Morphogenic Proteins

Among all the bioactive factors related with bone functions, BMPs have been considered really important for bone repair and regeneration. More than 40 members of the BMP group have been identified.[46] They are implicated in skeletal development, in fracture healing processes and in bone formation during modeling and remodeling as key agents in osteoblastic differentiation. Recent evidence implicates them also with the cells of the osteoclastic lineage.[46] Their main action is to promote the differentiation of committed stromal cells into mature osteoblasts.[46–48] Out of the BMP family members, BMP-2 and BMP-7 are the most studied in the context of osteoporosis.[46] Whereas BMP-7 upregulates alkaline phosphatase (ALP) activity and increases mineralization though osteoblast differentiation rise, BMP-2 has osteoinductive characteristics improving fracture healing.[11]

Unfortunately, BMPs signaling takes place in many tissues presenting several off-target effects. They are also mitogenic and have a short half-life which limit their use for treatment of systemic osteoporosis.[9]

1.3.3 New Therapeutic Approaches

While these conventional drugs are effective, they present some limitations and side effects which restrict their long-term administration and adherence. Recognition of signaling pathway targets has led to the development of new antiosteoporotic agents. The research on these targets is in constant progression, and this thesis would discuss some examples of these new therapeutic approaches.

1.3.3.1 Cathepsin K inhibitors

Cathepsin K is a cysteine protease which is selectively expressed by osteoclasts. It is mainly responsible for the degradation of bone matrix during bone resorption phase. Cathepsin K inhibitors have been developed to block the action of this enzyme and limit bone resorption.[49] They target the resorption process itself, presenting a lower effect on osteoclast–osteoblast interaction than the available antiresorptive agents. Therefore, they might not interfere with osteoclast stimulation of bone formation.[49] In fact, when cathepsin K is absent or inhibited in mice, rabbits, or monkeys, bone formation is maintained or increased.[49] In humans, inhibition of cathepsin K is associated with sustained reductions in bone resorption markers.

Since Cathepsin K inhibitors do not bind specifically or are not sequestered into bone, they show pharmacokinetics that are substantially different from other bone resorption inhibitors, such as BPs and denosumab.[50] This non-selectivity produces several side effects, mainly skin reactions. New generation of cathepsin K inhibitors have been produced with more selective capabilities, such as odanacatib, which has reduced the potential for adverse events and drug–drug interactions.[50] The beneficial effects of odanacatib as a selective cathepsin k inhibitor on BMD were reported to be dose dependent and persist up to 5 years after treatment. In addition, its fracture risk reduction effect is comparable with the effects of BPs and denosumab on similar bone sites.[24,51,52]

1.3.3.2 Anti-Sclerostin antibodies

Wnt/β-catenin is a major signaling pathway that regulates bone development and remodeling. Wnt ligands normally bind to LRP5/6 and Frizzled co-receptors at the cell surface. This binding would cause transduction of a signal that would stimulate the activation and accumulation of intracellular β-catenins. These molecules would translocate to the nucleus and would stimulate transcription of target genes in osteoblasts.

This pathway is inhibited by different molecules such as the protein sclerostin or DKK1 inhibitors, leading to reduced osteoblast proliferation, differentiation, and survival. Sclerostin (encoded by SOST) binds to the first propeller domain of the LRP5/6 receptor, inhibiting the formation of the LRP5/6–Frizzled co-receptor complex, which results in inhibition of the Wnt-signaling pathway (Figure 1.8).[14,16] This protein is produced by osteocytes at a late stage in their differentiation, once the surrounding matrix mineralization has already began.

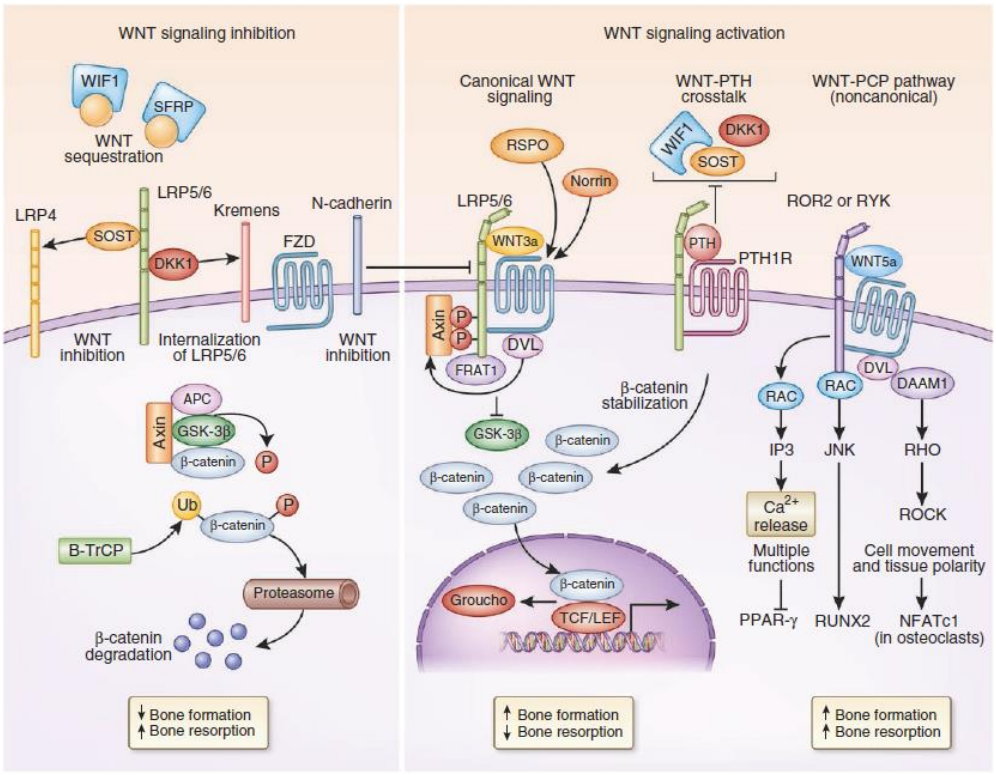

Figure 1.8 Wnt signaling: a simplified view. In the absence of Wnt or the action of either SOST or DKK1 inhibitors, bone formation is suppressed and bone resorption stimulated. Reproduced from Ref 16 with permission from Nature Medicine.

Several types of sclerostin blocking monoclonal antibodies have been developed for osteoporosis treatment. They would act as anabolic drugs blocking the activity of sclerostin and increasing osteoblast differentiation.[53] Romosozumab is a humanized antibody against sclerostin that is administrated as monthly subcutaneous injections. A single dose of romosozumab caused a dose-dependent increase in bone formation markers and a dose-dependent decrease in bone resorption ones. A dose-dependent increase in BMD was seen after one-month administration.[54]

The most frequently reported adverse effects are increased liver enzymes after first dose, which would be normalized nearly after one month, and injection site reactions. Moreover, these antibodies can cause an immune response, which limits the use of this treatment.[26,54]

1.3.3.3 Strontium Ranelate

Strontium ranelate is an antiresorptive agent for treatment of severe osteoporosis. It is mainly used in postmenopausal women at high risk of vertebral and hip fractures who cannot use or tolerate other pharmacological agents. Although its mechanism of action is unclear, it has been noted a modest antiresorptive effect and a little beneficial response on bone formation. The inhibition of osteoclast function as well as the promotion of osteoblast activity through calcium sensing receptor produced by strontium ralenated resulted in increasing BMD and decreasing fracture risk. In addition, it has been shown that strontium ranelate presents effect on osteoblast

differentiation and proliferation.[47] However, although the replacement of Ca ions in the hydroxy-apatite crystals by strontium leads to a larger apparent increase in BMD, the magnitude of changes observed in BMD is not suggestive of a greater reduction in fracture risk.[36] Therefore, it should be considered to include correction factors in BMD data of the strontium ranelate administrated patients.

The most common reported adverse effects are cardiovascular events, venous thromboembolism, myocardial infarction, gastrointestinal discomfort, and nervous system alterations, such as headache, seizure or memory loss. Due to the cardiovascular events, is recommended that strontium ranelate should only be used to treat severe osteoporosis in postmenopausal women or in men at high risk of fracture. Additional measures, including restrictions in patients with heart or circulatory problems, were also recommended to minimize the heart risks of the medicine.[9,36]

1.3.3.4 Osteostatin

In previous sections, it has been mentioned that intermittent administration of the N-terminal fragment of PTHrP increases cancellous bone volume and cortical thickness, and improves bone strength in osteoporotic patients. However, their side effects and narrow window of treatment lead to a further study of different analogues of PTH. The osteogenic effect of the C-terminal alternative PTHrP analogues for osteoporosis treatment has been under evaluation. *In vitro* and *in vivo* studies indicated that the native C-terminal PTHrP (107–139) fragment can inhibit osteoclastic bone resorption by affecting osteoclastic growth and/or differentiation. This effect has been ascribed to its N-terminal sequence 107–111 (Thr–Arg–Ser–Ala–Trp), called osteostatin (Figure 1.9).[38]

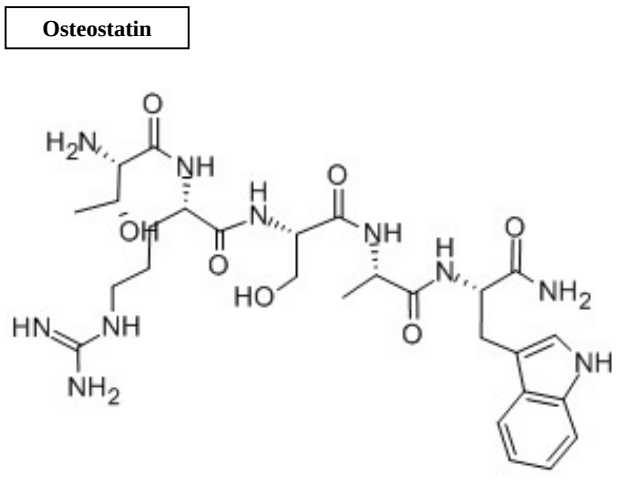

Figure 1.9 Osteostatin molecule structure

It has also been found that osteostatin increases differentiation, proliferation and viability in osteoblastic cells *in vitro* and *in vivo*.[55,56] Finally, it has been proved that osteostatin induce the

recruitment and activation of osteoprogenitors to promote bone regeneration in osteoporotic rabbits. Therefore, osteostatin could be a potential alternative for osteoporosis treatment.[41]

However, since osteostatin is a pentapeptide, is rapidly degraded by proteases in blood circulation, therefore new nanocarrier to deliverer this type of peptides are needed.

1.3.3.5 Gene expression modification therapies

Therapies based on gene expression modification have merged as potential alternative treatments to bone diseases. RNA interference (RNAi) is a natural cellular process that regulates gene expression. It enables the degradation of a specific messenger RNA (mRNA) and, therefore, knockdown specific proteins.[57]

The sequence of the therapeutic small interfering RNA (siRNA) could be identified based on the knowledge of the mRNA sequence that would encode the target protein. According to this, RNAi-based therapies could target genes that have been identified to down-regulate bone formation, leading to an alternative treatment for osteoporosis. In this sense, gene silencing through the delivery of siRNA has gained great attention as a method to increase bone formation.[58,59]

RNAi is mediated by siRNAs as it can be appreciated in Figure 1.10. Once in the cytoplasm, siRNA associates with the RNA-induced silencing complex (RISC). After being loaded inside the complex, the two strands of RNA that form the siRNA will be separated and the sense strand of siRNA will be cleaved and removed from the complex. This would trigger RISC activation, and the antisense sequence then would seek and bind to the complementary mRNA sequence. The catalytic RISC protein, Argonaute endoribonuclease (Ago2), will cleavage the mRNA preventing it from being translated to the corresponding protein (Figure 1.10).[60]

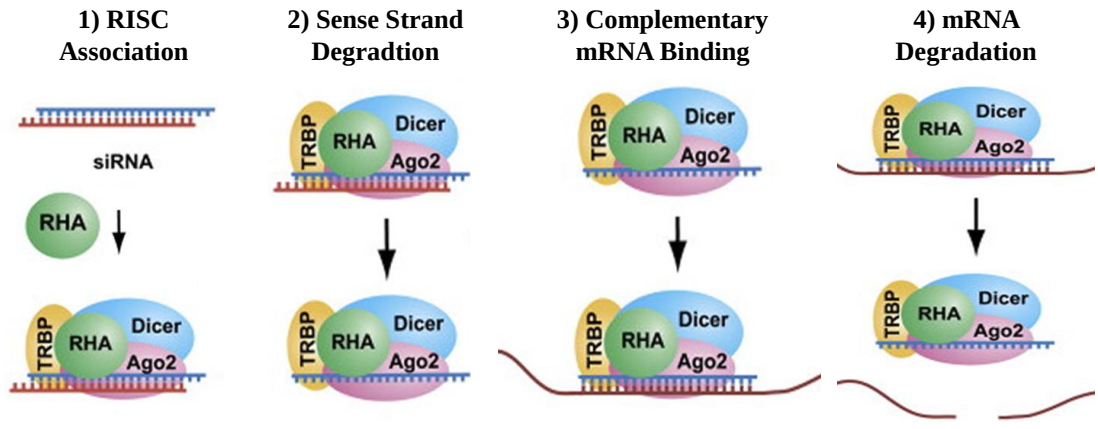

Figure 1.10 Mechanism of RNA interference process. Adapted from Ref 58 with permission from Elsevier.

Since siRNAs have a very short half-life and a poor penetration capacity through cell membranes, the delivery of these molecules has been the major challenge in the application of siRNA therapeutics in humans. This fact has induced the use of vectors to protect and transport siRNAs.[61]

Therefore, the use of siRNAs as therapeutics will begin with (1) the design of the siRNA which targets the mRNA of a protein related with a disease; (2) the incorporation of siRNAs into a delivery vehicle that can efficiently deliver the siRNAs *in vivo*, protecting them from RNases and making possible the penetration inside the cell and (3) the delivery of the siRNA/vehicle complex to the desired tissue/site, where the siRNA can effectively silence the gene and achieve the desired therapeutic response.

1.4 Nanotechnology and Osteoporosis

In the last decades, nanotechnology has been applied to a variety of fields, including medicine. The so-called nanomedicine combines medicine and nanotechnology for diagnosing, treating, and preventing diseases, preserving and improving human health. The nanomedicine has attracted the attention of many researchers, and it is expected to revolutionize the pharmaceutical and biotechnological fields in the near future.[62] Since nanotechnology has offered the possibility of developing particles with the capability of targeting and treating bone diseases, there is a growing interest in the research and development of this field for preventing and treating the consequences of osteoporosis. [63,64]

Conventional osteoporotic treatments that have been reviewed above, present a healing effect far from satisfactory, and their several side effects have limited their application in the clinic. In the last few years, nanoparticles have been found to be promising systems for efficient therapeutic delivery in bone disease therapy. The development of nanoparticles for bone regeneration in osteoporosis patients seems to be ideal since bone itself is a nanocomposite. In addition to this dimensional similarity, they can offer several benefits. First, they can enhance therapeutic delivery and increase tissue specificity, boosting therapy efficiency. They also provide drug protection from biodegradation and improve its pharmacokinetics, pharmacodynamics, biodistribution and targeting, decreasing doses without sacrificing treatment efficacy. Additionally, the nanoparticles would also reduce the exposure of the therapeutic agent to non-target cells, minimizing their potential side effects and improving the life quality of patients.

One of the biggest handicaps of nanoparticles is the rapid uptake by reticuloendothelial system (RES), which is traduced in a low circulation half-life. Incorporating poly(ethylenglycol) to their surface will decrease the uptake by RES so the time in blood stream will increase.[65]

In the frame of nanomedicine, and more specifically in the field of osteoporosis treatment, different nanoparticles have been developed (Figure 1.11).[66] Here, we reviewed some examples of the reported nanoparticles. Attending to their composition, they could be divided into two main groups, organic or inorganic nanoparticles.

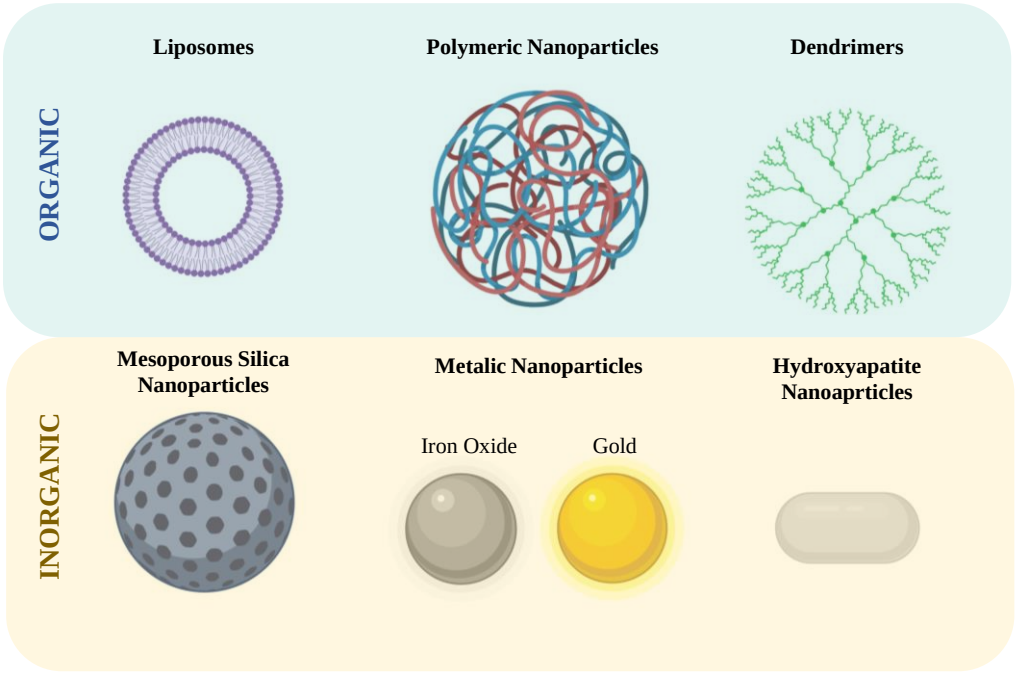

Figure 1.11 Examples of nanoparticles types investigated as delivery nanocarriers for osteoporosis treatment.

1.4.1 Organic Nanoparticles

1.4.1.1 Liposomes

Liposomes are made by the self-assembly of phospholipid molecules (natural or synthetic) with a hydrophilic head group and hydrophobic tail. They rearrange in aqueous environment to yield vesicles containing an aqueous compartment surrounded by a variable number of lipid bilayers. The mechanical properties of liposomes can be tuned using certain additives such as cholesterol. The amphiphilic nature of liposomes permits to load both hydrophilic and hydrophobic drugs in the core and in the lipid bilayer, respectively. Also, due to their biocompatibility and biodegradability, liposomes were the first drug delivery nanosystem to be successfully translated into the clinic.[67] Several examples of osteoporotic drugs loaded in liposomes have been reported. For example, Lu *et al.* reported a system based on ethinlyestradiol loaded liposomes that improved therapeutic effect compared with free drug after one month of treatment. The results obtained showed that BMD value increased *ca.* 38% after liposomes administration compared with a 20% after free drug administration.[68] Other example of lipid nanoparticles for osteoporosis is the work performed by Basha *et al.*[59] In this work they developed SOST siRNA liposomes for the potential stimulation of osteogenesis. This work set the stage for the development of a next-generation siRNA loaded liposome systems that may provide effective strategies for osteoporosis treatment. Also, liposomes were performed to reduce the main drawbacks of bisphosphonates. In this case, Hosny *et al.* formulated nanoliposomes for the encapsulation of alendronate. The new liposome-formula achieved better bioavailability and needed lower dose compared with free drug, avoiding the side effects produced by bisphosphonates.[69]

1.4.1.2 Polymeric Nanoparticles

Polymeric nanoparticles can be synthesized from a wide variety of polymers. Either biodegradable or non-biodegradable polymers can be employed as polymeric source, but synthetic biodegradable polymers as polylactide acid and the copolymer poly(lactide-co-glycolide acid) (PLGA) have been extensively used for the synthesis of nanoparticles.[70] They present excellent biocompatibility, non-toxicity, and tunable degradation rates. Furthermore, PLGA has already been approved by the FDA for its use in drug delivery and diagnostic.[71] Also, chitosan has been widely used as polymer for drug delivery in osteoporosis treatment.[72,73] It presents several interesting properties such as biocompatibility, non-toxicity and biodegradability with ecological safety which make it suitable for nanoparticles development.

Regarding osteoporosis treatment, some examples of polymeric nanoparticles have been reported. A poly(lactide-co-glycolide fumarate) nanoparticle-based system was proposed for BMP-2 delivery by Mercado *et al.*[74] They confirmed an increase osteogenic effect after the delivery of the BMP-2 by the polymeric nanoparticles. Sezlev-Bilecen *et al.* developed a PLGA based nanocapsules for transport and deliver siRNA to bone tissue for the treatment of bone specific diseases such as osteoporosis.[75] Also, Takeuchi *et al.* showed in their work estradiol-loaded PLGA nanoparticles which improved bone mineral density of cancellous bone in an animal model for osteoporosis.[76]

1.4.1.3 Dendrimers

Dendrimers are nano-sized, radially symmetric molecules with well-defined, homogeneous, and monodisperse structure consisting of polymeric tree-like arms or branches. They are monodispersed molecules which contain symmetric branching units around a small molecule or a linear polymer core.[77] The groups presented in the outer surface could also be functionalized, modifying their physicochemical or biological properties. They present diverse advantages that make them a potential macromolecular nanoscale delivery device. Dendritic macromolecules tend to linearly increase in diameter and adopt a more globular shape with increasing dendrimer generation. Therefore, dendrimers have become an ideal delivery vehicle candidate for the evaluation of the effects of polymer size, charge, and composition on biologically relevant properties such as lipid bilayer interactions, cytotoxicity, internalization, blood plasma retention time, biodistribution among others.[77] In the case of osteoporosis treatment, some examples have been reported. Oliveira *et al.* synthesized poly(amidoamine) dendrimers functionalized with biodegradable polymer carboxymethylchitosan and after loaded them with dexamethasone. They confirmed that the combination of the dexamethasone-loaded dendrimer combined with HA enhanced osteogenesis by increasing alkaline phosphatase activity and mineralization of the extra-cellular matrix.[78]

1.4.2 Inorganic Nanoparticles

1.4.2.1 Metal Nanoparticles

The synthesis of novel metal nanoparticles and their application to nanomedicine have increased in the last few years. Iron oxide (Fe_3O_4, Fe_2O_3) nanoparticles are chemically stable, non-toxic, and cost efficient. Coating iron oxide nanoparticles with calcium phosphate nanoparticles helps in increasing bone density and holds promising role in bone regeneration.[79] Thermotherapy has also been attractive for the treatment of osteoporosis. Iron oxide nanoparticles have a high magnetic field that can be used to increase local temperature, and in this way trigger osteoclast regulation. The temperature increment is capable of generating cell death by disrupting cell membranes and denaturing intracellular proteins. It has been used in order to control osteoporosis by destroying osteoclasts through thermolysis.[80] Other metal nanoparticles, such as gold nanoparticles, have been studied for osteoporosis applications. Recent studies reported that gold nanoparticles can promote osteoblast differentiation and inhibit osteoclast differentiation. One example is the work developed by Choi *et al.*, where chitosan-conjugated gold nanoparticles increased the deposition of calcium content and the expression of osteogenic markers differentiation in human adipose-derived mesenchymal stem cells at nontoxic concentrations. These results indicated that chitosan-conjugated gold nanoparticles promoted osteogenesis through the Wnt/β-catenin signaling pathway. Therefore, they could be used as a potential approach for promoting bone formation.[81] Another example of chitosan coated nanoparticles is the work performed by Shi *et al.*[82] In this case, they coated iron oxide nanoparticles with chitosan and it has also been reported to enhance osteoblast proliferation, promoting cell differentiation as indicated by the increase in alkaline phosphatase and extracellular calcium deposition. The effect was attributed to the capability of chitosan to up regulate the expression of bone formation associated genes and to improved osteoblast adhesion by altering the surface chemistry, energy and topography.

1.4.2.2 Hydroxyapatite Nanoparticles

HA is a biomineral, one of the principal constituents of human bones matrix and teeth. HA is biocompatible, biodegradable, and has excellent osteoconductive properties. Early studies demonstrated that nano-sized HA promotes osteoblast bioactivity enhancing bone regeneration.[83,84] In this regard, a nanocarrier based on HA would produce itself bone tissue and increase bone mass deposition. Some studies reported that HA-based nanoparticles loaded with a bisphosphonates increased bone density and improved stiffness and strength of bone in a better way than the administration of the bisphosphonates alone.[85] Other example of HA nanoparticles was reported by Hwang *et al.*[86] They designed HA-based nanoparticles which were coated by a layer-by-layer method with three layers of poly(allylamine) (PAA) and alginate (ALG). Then, at the outmost layer, ALN was conjugated, which conferred the capacity of binding bone tissue to

the nanoparticles. ALN was used as a targeting moiety but also as antiresorptive drug. The HA acted as core for the nanoparticles and when they arrived to the bone matrix, they increased bone density by inducing osteoconduction (Figure1.12).

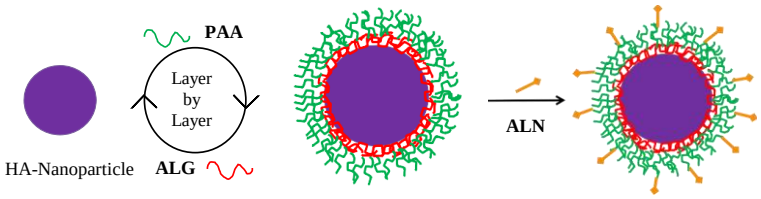

Figure 1.12 Schematic representation of alendronate functionalized hydroxyapatite nanoparticles synthetic process.[66] Adapted from Ref 61 with the permission from AIMS.

HA nanoparticles could also be doped with zinc to improve their therapeutic properties. Zinc enhances bone growth and mineralization by stimulating osteoblast activity and therefore osteogenesis.[87] Khajuria *et al.* chose zinc doped hydroxyapatite (ZnHA) to design their nanoparticles.[88] These ZnHA-based nanoparticles were loaded with risedronate (RIS) and the results demonstrated that the nanoparticles presented a therapeutic advantage over pure RIS or RIS loaded HA nanoparticles.

Several nanoparticles have been proposed as potential alternatives for osteoporosis treatment but still without satisfying results, therefore the investigations in this field are promoted. Table 1.3 includes a summary of the nanoparticles reviewed in this chapter.

Table 1.3 Examples of nanoparticles reported for potential osteoporosis treatment.

Nanoparticle Nature	Type of Nanoaprticle	Loaded Drug	Effect	Ref
Liposomes	Liposome	Ethinlyestradiol	BMD value increased compared with free drug administration	[63]
	Liposomes	SOST siRNA	Potential stimulation of osteogenesis	[64]
	Liposomes	ALN	Reduced the main side effects of ALN administration	[65]
Polymeric Nanoparticles	PLCGF nanoparticles	BMP-2	Increased osteogenic effect	[70]
	PLGA nanocapsules	siRNA	-	[71]
	PLGA nanoparticles	Estradiol	Improved bone mineral density of cancellous bone in animal model	[72]
Dendrimers	Poly(amidoamine) dendrimers	Dex	Enhanced osteogenesis by increasing alkaline phosphatase activity and mineralization of the extra-cellular matrix	[74]
Metal Nanoparticles	Iron oxide nanoparticles	Calcium	Increased bone density and holds promising role in bone regeneration	[75]
	Iron oxide nanoparticles	-	Thermotherapy; cell death, control osteoporosis by destroying osteoclasts	[76]
	Chitosan coated Gold Nanoparticles	-	Increased the deposition of calcium content and the expression of osteogenic markers differentiation	[77]
	Chitosan coated Iron oxide nanoparticles	-	Enhanced osteoblast proliferation, promoted cell differentiation, increased alkaline phosphatase and extracellular calcium deposition	[78]
HA nanoaprticles	HA nanoparticles	-	Promoted osteoblast bioactivity enhancing bone regeneration	[79,80]
	HA nanoparticles	RIS	Increased bone density and improved stiffness and strength of bone	[81]
	PAA and ALG coated HA nanoaprticles	ALN	Increased bone density by inducing osteoconduction	[82]
	Zinc doped HA nanoparticles	RIS	Presented a therapeutic advantage over pure RIS or RIS loaded HA nanoparticles	[84]

1.5 Mesoporous Silica Nanoparticles

Mesoporous silica nanoparticles (MSNs) have attracted research interest in biomedicine since Prof. Vallet-Regí and co-workers reported the use of mesoporous silica materials as drug delivery system back in 2001 for the first time.[89] These materials are characterized by high specific surface area (up to 1500 cm^2/g); high pores volumes (*ca.* 1 cm^3); adjustable pore structures and tunable and narrow pore size distributions (2-30 nm).[90] These properties provide these materials with a high loading capacity, being able to absorb many different types of molecules within their pores. In fact, conventional polymeric nanoparticles usually present low drug capacity, usually less than 5% of total weight, whereas these silica-based mesoporous nanoparticles offer greater values.[91] They have also high silanol density on their surface which allows further modifications for different purposes.

Compared with other types of particles, MSNs present higher robustness due to their silica framework. They are mechanically, thermally and chemically stable, allowing harsh reaction conditions for their modification.

It should be mentioned that silica is recognized as safe by the United States FDA, and it is often used as excipient in drug formulations and as dietary supplement.[92] However, the translation of these type of particles to clinic remains challenging.[93,94] Multiple biomedical applications of MSNs raised in light of their great properties mentioned above, such as controlled drug delivery,[90,95] efficient gene transfection[96] and diagnosis,[97] among others.

1.5.1 Synthesis

The synthesis of MSNs is based on a modification of the Stöber method. By this modification, the addition of surfactants as structure-directing agents results in silica nanoparticles with mesoporosity and excellent physico-chemical properties. This methodology allows obtaining homogenous nanoparticles within the range 50–300 nm. The morphology and dimensions of these surfactant-templated mesoporous silicas can be tailored by controlling the reaction conditions (*e.g.*, pH, temperature, surfactant concentration or silica precursor).[98] The mechanism proposed for the formation of MSNs (Cooperative *Liquid Cristal template*) is showed in Figure 1.13.

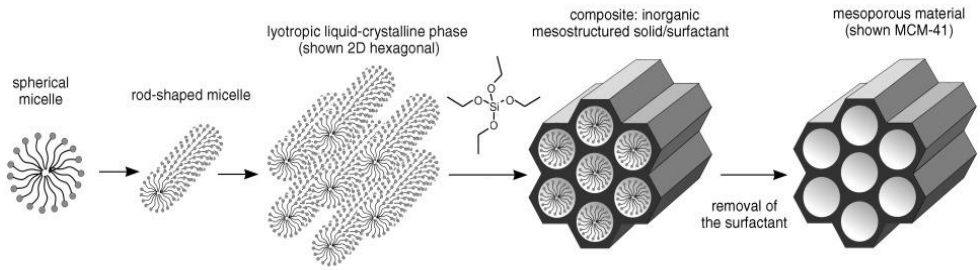

Figure 1.13 Mechanism proposed for the formation of MCM-41 mesoporous materials. The surfactant molecules self-assembly and the silica precursors polymerize around them from the beginning, leading to the formation of a silica backbone with hexagonally ordered pores. Adapted from Ref 99 with permission from Wiley.[99]

The formation of MSNs depends on several factors. The mesostructure would be highly related with the selection of the surfactant (anionic, cationic or neutral) and its concentration. Also, the interactions among the inorganic precursor, the polar head of the surfactant and the ions present in the solution as a function of the synthesis pH could modify the obtained structure of the MSNs.[100]

In the case of MCM-41 mesoporous silica, the inorganic precursor is negatively charged and the polar head positively charged. The polar heads of the surfactant molecules interact with the silica precursors leading to the formation of the silica framework. The hydrolysis, condensation and polymerization of the silica precursors occur from the very beginning, being deposited onto the self-assembled rod-like surfactant micelles and finally arranged, in the case of MCM-41, in a hexagonal fashion. Then, the organic template is removed using a solvent extraction method based on ammonium nitrate solution, generating MSNs with empty mesopores ready to be filled with therapeutic molecules. The organic template could also be removed by other methods like calcination, but this method is usually avoided. It will cause degradation of the present organic moieties and irreversible aggregation of the particles. Furthermore, cytotoxic by-products could be generated from the thermal degradation, limiting their potential application.[101] However, in some cases, the solvent extraction method may cause higher cytotoxicity if surfactant molecules are not completely removed, therefore, several extraction steps are usually needed to remove all the surfactant.[94]

1.5.2 Functionalization

One of the most attractive characteristics of MSNs is their surface with a high density of silanol groups. These chemical groups allow the easy functionalization of the nanoparticles surface, usually using organosilanes which will provide different functionalities (amine, carboxylic acid, thiol, among others), increasing the versatility of the produced nanocarriers. The organosilane employed would tune the interactions between the payload and the silica matrix (porous functionalization) or between the nanoparticles surface and the external medium (surface functionalization).[102] The functionalization can be accomplished through two different approximations: post-synthesis and co-condensation (Figure 1.14).[99]

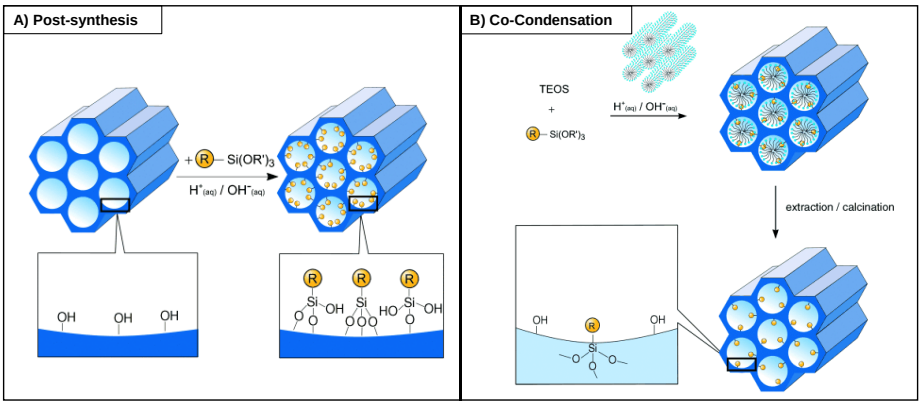

Figure 1.14 Functionalization of MSNs. A) Post-synthesis method. The functional groups are introduced after the synthesis of MSNs. b) Co-condensation method. The functional groups are introduced during the synthesis of the MSNs. Adapted from Ref 99 with permission of Wiley.[99]

The post-synthesis method involves the modification of the surface after the synthesis (Figure 1.14A). This approximation can lead to different groups inside and outside the pores, depending on whether the process is performed before or after removing the template. The co-condensation approach consists in the simultaneous addition of the silica precursor and the functional organosilane during the formation of the particles (Figure 1.14B). This approximation can yield nanoparticles with various functional groups homogenously distributed throughout the silica backbone or biodegradable periodic nanoparticles with labile bonds within the silica framework.[99,103]

The functionalization of the nanoparticles surface would be the key point of these type of nanocarriers. It will allow the modification of the surface charge, the adhesion of targeting ligands, the grafting with polymers, conferring new properties to the synthesized nanoparticle. Functionalization of the external surface is commonly carried out by silylation on free silanol groups.[104] If a high surface coverage with functional groups is desired, it is important to maintain a large amount of surface silanol groups after removal of the surfactant. Therefore, if the surfactant removal is performed by calcination, it will promote condensation of unreacted silanol groups reducing the number of free silanol groups for post-synthesis functionalization. Also, calcination might affect to surface functional groups functionalized by co-condensation during the synthesis process, which will be lost. Thus, as mentioned before, it would be better option the solvent extraction method for the removal of the surfactant.[95]

The main reasons of using nanoparticles as drug delivery carriers are their capacity of (1) maximize the amount of therapeutic loaded, (2) minimize the premature release, and (3) deliver the cargo only in the target tissue. In this sense, the extraordinary textural properties of MSNs empower them with great loading capacities, being able to load huge amounts of therapeutic molecules within their pores, providing a protective shell for the molecules against potential pH or enzymatic-mediated drug degradation in the organism.[90]

The loading of therapeutic molecules within MSNs can be easily accomplished through their open porous structure. However, this also means that the cargo molecules might easily diffuse out of the pores before reaching the target area. A smart approximation to minimize that premature drug release would be the use of gatekeepers, which are structures able to open and close the pore entrances in response to certain stimuli. Several stimuli have been studied in order to develop stimuli-responsive nanocarriers. They can be characteristic of a particular disease or tissue such as, pH,[105] redox,[106] or enzymes,[107] or they can also be externally administrated like ultrasounds,[108] light,[109] magnetic fields,[110] ultraviolet ligth[111] among others. The application of the stimuli will open the pores triggering the release only in the area of interest. The high amount of silanol groups on the surface of MSNs allows the functionalization with different polymers or molecules that can act as gatekeepers.

The surface could be functionalized in order to improve the targeting ability of the nanoparticles. In this sense, the nanoparticles can be functionalized with molecules that would target the tissue of interest, reducing the off-target effects and therefore minimizing the administrated dose needed to achieve the effect desired. For example, in the case of osteoporosis treatment, bone is made mainly by HA, therefore, HA would represent a promising target for selective delivery. Different molecules with high affinity to HA, such as BPs, have been proposed as bone targeting moieties for osteoporosis drug delivery.[86,112]

1.5.3 Mesoporous Silica Nanoparticles and Osteoporosis

In the field of osteoporosis treatment, MSNs have been widely used for delivery of conventional osteoporosis drugs. The first example of mesoporous silica materials (MCM-41 and SBA-15) applied for the controlled release of anti-resorptive molecules (alendronate) were reported by Vallet-Regí and co-workers in 2006.[113] Additionally, SBA-15 matrices were functionalized with phosphorous groups, enhancing the loading and controlled release of alendronate and inducing the formation of an apatite-like layer (typical from a bioactive material), being a promising alternative treatment for osteoporosis.[114] Further examples of anti-resorptive molecules loaded in MSNs are ipriflavone,[115] raloxifene,[116] salmon calcitonin[117] or zolendronic acid.[118] All of them showed promising results inhibiting osteoclast activity and enhancing osteogenesis.

Other great property of mesoporous silica-based nanoparticles is their capacity of loading hydrophobic compounds. Hence, barely soluble anabolic agents could be incorporated within their pores enhancing their bioavailability to induce bone formation. Dexamethasone[119] or estradiol[120] are some examples of molecules loaded inside MSNs increasing the biological functions of osteoblast and therefore inducing bone regeneration.

New alternative treatments for osteoporosis have also been developed using mesoporous silica nanomatrices. In this sense, osteostatin, the C-terminal fragment of parathyroid hormone-related

protein (107-111), was loaded and delivered from mesoporous materials. It was shown that osteostatin-loaded SBA-15 induced osteogenic features while inhibited the osteoclast activity *in vitro*[39,40,56] and stimulated bone regeneration *in vivo*.[55,121] This fact was the first step which led to further investigations of osteostatin delivery from mesoporous silica nanoparticles instead from nanomatrices.

As mentioned before, therapies based on gene expression modification have merged as potential alternative treatments to bone diseases. MSNs have been widely studied as genetic molecules nanocarriers. In this sense, MSNs could be used for the delivery of specific siRNAs related with osteoporosis disease such as RANK siRNA, for the potential reduction of osteoclastogenesis through the knockdown of RANK expression, as it was appreciated by the release of this silencing molecule from different silica-based mesoporous materials.[122]

The mesoporous structure of the nanoparticles also allows the loading of several drugs, and therefore empowers a dual treatment as it would be discussed in chapter 4. Thus, MSNs are useful for the co-delivery of dexamethasone and the BMP-2 to achieve great bone regeneration *in vivo*, through the osteoblast differentiation induced by both therapeutics.[123]

Although a lot of research has been developed to use nanoparticles for the treatment of osteoporosis, the translation from the bench to the bed still constitutes the bottleneck of this field, therefore, further studies and improvements remain necessary.

This doctoral thesis is focused on the application of mesoporous silica nanoparticles as therapeutic drug delivery nanocarriers. We used the nanoparticles for the transport and release of SOST siRNA to the bone tissue cells, and the co-delivery of an osteogenic peptide, osteostatin.

1.6 References

1. Kanis, J. A. *et al.* A reference standard for the description of osteoporosis. *Bone* 42, 467–475 (**2008**).

2. Kanis, J. A. Assessment of fracture risk and its application to screening for postmenopausal osteoporosis: Synopsis of a WHO report. *Osteoporos. Int.* 4, 368–381 (**1994**).

3. Moshiri, A., Sharifi, A. M., Oryan, A. Current knowledge, drug-based therapeutic options and future directions in managing osteoporosis. *Clin. Rev. Bone Miner. Metab.* 15, 1–23 (**2017**).

4. Rachner, T. D., Khosla, S., Hofbauer, L. C. Osteoporosis: now and the future. *Lancet* 377, 1276–1287 (**2011**).

5. Boskey, A. L. Bone composition: relationship to bone fragility and antiosteoporotic drug effects. *Bonekey Rep.* 2, 1–11 (**2013**).

6. Koons, G. L., Diba, M., Mikos, A. G. Materials design for bone-tissue engineering. *Nat. Rev. Mater.* 5, 584–603 (**2020**).

7. Yedavally-Yellayi, S., Ho, A. M., Patalinghug, E. M. Update on Osteoporosis. *Prim. Care - Clin. Off. Pract.* 46, 175–190 (**2019**).

8. Langdahl, B., Ferrari, S., Dempster, D. W. Bone modeling and remodeling: potential as therapeutic targets for the treatment of osteoporosis. *Ther. Adv. Musculoskelet. Dis.* 8, 225–235 (**2016**).

9. Íñiguez-Ariza, N. M., Clarke, B. L. Bone biology, signaling pathways, and therapeutic targets for osteoporosis. *Maturitas* 82, 245–255 (**2015**).

10. Raggatt, L. J., Partridge, N. C. Cellular and molecular mechanisms of bone remodeling. *J. Biol. Chem.* 285, 25103–25108 (**2010**).

11. Toosi, S., Behravan, J. Osteogenesis and bone remodeling: A focus on growth factors and bioactive peptides. *BioFactors* 46, 326–340 (**2019**).

12. Boyle, W. J., Simonet, W. S., Lacey, D. L. Osteoclast differentiation and activation. *Nature* 423, 337–342 (**2003**).

13. Wang, Y. *et al.* Wnt and the Wnt signaling pathway in bone development and disease. *Front. Biosci.* 19, 379–407 (**2014**).

14. Baron, R., Kneissel, M. Wnt signaling in bone homeostasis and disease: from human mutations to treatments. *Nat. Med.* 19, 179–192 (**2013**).

15. Moester, M. J. C., Papapoulos, S. E., Löwik, C. W. G. M., Van Bezooijen, R. L. Sclerostin: Current knowledge and future perspectives. *Calcif. Tissue Int.* 87, 99–107 (**2010**).

16. Duan, P., Bonewald, L. F. The role of the wnt/β-catenin signaling pathway in formation and maintenance of bone and teeth. *Int. J. Biochem. Cell Biol.* 77, 23–29 (**2016**).

17. Karsenty, G. Transcriptional control of skeletogenesis. *Annu. Rev. Genomics Hum. Genet.* 9, 183–196 (**2008**).

18. Liu, J., Curtis, E. M., Cooper, C., Harvey, N. C. State of the art in osteoporosis risk assessment and treatment. *J. Endocrinol. Invest.* 42, 1149–1164 (**2019**).

19. Compston, J. E., McClung, M. R., Leslie, W. D. Osteoporosis. *Lancet* 393, 364–376 (**2019**).

20. Gennari, L. *et al.* Emerging therapeutic targets for osteoporosis. *Expert Opin. Ther. Targets* 24, 115–130 (**2020**).

21. Russow, G. *et al.* Anabolic therapies in osteoporosis and bone regeneration. *Int. J. Mol. Sci.* 20, 83 (**2019**).

22. Arcos, D. *et al.* The relevance of biomaterials to the prevention and treatment of osteoporosis. *Acta Biomater.* 10, 1793–1805 (**2014**).

23. Vidal, M., Thibodaux, R. J., Neira, L. F. V., Messina, O. D. Osteoporosis: a clinical and pharmacological update. *Clin. Rheumatol.* 38, 385–395 (**2019**).

24. Appelman-Dijkstra, N. M., Papapoulos, S. E. Novel approaches to the treatment of osteoporosis. *Best Pract. Res. Clin. Endocrinol. Metab.* 28, 843–857 (**2014**).

25. Harslof, T., Langdahl, B. L. New horizons in osteoporosis therapies. *Curr. Opin. Pharmacol.* 28, 38–42 (**2016**).

26. Langdahl, B. L. Overview of treatment approaches to osteoporosis. *Br. J. Pharmacol.* 1, 1–16 (**2020**).

27. Lipton, A., Smith, M. R., Ellis, G. K., Goessl, C. Treatment-induced bone loss and fractures in cancer patients undergoing hormone ablation therapy: efficacy and safety of denosumab. *Clin. Med. Insights. Oncol.* 6, 287–303 (**2012**).

28. Cummings, S. R. *et al.* Denosumab for prevention of practures in postmenopausal women with osteoporosis. *N. Engl. J. Med.* 361, 756–765 (**2009**).

29. Bone, H. G. *et al.* 10 years of denosumab treatment in postmenopausal women with osteoporosis: results from the phase 3 randomised FREEDOM trial and open-label extension. *Lancet Diabetes Endocrinol.* 5, 513–523 (**2017**).

30. Lindsay, R., Hart, D. M., Forrest, C., Baird, C. Prevention of spinal osteoporosis in oophorectomised women. *Lancet* 316, 1151–1154 (**1980**).

31. Gennari, L. *et al.* Appropriate models for novel osteoporosis drug discovery and future perspectives. *Expert Opin. Drug Discov.* 10, 1201–1216 (**2015**).

32. Cauley, J. A. *et al.* Effects of estrogen plus progestin on risk of fracture and bone mineral density the women's health initiative randomized trial. *JAMA* 290, 1729–1738 (**2003**).

33. Stefanick, M. L. Estrogens and progestins: background and history, trends in use, and guidelines and regimens approved by the US Food and Drug Administration. *Am. J. Med.* 118, 64–73 (**2005**).

34. Lee, J.-H. *et al.* Development and evaluation of raloxifene-hydrochloride-loaded supersaturatable SMEDDS containing an acidifier. *Pharmaceutics* 10, 78 (**2018**).

35. Chesnut, C. H. *et al.* Salmon calcitonin: a review of current and future therapeutic indications. *Osteoporos. Int.* 19, 479–491 (**2008**).

36. Tabatabaei-Malazy, O., Salari, P., Khashayar, P., Larijani, B. New horizons in treatment of osteoporosis. *DARU, J. Pharm. Sci.* 25, 1–16 (**2017**).

37. Dean, T., Vilardaga, J.-P., Potts Jr, J. T., Gardella, T. J. Altered selectivity of parathyroid hormone (PTH) and PTH-related protein (PTHrP) for distinct conformations of the PTH/PTHrP receptor. *Mol. Endocrinol.* 22, 156–166 (**2008**).

38. Esbrit, P. *et al.* Parathyroid hormone-related protein analogs as osteoporosis therapies. *Calcified Tissue International*. 98, 359–369 (**2016**).

39. Cornish, J. *et al.* Stimulation of osteoblast proliferation by C-terminal fragments of parathyroid hormone-related protein. *J. Bone Miner. Res.* 14, 915–922 (**1999**).

40. Fenton, A. J. *et al.* A Carboxyl-Terminal peptide from the parathyroid hormone-related protein inhibits bone resorption by osteoclasts. *Endocrinology* 129, 1762–1768 (**1991**).

41. Lozano, D. *et al.* Parathyroid hormone-related protein (107-111) improves the bone regeneration potential of gelatin – glutaraldehyde biopolymer-coated hydroxyapatite. *Acta Biomater.* 10, 3307–3316 (**2014**).

42. Rihani-Basharat, S., Lewinson, D. PTHrP(107-111) inhibits in vivo resorption that was stimulated by PTHrP(1-34) when applied intermittently to neonatal mice. *Calcif. Tissue Int.* 61, 426–428 (**1997**).

43. Meier, C. *et al.* The role of teriparatide in sequential and combination therapy of osteoporosis. *Swiss Med. Wkly.* 144, w13952 (**2014**).

44. Miller, P. D. *et al.* Effect of Abaloparatide vs placebo on new vertebral fractures in postmenopausal women with osteoporosis. *JAMA* 316, 722 (**2016**).

45. Jolette, J. *et al.* Comparing the incidence of bone tumors in rats chronically exposed to the selective PTH type 1 receptor agonist abaloparatide or PTH(1–34). *Regul. Toxicol. Pharmacol.* 86, 356–365 (**2017**).

46. Kanakaris, N. K., Petsatodis, G., Tagil, M., Giannoudis, P. V. Is there a role for bone morphogenetic proteins in osteoporotic fractures? *Injury* 40, S21–S26 (**2009**).

47. Yamaguchi, M., Neale Weitzmann, M. The intact strontium ranelate complex stimulates osteoblastogenesis and suppresses osteoclastogenesis by antagonizing NF-κB activation. *Mol. Cell. Biochem.* 359, 399–407 (**2012**).

48. Canalis, E. Update in new anabolic therapies for osteoporosis. *J. Clin. Endocrinol. Metab.* 95, 1496–1504 (**2010**).

49. Boonen, S. *et al.* Inhibition of cathepsin K for treatment of osteoporosis. *Curr. Osteoporos. Rep.* 10, 73–79 (**2012**).

50. Costa, A. G. *et al.* Cathepsin K: Its skeletal actions and role as a therapeutic target in osteoporosis. *Nat. Rev. Rheumatol.* 7, 447–456 (**2011**).

51. Deal, C. Potential new drug targets for osteoporosis. *Nat. Clin. Pract. Rheumatol.* 5, 20–27 (**2009**).

52. Stoch, S. A., Wagner, J. A. Cathepsin K inhibitors: A novel target for osteoporosis therapy. *Clin. Pharmacol. Ther.* 83, 172–176 (**2008**).

53. Suen, P. K., Qin, L. Sclerostin, an emerging therapeutic target for treating osteoporosis and osteoporotic fracture: A general review. *J. Orthop. Transl.* 4, 1–13 (**2016**).

54. Haas, A. V, LeBoff, M. S. Osteoanabolic Agents for Osteoporosis. *J. Endocr. Soc.* 2, 922–932 (**2018**).

55. Lozano, D. *et al.* The C-terminal fragment of parathyroid hormone-related peptide promotes bone formation in diabetic mice with low-turnover osteopaenia. *Br. J. Pharmacol.* 162, 1424–1438 (**2011**).

56. Lozano, D. *et al.* Osteostatin-loaded bioceramics stimulate osteoblastic growth and differentiation. *Acta Biomater.* 6, 797–803 (**2010**).

57. Weng, Y. *et al.* RNAi therapeutic and its innovative biotechnological evolution. *Biotechnol. Adv.* 37, 801–825 (**2019**).

58. Mora-Raimundo, P., Lozano, D., Manzano, M., Vallet-Regí, M. Nanoparticles to Knockdown Osteoporosis-Related Gene and Promote Osteogenic Marker Expression for Osteoporosis Treatment. *ACS Nano* 13, 5451–5464 (**2019**).

59. Basha, G. *et al.* Lipid nanoparticle delivery of siRNA to osteocytes leads to effective silencing of SOST and inhibition of sclerostin in vivo. *Mol. Ther. Nucleic Acids* 5, 1–15 (**2016**).

60. Saw, P. E., Song, E.-W. siRNA therapeutics: a clinical reality. *Sci. China Life Sci.* 63, 485–500 (**2020**).

61. Dong, Y., Siegwart, D. J., Anderson, D. G. Strategies, design, and chemistry in siRNA delivery systems. *Adv. Drug Deliv. Rev.* 144, 133–147 (**2019**).

62. Tibbitt, M. W., Dahlman, J. E., Langer, R. Emerging Frontiers in Drug Delivery. *J. Am. Chem. Soc.* 138, 704–717 (**2016**).

63. Gao, C. *et al.* Nanotechnology for treating osteoporotic vertebral fractures. *Int. J. Nanomedicine* 10, 5139–5157 (**2015**).

64. Wei, D. *et al.* Nanotechnology Treatment Options for Osteoporosis and Its Corresponding Consequences. *Curr. Osteoporos. Rep.* 14, 239–247 (**2016**).

65. La-Beck, N. M. *et al.* Factors affecting the pharmacokinetics of pegylated liposomal doxorubicin in patients. *Cancer Chemother. Pharmacol.* 69, 43–50 (**2012**).

66. Mora-Raimundo, P., Manzano, M., Vallet-Regí, M. Nanoparticles for the treatment of osteoporosis. *AIMS Bioeng.* 4, 259–274 (**2017**).

67. Allen, T. M., Cullis, P. R. Liposomal drug delivery systems: From concept to clinical applications. *Adv. Drug Deliv. Rev.* 65, 36–48 (**2013**).

68. Lu, T. *et al.* Ethinylestradiol liposome preparation and its effects on ovariectomized rats' osteoporosis. *Drug Deliv* 18, 468–477 (**2011**).

69. Hosny, K. M., Ahmed, O. A. A., Al-Abdali, R. T. Enteric-coated alendronate sodium nanoliposomes: a novel formula to overcome barriers for the treatment of osteoporosis. *Expert Opin. Drug Deliv.* 10, 741–746 (**2013**).

70. Zhang, L., Webster, T. J. Nanotechnology and nanomaterials: Promises for improved tissue regeneration. *Nano Today* 4, 66–80 (**2009**).

71. Danhier, F. *et al.* PLGA-based nanoparticles: An overview of biomedical applications. *J. Control. Release* 161, 505–522 (**2012**).

72. Saini, D. *et al.* Formulation, development and optimization of raloxifene-loaded chitosan nanoparticles for treatment of osteoporosis. *Drug Deliv.* 7544, 1–14 (**2014**).

73. Narayanan, D., Anitha, A., Jayakumar, R., Chennazhi, K. P. In vitro and in vivo evaluation of osteoporosis therapeutic peptide PTH 1–34 loaded PEGylated chitosan nanoparticles. *Mol. Pharm.* 10, 4159–4167 (**2013**).

74. Mercado, A. E., Ma, J., He, X., Jabbari, E. Release characteristics and osteogenic activity of recombinant human bone morphogenetic protein-2 grafted to novel self-assembled poly(lactide-co-glycolide fumarate) nanoparticles. *J. Control. Release* 140, 148–156 (**2009**).

75. Sezlev Bilecen, D., Rodriguez-Cabello, J. C., Uludag, H., Hasirci, V. Construction of a PLGA based, targeted siRNA delivery system for treatment of osteoporosis. *J. Biomater. Sci. Polym. Ed.* 28, 1859–1873 (**2017**).

76. Takeuchi, I., Kobayashi, S., Hida, Y., Makino, K. Estradiol-loaded PLGA nanoparticles for improving low bone mineral density of cancellous bone caused by osteoporosis: Application of enhanced charged nanoparticles with iontophoresis. *Colloids Surf. B. Biointerfaces* 155, 35–40 (**2017**).

77. Abbasi, E. *et al.* Dendrimers: synthesis, applications, and properties. *Nanoscale Res. Lett.* 9, 247 (**2014**).

78. Oliveira, J. M. *et al.* The osteogenic differentiation of rat bone marrow stromal cells cultured with dexamethasone-loaded carboxymethylchitosan/poly(amidoamine) dendrimer nanoparticles. *Biomaterials* 30, 804–813 (**2009**).

79. Levingstone, T. J., Herbaj, S., Dunne, N. J. Calcium Phosphate Nanoparticles for Therapeutic Applications in Bone Regeneration. *Nanomater.* 9, 1570 (**2019**).

80. Lee, M. S. *et al.* Synthesis of composite magnetic nanoparticles Fe_3O_4 with alendronate for osteoporosis treatment. *Int. J. Nanomedicine*. 11, 4583–4594 (**2016**).

81. Lee, S. Y. *et al.* Gold nanoparticles promote osteogenic differentiation in human adipose-derived mesenchymal stem cells through the Wnt/β-catenin signaling pathway. *Int. J. Nanomedicine* 10, 4383–4392 (**2015**).

82. Shi, S.-F. *et al.* Biocompatibility of chitosan-coated iron oxide nanoparticles with osteoblast cells. *Int. J. Nanomedicine* 7, 5593–5602 (**2012**).

83. Webster, T. J. *et al.* Enhanced functions of osteoblasts on nanophase ceramics. *Biomaterials* 21, 1803–1810 (**2000**).

84. Lin, L., Chow, K. L., Leng, Y. Study of hydroxyapatite osteoinductivity with an osteogenic differentiation of mesenchymal stem cells. *J. Biomed. Mater. Res. - Part A* 89, 326–335 (**2009**).

85. Sahana, H. *et al.* Improvement in bone properties by using risedronate adsorbed hydroxyapatite novel nanoparticle based formulation in a rat model of osteoporosis. *J. Biomed. Nanotechnol.* 9, 193–201 (**2013**).

86. Hwang, S.-J. *et al.* Alendronate-modified hydroxyapatite nanoparticles for bone-specific dual delivery of drug and bone mineral. *Macromol. Res.* 24, 623–628 (**2016**).

87. Ito, A. *et al.* Zinc-containing tricalcium phosphate and related materials for promoting bone formation. *Curr. Appl. Phys.* 5, 402–406 (**2005**).

88. Khajuria, D. K. *et al.* Risedronate/zinc-hydroxyapatite based nanomedicine for osteoporosis. *Mater. Sci. Eng. C* 63, 78–87 (**2016**).

89. Vallet-Regí, M., Rámila, A., Del Real, R. P., Pérez-Pariente, J. A new property of MCM-41: Drug delivery system. *Chem. Mater.* 13, 308–311 (**2001**).

90. Manzano, M., Vallet-Regí, M. Mesoporous silica nanoparticles in nanomedicine applications. *J. Mater. Sci. Mater. Med.* 29, (**2018**).

91. Douroumis, D., Onyesom, I., Maniruzzaman, M., Mitchell, J. Mesoporous silica nanoparticles in nanotechnology. *Crit. Rev. Biotechnol.* 33, 229–245 (**2013**).

92. Zhou, Y. *et al.* Mesoporous silica nanoparticles for drug and gene delivery. *Acta Pharm. Sin. B* 8, 165–177 (**2018**).

93. Narayan, R., Nayak, U. Y., Raichur, A. M., Garg, S. Mesoporous silica nanoparticles: a comprehensive review on synthesis and recent advances. *Pharmaceutics* 10, 118 (**2018**).

94. Möller, K., Bein, T. Talented Mesoporous Silica Nanoparticles. *Chem. Mater.* 29, 371–388 (**2017**).

95. Slowing, I. I., Vivero-Escoto, J. L., Wu, C.-W. Mesoporous silica nanoparticles as controlled release drug delivery and gene transfection carriers. *Adv. Drug Deliv. Rev.* 60, 1278–1288 (**2008**).

96. Paris, J. L. *et al.* Suicide-gene transfection of tumor-tropic placental stem cells employing ultrasound-responsive nanoparticles. *Acta Biomater.* 83, 372–378 (**2019**).

97. Simmchen, J. *et al.* Asymmetric hybrid silica nanomotors for capture and cargo transport: Towards a novel motion-based DNA sensor. *Small* 8, 2053–2059 (**2012**).

98. Wu, S.-H., Mou, C.-Y., Lin, H.-P. Synthesis of mesoporous silica nanoparticles. *Chem. Soc. Rev.* 42, 3862–3875 (**2013**).

99. Hoffmann, F., Cornelius, M., Morell, J., Fröba, M. Silica-based mesoporous organic-inorganic hybrid materials. *Angew. Chemie - Int. Ed.* 45, 3216–3251 (**2006**).

100. Huo, Q. *et al.* Generalized synthesis of periodic surfactant/inorganic composite materials. *Nature* 368, 317–321 (**1994**).

101. Kecht, J., Bein, T. Oxidative removal of template molecules and organic functionalities in mesoporous silica nanoparticles by H_2O_2 treatment. *Microporous Mesoporous Mater.* 116, 123–130 (**2008**).

102. Wang, G. *et al.* Functionalized mesoporous materials for adsorption and release of different drug molecules: A comparative study. *J. Solid State Chem.* 182, 1649–1660 (**2009**).

103. Croissant, J. *et al.* Biodegradable Ethylene-Bis(Propyl)Disulfide-Based Periodic Mesoporous Organosilica Nanorods and Nanospheres for Efficient In-Vitro Drug Delivery. *Adv. Mater.* 26, 6174–6180 (**2014**).

104. Slowing, I. I. *et al.* Effect of surface functionalization of MCM-41-type mesoporous silica nanoparticles on the endocytosis by human cancer cells. *J Am Chem Soc* 128, 14792–14793 (**2006**).

105. Gisbert-Garzarán, M., Lozano, D., Vallet-Regí, M., Manzano, M. Self-immolative polymers as novel pH-responsive gate keepers for drug delivery. *RSC Adv.* 7, 132–136 (**2017**).

106. Guo, X. *et al.* Advances in redox-responsive drug delivery systems of tumor microenvironment. *J. Nanobiotechnology* 16, 74 (**2018**).

107. de la Torre, C. *et al.* Cathepsin-B Induced Controlled Release from Peptide-Capped Mesoporous Silica Nanoparticles. *Chem. - A Eur. J.* 20, 15309–15314 (**2014**).

108. Paris, J. L., Cabañas, M. V., Manzano, M., Vallet-Regí, M. Polymer-grafted mesoporous silica nanoparticles as ultrasound-responsive drug carriers. *ACS Nano* 9, 11023–11033 (**2015**).

109. Martínez-Carmona, M. *et al.* A novel visible light responsive nanosystem for cancer treatment. *Nanoscale* 9, 15967–15973 (**2017**).

110. Guisasola, E. *et al.* Magnetic-responsive release controlled by hot spot effect. *Langmuir* 31, 12777–12782 (**2015**).

111. Martínez-Carmona, M. *et al.* Mesoporous silica nanoparticles grafted with a light-responsive protein shell for highly cytotoxic antitumoral therapy. *J. Mater. Chem. B* 3, 5746–5752 (**2015**).

112. Cenni, E. *et al.* The effect of poly(D,L-lactide-co-glycolide)-alendronate conjugate nanoparticles on human osteoclast precursors. *J. Biomater. Sci. Polym. Ed.* 23, 1285–1300 (**2012**).

113. Balas, F., Manzano, M., Horcajada, P., Vallet-Regí, M. Confinement and controlled release of bisphosphonates on ordered mesoporous silica-based materials. *J. Am. Chem. Soc.* 128, 8116–8117 (**2006**).

114. Colilla, M., Izquierdo-Barba, I., Vallet-Regí, M. Phosphorus-containing SBA-15 materials as bisphosphonate carriers for osteoporosis treatment. *Microporous Mesoporous Mater.* 135, 51–59 (**2010**).

115. Casarrubios, L. *et al.* Incorporation and effects of mesoporous SiO_2-CaO nanospheres loaded with ipriflavone on osteoblast/osteoclast cocultures. *Eur. J. Pharm. Biopharm.* 133, 258–268 (**2018**).

116. Shah, P., Rajput, S. J. Investigation of in vitro permeability and in vivo pharmacokinetic behavior of bare and functionalized MCM-41 and MCM-48 mesoporous silica nanoparticles: a burst and controlled drug release system for raloxifene. *Drug Dev. Ind. Pharm.* 45, 587–602 (**2019**).

117. Yu, P. *et al.* Pentapeptide-decorated silica nanoparticles loading salmon calcitonin for in vivo osteoporosis treatment with sustained hypocalcemic effect. *Mater. Today Chem.* 14, 100189 (**2019**).

118. Zhu, M. *et al.* Mesoporous silica nanoparticles/hydroxyapatite composite coated implants to locally inhibit osteoclastic activity. *ACS Appl. Mater. Interfaces* 6, 5456–5466 (**2014**).

119. Ren, H. *et al.* A traceable and bone-targeted nanoassembly based on defect-related luminescent mesoporous silica for enhanced osteogenic differentiation. *J. Mater. Chem. B* 5, 1585–1593 (**2017**).

120. Hu, Y., Cai, K., Luo, Z., Jandt, K. D. Layer-by-layer assembly of β-estradiol loaded mesoporous silica nanoparticles on titanium substrates and its implication for bone homeostasis. *Adv. Mater.* 22, 4146–4150 (**2010**).

121. Lozano, D. *et al.* Osteostatin-loaded onto mesoporous ceramics improves the early phase of bone regeneration in a rabbit osteopenia model. *Acta Biomater.* 8, 2317–2323 (**2012**).

122. Kim, T. *et al.* Inhibition of osteoclastogenesis through siRNA delivery with tunable mesoporous bioactive nanocarriers. *Acta Biomater.* 29, 352–364 (**2016**).

123. Gan, Q. *et al.* A dual-delivery system of pH-responsive chitosan-functionalized mesoporous silica nanoparticles bearing BMP-2 and dexamethasone for enhanced bone regeneration. *J. Mater. Chem. B* 3, 2056–2066 (**2015**).

Chapter II:
Materials and Methods

El arte de vivir mucho es resignarse
a vivir poco a poco
Dr. Santiago Ramón y Cajal

2. Materials and Methods

This chapter is focused on the methods used during all the research here presented. Here it is described the details of the protocols followed during this doctoral thesis, regarding nanoparticle synthesis, polymer modifications, methods of optimization and *in vitro* and *in vivo* assays.

2.1 Synthesis and Surface Modification of Mesoporous Silica Nanoparticles

2.1.1 Synthesis of Mesoporous Silica Nanoparticles

Mesoporous silica nanoparticles were synthesized following a modification of the Stöber method.[1] Cetyltrimethylammonium bromide (CTAB (1 g, 2.74 mmol)), the structure directing agent, was dissolved in H_2O (480 mL) and NaOH (3.5 mL, 2 M) in a 1 L round-bottom flask under moderate magnetic stirring. The mixture was heated for 20 minutes at 80°C and then, tetraethyl orthosilicate (TEOS (4.5 mL, 20.15 mmol)), the silica precursor, was added drop-wise at 0.33 mL/min rate with a pump. After 30 min of TEOS addition, 3-trihydroxysilylpropyl methylphosphonate (TSPMP (0.5 mL, 1.31 mmol)) was added for the phosphonate modification and heated for a further 1.5 hours at 80°C under magnetic stirring. Then, the solution was centrifuged and washed once with water and twice with ethanol. The product was dried at room temperature under vacuum obtaining a white powder.[2]

The surfactant was removed by ionic exchange using 350 mL of a solution of ammonium nitrate (NH_4NO_3) (10 mg/mL) in ethanol (95%) at 80°C overnight under magnetic stirring. The process was repeated but this time for 2 hours. Then, the product was centrifuged, washed 3 times with ethanol and dried under vacuum.[3]

Rhodamine B-labeled nanoparticles and fluorescein (FITC)-labeled nanoparticles were synthesized by reacting 1 mg of Rhodamine-B isothiocyanate or FITC with 2.2 mL (0.009 mmol) of 3-aminopropyltriethoxysilane (APTES) in 40 μL of ethanol for 2 hours at room temperature.[4] Then, this solution was mixed with 4.5 mL of TEOS, and the whole mixture was added to the surfactant solution as previously described. The rest of the procedure (silica precursor, functionalization and surfactant removal) was carried out as described above. For the synthesis of cyanine-7(Cy7)-labeled nanoparticles, 5 mg of Cy7 with 4.4 μL of APTES were dissolved in 140 μL of dimethyl sulfoxide (DMSO) and stirred overnight. Then, this solution was mixed with 4.5 mL of TEOS, and the whole mixture was added to the surfactant solution as previously described. The rest of the procedure was carried out as described above.

The as-produced particles were characterized in terms of X-Ray Diffraction (XRD), Fourier Transformed Infrared (FTIR) spectroscopy, Thermogravimetric Analysis (TGA) N_2 adsorption analysis, Transmission Electron Microscopy (TEM), Dynamic Light Scattering (DLS) and Zeta potential.

2.1.2 Synthesis and Characterization of PEG-Alendronate Conjugate

The reaction for obtaining the poly(ethylene glycol) (PEG)-alendronate (PA) conjugate was divided in two steps. The reaction between the amino group of alendronate (ALN) and the activated carboxylic acid of the PEG was performed.

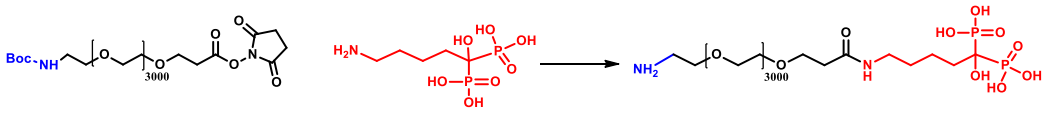

Scheme 2.1. Reaction between activated PEG and ALN.

The amino group of PEG was functionalized with tert-butyloxycarbonyl protecting group (Boc-) to avoid reactions between different chains of PEG, so the only amino group available was from ALN which will react with the activated acid group of PEG. The reaction was performed in a mixture of H_2O and DMSO (40:60). In a N_2-purged flask, a commercial O-[2-(Boc-amino) ethyl]-O′-[3-(N-succinimidyloxy)-3-oxopropyl] poly(ethylene glycol) (3500 Da) (153 mg) and sodium alendronate (30 mg) were solved in 100 µL of a mixture of DMSO/H_2O 60:40 at room temperature.[5] Triethylamine (30 µL) was added and the temperature was increased to 50ºC. The reaction was magnetically stirred overnight under inert atmosphere. The product (Boc-NH-PA) was precipitated in cold ether and purified by flash molecular exclusion chromatography (G-25/H_2O). The obtained product was characterized by ^{1}H-NMR as it can be appreciated in Figure 2.1

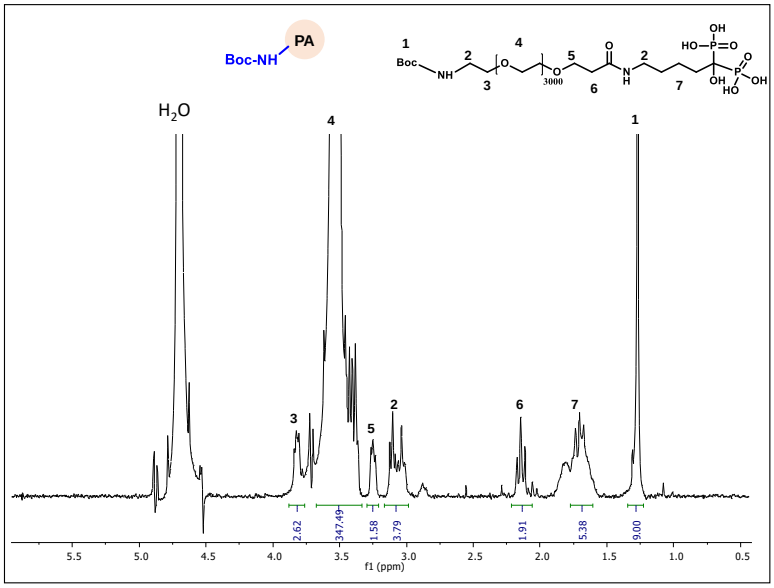

Figure 2.1 ^{1}H-NMR (D_2O) Boc-NH-PA. ^{1}H NMR (250 MHz, D_2O) δ (ppm) 3.92 – 3.81 (m, 2H, CH_2, PEG), 3.59 (s, 324H, CH_2, PEG), 3.33 – 3.24 (m, 2H, CH_2, PEG), 3.20 – 3.01 (m, 4H, 2xCH_2, PEG), 2.19 (t, 2H, CH_2, alendronate), 1.76 (dd, 4H, 2xCH_2, alendronate), 1.32 (s, 9H, 3xCH_3, Boc).

After the isolation and purification of the product, the amino group of the PEG was unprotected by the addition of TFA in dichloromethane, obtaining the final PA product (Figure 2.2). Boc-NH-PEG-ALN was solved in a solution of dichloromethane/trifluoroacetic acid (DCM/TFA) 1% to

remove the protecting Boc from the amino group. The mixture was stirred at room temperature for 1 hour. The product was obtained by precipitation in cold ether. The obtained product was characterized by ^{1}H-NMR as it can be appreciated in Figure 2.2

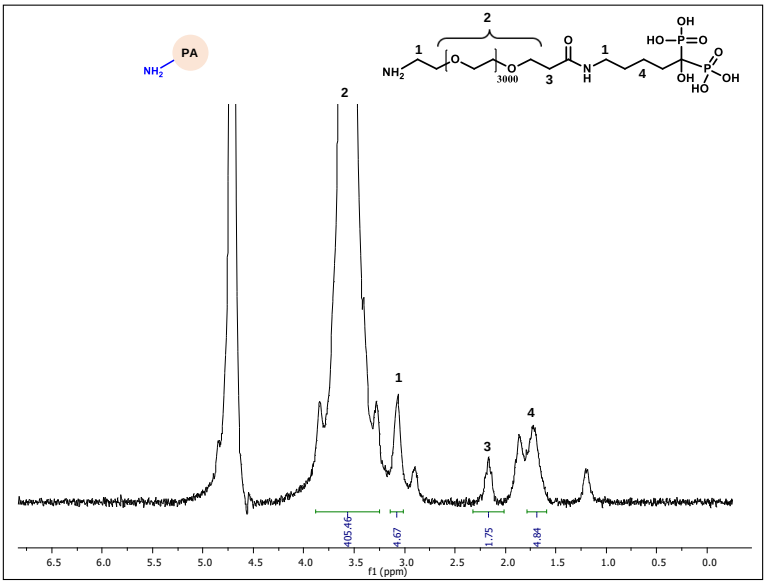

Figure 2.2 ^{1}H-NMR (D_2O) NH_2-PA. ^{1}H NMR (250 MHz, D_2O) δ (ppm) 3.59 (s, 340H, CH_2, PEG), 3.09 (s, 2H, CH_2, PEG), 2.20 (t, 2H, CH_2, alendronate), 1.77 (d, 4H, 2xCH_2, alendronate).

2.1.3 Synthesis and Characterization of Amine Functionalized PEG

A commercial PEG (2000 Da) was also modified with a glycine to obtain an amino end (Scheme 2.2) for further nanoparticle functionalization.

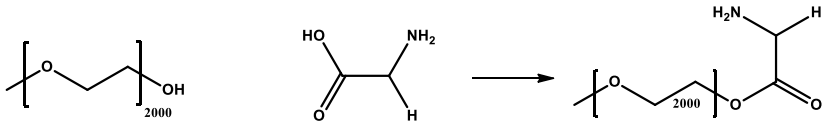

Scheme 2.2 Reaction of PEG with Glycine.

Glycine amino group was functionalized with fluorenylmethyloxycarbonyl (Fmoc) protecting group, to avoid cross reactions between different molecules of amino acid. PEG-methyl eter (2000 Da) (80 mg) and glycine-Fmoc (24 mg) were solved in a mixture of dried DMSO (0.1 mL) / CH_2Cl_2 (2 mL). N,N'-dicyclohexylcarbodiimide (DCC) (20 mg) and 4-dimethylaminopyridine (DMAP) (2 mg, 0.015 mmol) were solved in 0.5 mL of dried CH_2Cl_2 and added dropwise the PEG solution. The reaction was performed in presence of DCC for the acid activation of the glycine, and with DMAP as catalyst. The reaction was magnetically stirred overnight. Finally, the alcohol group of PEG reacted with the activated acid of the glycine, obtaining the desired amino functionalized PEG. The product was precipitated in cold ether, solved in N,N-dimethylformamide (DMF)/piperidine 20% and stirred for 2 hours for the Fmoc amino group deprotection from the glycine. The obtained product was characterized by ^{1}H-NMR as it can be appreciated in Figure 2.3

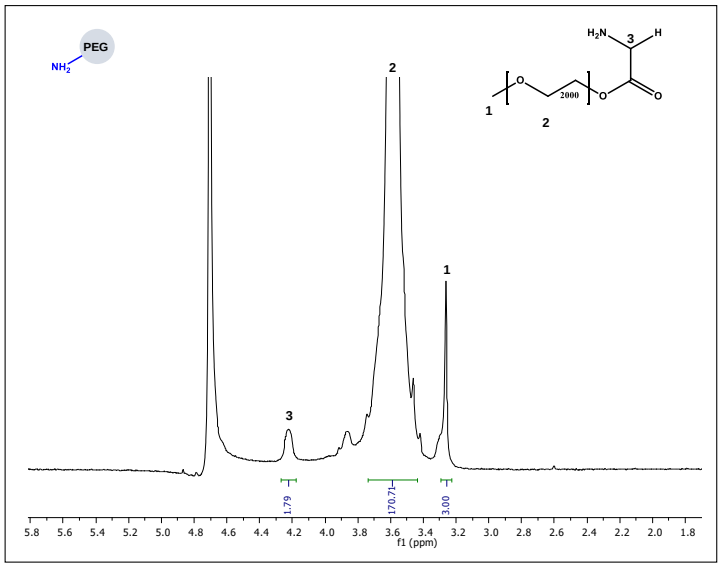

Figure 2.3 ^{1}H-NMR (D_2O) NH_2-PEG. ^{1}H NMR (250 MHz, D_2O) δ (ppm) 3.59 (s, broad, 182H, CH_2, PEG), 3.25 (s, 3H, CH_3, PEG), 4.26 (t, 2H, CH_2, glycine).

2.1.4 MSNs Polymer Coatings

2.1.4.1 Poly(ethylene glycol) and Alendronate modified Poly(ethylene glycol) Grafting

PA (1.5 mg) and PEG (1.5 mg) were added to a glass vial. The vial was purged with N_2 and 1 mL of dry toluene was added. Then, dry toluene (0.5 mL) with 1 µL of 3-triethoxysilylpropylsuccinic anhydride (SATES) were added dropwise to PEG mixture under N_2 atmosphere and with magnetic stirring. A catalytic amount of DMAP was solved in 1 mL of toluene and finally added to the whole solution. The reaction was stirred overnight (Solution 1, sililated polymers solution).

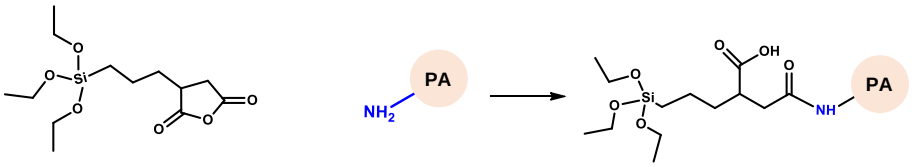

Scheme 2.3 Reaction between PEG and PA residues with SATES (Solution 1).

Then, 1 mL of Solution 1 was added dropwise to 5 mL of toluene containing 50 mg of previously dispersed MSNs under vigorous stirring. The reaction medium was heated (80°C) under reflux. After 1 hour, the remaining Solution 1 was added. The reaction was left under vigorous stirring for 24 hours. Then, the functionalized MSNs were collected by centrifugation and washed with toluene (twice), and ethanol (twice). Afterwards, the nanoparticles (MSNs-PA) were dried under vacuum for 16 h.

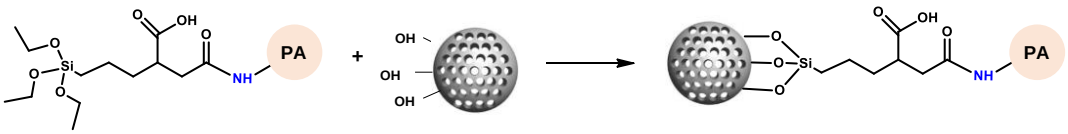

Scheme 2.4 Condensation of sililated polymer onto MSNs.

The same procedure was used to functionalize the nanoparticles only with PEG to obtain pegylated nanoparticles (MSNs-PEG) for experiment controls. PEG (3 mg) were solved in dry toluene under N_2 atmosphere. Then, dry toluene (0.5 mL) with 1 µL SATES were added dropwise to PEG mixture with magnetic stirring. A catalytic amount of DMAP was solved in 1 mL of toluene and finally added to the whole solution. The reaction was stirred overnight. The same protocol described above was followed for the sililated polymer condensation onto the nanoparticle surface.

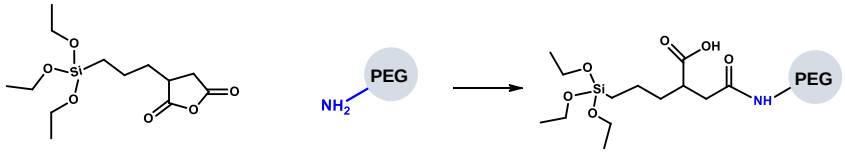

Scheme 2.5 Reaction between PEG and SATES.

2.1.4.2 Poly(ethylenimine) Grafting

Different nanoparticles, 5 mg of MSNs, MSNs-PA or MSNs-PEG nanoparticles were dispersed in a solution of 2.5 mg of poly(ethylenimine) (PEI) (5 kDa) in 1 mL of absolute ethanol to perform the PEI coating. After sonicating for 20 seconds and stirring for 30 min, the PEI coated nanoparticles (MSNs@PEI, MSNs-PA@PEI, MSNs-PEG@PEI) were consequently washed with PBS and ethanol.[6] The amount of MSNs was increased to achieve the different PEI:MSNs ratios needed. It was performed 1:1 and 1:2 mass ratio for MSNs@PEI, and 1:2, 1:3, 1:6 for MSNs-PA@PEI. In the case of MSNs@PEI it was also evaluated different PEI molecular weights (5 kDa, 8 kDa, and 10 kDa).

2.2 Physicochemical Characterization of MSNs

All the materials were characterized by different techniques. Surface morphology was analyzed by TEM (Figure 2.4), which was carried out in a JEOL JEM 2100 instrument operated at 200 kV, equipped with a charge-coupled device camera (KeenView Camera). The TEM micrographs here presented (Figure 2.4) show the spherical shape, monodispersity and structure of the nanoparticles. Also, the disposition of their pores could be appreciated (Figure 2.4 inset).

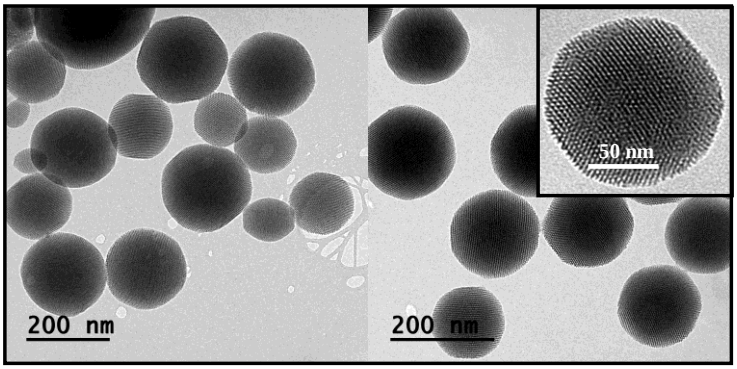

Figure 2.4 MSNs TEM micrographs.

The Zeta (ζ) potential and hydrodynamic size of nanoparticles were measured by means of a Zetasizer Nano ZS (Malvern Instruments) equipped with a 633 nm "red" laser. As observed in Figure 2.5, the distribution was centered at 164 nm. In addition, there were no aggregates, confirming the suitability of the particles for their biological application.

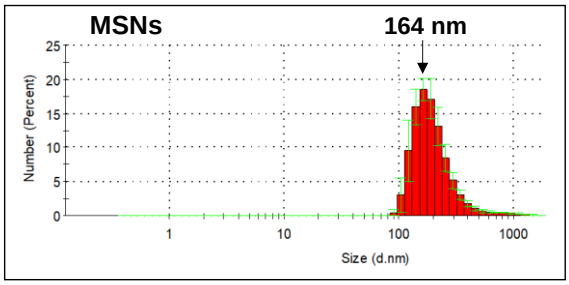

Figure 2.5 DLS measurements of MSNs. The analysis showed a homogenous distribution centered at 164 nm and well dispersed, in agreement with the electronic micrographs.

A Nicolet Nexus spectrometer (Thermo Fisher Scientific) was used to obtain the FTIR spectra (Figure2.6A). The spectrum shows the typical bands of mesoporous silica nanoparticles (490-1090 cm^{-1} Si-O-Si and 1700 cm-1 of Si-OH). The Si-O-Si vibration bands confirmed the proper hydrolysis, condensation and subsequent polymerization of the silica precursors during the synthesis, leading to a network of Si-O-Si bonds as backbone. In addition, the Si-OH bands confirmed the expected presence of silanol groups on surface of MSNs. TGA/DTA were performed in a PerkinElmer Pyris Diamond TG/DTA analyzer, with 5°C/min heating ramping up from room temperature to 600°C (Figure2.6B). By this technique the organic matter presented in the sample would be burned increasing gradually the temperature. Therefore, it can be possible to determine the percentage of organic matter lost at every temperature point. After solvent extraction of the surfactant, by TGA it could be confirmed that the process was successfully performed.

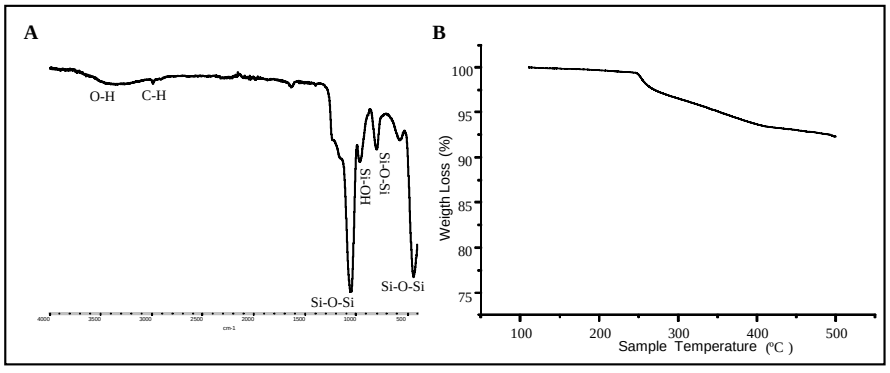

Figure 2.6 Physicochemical characterization of MSNs A) FTIR spectrum. B) TGA graphic.

N_2 adsorption was carried out to obtain surface area and pore size and pore volume values. Micromeritics ASAP 2010 instrument was used; surface area was obtained by applying the BET equation, and the pore size distribution was determined by the BJH method from the desorption branch of the isotherm.[7] The mesopore diameter was determined from the maximum of the pore

size distribution curve (Figure 2.7A). The N_2 adsorption analysis confirmed the excellent textural properties of this kind of material, showing a surface area of ca. 900 m^2/g and pore width and volume of 2.34 nm and 1.05 cm^3/g, respectively. The pore size would allow the loading of therapeutic compounds. The shape of the isotherm provides structural information about the material. XRD was carried out to confirm the order of the mesostructured from the mesoporous nanoparticles in a Philips X-Pert MPD diffractometer equipped with Cu Kα radiation (Figure 2.7B).[8] The maxima shown in the diffractogram, ([100], [110] and [200]), confirmed the hexagonally ordered pore distribution typical of MCM-41-like materials.

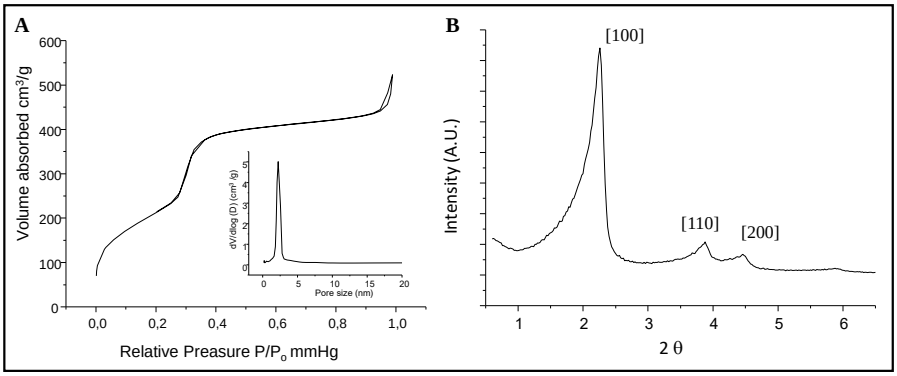

Figure 2.7 Physicochemical characterization of MSNs. A) N_2 adsorption. B) X-ray diffraction.

Fluorescence spectrometry was used to determine cargo released by nanoparticles by means of a Biotek Synergy 4 device. Fluorescence microscopy was used to verify the colocalization on MSNs and siRNA constructs. It was performed with an Evos FL Cell Imaging System equipped with three LED light cubes (lEX, nanometers; lEM, nanometers): DAPY (357/44; 447/60), GFP (470/22; 525/50), and RFP (531/40; 593/40) from AMG (Advanced Microscopy Group).

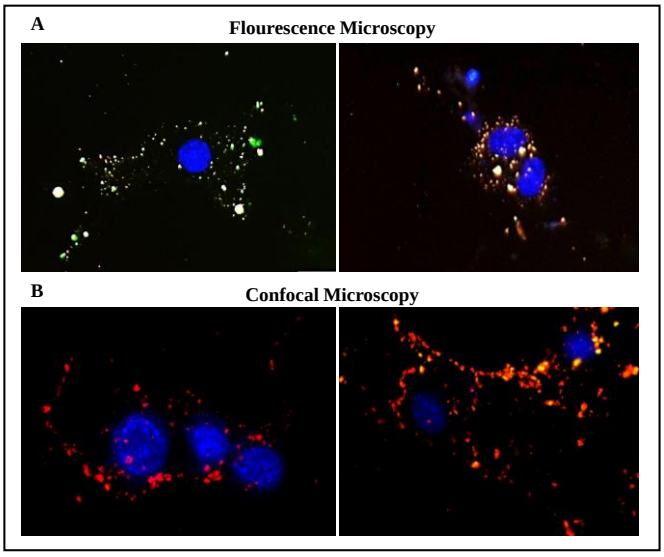

Figure 2.8 Fluorescence microscopy images of MEF cells incubated with MSNs (A). Confocal laser scanning microscopy images of MEF cells incubated with MSNs (B). Red fluorescence MSNs, green fluorescence siRNA, blue fluorescence cell nuclei.

2.3 Optimization of MSNs@PEI and MSNs-PA@PEI

2.3.1 SiRNA Binding Capability

The transfection conditions and the release efficiency of the siRNA from nanoparticles were optimized using a siRNA-analog called siGLO Green Transfection Indicator (Abs/Em max 494/520 nm). The siRNA binding capability of MSNs@PEI or MSNs-PA@PEI was determined by agarose gel retardation assay.[9] Different amounts of MSNs@PEI ranging from 0.8 to 6.4 μg were mixed with 0.1 μg of siGLO in aqueous solution to obtain nanoparticle to nucleic acid ratios (N/P) of 8−64. N/P is a mass ratio in which N and P, respectively, correspond to the positive (nitrogen (MSNs@PEI)) and negative (phosphonate (siGLO)) charges. Free siGLO was used as control. A total of 20 μL of MSNs@PEI and siGLO complex solution were mixed with 5 μL of loading buffer and electrophoresed in a 2% agarose gel containing 0.5 μg/mL of GelRed (Nucleic Acid Gel Stain) at 80 V for 40 minutes in Tris/Borate/ ethylenediaminetetraacetic acid (EDTA) running buffer. Nucleic acid bands were detected by ultraviolet (UV) light (254 nm). It is important to mention that only uncomplexed siGLO was able to migrate to the positive electrode and, therefore, be observed on the gel. Then, when the spot of free siGLO was no longer visible means that the amount of nanoparticles added had complexed with all the siGLO present (total binding particle/nucleic acid). The lowest N/P ratio that complexed all the siGLO is called threshold.[2]

For MSN@PEI it was compared PEI with different molecular weights, 5, 8, and 10 kDa, and different PEI:MSNs ratio (1:1 and 1:2). The results can be found in chapter 3. In the case of 8 and 10 kDa MSN@PEI appeared the same threshold, 32, but for 5 kDa PEI, the threshold was 16.

On the other hand, for MSNs-PA@PEI, the procedure was the same, but in this case, we compared the 3 different ratios with just 5 kDa PEI. Different amounts of MSNs@PEI ranging from 0.8 to 25.6 μg were mixed with 0.1 μg of siGLO in aqueous solution to obtain nanoparticle-to nucleic acid ratios of 8−256. For MSNs-PA@PEI 1:2 the threshold was 34, for 1:3 ratio was 64, and 1:6 ratio was not able to bind properly the siGLO therefore the nucleic acid band did not disappear even in 256 N/P ratio.

2.3.2 SiGLO Release from MSNs@PEI

The final concentration to bind siGLO to the polymer (N/P ratio of 32) was achieved adding 165 μL of siGLO (20 μM) to 0.35 mL of a 4 mg/mL solution of MSNs@PEI in PBS 7.4 (10 mM). A 24-transwell plate was employed to determine the siGLO release. To perform the assay, 0.1 mL of the nanoparticle dispersion were placed on a Transwell permeable support (three replications were performed). The well was filled with 0.6 mL of PBS pH 7.4 (10 mM), and the suspension was orbitally stirred (100 rpm) at 37°C during all the experiment. At every time point studied, the

solution outside the transwell insert was removed and replaced with fresh PBS. The amount of cargo released in the solution removed was determined by fluorescence (absorbance/emission: 494/520 nm).

2.3.3 Cell Cultures

Cell culture tests were performed using mouse embryonic fibroblast (MEFs) because they are known to express SOST gene.[10] MEF cells were plated at a density of 10^4 cells per square centimeter in 1 mL of Dulbecco's modified eagle's medium (DMEM), containing 10% of heat-inactivated fetal bovine serum and 1% penicillin−streptomycin at 37°C in a humidified atmosphere of 5% CO_2, and incubated for the specific time of each experiment. The tested nanoparticles were placed into each well of 12 or 24-well plates after cell seeding. Some wells without nanoparticles were seeded as controls.

2.3.4 Cell Viability

MEF viability was determined by addition of Alamar Blue solution at 10% (v/v) to the cell culture. After 2 hours of contact with different concentrations of MSNs (n = 3), the cells were grown for 48 hours in 24 well plates at a density of 10^4 cells per square centimeter. Afterward, Alamar Blue solution was added following the manufacturer's instructions.[11] Fluorescence intensity was measured using excitation emission wavelengths of 570 and 600 nm, respectively, in a Unicam UV-500 UV−visible spectrophotometer.

2.3.5 Cell MSNs-PA@PEI and MSNs@PEI Uptake

2.3.5.1 MSNs@PEI

MEF cells were cultured in each well of a 12-well plate and incubated at different times in the absence or presence of the tested FITC-labeled nanoparticles at a concentration of 50 μg/mL (MSNs, MSNs@PEI, and MSNs@PEI-siGLO). After 2 hours, cells were washed twice with PBS and incubated at 37°C with trypsin−EDTA solution for cell detachment. The reaction was stopped with culture medium after 5 minutes, and cells were centrifuged at 1000 rpm for 10 minutes and resuspended in fresh medium. Then, the fluorescence present in the surface of the cells was quenched with Trypan blue (0.4%) to confirm the presence of intracellular and, therefore, internalized fluorescent signal.

Flow cytometry measurements were performed at an excitation wavelength of 488 nm, and green fluorescence was measured at 530 nm (FL1). The trigger was set for the green fluorescence channel (FL1). The conditions for the data acquisition and analysis were established using negative and positive controls with the CellQuest Program of Becton−Dickinson, and these conditions were maintained during all the experiments. Each experiment was carried out three times and single representative experiments were displayed. For statistical significance, at least

10^4 cells were analyzed in each sample in a FACScan machine (Becton, Dickinson and Company) and the mean of the fluorescence emitted by these single cells was used.

The cell uptake of MSNs was evaluated using fluorescence and confocal laser scanning microscopy incubating the cells with Rhodamine-B-labeled MSNs, MSNs@PEI, and MSNs@PEI-siGLO for 2 hours. Each well was washed with PBS three times to clear the no internalized nanoparticles and then fixed with 75% ethanol for 10 minutes. Cells were permeabilized with 0.5% of Triton X-100 during 5 min. The non-specific background was reduced through the addition of 1% bovine serum albumin to the solution and left for 20 min. The nucleus of both types of cells were stained with 4′,6-diamidino-2-fenilindol (DAPI, ≥ 98%) for 5 min, respectively, and then washed three times with PBS. The nanoparticles internalized into MEF cells were evaluated by fluorescence microscopy and performed with an Evos FL Cell Imaging System and with a confocal laser scanning microscope Olympus FV1200. The images were prepared for analysis using 3D Imaris software to project a single 2D image from the multiple Z sections by using an algorithm that displays the maximum value of the pixel of each Z slice of 1 μm of depth. The resulting projection was then converted into an image file using this software. The red channel was used for detecting Rhodamine-B-labeled MSNs@PEI, green channel for siGLO and blue for cell nucleus labelled with DAPI.

2.3.5.2 MSNs-PA@PEI

MEF cells were cultured in each well of a 12-well plate and incubated at different times in the absence or presence of the tested FITC-labeled nanoparticles at a concentration of 50 μg/mL (MSNs, MSNs-PA, MSNs-PA@PEI, and MSNs-PA@PEI-siGLO). After 2 hours, cells were washed twice with PBS and incubated at 37°C with trypsin−EDTA solution for cell detachment. The reaction was stopped with culture medium after 5 min, and cells were centrifuged at 1000 rpm for 10 min and suspended in fresh medium. Then, the fluorescence present in the surface of the cells was quenched with Trypan blue (0.4%) to confirm the presence of intracellular and, therefore, internalized fluorescent signal.

Flow cytometry measurements were performed following the protocol stated above.

2.3.6 Targeting Assay

To evaluate the targeting capacity of the nanoparticles, 500 μL of a solution of 1mg/mL of the different Rhodamine-B-labeled nanoparticles (MSNs, MSNs-PA, MSNs@PEI MSNs-PA@PEI) in PBS 1X (pH= 7.4) were incubated with a commercial HA (50 mg) tablet (ENGIPORE pre-formed bone substitute) at 37°C and 100 rpm during 8 hours. The tablet was washed 3 times in PBS 1X (1.5 mL) and incubated for further 48 hours at 37°C and 100 rpm with fresh PBS 1X to wash the nanoparticles retained inside the tablet due to its porosity nature. Then, the piece was

washed 4 times with fresh PBS 1X (1 mL). The tablets were analyzed by fluorescence microscopy to determine the presence of Rhodamine B-labeled nanoparticles.

2.3.7 Colloidal Stability Assay

To determine the stability of the different nanoparticles, 500 µL of a solution of 1mg/mL in PBS of the different FITC-labeled nanoparticles, PEGylated nanoparticles (MSNs-PA), and coated with PEI (MSNs-PA@PEI) and our previously reported non-PEGylated nanoparticles (MSNs), were kept at 37°C for 1 hours without stirring, to be then evaluated under visible and UV light. The suspension stability in 1 mM PBS was further evaluated by DLS to determine the hydrodynamic diameter of the different nanoparticles (MSNs, MSNs-PA, MSNs-PA@PEI) after different periods of time (0, 1, 2, 3, 6 and 24 hours).

2.3.8 RNase Stability

The MSNs-PA@PEI-siRNA RNase stability was determined by agarose gel retardation assay. Different conditions of siRNA and nanoparticles bound to siRNA were evaluated in order to determine their RNase stability. 1 μg of free siRNA was used as negative control (ϕ). Both Naked siRNA (1 μg) (Channel 1) and 32 μg of MSNs-PA@PEI-siRNA containing 1 μg of siRNA (Channel 2) were incubated with 2 μL of RNase (1 U/μL) in phosphate buffer (pH 7.0) at 4°C, for 2 hours. After time periods, 1 μL of EDTA 100 nM was added to the samples and incubated at 70°C for 30 min for RNase inactivation. The siRNA was released from the polymers by incubating the sample with 2.5 μL of sodium dodecyl sulfate (SDS) 1% solution at room temperature for 15 min. The extracted siRNA was analyzed on 1% agarose gel electrophoresis carried out at 80 V for 60 min. The results are shown in chapter 5.

2.4 SOST mRNA Expression and siRNA Transfection

MEFs were seeded in 12-well plates and incubated during 3, 7, 14, and 21 days (n= 3). Total RNA was isolated from MEF cells by a standard procedure (Trizol, Invitrogen), and cDNA synthesis was performed using a high-capacity RNA-to-cDNA kit. Gene expression was analyzed by real-time quantitative reverse transcription polymerase chain reaction (qRT-PCR) using a QuantStudio 5 Real-Time PCR System. Unlabeled mouse-specific primers for SOST, Runx2, Alp, and TaqMan MGB probe were used to perform qRT-PCR assay. The mRNA copy numbers were calculated for each sample by using the cycle threshold (Ct) value. Glyceraldehyde 3-phosphate dehydrogenase (GAPDH) RNA (a housekeeping gene) was amplified in parallel with tested genes. The relative gene expression was represented by $2^{-\Delta\Delta Ct}$, where $\Delta\Delta C_t = \Delta C_{ttargetgene} - \Delta C_{tGAPDH}$.

The efficacy of gene silencing using specific SOST siRNA on MEFs *in vitro* was tested seeding cells in 12-well plates and incubated for 2 weeks. Cells were then transfected with the specific siRNAs at 0.5 μM concentration and incubated as required (experiments run for triplicate). To optimize the experiment, two controls were used: a negative control siRNA ("non-targeting control", which targets a site that is absent in human, mouse, and rat genomes) as well as a positive control ("GAPDH control", which targets GAPDH, a gene common between human, mouse, and rat). SiRNA transfection was promoted using Accell siRNA transfection media. Transfection progressed for 2 hours and after that cells were lysed with 500 μL of Trizol. Then, gene expression was analyzed by qRT-PCR as described above. Bar graphs represent expression of SOST mRNA relative to GAPDH.

2.5 Osteostatin Loading and Release

The MSNs were loaded before PEI coating with osteostatin (OST) by incubating 5 mg of MSNs in a solution of OST 10^{-4} M in PBS overnight at 4°C to ensure osteostatin stability. Then, the nanoparticles were recovered by centrifugation and washed with PBS. The loaded nanoparticles were functionalized with PEI, as previously described. Then, the OST loaded MSNs@PEI nanoparticles (OST-MSNs@PEI) were centrifuged and washed with PBS. A 24-transwell plate was employed to determine the OST release. From a 14 mg/mL dispersion of OST-MSNs@PEI dispersed in PBS with a pH of 7.4 (10 mM), 0.1 mL were placed on a Transwell permeable support (3 replications were performed). The well was filled with 0.6 mL of PBS pH 7.4 (10 mM), and the suspension was stirred at 100 rpm at 37°C during the experiment. At every time point studied, the solution outside the transwell insert was measured by fluorescence and replaced again on the plate. The amount of cargo released was determined by fluorescence at a wavelength of absorbance/emission of 280/320 nm. It was confirmed by a gel electrophoresis assay that osteostatin loading process keeps unaffected the binding ability of OST-MSNs@PEI to siGLO.

2.6 *In Vitro* Evaluation

2.6.1 SOST mRNA Knockdown by MSNS@PEI-siRNA

MSNs@PEI-siRNA complexes were prepared with the N/P ratios previously described. For the complexes formation, 15 μL of 20 μM SOST siRNA or negative (SiCtl) or positive (PosControl) control siRNA were added to 70 μg of MSNs@PEI 5kD (N/P ratio =16) in 600 μL of DMEM. The complexes were added to MEFs cells after 14 days and exposed for 2 hours. Then, the medium was replaced with fresh medium and cultured for further 48 hours. Cells were then lysed using 500 μL of Trizol, and the SOST, Runx2, and Alp expression levels were quantified by qRT-PCR, as previously described.

2.6.2 Osteostatin Delivery in MEF Cells in the Presence and Absence of siRNA SOST

For the performance of the experiment, MSNs were loaded with osteostatin as described before; afterwards, they were coated with PEI and bound to siRNA (OST-MSNs@PEI-siRNA). Then, 15 μL of 20 μM SOST siRNA or negative or positive control siRNA were added to 70 μg of OST-MSNs@PEI 5kD (N/P ratio of 16) in 600 μL of DMEM. The complexes were added to MEFs cells after 14 days of culture and exposed for 2 hours. OST-MSNs@PEI were also used as control. Then, the medium was replaced with fresh medium and cultured for further 48 hours. Cells were then lysed using 500 μL of Trizol, and the SOST, Runx2, and Alp expression levels were quantified by quantitative real-time PCR, as previously described.

2.7 *In Vivo* Evaluation

2.7.1 Local *In Vivo*

Young mature female C57BL/6J mice (Charles River) that underwent bilateral ovariectomy after 4 weeks of age (OVX) or sham operations (placebo surgery) (control) of 12 weeks of age were used. They were assigned to 6 groups (n = 5 per group), OVX, MSNs, MSNs@PEI-siCtl, MSNs@ PEI-siRNA, OST-MSNs@PEI, OST-MSNs@PEI-siRNA, and one more control group with 5 mice. They were stabled in the Animal Research Facility at Hospital 12 de Octubre for 2 weeks. All animal experiments in this study were performed according to approved animal protocols. Animals were given free access to water and fed a standard diet (8.8 g/kg calcium and 5.9 g/kg phosphate) in a room maintained at 22°C on 12 h light/12 h dark cycles. Mice were anesthetized with isoflurane, and 50 μL of nanoparticle dispersion (0.8 mg/mL) were injected in the femur bone marrow by bilateral oblique incisions that were made over the patellar ligament. A hole was made through patellar ligament using the needle from the syringe, and then the dispersion was injected. After 5 days, mice were euthanized by exposing them to 5% isoflurane in oxygen, and both femurs, the one injected with nanoparticles and the other one as control, were removed. Bone samples were crushed under liquid nitrogen. Total RNA was extracted from these homogenized samples with Trizol following the manufacturer's instructions (Invitrogen). SOST, Runx2, and Alp expression levels were quantified by qRT-PCR, as previously described.

2.7.2 Systemic *In Vivo*

Young mature female C57BL/6J mice (Charles River) that underwent bilateral ovariectomy after 6 weeks of age (OVX) or sham operations (control) of 14 weeks of age were used. They were assigned to 4 groups (n = 5 per group), OVX, MSNs-PA@PEI (MSNs), PTH (PTH), OST-MSNs-PA@PEI-siRNA (OST-siRNA) and one more group as control (Control) with 5 healthy mice. They were stabled in the Animal Research Facility at Hospital 12 de Octubre for 2 weeks. All animal experiments in this study were performed according to approved animal protocols.

Animals were given free access to water and fed a standard diet (8.8 g/kg calcium and 5.9 g/kg phosphate) in a room maintained at 22°C on 12 h light/12 h dark cycles.

Mice were anesthetized with isoflurane for every injection. Every two days for a period of 2 or 3 weeks mice were injected with 100 μL of either the different nanoparticle dispersion (MSNs-PA@PEI; OST-MSNs-PA@PEI-siRNA) (0.8 mg/mL), 100 μL of PTH or 100 μL PBS depending on the group. The injections were performed subcutaneously in the left side of the ovariectomized mice. After 2 or 3 weeks of treatment, mice were euthanized by exposing them to 5% isoflurane in oxygen, and both femurs and tibiae were removed.

For the gene expression analysis, one site bone samples were crushed under liquid nitrogen. Total RNA was extracted from these homogenized samples with Trizol following the manufacturer's instructions. SOST, Runx2, Alp, OPG, OSX, and VEGF expression levels were quantified by qRT-PCR as previously described.

2.7.3 Dual-Energy X-Ray Absorptiometry

The bone mineral density of femur was measured in anaesthetized control and ovariectomized mice at the start of the study to confirm decreased bone mass using PIXImus (GE Lunar Corp).

2.7.4 Micro-Computed Tomography

The removed femur and tibiae bones were fixed in 10% neutral buffered formalin. Before CT scanning, they were washed with running water for 15 min. The imaging of three-dimensional microcomputed tomography was performed with a CompactCT micro-CT scanner (SEDECAL). Data were acquired at 27 μm isotropic voxel size with 720 projections by 360-degree scan, integration time of 2,000 ms with three frames, photon energy of 80 KeV, and current of 450 uA. The duration of imaging time was 10 min per scan and followed by projection correction and volume reconstruction of three-dimensional representation. Three-dimensional render images of the bones were generated through original volumetric reconstructed images by MicroView software (GE Healthcare). The analysis of the results obtained in the microcomputed tomography were quantified from Micro-Computed Tomography scans using GE MicroView software v2.2.

2.8 References

1. Stober, W., Fink, A. Controlled Growth of Monodispersed Silica Spheres in the Micron Size Range. *J. Colloid Interface Sci.* 26, 62–69 (**1968**).

2. Meng, H. *et al.* Engineered Design of Mesoporous Silica Nanoparticles to Deliver Doxorubicin and P-Glycoprotein siRNA to Overcome Drug Resistance in a Cancer Cell Line. *ACS Nano* 4, 4539–4550 (**2010**).

3. Martínez-Carmona, M. *et al.* A novel visible light responsive nanosystem for cancer treatment. *Nanoscale* 9, 15967–15973 (**2017**).

4. Paris, J. L. *et al.* From proof-of-concept material to PEGylated and modularly targeted ultrasound-responsive mesoporous silica nanoparticles. *J. Mater. Chem. B* 6, 2785–2794 (**2018**).

5. Villaverde, G., Nairi, V., Baeza, A., Vallet-Regí, M. Double Sequential Encrypted Targeting Sequence: A New Concept for Bone Cancer Treatment. *Chem. Mater.* 23, 7174–7179 (**2017**).

6. Xia, T. *et al.* Polyethyleneimine coating enhances the cellular uptake of mesoporous silica nanoparticles and allows safe delivery of siRNA and DNA constructs. *ACS Nano* 3, 3273–3286 (**2009**).

7. Ishii, Y., Nishiwaki, Y., Al-zubaidi, A., Kawasaki, S. Pore Size Determination in Ordered Mesoporous Materials Using Powder X-ray Diffraction. *J. Phys. Chem. C* 117, 18120–18130 (**2013**).

8. Vallet-Regí, M., Rámila, A., Del Real, R. P., Pérez-Pariente, J. A new property of MCM-41: Drug delivery system. *Chem. Mater.* 13, 308–311 (**2001**).

9. Furst, T. *et al.* Capillary electrophoresis method to determine siRNA complexation with cationic liposomes. *Electrophoresis* 37, 2685–2691 (**2016**).

10. Basha, G. *et al.* Lipid nanoparticle delivery of siRNA to osteocytes leads to effective silencing of SOST and inhibition of sclerostin in vivo. *Mol. Ther. Nucleic Acids* 5, 1–15 (**2016**).

11. Invitrogen. alamarBlue ® Assay. *US Pat. No 5501959* 1–27 (**2007**) doi:U.S. Patent No. 5,501,959.

Chapter III: Mesoporous Silica Nanoparticles for SiRNA Delivery

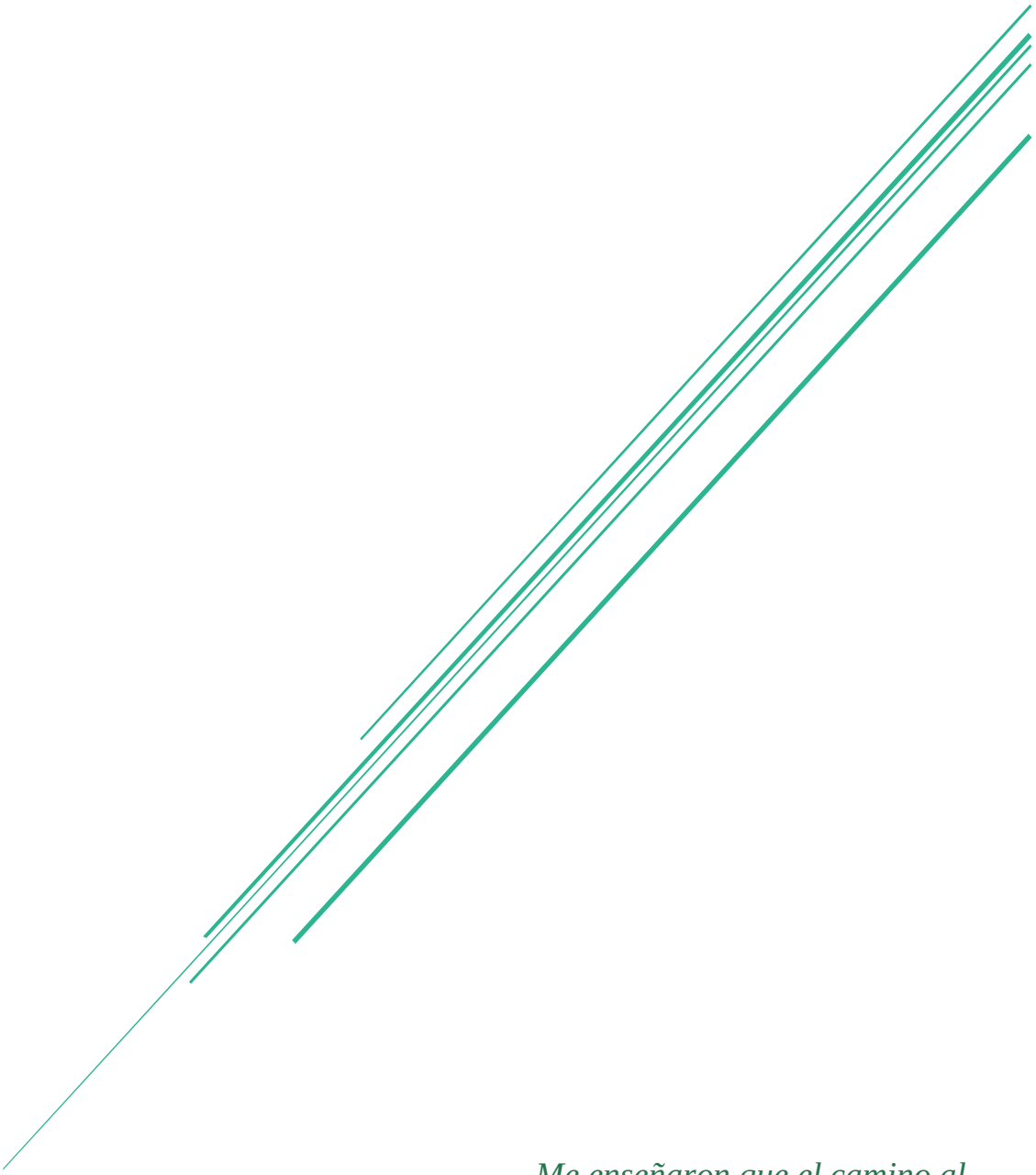

Me enseñaron que el camino al progreso no era rápido ni fácil
Marie Curie

3. Mesoporous Silica Nanoparticles for SiRNA Delivery

3.1 Introduction

This chapter is focused on the design of a mesoporous silica nanoparticle-based nanocarrier for the delivery of nucleic acids, more specifically siRNAs, for the potential application in osteoporosis treatment.

3.1.1 Genes Involved in Osteoporosis

Osteoporosis is a complex disease in which different genes take part in the development and progress of the bone degeneration. Those genes that have been identified to down-regulate bone formation could be targeted, which could lead to an alternative treatment for osteoporosis.

There are two main signaling pathways related with bone formation or bone resorption. The RANK/RANKL/OPG regulatory axis, where RANKL acts as activator of the pathway and OPG as negative regulator, regulates bone formation and degradation by the coordinated competition of these two molecules with RANK receptor (Figure 3.1). When RANKL activates RANK receptor, induces mainly osteoclasts differentiation and survival, and therefore the maintenance of bone resorption by mature osteoclasts.[1]

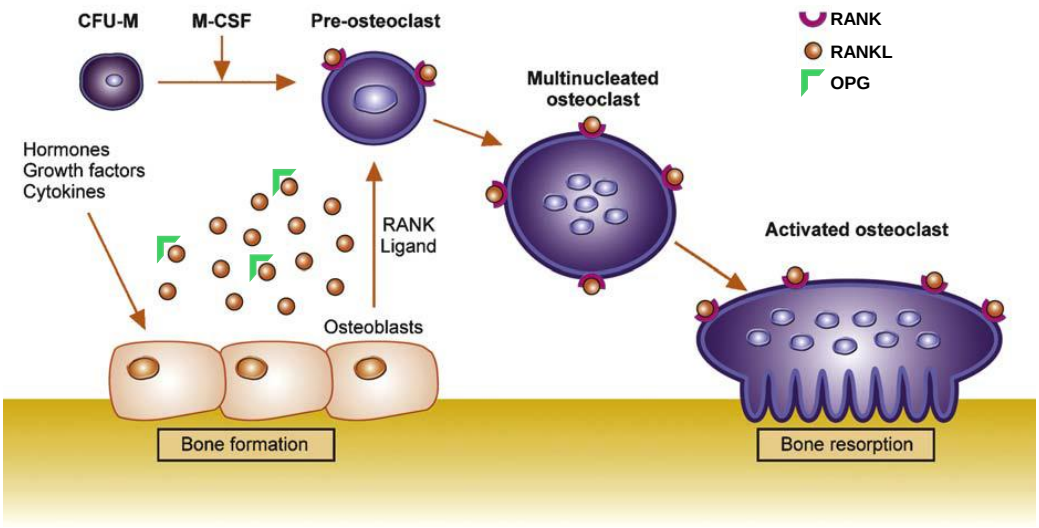

Figure 3.1 Role of RANK/RANKL/OPG regulatory axis in osteoclast formation, function, and survival. Adapted from Ref 1 with the permission of Nature. Colony-forming unit macrophage (CFU-M), macrophage colony-stimulating unit (M-CSF).

Thus, RANKL could be chosen as knock-down target to downregulate osteoclast bone resorption. Additionally, there are several transcription factors, such as c-FOS, NF-κB, c-Jun, NFATc1,

activated by the interaction of RANK with RANKL, that could be targeted with siRNAs in order to downregulate osteoclast formation and activation.[1,2]

As mentioned in the first chapter, the wnt-β-catenin signaling pathway is the second route highly related to bone formation. This pathway is activated by the interaction of wnt proteins with low density lipoprotein receptor-related protein 5/6 (LRP5/6) and with Frizzled membrane receptors.[3] The activation of this pathway leads to an increased osteoblastic differentiation and the subsequent bone formation stimulation. This bone-anabolic pathway is negatively regulated by sclerostin and dickkopf-1 (Dkk-1), which block the LRP5/6 receptor protein.[4–6] Thus, knocking-down the corresponding genes of these inhibitors would permit the activation of the pathway with the consequent osteoblast activation and bone formation.

During the present work, we have focused in SOST, the gene that encodes sclerostin, since its knock-down would produce an anabolic effect and potential bone formation. Several types of sclerostin monoclonal antibodies have been developed as anabolic drugs to block the activity of sclerostin, increasing osteoblast differentiation for osteoporosis treatment.[7,8] However, these antibodies have been observed to cause an immune response, which limits their use for this treatment.[7] Silencing SOST gene with a specific siRNA in osteocytes could be a more effective approach that could promote osteoblast differentiation and the subsequent bone formation overcoming the immune response limitation.

3.1.2 SiRNAs Delivery Challenge

SiRNA-based therapeutics are under development for the treatment of several diseases such as, cancer, bone diseases, viral infections, etc.[9,10] The major bottleneck for siRNA-based treatments is the necessity of a delivery method to transport siRNAs into targeted cells. SiRNAs are well known for having a very short half-life, a poor cell membrane penetration capacity, and a low stability against serum nucleases.[11,12] SiRNA molecules must be delivered inside the target cells for be incorporated in the RNAi machinery, the so-called RNA-induced silencing complex (RISC), and therefore achieve the desired knock-down effect. Thus, siRNAs might face many physiological barriers to reach its site of action (Figure 3.2)[13], such us the degradation by RNases, the recognition by the immune system, and the cell membrane penetration. For this reason a delivery system must be engineered to overcome all these barriers and allow the siRNA to reach its side of action.[9,14]

Typical siRNA delivery challenges have been approached from different perspectives using both viral and non-viral vectors. While viral vectors have the main drawback of safety issues, including high viral toxicity, possible carcinogenicity and immunogenicity, together with significant cost limitations; non-viral vectors instead have the extremely inefficient targeting and transfection

capacity. These unresolved issues have inspired the research and development of new nanocarriers to deliver siRNAs unaffected. Among them, different polymeric nanoparticles, including liposomes[15,16] or cationic-polymeric nanoparticles[13,17], have been proposed as siRNA nanocarriers. In this sense, PEI-siRNA complexes have been investigated for siRNA delivery, although the high cytotoxicity of high molecular PEIs has compromised their use.[18] Therefore, novel siRNA nanocarriers need to be further explored to fully exploit the siRNA therapy potential.

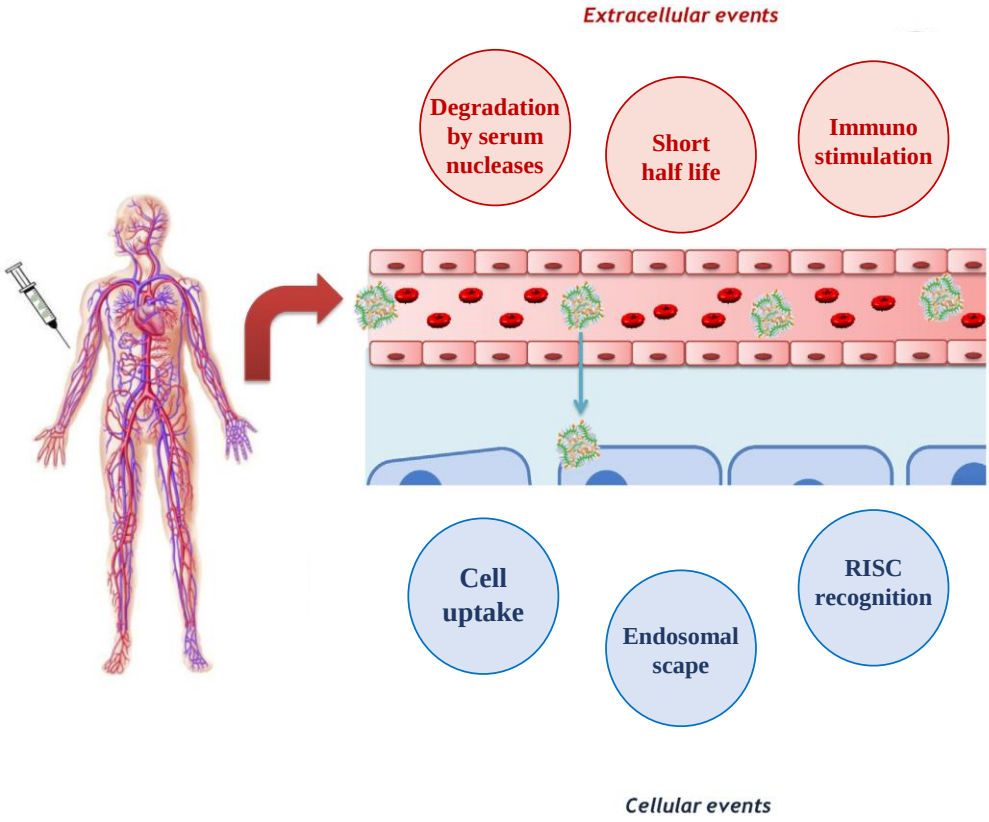

Figure 3.2 Extracellular and cellular events in siRNA delivery following the intravenous administration. Adapted from Ref 13 with permission of Elsevier.

3.1.3 Mesoporous Silica Nanoparticles for SiRNA Delivery

Nowadays, MSNs have attracted research interest in biomedicine due to their great properties for drug delivery, such as huge pore volume and surface area, high loading capacity and biocompatibility, among others.[19–22] Additionally, their surface can be easily chemically modified with different moieties to provide MSNs with different capabilities such as targeting[23,24] and responsive behaviours.[25,26] Since siRNAs face many physiological barriers to reach its site of action, a delivery system might be developed to overcome all these barriers. Due to all their physical properties, MSNs could be an appropriated platform to deliver siRNAs. They can load nucleic acids inside their pores, being necessary in this case to obtain high pore diameter nanoparticles (above 4 nm pore) to achieve the siRNA encapsulation.[27] Additionally, as mentioned before, MSNs can be functionalized in the surface to obtain different capabilities, for

example, loading nucleic acids.[28] The negative nature of nucleic acids makes necessary the surface modification of MSNs to achieve the desired positive charge in their surface. Althougth there is not a particular surface charge that has been shown to be the ideal, there is a consensus that a positive charge between +5 and +30 mV zeta potential before nucleic acid complexation might be necessary for ensuring efficient siRNA encapsulation and delivery.

Different cationic polymers have been grafted to nanoparticles surface for nucleic acids transport and delivery. Poly(allylamine hydrochloride) is one of the cationic polymers that has been used for nucleic acids complexation on the MSN surface enhancing the transfection efficiency.[29] Poly-2-dimethylaminoethyl methacrylate is another alternative polymer that was demonstrated to enhance transfection efficiency. Though this polymer is cytotoxic on its own, its toxicity is reduced when it is grafted to the MSNs surface.[30] Other ways to introduce a positive charge on the MSN surface different from cationic polymers are to conjugate small molecules. For example, it has been used aminopropyltriethoxysilane to impart a positive charge to the MSNs surface through its amine group.[29] Furthermore, it has been used amine functionalized lipids or positively charged lipid bilayers to confer the positive charge to the MSNs surface.[29]

PEI is considered one of the most successful and widely used gene delivery polymers due to its membrane destabilization capability, high positive charge density which permits DNA condensation, and its ability to protect nucleic acids from enzymatic degradation.[18] PEIs are synthetic cationic polymers that compact DNA and siRNA into complexes that are effectively taken up in cells to make nucleic acid delivery and gene therapy possible. As it has been mentioned before, PEI could be used itself as a siRNA delivery vehicle, but high cytotoxicity was observed.[18] In a different approach, PEI can be attached to nanoparticles surface either through covalent or electrostatic interactions to confer them the capability of transporting siRNA constructs. In this regard, MSNs coated with PEI have been reported to be biocompatible, showing much less cytotoxicity to cells than the PEI-siRNA complexes mentioned above.[27]

Additionally to the capability of carrying, protecting, and releasing nucleic acids, PEI also enhance the particle uptake. Due to its cationic nature, PEI confers a positive charge to the nanoparticles surface, being easier for the negatively charged cell membrane to endocyte the positively charged nanoparticles. Moreover, PEI is known as endosomal escape agent, due to a proton-sponge effect, being this fact crucial for the delivery of the biomolecules to the cytoplasm. The large number of amine groups on each PEI polymer confers the nanoparticles with protonable groups under acidic conditions. Once the nanoparticles are inside the endosomes after endocytosis, at the endosomal low pH, the protonable groups acquire a high positive charge, which would tend to be neutralized by the entrance of chloride anions. These osmotically active

ions enter the endosomes accompanied by water, making the endosome swell until it bursts, releasing the nanoparticles in the cytoplasm.[31]

Here we have chosen PEI as cationic polymer for MSNs grafting in order to enhance the particle uptake into cells[27,28] and facilitate endosomal escape for the nucleic acid delivery.[32]

3.1.4 Aims

The objective of this chapter was to engineer a system based on mesoporous nanoparticles that can effectively boost bone formation to become a potential alternative to the current treatments for osteoporosis.[33] This work was carried out within the frame of the European Research Council proposal "VERDI" ("polyValent mEsopoRous naosystem for bone DIseases"). According to VERDI AdG-ERC proposal, the objective of the project coulds be stated as follows:

"The aim of this proposal consists of developing a versatile polyvalent system that can be adapted to the treatment of three situations of clinical relevance in bone pathology: bone infection, cancer in bone (primary tumors and bone metastases) and osteoporosis. To achieve this goal, we proposed to design a nanosystem that will incorporate a series of common elements based on cutting edge technology that will be easily translated to a high-scale manufacturing level"

In particular, this PhD thesis is focused in the osteoporosis treatment, being the main objective of this chapter to develop a system based on MSNs that can effectively bind and deliver siRNAs in an attempt to deal with the disease from a genetic point of view.

Although the use of MSNs for siRNA delivery has been studied before,[29,34,35] this is the first time that they will be used for osteoporosis treatment. One of the possibilities to provide the MSNs the capability of transporting siRNAs is by grafting their surface with cationic polymers as PEI. However, high molecular weight PEI has been reported to be toxic for some cells.[36] So, the initial aim consisted on finding the optimum PEI molecular weight to bind the maximum amount of siRNA without compromising the viability of cells.

The second objective of this chapter was to overcome another drawback of free siRNAs, their poor penetration capacity through cell membranes, using nanocarriers to deliver siRNAs inside the cells. It is important that the delivery process might not affect the cargo properties, so it was necessary to verify that siRNA knock-down capability should be maintained after being loaded and released from MSNs. To demonstrate this fact, it was necessary to have a cell line that overexpress SOST gene. In this sense, mouse embryonic fibroblasts (MEFs) have been reported to generate detectable levels of SOST expression in certain conditions.[16] Then, the third objective was to find and optimize the best conditions to obtain a cell model with increased levels of SOST expression to evaluate the silencing capacity of the system. After the *in vitro* validation of the

system, the next step was the *in vivo* evaluation in a reduced bone mass model. In this sense, the last aim of this chapter was to confirm the effectiveness of the here developed platform for knocking down SOST gene after one injection in the femur bone marrow of ovariectomized mice.

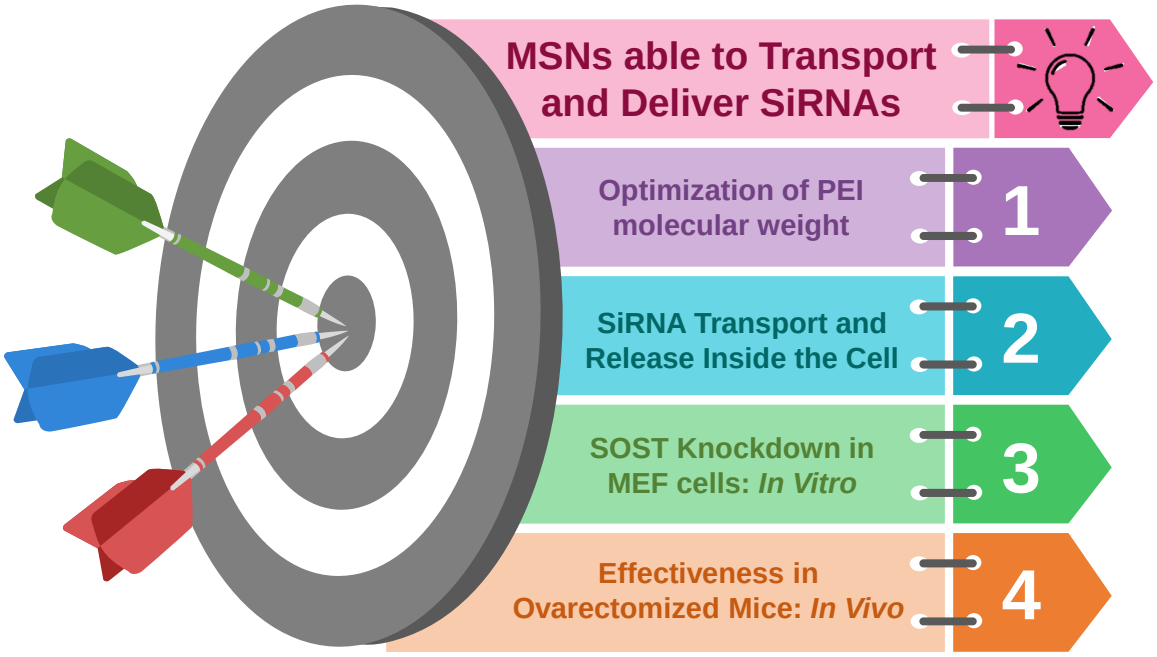

Figure 3.3 Schematic representation of Chapter III aims.

3.2 MSNs Grafting Optimization and Effective Loading and Delivering of SOST SiRNA inside Cells

This first piece of research consisted in developing a drug delivery system using mesoporous silica nanoparticles as carrier.

Mesoporous silica nanoparticles with diameter of *ca.* 150 nm and mesopores of 2 nm were synthesized following a modification of the Stöber method.[37] The experimental details were described in the Methods section in chapter 2. During the synthesis process, the external surface of the nanoparticles was functionalized with phosphonate groups, to provide the strong negative charge needed to coat them afterwards with the cationic polymer. The polymer grafting was explored using PEIs with different molecular weights (5, 8 and 10 kDa) and different MSNs:PEI ratios (1:1 and 1:0.5), to optimize the siRNA loading.

The aim of covering the surface of MSNs with PEI was to provide them with the ability to bind siRNA. However, depending on the molecular weight employed, PEI could damage the cell membrane, mitochondria and lysosomes.[36,38] While low molecular weight PEI is not cytotoxic, these polymers are ineffective at transfecting nucleotides in contrast to the high molecular weight PEI. However, high molecular weight PEI has shown cytotoxicity in cells. In this regard, it has

been demonstrated that the size, compactness, and chemical modification of PEI affect the efficacy and toxicity of the polymer.[36] PEI cytotoxicity occurs via a proton sponge effect, as mentioned before, it involves proton sequestration by the polymer surface that leads to intense proton pump activity inside the cell, osmotic swelling of the endocytic compartment, endosomal rupture, and finally cell death by a mitochondrial-mediated mechanism. It has been demonstrated that the reduction of the polymer size is capable of scaling back the cytotoxic effect of the polymer. Therefore, optimization of PEI coating with different molecular weights PEI was the first task to accomplish.

The PEI coating was confirmed through Transmision Electron Microscopy (TEM). To determine the presence of organic matter in the nanoparticles, a negative stain with phosphotungstic acid was performed. Phosphotungstic acid is electron dense, *i.e.* opaque for electrons and it links to organic matter, therefore, the stained-layer covering the surface of PEI functionalized nanoparticles that could be appreciated in Figure 3.4 confirmed the coating. TEM also showed that the nanoparticles were spherical, monodispersed and with a diameter around 150 nm.

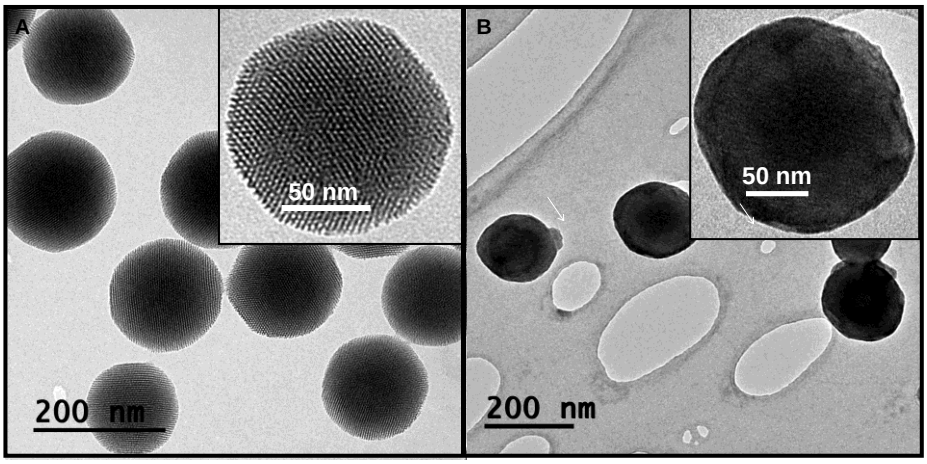

Figure 3.4 PEI grafting to MSNs surface. TEM micrographs of the nanoparticles (A) before and (B) after coating with 5 kDa PEI polymer. The nanoparticles before coating did not present the stain-layer, compared to the nanoparticles after coating. Phosphotungstic acid presented affinity to the organic polymer, a black stain layer appeared onto the nanoparticles confirming the proper PEI grafting. More detailed micrographs could be appreciated in the insets, nanoparticles with a diameter around 150 nm were represented. Adapted from Ref 33 with permission of ACS.

For the evaluation of the correct PEI coating, the surface charge was measured and compared between naked and functionalized nanoparticles (Figure 3.5). The nanoparticles before PEI grafting presented a strong negative zeta potential of −21.5 mV at pH = 7, due to the presence of phosphonate groups in the surface. This value, after the polymer coating, was shifted to strong positive, 31 mV at pH = 7, due to the presence of the amino groups of the cationic PEI coating. Different molecular weights (5 kDa, 8 kDa, and 10 kDa) were used for the future optimization of siRNA loading. In this case we could confirm that the values of zeta potential were similar between the different PEIs.

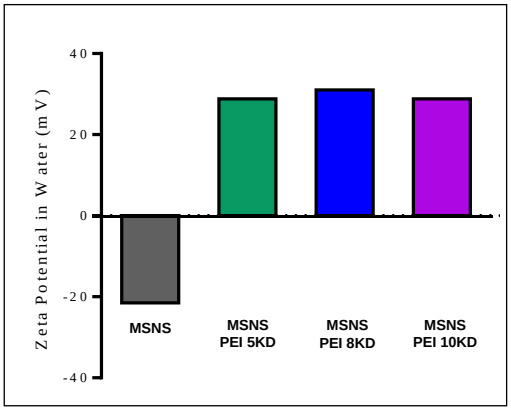

Figure 3.5 Zeta potential before and after coating with 5, 8, and 10 kDa PEI polymer. Adapted from Ref 33 with permission of ACS

The particle size could also show if the grafting was performed successfully. In this sense, the particle size should increase after grafting the polymer to the nanoparticles. The particle sizes and size distribution graphics are showed in the Figure 3.6. As it can be appreciated, after the polymer coating, the size of the nanoparticles slightly increased, and it was not modified after binding the siRNA molecule. Both data indicate that the PEI grafting was successfully performed. It can also be appreciated that the nanoparticles present a narrow size distribution, indicating that the nanoparticles were homogenous and monodispersed.

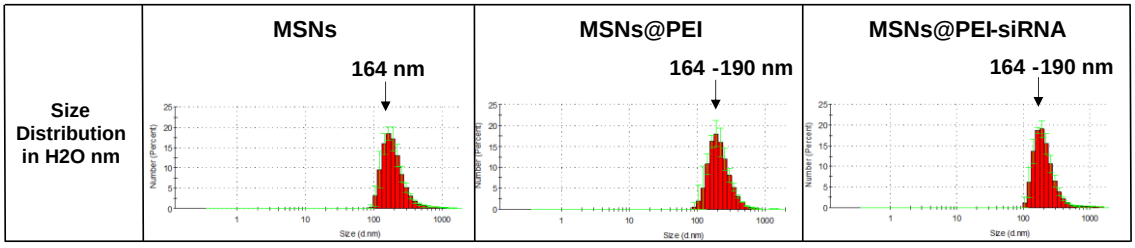

Figure 3.6 Particle size and size distribution graphics of MSNs, MSNs coated with PEI, and MSNs coated with PEI and bound with siRNA. Adapted from Ref 33 with permission of ACS.

In the Fourier Transform Infrared (FTIR) spectra we could observe the presence of silica and after coating. The presence of the typical vibration bands of silica (490-1090 cm^{-1} Si-O-Si and 1700 cm^{-1} of Si-OH) in both naked and coated nanoparticles confirms the silica frame of the nanoparticles. The Si-O-Si vibration bands confirmed the proper hydrolysis, condensation and subsequent polymerization of the silica precursors during the synthesis, leading to a network of Si-O-Si bonds as backbone. In addition, the Si-OH bands confirmed the expected presence of silanol groups on surface of MSNs. After PEI grafting, new bands related with the presence of PEI appeared (3500 cm^{-1} stretching (δ) vibrations of -NH- groups; 2900-2800 cm^{-1} C-H from CH_2 and CH_3 groups; 1600-1400 cm^{-1} bending (ν) vibrations of -NH- groups) confirming the functionalization processes (Figure 3.7A).

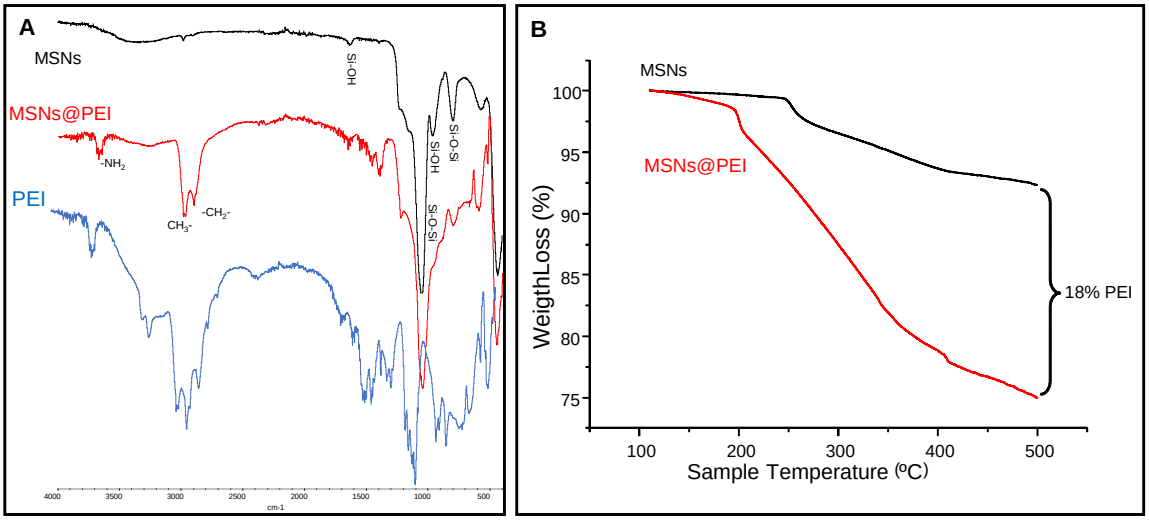

Figure 3.7 Physicochemical characterization of MSNs and PEI coated MSNs. The nanoparticles before and after coating with 5 kD PEI polymer were characterized by (A) Fourier Transform Infrared spectroscopy (FTIR), (B) thermogravimetric analysis (TGA), Adapted from Ref 33 with permission of ACS.

For evaluating the amount of polymer grafted onto the nanoparticles, Thermogravimetric Analysis (TGA) assays were carried out confirming and quantifying the amount of organic matter in the coated nanoparticles. By this technique the organic matter present in the sample would be burned increasing gradually the temperature. Therefore, we were able to determine the percentage of organic matter lost at every temperature point and correlate it with the polymer added to the nanoparticles. It showed that 18% of the weight was organic matter, which corresponds to PEI matrix (Figure 3.7B).

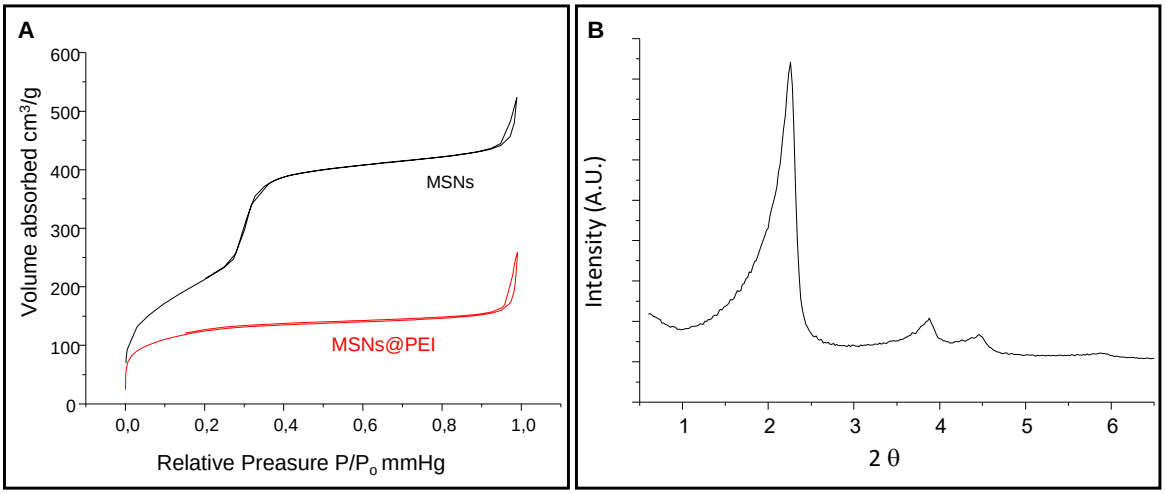

Figure 3.8 Physicochemical characterization of MSNs and PEI coated MSNs. The nanoparticles before and after coating with 5 kD PEI polymer were characterized by (A) N_2 adsorption and (B) X-ray diffraction (XRD). Adapted from Ref 33 with permission of ACS.

Nitrogen absorption analyses confirmed the porous structure of the material as it can be appreciated in the isotherm graphic (Figure 3.8A). By the same technique we were able to evaluate the size of the mesopores (*ca.* 2.5 nm before coating, and 1.35 nm after coating) and the reduction

of the surface area, from 818 m^2/g in MSNs to 427 m^2/g in MSNs@PEI which also confirmed the successful polymer coating of the nanoparticles. The characteristic mesostructure of the MCM-41 type nanoparticles survived the functionalization process as revealed through low-angle XRD where the characteristic diffraction maxima of the 2D hexagonal symmetry were obtained (Figure 3.8B). These data confirmed that the external surface of the particles was successfully grafted with the polymer.

The optimization of PEI coating was the first task to accomplish in this work using different molecular weights (5, 8, and 10 kDa) and different MSNs:PEI ratios, 1:1 and 1:0.5 as mentioned above. The selection of the different molecular weights is based on the fact that the nanoparticles coated with 10kD PEI or even smaller molecular weight, still maintain the feature of improving the cell uptake. They preserve the membrane binding avidity and membrane wrapping efficiency, allowing these particles to penetrate into cellular endocytic compartments.[36] As mentioned before, their capacity of binding to siRNA *versus* reduction of toxicity was one of the main facts to optimize. It was evaluated using a fluorescent siRNA analog (siGLO Green Transfection Indicator), which is a fluorescent–labeled RNAi control for evaluating transfection efficiency as it provides a rapid visual evaluation.

The potential toxicity of the platforms decorated with different molecular weight PEIs was evaluated so the proper molecular weight PEI could be selected. *In vitro* cell viability of MSNs coated with different PEIs (MSNs@PEI) was evaluated by incubating different concentrations of nanoparticles (200, 100 and 50 μg/mL) with mouse embryonic fibroblast (MEF) cells for 2 hours. The media was refresh and after 48 hours of incubation the cell viability was measured. As it can be appreciated in Figure 3.9 the nanoparticles coated with 10 kDa PEI at both PEI:MSNs ratios were non-toxic at 50 μg/mL. However, while the concentration of the nanoparticles was increasing, the toxicity of them increased, reaching values of *ca.* 70% of viability. Therefore, it was found that MSNs@PEI of 10 kDa in both ratios (1:1 and 1:2) reduced the cellular viability at concentrations above 100 μg/mL. On the other hand, when we evaluated the nanoparticles coated with 8 or 5 kDa PEI, they showed no toxic effects at concentrations as high as 200 μg/mL in both ratios. This would confirm the fact stated above that by reducing the polymer size, the cytotoxicity of the nanoparticles could be reduced to be non-toxic at all. It should be noted that bare nanoparticles without PEI coating were non-toxic for MEF cells at concentrations as high as 200 μg/mL. Therefore, MSNs@PEI of 10 kDa were refused due to their toxicity, and we focused on MSNs@PEI of 5 kDa. It has been also proved that the increase of the ratio did not affect to the cell viability, therefore the selection of the proper MSNs:PEI ratio would be decided regarding the binding capacity of the siRNA.

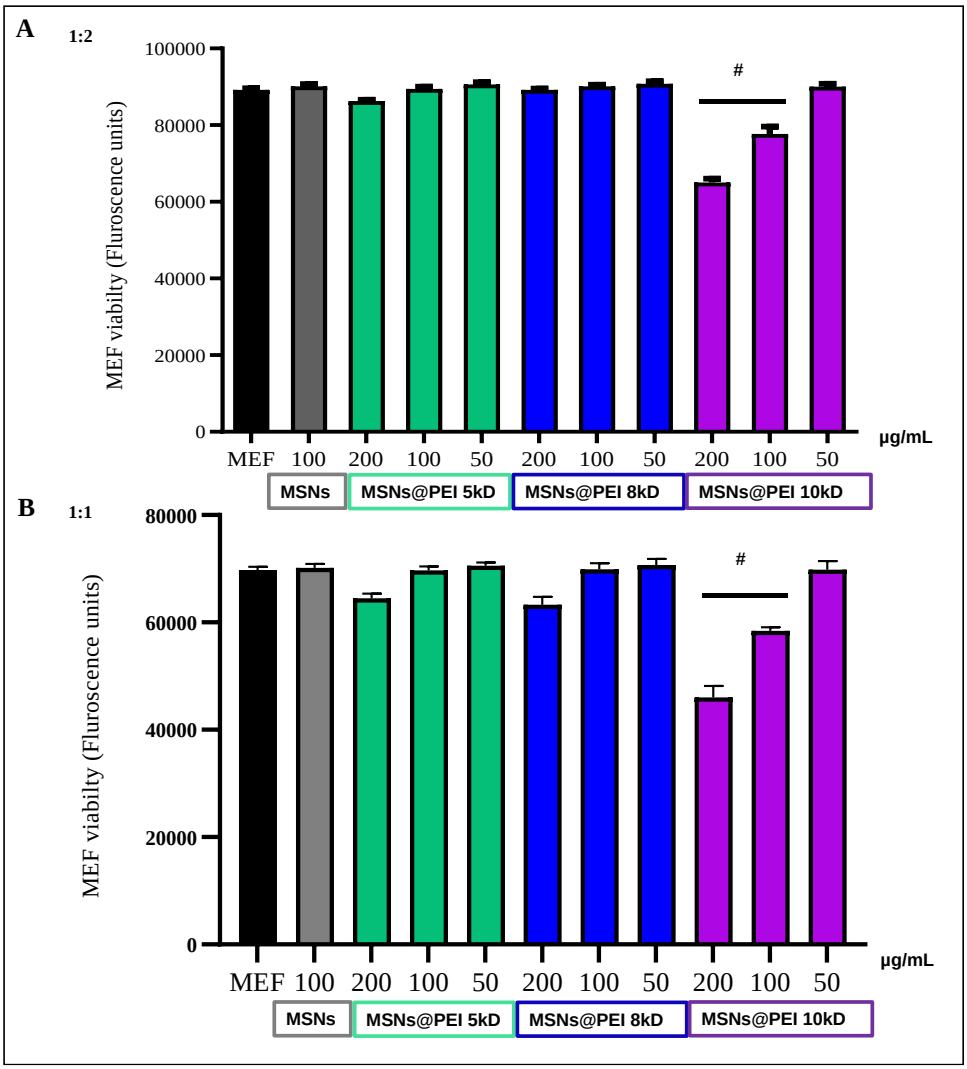

Figure 3.9 MSNs@PEI cell viability in mouse embryonic fibroblast (MEF) cells. MEF cell viability (measured by Alamar Blue) in contact with different concentrations of MSNs@PEI nanoparticles at 48 h of cell culture. (A) MEF cell viability with MSNs@PEI of 1:2 ratio. (B) MEF cell viability with MSNs@PEI of 1:1 ratio. Data are mean ± SEM of three independent experiments performed in triplicate. Hastag signs indicate $p < 0.01$ *vs* MSN, MSNs@PEI 5kD, and MSNs@PEI 8kD. Adapted from Ref 33 with permission of ACS.

The siRNA loading from MSNs@PEI was initially determined by the binding capacity of the polymeric coating towards the nucleic acid. The interaction between the positively charged NPs and the negatively charged siRNA plays an important role in the transfection efficiency of the system. The interactions should be strong enough to load the siRNA and carry it successfully into the cell, but lax enough to release it into the intracellular cytoplasm for the activation of the RNAi process in order to knockdown the desired gene. The highest amount of siRNA that could be bound to MSNs@PEI was determined by agarose gel electrophoresis (Figure 3.10). In particular, different amounts of PEI coated MSNs ranging from 0.8 to 6.4 µg (with PEI of different molecular weights and the different MSNs:PEI ratios) were dispersed with 0.1 µg of siRNA in aqueous solution to obtain nanoparticles-to-nucleic acid ratios (N/P) of 8− 64. The so-called N/P ratio, is

a mass ratio in which N and P, respectively, correspond to the mass of positive (nitrogen N (MSNs@PEI)) and negative (phosphonate P (siGLO)) charges. The ratio results from dividing the μg of nanoparticles (N) by the μg of siRNA (P). One channel was filled just with siGLO as control (ϕ). Then, these dispersions with different nanoparticle to siRNA (N/P) ratios were electrophoresed. Only the uncomplexed siGLO was able to migrate to the positive electrode and, therefore, be observed on the gel. Thus, when the band generated by siGLO is no longer visible means that all the nucleic acid has been complexed with the added nanoparticles, and that would be the optimal concentration of nanoparticles needed to complex the siGLO present. The results observed in Figure 3.10A indicates that for the PEI:MSNs ratio of 1:2, all siGLO was bound to the nanoparticles at a N/P ratio of 16 or higher (for PEI 5 kDa) and 32 or higher (for PEI 8 and 10 kDa). Thus, 16 μg of MSNs@ PEI 5 kDa were needed to load 1 μg of siGLO and 32 μg of the MSNs@PEI 8 and 10 kDa.

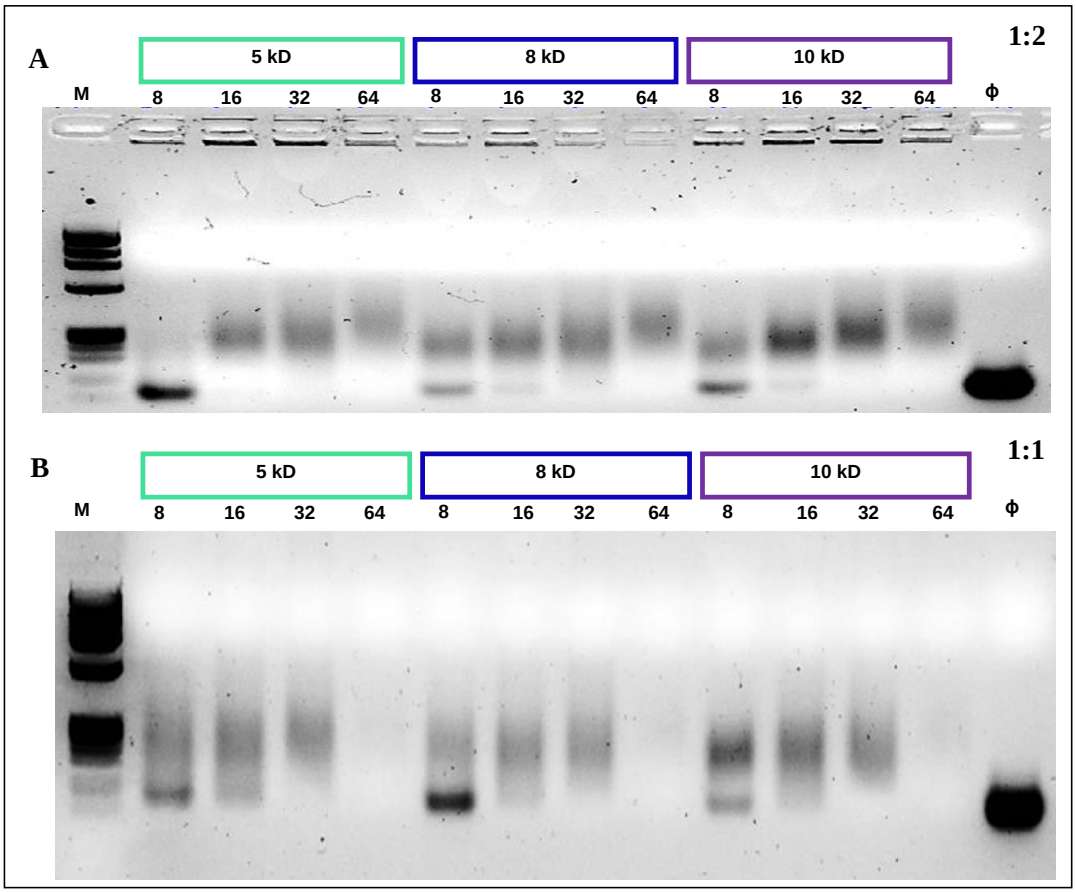

Figure 3.10 Agarose gel electrophoresis of MSNs@PEI and complexed siGLO siRNA in different N/P ratios. M: molecular weight marker. The ϕ lane contains only siRNA. After the loading of osteostatin, the N/P ratio and the electrophoretic mobility did not change. The data showed that all siRNA was bound when the N-to-P ratio was over 16 in MSNs@PEI 5 kDa, and over 32 in the case of PEI 8 kDa and PEI 10 kDa. Adapted from Ref 33 with permission of ACS.

Consequently, the siRNA loading capacity of the nanoparticles was found to be *ca.* 5 wt %. The amount of siRNA recommended by the manufacturer to achieve a proper knockdown effect was around 0.5−1 μM, *i.e.* 6.65-13.3 μg/mL. Considering that the N/P ratio obtained was 16 (16 μg of nanoparticles per μg of siRNA), therefore, we can approximate that the nanoparticle concentration should be around 106-213 μg/mL. This concentration interval is within the nontoxicity window for 5 kDa PEI regarding the data obtained in the cell viability assays. Then, the loading capacity was found to be good enough to transport the efficient amount of siRNA needed for an effective knockdown of the gene. On the other hand, for the MSNs:PEI ratio of 1:1, the binding capacity of the nanoparticles was lower, being the N/P ratio for the 5 kDa PEI 32 instead of 16. Therefore, since the cell viability almost did not change between different MSNs:PEI ratios as observed in Figure 3.9, and the binding capacity was higher for the 1:2 ratio (Figure 3.10), we decided to continue with these conditions for further studies. Also, the 5 kDa PEI resulted on the lowest cell toxicity of MSNs@PEI while maintaining the effective siRNA bind and delivery ability. Based on these results, the 5 kDa PEI was selected and further used for the next steps in our research. It is worth mentioning that the siRNA presence in the PEI mesh remained the cell viability unchanged (Figure 3.11).

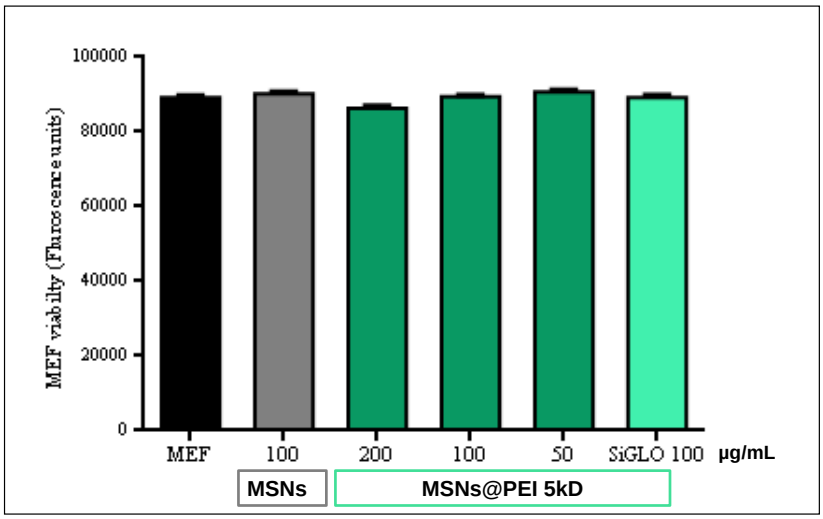

Figure 3.11 MEF cell viability (measured by Alamar Blue) in contact with different concentrations of MSNs@PEI 5kD and MSNs@PEI-siGLO at 48 h of cell culture. Adapted from Ref 33 with permission of ACS.

As stated above, PEI was selected as grafting polymer for siRNA delivery due to its capability of enhancing the particle uptake into cells and to its endosomal scape capacity due to the proton sponge effect,[39] allowing the delivery of siRNA inside cells. Therefore, the next step consisted on the evaluation of the cellular uptake of the MSNs@PEI through flow cytometry (Figure 3.12) and confocal laser scanning microscopy (Figures 3.13 and 3.14).

For the flow cytometry assay, fluorescein isothiocyanate (FITC) labeled nanoparticles coated with PEI and bound with siGLO were used. The different nanoparticles were incubated with MEF cells for 2 hours and then evaluated by flow cytometry. After coating the MSNs with PEI, the nanoparticle uptake significantly increased, which could be ascribed to the drastic change on the surface charge previously mentioned, from negative (MSNs) to positive (MSNs@PEI) as observed in the zeta potential measurements (Figure 3.5). This is in agreement with the literature, since it is easier for the cell membrane (negative) to endocyte the positively charged nanoparticles (Figure 3.12).[36]

After the binding of siGLO to the PEI coated nanoparticles, the amount of nanoparticles internalized was approximately the same as the PEI coated particles without siGLO (Figure 3.12), confirming that the presence of siRNA was not affecting the cellular internalization capacity of MSNs. Aditionally, the fluorescence intensity doubled, confirming that siGLO was inside the cells being responsible for the fluorescence intensity increase.

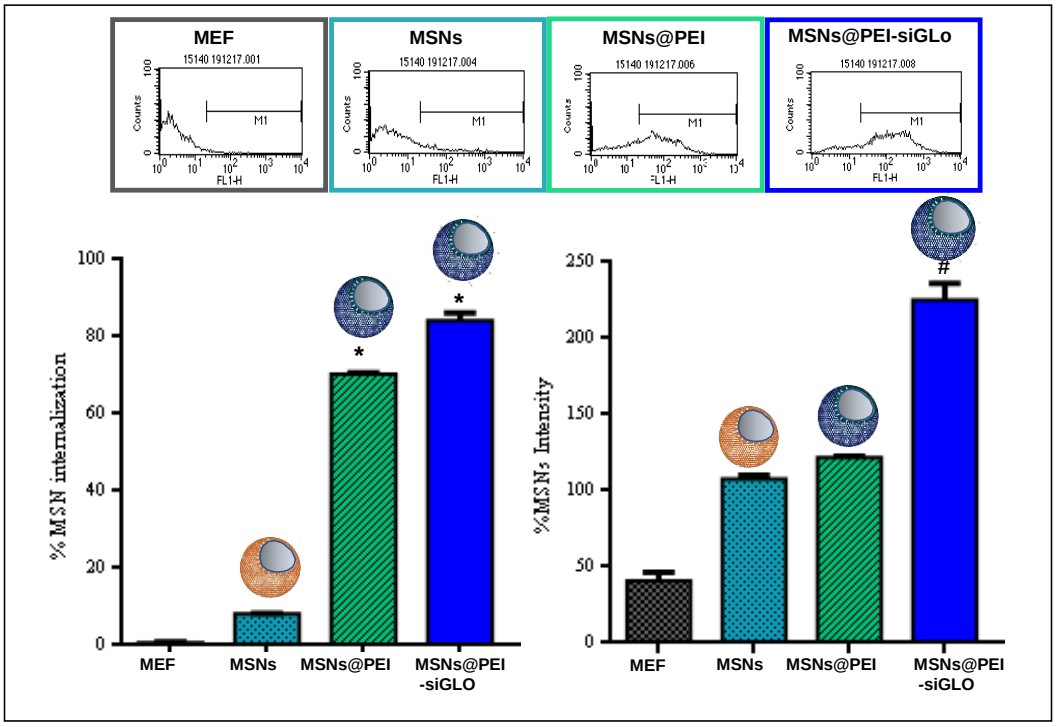

Figure 3.12 MSNs@PEI-siGLO uptake by mouse embryonic fibroblast (MEF) cells by flow cytometry. Cellular uptake of different FITC-labeled MSNs, MSNs@PEI, and MSNs@PEI-siGLO was measured by flow cytometry at 2 h of internalization in MEF cells. Representative flow cytometry images are shown on the top. Data are mean ± SEM of three independent experiments performed in triplicate. Asterisks indicate $p < 0.03$ *vs* MSN; hastag signs indicate $p < 0.01$ *vs* MSN and MSNs@PEI. Adapted from Ref 33 with permission of ACS.

The particle uptake was also evaluated by microscopy assays, both confocal and fluorescence microscopy, in order to test the internalization capacity of the different nanoparticles. For this purpose, rhodamine B-labeled nanoparticles coated with PEI and bound with siGLO (Rh-

MSNs@PEI-siGLO) were employed. In this case, the nanoparticles were labeled with a different dye than siRNA in order to distinguish them by fluorescence in the microscope. The nanoparticles were incubated with cells for 2 hours and after this time the media was refresh. Then, the cells were fixated and dyed with 4′,6-diamidino-2-phenylindole (DAPI), which binds strongly to adenine–thymine-rich regions in DNA and therefore will stain in blue the nuclei of live and fixated cells. The MSNs (red) and siGLO (green) co-localize in the cell, proving that the nucleic acid was attached to the PEI mesh at the initial stage of the experiment (Figure 3.13).

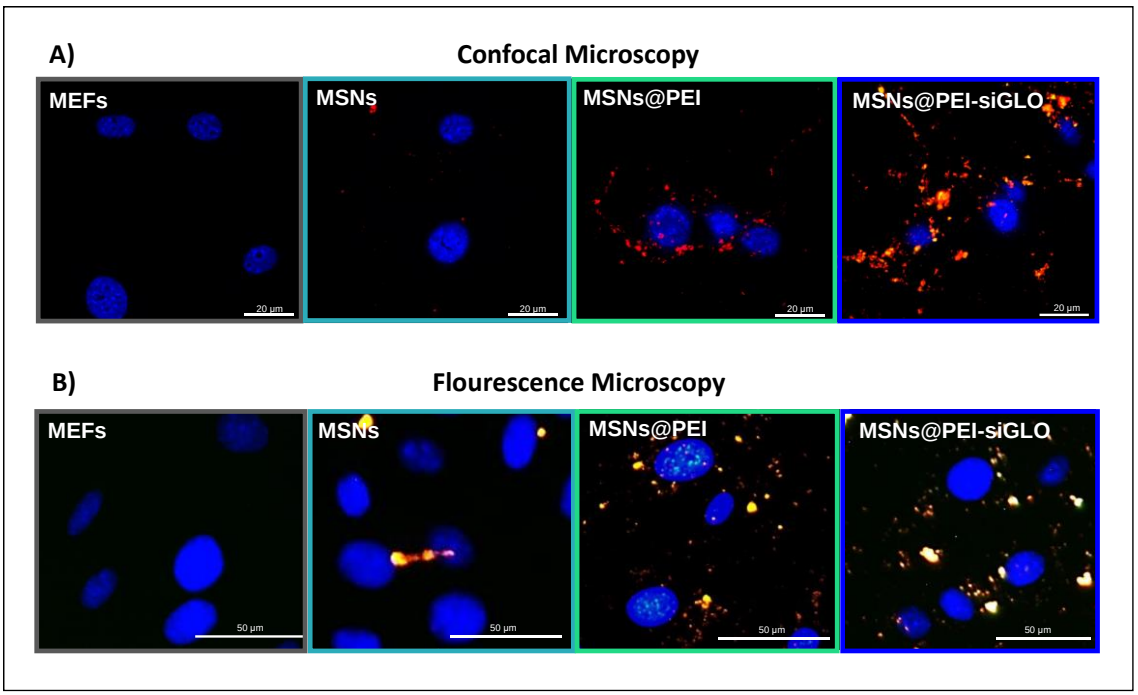

Figure 3.13 MSNs@PEI-siGLO uptake by mouse embryonic fibroblast (MEF) cells by confocal and fluorescence microscopy. (A) Representative confocal laser scanning microscopy images of MEF cells incubated with Rhodamine-B-labeled MSNs, MSNs@PEI, and MSNs@PEI-siGLO nanoparticles at 2 h of internalization. Blue fluorescence (nuclei), red fluorescence (Rh-MSNs@PEI), and green fluorescence (siGLO). (B) Representative fluorescence microscopy images of MEF cells incubated with, Rh-MSNs, Rh-MSNs@PEI and Rh-MSNs@PEI-siGLO nanoparticles at 2 h of internalization. Blue fluorescence (nuclei), red fluorescence (Rh-MSNs@PEI) and green fluorescence (siGLO). Adapted from Ref 33 with permission of ACS.

The release of siGLO from the PEI matrix was also evaluated. The Rh-MSNs@PEI-siGLO were added to the cells and after 2 h, the media, including the non-internalized nanoparticles, were removed and refreshed. At that moment (0 h), green (siRNA) and red (MSNs) fluorescence co-localize, while after 48 h, the green fluorescence started to spread, turning green the cytoplasm, which could be ascribed to the siGLO being released from the Rh-MSNs@PEI (Figure 3.14). These results confirm one of the concerns of the present approach: the ability not only to transport the siRNA, but also to release it inside the cell cytoplasm which could be considered a keystone of the present technology.

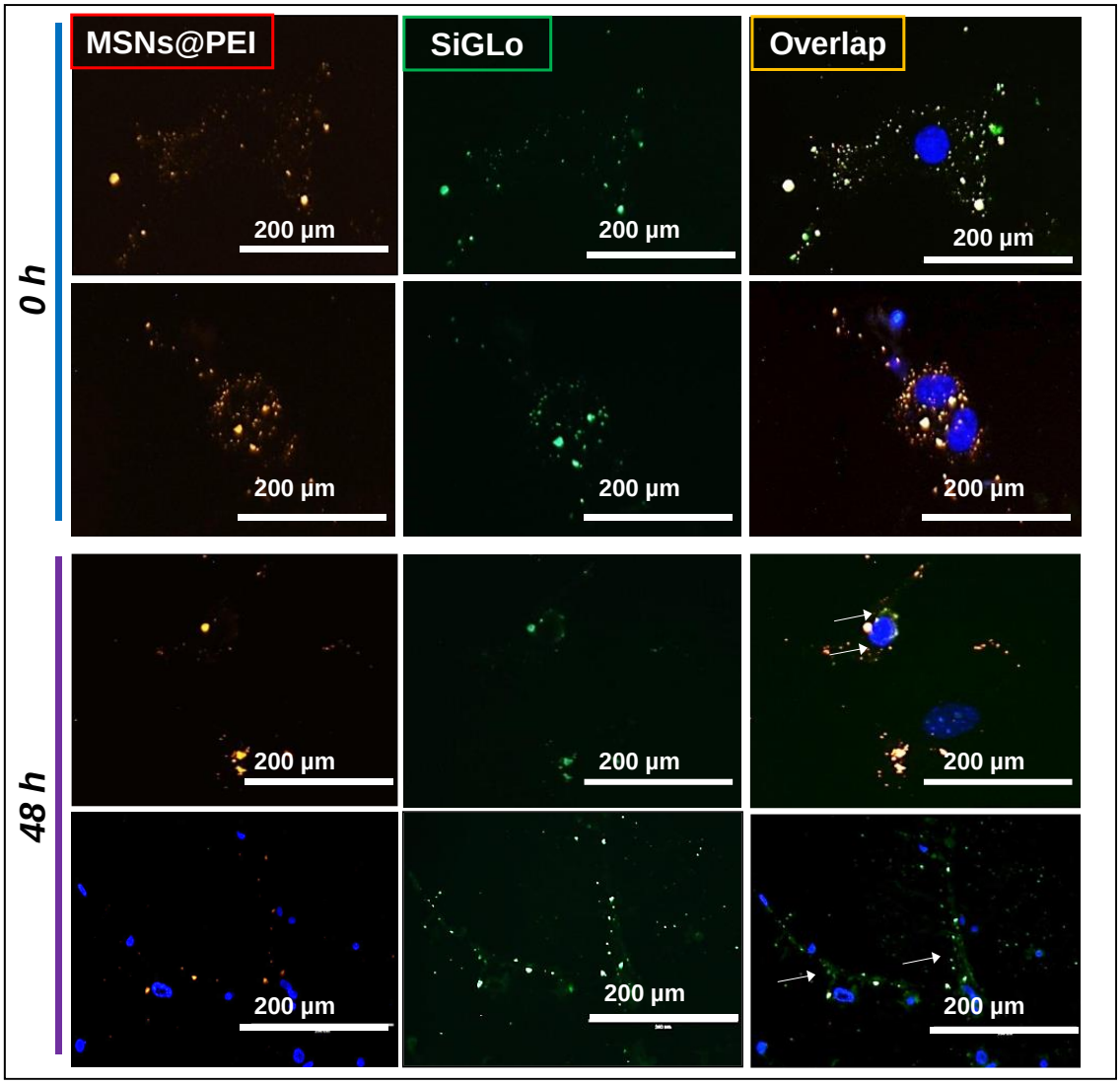

Figure 3.14 SiGLO release from MSNs@PEI in MEF cells. Representative fluorescence microscopy images of MEF cells incubated 2 h with MSNs@PEI nanoparticles with siGLO at 0 and 48 h after nanoparticle incubation. Blue fluorescence (nuclei), red fluorescence (MSNs@ PEI), and green fluorescence (siGLO). Arrows denote the siGLO released. Adapted from Ref 33 with permission of ACS.

The release kinetic of the MSN@PEI carrier was evaluated using siGLO as a siRNA model. Loaded nanoparticles were suspended in phosphate-buffered saline (PBS) and placed on a Transwell permeable support. At every time point studied, the amount of cargo released in the solution outside the transwell was determined by fluorescence. Figure 3.15 shows the release profile of siGLO from MSNs@PEI.

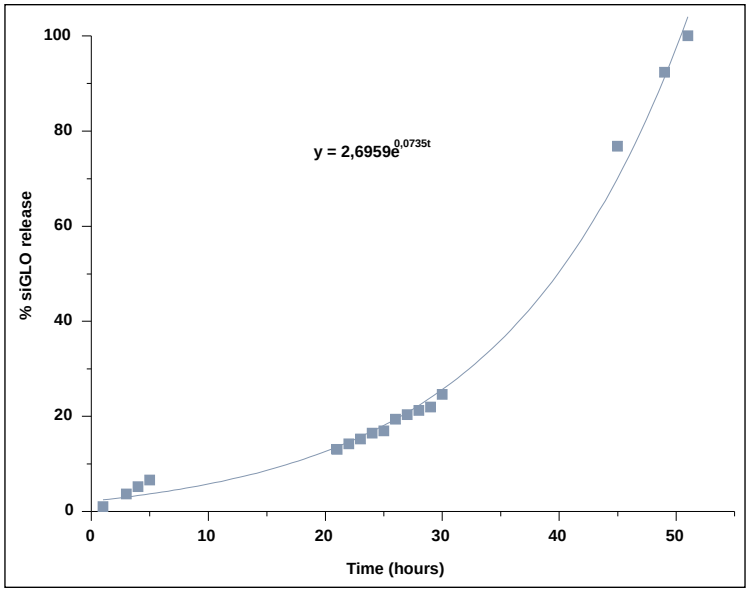

Figure 3.15 Time-dependent SiGLO release from MSNs@PEI (PEI 5kD) in PBS. Adapted from Ref 33 with permission of ACS.

SiGLO release data showed in Figure 3.15 can be fitted to an exponential model, (eq 3.1).

$$Y=(I_t/I_{max})x100=2{,}6959e^{0.0735t} \quad \text{(eq 3.1)}$$

The % of siGLO released is related to time in an exponential manner. The equation parameters could be described as Y being the % of siGLO released. This percentage is related with the siGLO fluorescence intensity. In this way, the percentage of siGLO released was $(I_t/I_{max})100$, being I_t defined as the florescence intensity of released siGLO at certain time point (t); Imax as total siGLO fluorescence signal obtained after repeated PBS washing during more than 60 hours (considered as 100%). The release data showed that at the beginning, only a small amount of the cargo was released (around 20% of the cargo after 24 h), possibly due to the strong interactions between PEI and siRNA.[17] However, over 80% of the cargo was released after 48 h as a consequence of the reduction of the electrostatic interaction between siGLO and the cationic mesh. This release delay would provide the system with the necessary time to arrive to the target area (osteoporotic bone) before releasing the cargo, providing the protection that siRNA needs around system circulation.

3.3 *In Vitro* Evaluation of MSNs@PEI-SiRNA Knockdown Capability

The final purpose of this research is to reduce the expression levels of SOST gene, in order to decrease the amount of sclerostin secreted by the osteocytes which will inhibit the Wnt/β-catenin pathway. Since SOST gene is mainly expressed by osteocytes *in vivo*, and osteocyte-like cell lines (such as, MLO-Y4 cells) express low to undetectable levels of this gene,[40] it was necessary to find a cell line which express noticeable levels of SOST to validate the silencing capacity of our

approach *in vitro*. In particular, it has been reported that MEFs generate detectable levels of SOST expression.[16] Thus, we cultured MEFs for 3 weeks and evaluated the levels of SOST expression by real-time quantitative reverse transcription polymerase chain reaction (qRT-PCR). This technique is a major development of PCR technology which allows a reliable detection and measurement of products generated during each cycle of PCR process. In our case, we wanted to measure mRNA, therefore it was necessary a first step to obtain the cDNA from the mRNA samples, with the retro-transcriptase enzyme. After this first step, the PCR was performed to detect the cDNA templates (amplicons). PCR is a method where an enzyme, thermostable DNA polymerase, amplifies a short specific part of the DNA amplicon in cycles. In every cycle, the number of short specific sections of DNA is doubled, leading to an exponential amplification of targets. After performing the qRT-PCR we observed increased levels of SOST expression detectable after 3 days, which were increased up to 20-fold after 14 days (Figure 3.16).

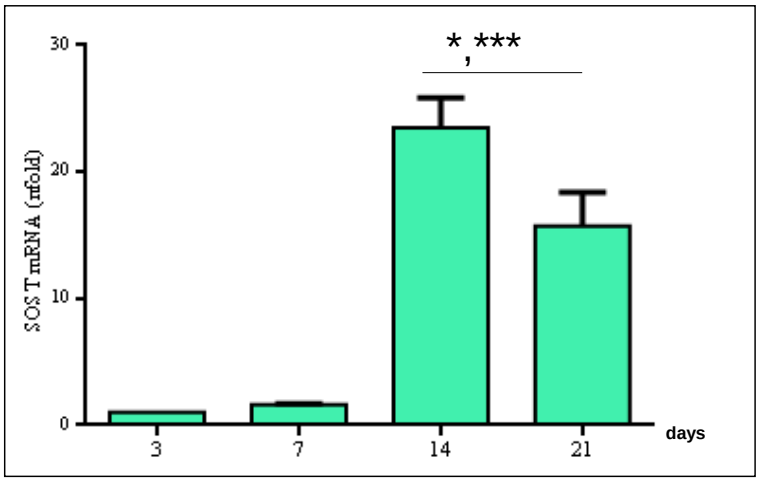

Figure 3.16 Changes in SOST mRNA levels in MEF cells. SOST gene expression (measured by real-time qRT-PCR) in MEF cells at different days. Data are mean ± SEM of three independent experiments performed in triplicate. Single asterisks indicate $p < 0.01$ *vs* 3 days; triple asterisks indicate $p < 0.001$ *vs* 3 and 7 days. Adapted from Ref 33 with permission of ACS.

It was also observed that as SOST mRNA levels lessened after the 14th day, the expression of two osteoblastic differentiation markers, Runx2 and Alp, increased (Figure 3.17), reaching higher values at day 21. As mentioned above, SOST gene is involved in different developmental processes, particularly, inhibits osteoblastic activity and differentiation, therefore modulates bone formation. Then, when cells differentiate, SOST expression falls and decreases to lower values. On the other hand, different genes like Runx2 or Alp, known as osteogenic markers,[16,41] increased their expression. The results obtained by qRT-PCR are in agreement with this statement.

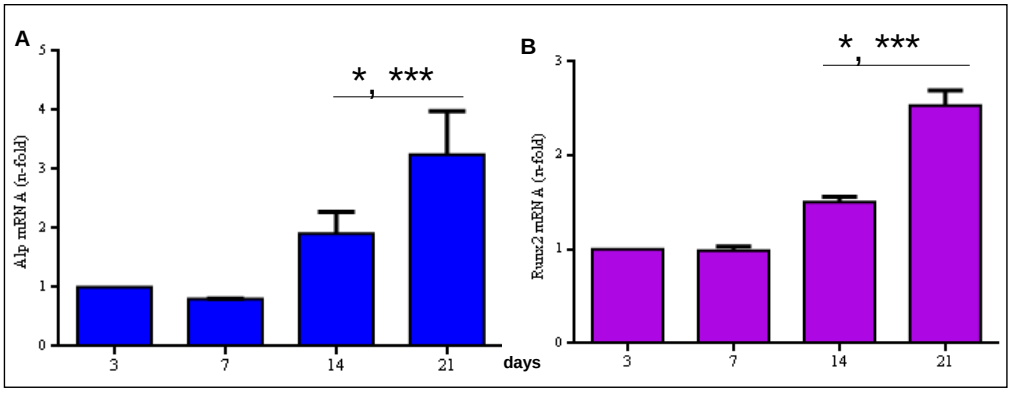

Figure 3.17 Changes in Runx2 and Alp mRNA bone osteogenic markers in MEF cells. (A) Alp, (B) Runx2 gene expression (measured by real-time qRT-PCR) in MEF cells at different times. Data are mean ± SEM of three independent experiments performed in triplicate. Single asterisks indicate $p < 0.01$ *vs* 3 days; triple asterisks indicate $p < 0.001$ *vs* 3 and 7 days. Adapted from Ref 33 with permission of ACS.

In consequence, MEFs provides an *in vitro* system in which SOST is greatly expressed after 2 weeks of incubation without the necessity to expose the cells to any osteogenic inductors. This system would permit us to validate our approach evaluating the SOST knockdown efficiency by the specific siRNA. In addition, the modified expression of osteogenic markers as well as SOST gene in MEF cells permits its use to evaluate the impact of SOST knockdown on bone osteogenic marker genes.

After optimizing a cell model for evaluating the knockdown capability of MSNs@PEI-siRNA, it was necessary to evaluate the free siRNA capacity to silence *in vitro* SOST gene in the MEF model. The transfection of SOST siRNA to MEF cells was evaluated after 14 days of incubation in DMEM. That period of time was selected after the previous experiment, in which the maximum expression of SOST in MEF cells was observed after 14 days of culture, so the potential silencing effect would be easier to detect. SiRNA transfection was promoted using Accell siRNA delivery media (free from BSA, which inhibit the transfection of free Accell siRNA). qRT-PCR was used to evaluate SOST expression after 2 h of transfection at day 14 of cell culture. In this case, a pair of controls were used to optimize the experiment: a negative control siRNA (SiCtl) ("non-targeting control", which targets a site that is absent in human, mouse, and rat genomes), as well as positive control (PosControl) ("GAPD control", which targets GAPDH, a gene common between human, mouse, and rat). SiCtl is necessary to verify that the silencing resulted from a sequence-specific process, and it is not due to a nonspecific effect. In contrast, PosControl targets a housekeeping gene, which means that the target gene is expressed in all cell types at a level that does not fluctuate with cell cycle. In this sense, PosControl would verify the efficiency of siRNA delivery into cells. It was also used an untreated-siRNA control (MEF) to determine a baseline of target gene level (Figure 3.18).

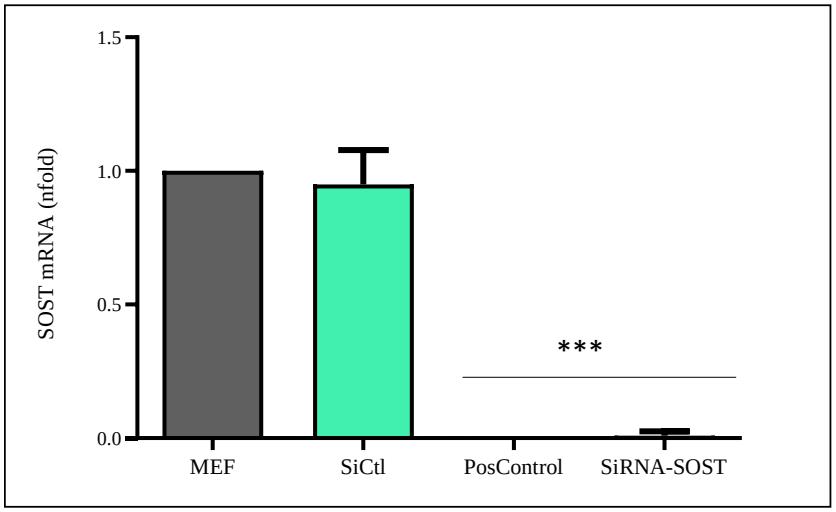

Figure 3.18 SOST gene expression knockdown in presence of SiRNA-SOST in MEF cells. SOST mRNA expression (measured by real-time qRT-PCR) in MEF cells after 14 days of cell culture. A Negative control siRNA (SiCtl) and positive control (PosControl) were used. Data are mean ± SEM of 3 independent experiments performed in triplicate. Triple Asterix indicate p<0,001 *vs* MEF control cells. Adapted from Ref 33 with permission of ACS.

After evaluation of the gene expression levels (Figure 3.18), it was found that when treating the cells with the SiCtl, SOST expression was very similar to the untreated control (MEF). Instead, after applying the PosControl, SOST expression decreased to significantly lower levels, confirming that siRNA transfection was carried out successfully. The data obtained showed that the expression of SOST decreased notably (*ca.* 98%) after treatment with SOST siRNA, verifying its functionality and the utility of the *in vitro* model to assess the capability of our nanoparticles to transfect SOST siRNA into cells.

After confirming the siRNA activity, the efficacy of SOST siRNA delivered by MSNs@PEI was evaluated in MEFs. In this case, the MSNs would be the transfection vector, so it was not necessary to use the Accell siRNA delivery media; hence, DMEM was used instead. At day 14 of culture, MSNs@PEI dispersion bound with siRNA were added to the cells, and after 2 h, the media were refreshed. Considering the amount of siRNA bound to the nanoparticles as well as the nanoparticles internalized inside the cells, we could approximate the amount of siRNA delivered to the cells, assuming that all the siRNA loaded would be released. A total of 600 µL of a 115 µg/mL MSNs@PEI dispersion bound with 15 µL of 20 µM of siRNA was added to cells, *i.e.* 70 µg of nanoparticles loaded with 4 µg of siRNA were administrated. The 80% of the loaded nanocarriers were internalized as observed by flow cytometry in the internalization assay (Figure 3.12). Therefore, 56 µg of nanoparticles were taken up, and 3.2 µg of siRNA were released into cells. This approximated amount of siRNA would be the responsible of the effect produced by our loaded nanoparticles.

After 48 h, SOST-mRNA was measured using qRT-PCR. MEFs transfected with SOST siRNA presented a significant reduced expression of SOST compared to the negative control (MSNs@PEI SiCtl) (*ca.* 95%) as well as the untreated-siRNA control (MSNs@PEI MEF) (Figure 3.19). The results obtained with our nanosystem were quite similar to the ones obtained in the previous assay, therefore our nanoparticles achieved a knockdown capacity as effective as the one obtained by the Accell siRNA transfected with the Accell siRNA delivery media. Our nanoparticles would act as a transfection vector, making unnecessary the application of an Accell siRNA delivery media.

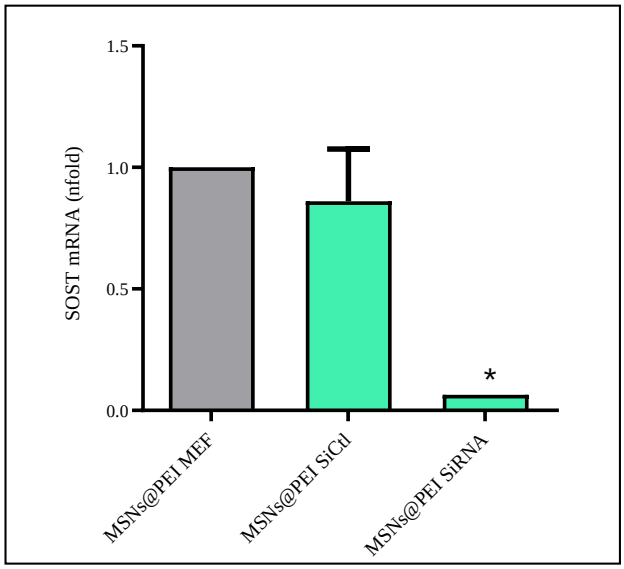

Figure 3.19 SOST gene expression in the presence of SiRNA-SOST bound to MSNs@PEI in MEF cells. SOST mRNA expression (measured by real-time qRT-PCR) in MEF cells at day 14th of cell culture. A negative-control siRNA (SiCtl) was used. MSNs@PEI nanoparticles bound to SiCtl (MSNs@PEI SiCtl). Data are mean ± SEM of three independent experiments performed in triplicate. Asterisks indicate $p < 0.01$ *vs* MSNs@PEI MEF control cells. Adapted from Ref 33 with permission of ACS.

Osteogenic markers gene levels (Runx2 and Alp) were also measured to determine the impact of SOST down-regulation (Figure 3.16). As it has been mentioned above, SOST is a gene involved in cell differentiation inhibition, so its knockdown is expected to increase the expression of these osteogenic markers.

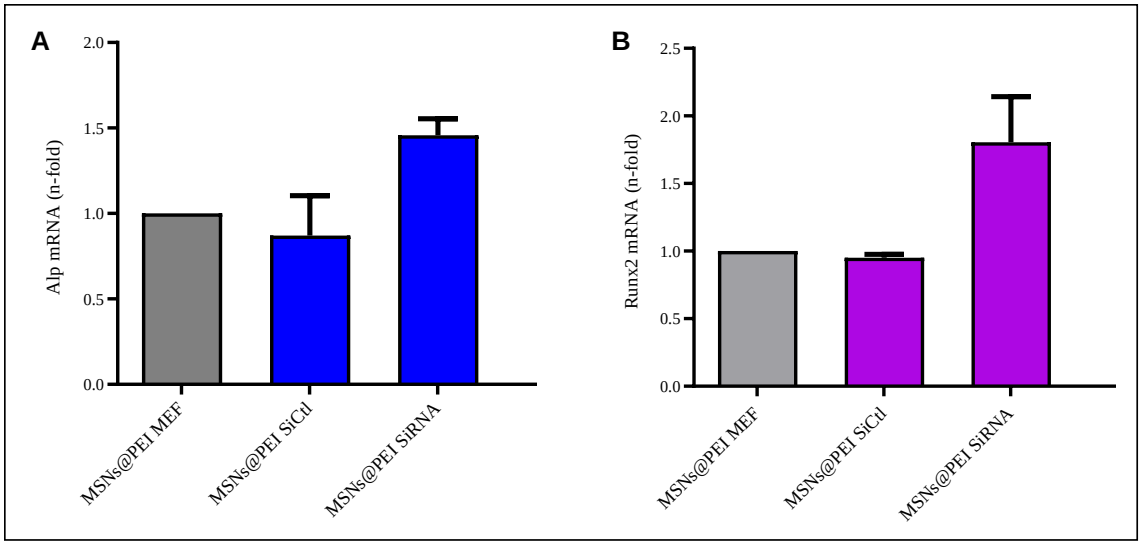

Figure 3.20 Runx2 and ALP gene expression in the presence of SiRNA-SOST bound to MSNs@PEI in MEF cells. (A) Alp and (B) Runx2 mRNA expression (measured by real-time PCR) in MEF cells at day 14th of cell culture. A negative-control siRNA (SiCtl) was used. MSNs@PEI nanoparticles bound to SiCtl (MSNs@PEI SiCtl). Data are mean ± SEM of three independent experiments performed in triplicate. Adapted from Ref 33 with permission of ACS.

The data showed, that when SOST was knocked down, the expression of the osteogenic markers increased as expected, being possibly correlated with an enhancement in cell differentiation at complex environment, such as osteoporotic bone. As it can be observed in Figure 3.20, the expression of Runx2 increased up to 2-fold and Alp up to 1.5-fold after siRNA transfection compared to empty MSNs@PEI treated MEF cells expression.

3.4 *In Vivo* Evaluation of MSNs@PEI-SiRNA Knock-down Capability and Gene Expression Modulation

After the successful *in vitro* validation of the system, the next step was the *in vivo* evaluation in a reduced bone mass model. The most frequent types of osteoporosis in humans are postmenopausal osteoporosis, disuse osteoporosis, and glucocorticoid-induced osteoporosis.[42] Therefore, in this thesis the focus was on postmenopausal osteoporosis for the animal model here evaluated. Estrogen deficiency enhances bone resorption, being the main cause of this type of osteoporosis, thus, the most popular animal model of postmenopausal osteoporosis is generated by ovariectomy. The depletion of estrogen would produce significant bone loss after at least 14 days of surgery.[43] For the evaluation of our new system, ovariectomized C57/BL6 female mice with a decreased femoral bone mineral density compared to nonovariectomized (62.98 ± 0.28 mg/cm2 *versus* 66.56 ± 0.47 mg/cm2; $p < 0.001$) were employed.[44] First, 50 μL of the complete nanocarrier (MSNs@PEI-siRNA) dispersion (0.8 mg/mL) in PBS were injected in the femur bone marrow of ovariectomized mice (Figure 3.21 left). Even-higher concentrations of this type nanoparticles have been used in different works without any toxic effects.[45–47]

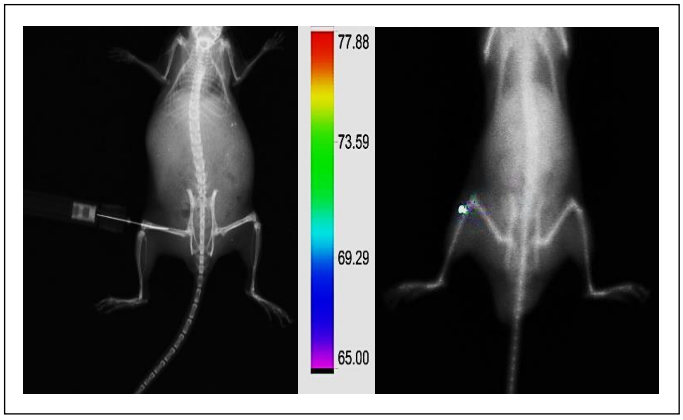

Figure 3.21 *In vivo* injection of MSNs@PEI-siRNA. Femur bone-marrow injection in ovariectomized female mice and cyanine-7 labeled nanoparticles accumulation. Color bar express the intensity of fluorescence. Adapted from Ref 33 with permission of ACS.

After 5 days, the mice were sacrificed and the femur bone was extracted and processed to analyze the gene expression. SOST, Runx2, and Alp mRNA were measured by qRT-PCR (Figure 3.22 and 3.23). Because the injection of the nanoparticles was local, *i.e.*, the nanoparticles were already at the target tissue, we did not evaluate the biodistribution of the nanoparticles in the animals, but we ensured that after 2 hours the nanoparticles remained in the injection area (Figure 3.21 rigth). It should be mentioned that the expression of SOST in ovariectomized mice (OVX) increased compared to non-ovariectomized mice (Control) and were statistically significant. However, the injection of the nanoparticles, with SOST siRNA notably decreased the expression of SOST (*ca.* 50%) (Figure 3.22).

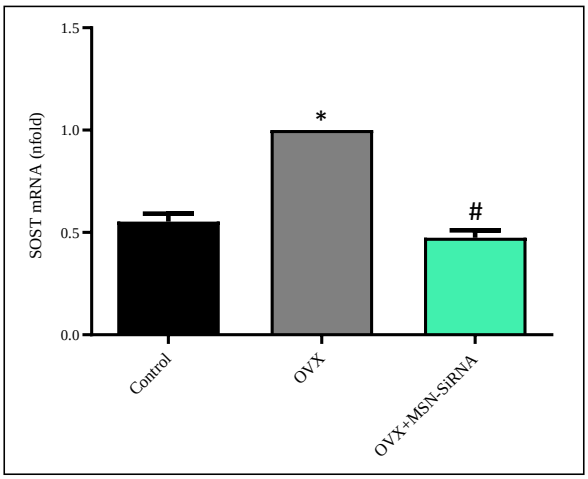

Figure 3.22 *In vivo* injection of MSNs@PEI-siRNA. SOST gene expression in the presence of SiRNA-SOST bound to MSNs@PEI in ovariectomized mice (OVX). SOST mRNA expression (measured by real time qRT-PCR) in femur bone. To optimize the experiment, one control was used: a negative control siRNA (SiCtl) ("non-targeting control", which targets an absent site in human, mouse, and rat genomes) and MSNs@PEI nanoparticles bound to SiCtl (MSNs@PEI SiCtl). Data are mean ± SEM of three independent experiments performed in triplicate. Asterix indicate $p < 0.0005$ *vs* OVX. Adapted from Ref 33 with permission of ACS.

The osteogenic markers, Runx2 and Alp, decreased their expression in OVX compared to Control group, as expected (Figure 3.23). The results also showed that Runx2 and Alp expression notably increased when SOST siRNA was released by the system (1.5-fold and 1.8-fold respectively compared with OVX), in total agreement with the previously *in vitro* results, demonstrating that our approach worked in an *in vivo* scenario (Figure 3.23).

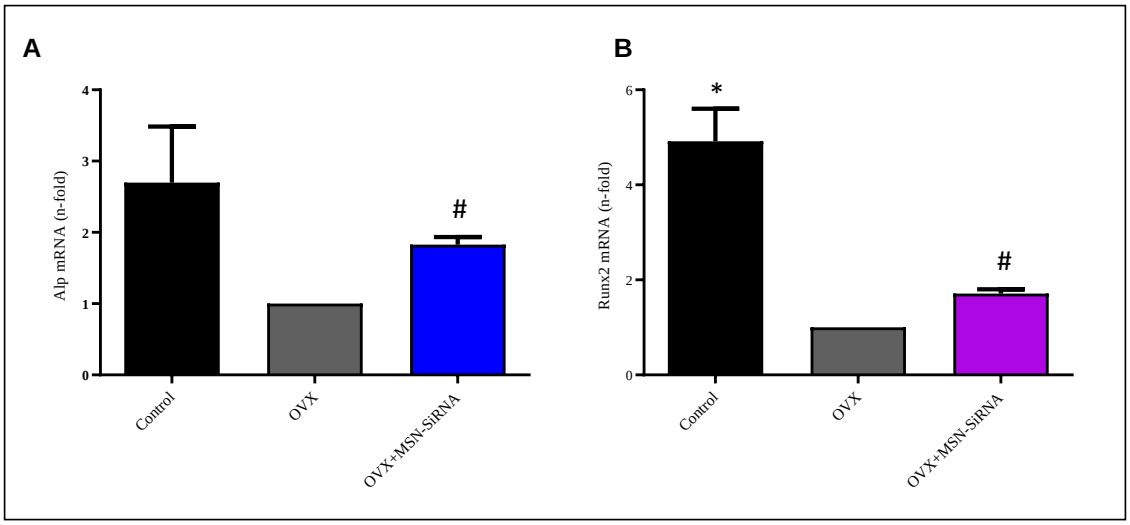

Figure 3.23 *In vivo* injection of MSNs@PEI-siRNA. Alp and Runx2 bone osteogenic markers gene expression in the presence of SiRNA-SOST bound to MSNs@PEI in ovariectomized mice (OVX). (A) Alp and (B) Runx2 mRNA expression (measured by real-time qRT-PCR) in femur bone. To optimize the experiment, one control was used: a negative control siRNA (SiCtl) ("non-targeting control", which targets an absent site in human, mouse, and rat genomes) and MSNs@PEI nanoparticles bound to SiCtl (MSNs@PEI-SiCtl). Data are mean ± SEM of three independent experiments performed in triplicate. Asterix indicate $p < 0.0005$ *vs* OVX, and pound indicate $p < 0.001$ *vs* OVX. Adapted from Ref 33 with permission of ACS.

The design of the delivery nanosystem enhanced the expression of osteogenic markers and, effectively, knockdown SOST gene through the effect of SOST siRNA *in vivo*. This system could provide a potential alternative to the current treatment of osteoporosis, empowering cell differentiation by osteogenic features.

3.5 Conclusions

Current clinical osteoporosis treatments are not able to offer a fully satisfying curative effect, so the research of new effective approaches is pursued. Gene silencing through siRNA delivery has gained great attention as a potential treatment for bone diseases. The knoc-down of osteoporotic related genes such as SOST could be an effective approach against osteoporosis. However, the main problem of using siRNAs as therapeutic agents relies on their delivery, due to their very short half-life and poor internalization capacity through cell membranes. The objective of this

work was to develop a system capable of transporting and delivering siRNA inside cells knocking down SOST gene.

We designed a system based on MSNs coated with a cationic polymer (PEI) able to transport and deliver siRNAs. We used different ratios of PEI:MSNs and different PEI molecular weights to optimize the cationic polymer coating considering siRNA loading capacity of the nanoparticles and potential cytotoxicity to cells. Regarding the PEI:MSNs ratios tested (1:1 and 1:2), we found that the 1:1 ratio presented less siRNA binding capacity compared with 1:2, while cell viability was the same. In the case of PEI molecular weights (5 kDa, 8 kDa, 10 kDa), 5 kDa PEI resulted on the lowest cell toxicity of MSNs@PEI while maintaining an effective siRNA binding capacity. Based on these results, the 1:2 ratio and 5 kDa PEI were selected and further used for the next steps in our research.

The optimized system was capable of increasing the cell uptake, being internalized around the 80% of the nanoparticles incubated with cells, overcoming another drawback of free siRNAs, poor cell membrane penetration capacity. It was also evaluated the release of the siRNA inside the cytoplasm, confirming not only the ability of the nanoparticles to transport siRNAs but also to release the siRNA loaded.

Osteocytes are the most abundant cells in bone tissue and are responsible for SOST gene expression. In face of the difficulties of finding an osteocyte *in vitro* model that expresses SOST, we had to use MEFs for our *in vitro* evaluations, which are known to generate detectable levels of SOST expression. Therefore, we optimized the conditions of MEFs cultures so we could use them as a platform to test the siRNA effectiveness.

The siRNA loaded nanoparticles were evaluated in MEFs cells, and it was concluded that they were able to deliver SOST siRNA inside cells, silencing SOST and increasing the expression levels of two osteogenic markers. After evaluation of the effect *in vitro* with promising results, the system was injected in the femoral bone marrow of ovariectomized mice, and the obtained results were in agreement with the *in vitro* experiments. Thus, it can be concluded that our system was able to transport, deliver, and transfect to cells SOST siRNA maintaining its activity and achieving an effective silencing effect. The knockdown of the gene promoted the expression of early markers of osteogenic differentiation in ovariectomized mice (Runx2 and Alp).

These promising results might lead to further investigations that would be discussed in the following chapters of this thesis. This system has demonstrated remarkable efficacy for an intra-bone marrow injection and would be the first step for the future systemic treatment approach. In consequence, this system will constitute a promising candidate as a platform for gene therapy in osteoporosis treatment.

3.6 References

1. Boyle, W. J., Simonet, W. S., Lacey, D. L. Osteoclast differentiation and activation. *Nature* 423, 337–342 (**2003**).

2. Takayanagi, H. Osteoclast differentiation and activation. *Clin. Calcium* 17, 484–492 (**2007**).

3. MacDonald, B. T., Tamai, K., He, X. Wnt/β-Catenin Signaling: Components, Mechanisms, and Diseases. *Dev. Cell* 17, 9–26 (**2009**).

4. Wang, Y. *et al.* Wnt and the Wnt signaling pathway in bone development and disease. *Front. Biosci.* 19, 379–407 (**2014**).

5. Duan, P., Bonewald, L. F. The role of the wnt/β-catenin signaling pathway in formation and maintenance of bone and teeth. *Int. J. Biochem. Cell Biol.* 77, 23–29 (**2016**).

6. Suen, P. K., Qin, L. Sclerostin, an emerging therapeutic target for treating osteoporosis and osteoporotic fracture: A general review. *J. Orthop. Transl.* 4, 1–13 (**2016**).

7. Li, X. *et al.* Inhibition of sclerostin by monoclonal antibody increases bone formation, bone mass, and bone strength in aged male rats. *J. Bone Miner. Res.* 25, 2647–2656 (**2010**).

8. Kim, S. W. *et al.* Sclerostin Antibody Administration Converts Bone Lining Cells Into Active Osteoblasts. *J. Bone Miner. Res.* 32, 892–901 (**2017**).

9. Saw, P. E., Song, E.-W. siRNA therapeutics: a clinical reality. *Sci. China Life Sci.* 63, 485–500 (**2020**).

10. Weng, Y. *et al.* RNAi therapeutic and its innovative biotechnological evolution. *Biotechnol. Adv.* 37, 801–825 (**2019**).

11. Kim, T. *et al.* Inhibition of osteoclastogenesis through siRNA delivery with tunable mesoporous bioactive nanocarriers. *Acta Biomater.* 29, 352–364 (**2016**).

12. Wang, Y., Tran, K. K., Shen, H., Grainger, D. W. Selective local delivery of RANK siRNA to bone phagocytes using bone augmentation biomaterials. *Biomaterials* 33, 8540–8547 (**2012**).

13. Cavallaro, G. *et al.* Polymeric nanoparticles for siRNA delivery: Production and applications. *Int. J. Pharm.* 525, 313–333 (**2017**).

14. Dong, Y., Siegwart, D. J., Anderson, D. G. Strategies, design, and chemistry in siRNA delivery systems. *Adv. Drug Deliv. Rev.* 144, 133–147 (**2019**).

15. Zhang, J., Li, X., Huang, L. Non-viral nanocarriers for siRNA delivery in breast cancer. *J. Control. Release* 190, 440–450 (**2014**).

16. Basha, G. *et al.* Lipid nanoparticle delivery of siRNA to osteocytes leads to effective silencing of SOST and inhibition of sclerostin in vivo. *Mol. Ther. Nucleic Acids* 5, 1–15 (**2016**).

17. Goyal, R. *et al.* Linear PEI nanoparticles: efficient pDNA/siRNA carriers in vitro and in vivo. *Nanomedicine* 8, 167-175 (**2012**).

18. Swami, A. *et al.* A unique and highly efficient non-viral DNA/siRNA delivery system based on PEI-bisepoxide nanoparticles. *Biochem. Biophys. Res. Commun.* 362, 835–841 (**2007**).

19. Mora-Raimundo, P., Manzano, M., Vallet-Regí, M. Nanoparticles for the treatment of osteoporosis. *AIMS Bioeng.* 4, 259–274 (**2017**).

20. Manzano, M., Vallet-Regí, M. Mesoporous silica nanoparticles in nanomedicine applications. *J. Mater. Sci. Mater. Med.* 29, 65 (**2018**).

21. Gisbert-Garzarán, M., Manzano, M., Vallet-Regí, M. Mesoporous silica nanoparticles for the treatment of complex bone diseases: Bone cancer, bone infection and osteoporosis. *Pharmaceutics* 12, 83 (**2020**).

22. Vallet-Regí, M., Balas, F., Arcos, D. Mesoporous Materials for Drug Delivery. *Angew. Chemie Int. Ed.* 46, 7548–7558 (**2007**).

23. Villaverde, G., Nairi, V., Baeza, A., Vallet-Regí, M. Double Sequential Encrypted Targeting Sequence: A New Concept for Bone Cancer Treatment. *Chem. Mater.* 23, 7174–7179 (**2017**).

24. Baeza, A. *et al.* Multifunctional Protocells for Enhanced Penetration in 3D Extracellular Tumoral Matrices. *Chem. Mater.* 30, 112–120 (**2018**).

25. Gisbert-Garzarán, M., Lozano, D., Vallet-Regí, M., Manzano, M. Self-immolative polymers as novel pH-responsive gate keepers for drug delivery. *RSC Adv.* 7, 132–136 (**2017**).

26. Paris, J. L., Cabañas, M. V., Manzano, M., Vallet-Regí, M. Polymer-Grafted Mesoporous Silica Nanoparticles as Ultrasound-Responsive Drug Carriers. *ACS Nano* 9, 11023–11033 (**2015**).

27. Hom, C. *et al.* Mesoporous Silica Nanoparticles Facilitate Delivery of siRNA to Shutdown Signaling Pathways in Mammalian Cells. *Small* 6, 1185–1190 (**2010**).

28. Meng, H. *et al.* Engineered Design of Mesoporous Silica Nanoparticles to Deliver Doxorubicin and P-Glycoprotein siRNA to Overcome Drug Resistance in a Cancer Cell Line. *ACS Nano* 4, 4539–4550 (**2010**).

29. Keasberry, N. A., Yapp, C. W., Idris, A. Mesoporous silica nanoparticles as a carrier platform for intracellular delivery of nucleic acids. *Biochem.* 82, 655–662 (**2017**).

30. Lin, D. *et al.* Intracellular cleavable poly(2-dimethylaminoethyl methacrylate) functionalized mesoporous silica nanoparticles for efficient siRNA delivery in vitro and in vivo. *Nanoscale* 5, 4291–4301 (**2013**).

31. Lee, H. *et al.* PEGylated polyethyleneimine grafted silica nanoparticles: Enhanced cellular uptake and efficient siRNA delivery. *Anal. Bioanal. Chem.* 400, 535–545 (**2011**).

32. Duan, H., Nie, S. Cell-Penetrating Quantum Dots Based on Multivalent and Endosome-Disrupting Surface Coatings. *J. Am. Chem. Soc.* 129, 3333–3338 (**2007**).

33. Mora-Raimundo, P., Lozano, D., Manzano, M., Vallet-Regí, M. Nanoparticles to Knockdown Osteoporosis-Related Gene and Promote Osteogenic Marker Expression for Osteoporosis Treatment. *ACS Nano* 13, 5451–5464 (**2019**).

34. Li, X. *et al.* A mesoporous silica nanoparticle - PEI - Fusogenic peptide system for siRNA delivery in cancer therapy. *Biomaterials* 34, 1391–1401 (**2013**).

35. Zhou, X. *et al.* Dual-responsive mesoporous silica nanoparticles mediated codelivery of doxorubicin and Bcl-2 SiRNA for targeted treatment of breast cancer. *J. Phys. Chem. C* 120, 22375–22387 (**2016**).

36. Xia, T. *et al.* Polyethyleneimine coating enhances the cellular uptake of mesoporous silica nanoparticles and allows safe delivery of siRNA and DNA constructs. *ACS Nano* 3, 3273–3286 (**2009**).

37. Stober, W., Fink, A. Controlled Growth of Monodispersed Silica Spheres in the Micron Size Range. *J. Colloid Interface Sci.* 26, 62–69 (**1968**).

38. Fuller, J. E. *et al.* Intracellular delivery of core-shell fluorescent silica nanoparticles. *Biomaterials* 29, 1526–1532 (**2008**).

39. Xue, H. Y., Wong, H. L. Solid lipid-PEI hybrid nanocarrier: An integrated approach to provide extended, targeted, and safer siRNA therapy of prostate cancer in an all-in-one manner. *ACS Nano* 5, 7034–7047 (**2011**).

40. Stern, A. R. *et al.* Isolation and culture of primary osteocytes from the long bones of skeletally mature and aged mice. *Biotechniques* 52, 361–373 (**2012**).

41. Kyllönen, L., D'Este, M., Alini, M., Eglin, D. Local drug delivery for enhancing fracture healing in osteoporotic bone. *Acta Biomater.* 11, 412–434 (**2015**).

42. Permuy, M., López-Peña, M., Muñoz, F., González-Cantalapiedra, A. Rabbit as model for osteoporosis research. *J. Bone Miner. Metab.* 37, 573–583 (**2019**).

43. Komori, T. Animal models for osteoporosis. *Eur. J. Pharmacol.* 759, 287–294 (**2015**).

44. de Castro, L. F. *et al.* Comparison of the skeletal effects induced by daily administration of PTHrP (1-36) and PTHrP (107-139) to ovariectomized mice. *J. Cell. Physiol.* 227, 1752–1760 (**2012**).

45. Dogra, P. *et al.* Establishing the Effects of Mesoporous Silica Nanoparticle Properties on in Vivo Disposition Using Imaging-Based Pharmacokinetics. *Nat. Commun.* 9, 1–14 (**2018**).

46. Wen, S., Zheng, F., Shen, M., Shi, X. Surface modification and PEGylation of branched polyethyleneimine for improved biocompatibility. *J. Appl. Polym. Sci.* 128, 3807–3813 (**2013**).

47. Meng, H. *et al.* Codelivery of an Optimal Drug/siRNA Combination Using Mesoporous Silica Nanoparticles To Overcome Drug Resistance in Breast Cancer in Vitro and in Vivo. *ACS Nano* 7, 994–1005 (**2013**).

Chapter IV: Mesoporous Silica Nanoparticles for Gene Silencing and Anabolic Therapy

Conserva celosamente tu derecho a reflexionar,
porque incluso el hecho de pensar erróneamente
es mejor que no pensar en absoluto
Hipatia de Alejandría

4. Mesoporous Silica Nanoparticles for Gene Silencing and Anabolic Therapy

4.1 Introduction

Nowadays, several anti-osteoporotic drugs are currently in the market, but still without the desired outcome and with several adverse effects. One of the possible approaches considered for increasing treatment efficacy is the combined use of several drugs known as combination therapy. It is hoped that the combination therapy of different anti-osteoporotic drugs could show a synergistic or additive effect leading to better treatment results.

4.1.1 Combination Therapy for Osteoporosis Treatment

Even though different drugs with anti-osteoporotic activity have been reported,[1] the magic bullet remains missing. Researchers have been seeking possible alternatives for osteoporosis treatment considering not only the design of new anti-osteoporotic drugs. Due to the complexity of diverse diseases, such as osteoporosis, it has become increasingly clear that drugs administered alone targeted to specific molecular pathways have limitations. In the recent years, combination therapy has become a more valuable option than single therapy regarding (1) the several side effects that anti-osteoporotic drugs present and combined therapy may reduce, and (2) the potency and effectiveness of the different therapies that could be increased by the application of a combination approach. A combination therapy could therefore be a potential alternative to achieve more promising results in osteoporosis remission.

There are several conventional approaches for osteoporosis treatment. In this sense, a large number of possible combinations could be obtained. Combining agents with different mechanism of action (anabolic + antiresorptive) or two or more agents with similar effect but through different pathways could be a promising strategy to confront the disease. The combination therapy should exhibit synergistic or additive anti-osteoporotic effect, but the reality has proven that not every combination shows those effects.

It has been investigated the combination of different antiresorptive drugs with disappointing results, therefore, the use of both drugs at the same time is no longer justified.[2–4] In contrast, it has been speculated that the bone-forming effect of teriparatide or abaloparatide (common anabolic drugs) could be improved by their combination with an anti-resorptive drug. This possible combination is based on the secondary stimulation of bone resorption associated with the PTH analogues treatment.[5] In this sense, the treatment with the anabolic drugs would increase bone formation, and the antiresorptive agent would decrease the associated bone resorption activation.

Several combinations of teriparatide or abaloparatide using different anti-resorptive drugs have been evaluated reaching diverse conclusions. Teriparatide combined with bisphosphonates has been widely studied. Among them, the combination of teriparatide and alendronate was proposed taking into consideration the beneficial effect of PTH to avoid the osteonecrosis typically produced by bisphosphonates.[5,6] However, the PATH trial demonstrated that BMD in patients treated with a combination of teriparatide and alendronate was not higher than those treated with the separated drugs. In fact, alendronate appeared to impair the anabolic effect of teriparatide.[7] Other combinations of teriparatide with different bisphosphonates such as risedronate have been proposed, but similar results were found.[8] In contrast, the combined administration of teriparatide with zoledronate, showed higher BMD increases in the combination treatment than with either drug alone.[9]

Teriparatide combined with other anti-resorptive agents has been also evaluated. One alternative proposed was the treatment with the combination of teriparatide and denosumab. The DATA study demonstrated that combined treatment in this case, increased BMD more than either treatment alone.[10] Other studies has been developed to evaluate the combination of teriparatide and raloxifene, showing also higher BMD increases in the combination treatment compared with single drug treatment.[11] A synopsis of the efficacy of the different osteoporosis combinations treatments is provided in Table 4.1.

Table 4.1 Effects on BMD of different osteoporotic combination therapies. Bisphophonates (BPs), Selective Estrogen receptor modulators (SERMs), Hormone Replacement Therapy (HRT), Alendronate (ALN), Risedronate (RIS), Raloxifene (RLX), Bone Mineral Density (BMD), Parathyroid Hormone (PTH), Receptor Activator of Nuclear Factor κB Ligand (RANKL)

Combination Therapy	Drugs	Effects	Ref
Antiresorptive Combination			
BPs+HRT	ALN+HRT	1-year combination therapy of ALN and HRT did not increase bone mass over HRT alone.	[2]
	RIS+HRT	RIS and HRT had a favorable effect on BMD similar to that of HRT alone	[3]
SERMs+HRT	ALN+RLX	The combination of ALN and RLX produced a greater increase in femoral neck. Although the increases in lumbar spine BMD and in bone turnover markers with combination therapy were similar to either drug alone.	[4]
Anabolic+Antiresorptive Combination			
	Teriparatide+ALN	BMD in patients treated with a combination of teriparatide and alendronate was not higher than with either treatment alone	[7]
PTH+BPs	Teriparatide+RIS	BMD in patients treated with a combination of teriparatide and alendronate was not higher than with either treatment alone	[8]
	Teriparatide+Zolendronate	Higher BMD increases were achieved with the combination treatment than with either drug alone	[9]
PTH+RANKL Antibody	Teriparatide+Denosumab	Combined treatment in this case, increased BMD more than either treatment alone.	[10]
PTH+SERMs	Teriparatide+RLX	Higher BMD increases with the combination treatment than with either drug alone	[11]

Regarding the approach of a combination therapy, the administration of the different drugs involved in the treatment should be taken under consideration. The different combinations proposed present diverse administration routes.

In the cases of the administration of two different antiresorptive drugs stated above, both agents were administrated orally. ALN and RIS were administrated by a 10 mg/day and 5 mg/day cellulose film-coated tablet. The administration of the drugs was following the consumption recommendations of bisphosphonates, taking the drug with empty stomach (30-60 minutes before breakfast) and with a big amount of water (200-250 mL), and being upright after the ingestion of the capsule for 60 minutes.[2,3] Instead, the HRT consisted on the administration of 2 different drugs, 0.625 mg/day of equine estrogens and 2.5-5 mg/day of medroxyprogesterone acetate, both of them in the form of tablets. In the case of RLX, it was a tablet of 60 mg/day.[4] All the three combinations (ALN + HRT, RIS + HRT, ALN + RLX) were supplemented with the administration of calcium (1 g/day) and vitamin D (400 UI/day). Considering all the drugs administrated, the patients were taking between 4-5 tablets every day for 12 months, with their own posology indications. This fact made more difficult and complicated the adherence of the treatment, being easier to break the drug taking schedule.

On the other hand, the combination therapy based on bisphosphonates and teriparatide presented different ways of administration. ALN and RIS were administrated again orally by the administration of either 5 mg/day for ALN or 35 mg/day for RIS capsule film-coated tablet.[7,8] Again, the administration of both bisphosphonates was following the consumption recommendations mention above. In contrast, zoledronate was administrated by a single intravenous infusion of 5 mg.[9] The administration of teriparatide was subcutaneous in all cases, 20-100 µg/day by a subcutaneous injection (Froteo®). The three combinations (ALN + Teriparatide, RIS + Teriparatide, Zoledronate + Teriparatide) were also supplemented by the administration of calcium and vitamin D. In this case the patients were under 4 different drugs for 18 months, and not only with orally administrated drug but also everyday injections what complicates the adherence of the treatment.

The administration of PTH with other antiresorptive agents different from bisphosphonates involved also different types of posology. The combination of denosumab with teriparatide consisted of 60 mg subcutaneous injection every 6 months for denosumab, and 20 µg/day by a subcutaneous injection (Froteo®) for teriparatide.[10] Instead, the combination of RLX with teriparatide consisted of 60 mg/day orally administrated tablet for RLX and again 20 µg/day subcutaneous injection for teriparatide.[11] Again, both combinations were supplemented with calcium and vitamin D, and the adherence issue was also presented.

Considering the benefits of potential combination therapy, it can be very important in treating severe osteoporosis and osteoporosis related bone fractures. However, additional costs, adverse effects, pill burden as well as patient's likelihood of adherence to therapy have to be weighted into the individual's medical decision process. The common problem presented in every combination therapy was the high number of drugs administrated affecting the adherence to the treatment, each of them by different pharmaceutical formulas. Taking this fact into consideration, one possible alternative to reduce the number of medicaments administrated could be the mixture of different drugs in the same pharmaceutical form. For example, there is a combination medication available containing estrogen and the SERM basedoxifene (Duavee®) used in selected situations to help ameliorate hot flashes while also minimizing osteoporosis risk.[12]

Currently, there is no other combination device focused on osteoporotic agents administration. Research in new alternatives for the delivery of several drugs by the same agent could be interesting. In this regard, the interest of developing nanocarriers able to co-load and co-deliver two or more drugs is becoming more important. Nanoparticles, could play a key role in this field, offering the possibility of loading several drugs and transporting them to the target tissue. In this way the number of medications would be reduced and the adherence could be potentially improved.

4.1.2 MSNs for Combination Therapy

Lately, co-load and co-delivery two or more therapeutic agents, such as genes, proteins or drugs, with complementary or synergistic effect are attracting tremendously interest in nanomedicine.[13–16] The key for such therapy is the design of a dual delivery system able to deliver drugs controlling their release behavior. Several approaches have been developed for combination therapy using MSNs with different purpose than the here proposed. An example of a possible approach for combination therapy including nucleic acids is the work proposed by Cheng *et al*. for promoting neurite outgrowth. They used a MSNs-based system for co-delivering curcumin and a plasmid. However, the main field focused in combination therapy has been chemotherapy.

4.1.2.1 MSNs for Combination Therapy in Oncology

Lately, different approaches for cancer treatment have proposed the combination of different drugs with the application of siRNAs. It has received increased attention in recent years due to its excellent therapeutic efficacy, and MSNs have been widely proposed for this purpose.[14] In this way, the selected siRNA can prevent resistance towards chemotherapeutic drug, it can be involved in inducing cancer cell death by different mechanisims than the other drug applied or it can provide anticancer therapeutic effect through the inhibition of angiogenesis. Several examples have been selected to illustrate the different strategies using MSNs for co-delivery small molecules and siRNAs in this case in oncology (Table 4.1).

Avoid Resistance Against Chemotherapeutic

Chen *et al.* used MSNs coated with G2 polyamidoamine dendrimers to co-deliver the drug doxorubicin (Dox) and a Bcl-2 siRNA.[17] In this work, Dox would be responsible for inducing cancer cell death by inducing apoptosis, while the used Bcl-2 siRNA would act as a suppressor of cellular antiapoptotic defense (the Bcl-2 protein is the main player for in cancer chemotherapy resistance not concerning pumps). Ma *et al.* developed a system based on the same dual cargo system Bcl-2 siRNA/Dox, showing significant gene silencing in addition to the cytotoxic effect of Dox in an *in vivo* zebrafish model.[18] Another co-delivery system for Bcl-2 siRNA and Dox was also prepared by Zhao *et al.*[19] This system also showed improved therapeutic efficacy in an *in vivo* human breast adenocarcinoma MCF-7 xenograft mouse model. PEGylated PEI-coated MSNs have also been developed to co-deliver Bcl-2 siRNA, with, in this case, epirubicin as another chemotherapeutic drug, enhancing the antitumor effect both *in vitro* and *in vivo*, compared to particles carrying only the drug.[20] Another protein involved in chemotherapy resistance is connective tissue growth factor (CTGF). The overexpression of this protein is known to induce the up-regulation of Bcl-xL and the cellular inhibitor of apoptosis protein 1 (cIAP1) reducing the capacity of the cell for getting in apoptosis state. Multilayered hyaluronic acid-PEI-rattle MSNs prepared to co-deliver CTGF siRNA and Dox produced improved *in vivo* anti-cancer efficacy, compared with only chemotherapy, in an MDA-MB-231 tumor bearing mice model.[21]

Other mechanism driving chemotherapy resistance in tumors is pump-mediated resistance. The cancer cells acquire the ability to produce different pumps capable of expelling chemotherapeutic drugs to the extracellular environment, increasing the necessary concentration of drugs to achieve therapeutic effect. Among the different types of pumps known to exert this function, P-glycoprotein (Pgp) is probably the most well-known. Meng *et al.* developed PEI-coated MSNs to co-deliver Dox and a Pgp siRNA.[22] This dual delivery system produced an higher cytotoxic effect incubated with a multidrug resistant cell line compared to nanoparticles delivering just the drug. The same authors later improved the system by delivering an optimized ratio of Pgp siRNA and Dox with PEGylated PEI-coated MSNs in an *in vivo* model of multidrug-resistant breast cancer, achieving synergistic inhibition of tumor growth with significant Pgp knockdown at heterogeneous tumor sites.[23] A similar system was used by Wang *et al.*, PEI-coated MSNs were also used to co-deliver Dox and Pgp-1 siRNA, achieving a huge decrease in tumor size *in vivo* (over 80% decrease after 28 days).[24] A different type of pump-mediated resistance is related to the overexpression of transmembrane Ca^{2+} channels.[25] This overexpression is associated with an increase of Ca^{2+} influx, which is involved in proliferative pathways. Wang *et al.* developed amino-functionalized MSNs for co-delivery of T-type Ca^{2+} channel siRNA and Dox.[25] The obtained *in vitro* and *in vivo* results showed a high therapeutic efficacy, even in a drug-resistant breast cancer model. The combination of more than two molecules inside the nanoparticles could also be achieved. siRNAs against pump- and non-pump-mediated resistance mechanisms can also be

combined in a single nanocarrier in addition to different small molecule drugs, such as in the work of Taratula *et al.*[26] In this work, an MSNs-based carrier co-delivered small molecule drugs (Dox and cisplatin) and siRNAs (against Bcl-2 and pump Pgp1) for inhale-based administration in the context of lung cancer.

Directly Induced Tumor Cell Death

A different strategy that can be adopted when co-delivering nucleic acids and small molecule drugs in the context of cancer therapy is combining a chemotherapeutic drug with a siRNA that can induce cell death by itself, aiming to achieve a synergistic effect by exploiting two different cytotoxicity mechanisms simultaneously. It has been recently reported a strategy in which it was selected an anti-TWIST siRNA as the therapeutic nucleic acid cargo.[13] TWIST is a transcription factor that is linked to cancer in the context of angiogenesis, metastasis, cancer stem cell phenotype, and drug resistance. For this reason, it was co-delivered this siRNA in combination with the chemotherapeutic drug daunorubicin for ovarian cancer therapy. The delivery system employed was based on core-shell Fe_3O_4@MSNs coated by a functionalized PEI polymer. The cytotoxic effect of the system combining both therapeutic cargos was enhanced even further by activating the core magnetic particles with oscillating magnetic field.

Angiogenesis Inhibition

An alternative to chemotherapeutic-based cancer therapy consists of preventing cancer cells from obtaining enough nutrients to survive. One way to achieve this is by attacking the tumor blood supply, preventing it from forming new blood vessels which are essential for its survival. This strategy is known as antiangiogenic therapy, and one of the most common therapeutic targets is VEGF.[27] Delivering siRNA sequences directed against VEGF production is therefore an interesting approach with great potential. However, a common limitation in antiangiogenic therapy is the appearance of the resistance mechanism against monotherapies, which is why combination therapies are usually employed, either with chemotherapeutic agents or with other anti-vascular therapeutics.[28] In this context, Zheng *et al.* developed a co-delivery nanosystem, based on MSNs for the treatment of hepatocellular carcinoma.[29] In this work, sorafenib (an antiangiogenic drug) was introduced inside MSN mesopores, while a VEGF siRNA was adsorbed on the nanoparticle surface by electrostatic interactions. This nanosystem was capable of inducing cell cycle arrest and inhibiting the expresion of VEGF in Huh7 cells *in vitro*.

This anti-angiogenic therapy strategy can also be combined with traditional chemotherapy agents, achieving improved therapeutic efficacy. Han *et al.* prepared multilayered nanoparticles where Dox was included within the mesopores, and after several coatings VEGF siRNA was loaded by electrostatic interactions.[30] The different components in the particle enabled uptake by target cells followed by endosomal escape and intracellular delivery of both Dox and the siRNA with active subcellular targeting to the cell nuclei. This multi-step nanosystem produced potent antitumor

efficacies *in vivo*, even at low doses. In another example of this same type of combination, Zheng *et al.* developed a MSN carrier that was loaded with ursolic acid within its mesopores and with VEGF siRNA through electrostatic interaction with the particle surface.[31] The promising *in vitro* results in this work demonstrate a great potential of this system, although no *in vivo* evaluation was reported at this point.

Table 4.2 Small molecule and nucleic acid cargos co-delivered by MSN-based formulations for cancer therapy.

Molecule Drug	siRNA	In Vivo	SiRNA Function	Reference
Doxorubicin	Bcl-2 siRNA	None	Avoiding Resistance	[17]
Doxorubicin	Bcl-2 siRNA	Zebrafish	Avoiding Resistance	[18]
Doxorubicin	Bcl-2 siRNA	Mouse	Avoiding Resistance	[19]
Epirubicin	Bcl-2 siRNA	Mouse	Avoiding Resistance	[20]
Doxorubicin	CTGF siRNA	Mouse	Avoiding Resistance	[21]
Doxorubicin	Pgp siRNA	None	Avoiding Resistance	[22]
Doxorubicin	Pgp siRNA	Mouse	Avoiding Resistance	[23]
Doxorubicin	Pgp-1 siRNA	Mouse	Avoiding Resistance	[24]
Doxorubicin	T-type Ca2+ channel siRNA	Mouse	Avoiding Resistance	[25]
Doxorubicin and cisplatin	Bcl-2 and Pgp-1 siRNAs	Mouse	Avoiding Resistance	[26]
Daunorubicin	Anti-TWIST siRNA	None	Directly Induce cell death	[13]
Sorafenib	VEGF siRNA	None	Angiogenesis Inhibition	[29]
Doxorubicin	VEGF siRNA	Mouse	Angiogenesis Inhibition	[30]
Ursolic Acid	VEGF siRNA	None	Angiogenesis Inhibition	[31]

4.1.2.2 MSNs for Combination Therapy in Osteoporosis

Regarding the several examples presented in oncology for combination therapy using MSNs as nanocarrier, we decided to use the same technology but for different applications. Since a combined therapy for the osteoporosis remission has been proposed as a potent alternative, the application of MSNs would be interesting for this purpose. However, the development of this field for this precise disease is still in his infancy. Few examples have been reported in the application of MSNs for combination therapy against osteoporosis. Gan *et al.* developed BMP-2 and dexamethasone-loaded chitosan-functionalized MSNs to enhance bone regeneration. They took advantage of the MSNs pores to load the dexamethasone, and then, the hydrophilic chitosan was coated onto the MSNs surface for the following adsorption of BMP-2 molecule (Figure 4.1).[32] BMP-2 was quickly released activating the Smad signaling by binding to specific cell surface BMP receptors. Dexamethasone, instead, was delivered into cells after MSNs endocytosis and released in the lysosomes by the pH-triggered changing structure of chitosan. Therefore, BMP-2 and dexamethasone induced osteoblast differentiation, resulting in enhanced bone regeneration.

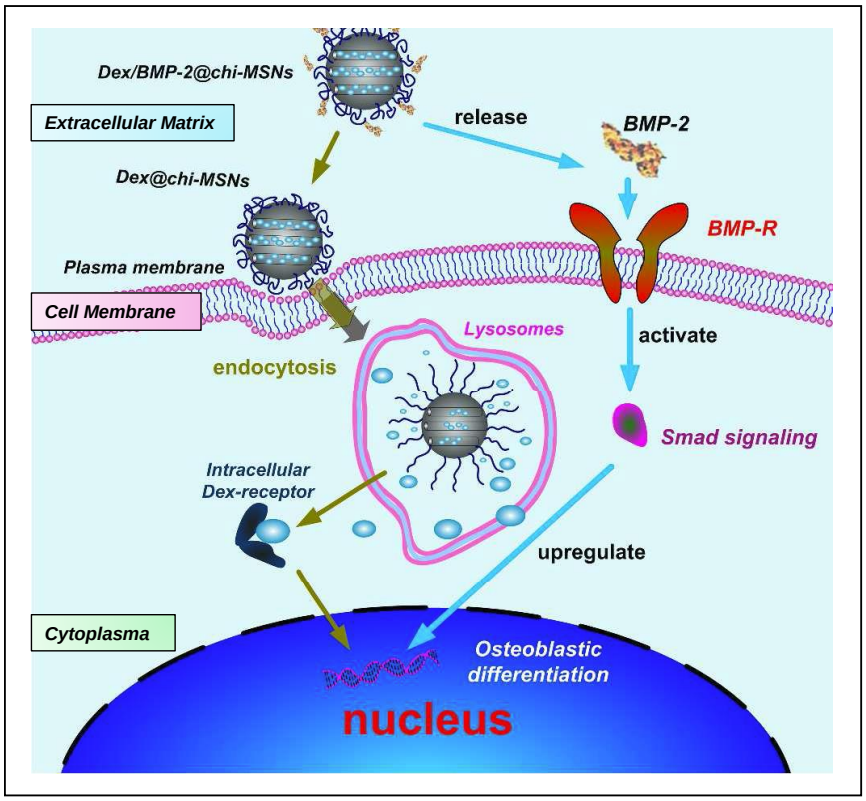

Figure 4.1 Schematic co-delivery diagram of dexamethasone and BMP-2 from MSNs for osteoblast differentiation. Bone morphogenetic proteins receptor (BMP-R), MSNs coated with chitosan and coloaded with Dexamethasone and BMP-2 (Dex/BMP-2@chi-MSNs), MSNs coated with chitosan and loaded with Dexamethasone (Dex@chi-MSNs). Reproduced from Ref 12 with the permission from The Royal Society of Chemistry.

In this chapter, we will develop a system based on MSNs for the potential co-delivery of two therapeutic agents. We will focus on the delivery of the previously mentioned SOST siRNA and an osteogenic peptide. This fact could be achieved due to the PEI coating performed in the MSNs which would be able to effectively bind and deliver SOST siRNA, as evaluated in the previous chapter, and the presence of empty mesoporous that will be loaded with osteostatin. We chose osteostatin as osteogenic peptide since its effect in osteoblastic cell growth and differentiation stimulation has been widely proved.[33–35] Osteostatin delivery from other mesoporous matrices, such as SBA15, has been previously explored *in vivo*, conferring osteoinductive features thanks to the peptide delivery. In fact, despite the non-controlled delivery of osteostatin, no clinical alterations were observed.[36] Even though osteostatin has been shown to be effective at inducing osteoblast differentiation *in vitro* (even in the sub-nanometer range)[37–40] and increasing bone regeneration *in vivo*,[35,36,41] its use in combination with siRNAs has never been reported. Therefore, we considered that osteostatin could be an appropriate option to be evaluated, supplying new information for new potential alternatives in osteoporosis treatments. (Figure 4.2). The main goal of this chapter is to evaluate the possible synergistic effect of both molecules regarding gene expression. This dual therapy could be expected to boost bone formation being a potential alternative to the current treatments for osteoporosis.[42]

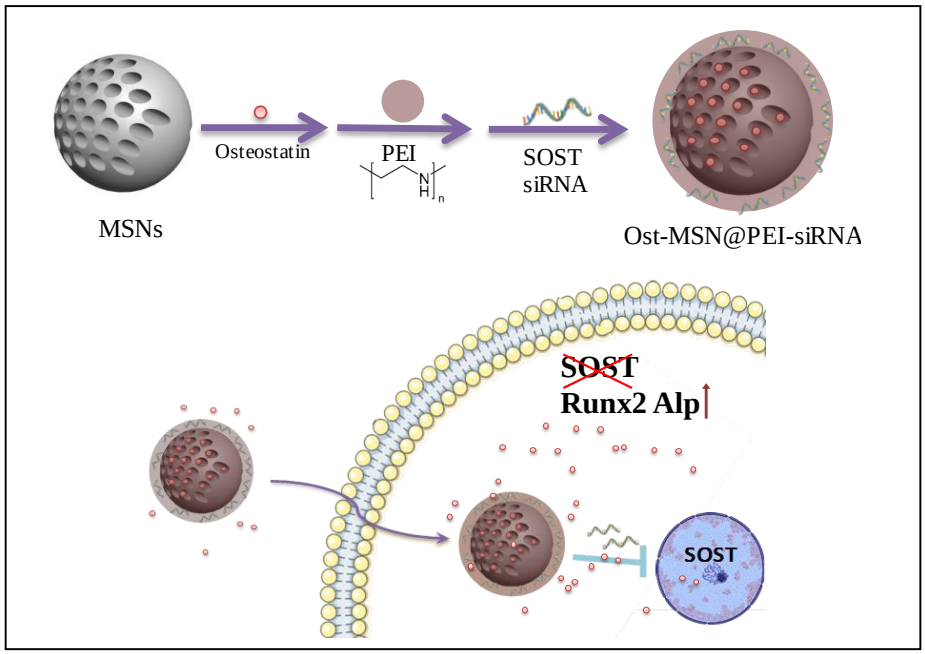

Figure 4.2 Schematic representation of the designed nanocarrier based on mesoporous silica nanoparticles loaded with osteostatin and siRNA to knockdown SOST and promote the expression of early markers of osteogenic differentiation both *in vitro* and *in vivo.*

4.1.3 Aims

Since Osteoporosis is considered a complex degenerative disease and the magic bullet against this disorder has not been found yet, it has become clear that drugs administrated alone against specific molecular pathways have limitations. New alternatives have been proposed but still without the desired outcome and with several adverse effects. The combination of two or more agents with similar or different effects could be a promising strategy to confront the disease.

Gene therapy has recently become more interesting for bone diseases. The delivery of siRNAs against osteoporotic related genes could be consider a potential alternative treatment for osteoporosis. After developing a nanocarrier able to deliver SOST siRNA inside cells, the increment in bone osteogenic markers expression by silencing SOST could be improved by co-delivering another molecule for obtaining better results. Thus, as stated above, a combination therapy has been proposed for boosting the potential osteogenic effects. The next step was to evaluate the coadministration with other anabolic agent to determine if an additive effect could be achieved.

Osteostatin, as the C-terminal fragment of PTHrP (107−111), has been found to be an important osteoclast inhibitor while inducing osteogenic features *in vitro* and stimulating bone regeneration *in vivo*.[37–40] Therefore, it could be a promising agent to co-administrate with the SOST siRNA to increase the effect obtained.

The interest of developing nanocarriers able to co-load and co-deliver two or more drugs is becoming more important. MSNs have been widely used for drug delivery. They could be coated with PEI (cationic polymer) through covalent or electrostatic interactions to become a delivery vehicle for nucleic acids. In this sense, the polymer coat could bind siRNA and the porous of the nanoparticles could be used to encapsulate small molecules, such as the previously mentioned osteostatin, combining both therapeutics to achieve a dual delivery of drugs and nucleic acids.

In this chapter we will focus on the evaluation of a combined therapy for osteoporosis, via the delivery of two different therapeutics at the same time by MSNs in the bone area. Therefore, the first objective of this chapter was to evaluate the PEI coated MSNs capacity of loading and releasing the osteogenic peptide, osteostatin, while transporting the SOST siRNA.

Although nanoparticles could load and deliver both molecules inside the cell, it was necessary to evaluate their action, therefore, the second objective of this chapter was to verify that the transported drugs were active *in vitro* by measuring the expression of different genes, the silenced gene, SOST, and two osteogenic markers Runx2 and Alp.

It was hoped that the combination therapy of different anti-osteoporotic drugs would show a synergistic or additive effect. So, this fact leads to our final objective of this chapter that was to evaluate the possible synergistic effect of both molecules *in vitro* and *in vivo* by one injection in the femur bone marrow of ovariectomized mice.

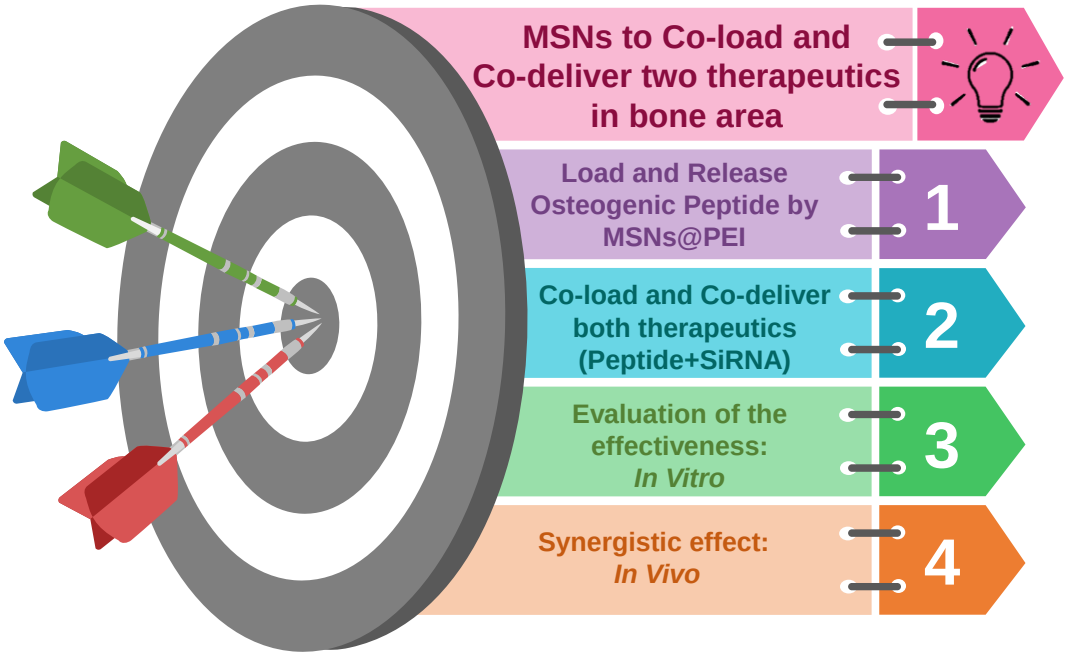

Figure 4.3 Schematic representation of Chapter IV aims.

4.2 Co-delivery of SOST SiRNA and Osteostatin

Since combination therapy has been proposed as a possible alternative for a better osteoporosis treatment, several combinations of different drugs have been evaluated but still there are new therapies pending to be evaluated. The combination of the previously evaluated SOST siRNA with is a C-terminal PTH fragment (107-111), osteostatin, could increase the anabolic effect of both SOST siRNA and osteostatin in an additive manner. Also, the capacity of osteostatin of reducing osteoclastic growth and differentiation could have a synergistic effect between an anabolic and an antiresorptive approach. As it has been mentioned above, MSNs could be used as nanocarrier for co-loading and co-delivering both molecules in order to explore that possible synergistic effect. For this reason, we designed a dual release system in which osteostatin would be loaded into the mesopores of the silica matrix, and the therapeutic siRNA would be bound to the PEI network attached to the surface of the nanoparticles by electrostatics interactions. In this sense, the system will be able to transport and release both molecules at the target destination, where the effect of their dual release would be evaluated.

4.2.1 Delivery of Osteostatin

The first task to accomplish was the loading and release of osteostatin from the MSNs matrix. Therefore, it was necessary to test whether the PEI coating grafted around the nanoparticles might affect the osteostatin release from the MSNs. Osteostatin was loaded into the mesopores of the MSNs by immersing the nanoparticles in a solution of osteostatin overnight. After, the nanoparticles were centrifuged and resuspended in ethanol for the PEI coating following the same procedure described in chapter 3. Afterwards, a release experiment was carried out, and the amount of osteostatin released was measured by fluorescence. The possibility of evaluating the osteostatin release by fluorescence was due to the presence of tryptophan (Trp) in the pentapeptide of osteostatin (Thr-Arg-Ser-Ala-Trp) (Figure 4.4). The indole group of Trp is considered the dominant source of UV absorbance at ~280 nm and emission at ~350 nm in proteins.[43]

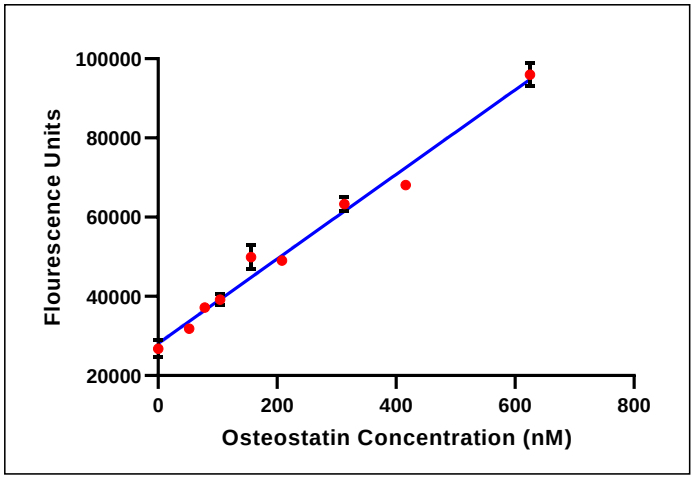

Figure 4.4 Osteostatin standar graph, relation between osteostatin concentration (nM) and fluorescence units.

Thanks to this fact, we were able to measure the release of osteostatin by the nanoparticles. Osteostatin release data showed in Figure 4.5 can be fitted to a first-order kinetic model, with a typical release profile from mesoporous materials (eq 4.1):[44]

$$Y = A(1 - e^{-kt}) \qquad \text{(eq 4.1)}$$

The equation parameters could be described as Y being the amount of osteostatin released (microgram of osteostatin per milligram of MSNs@PEI) at time t (h), with A being the maximum amount of osteostatin released (in micrograms of osteostatin per milligram of MSNs@PEI), and with k being the release rate constant.

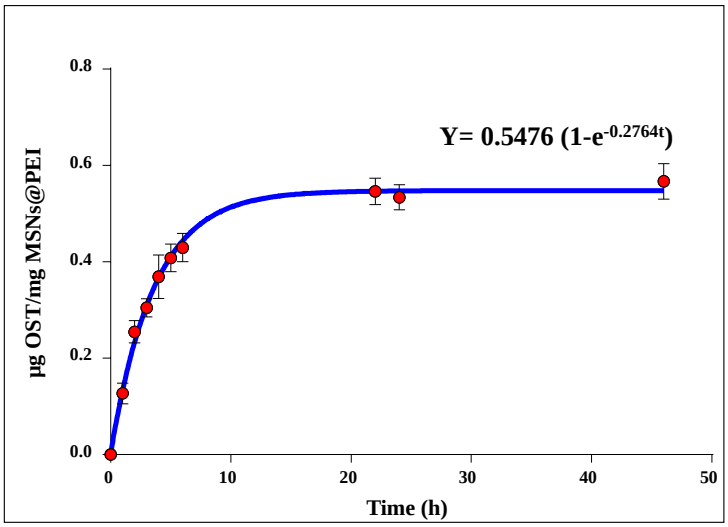

Figure 4.5 Time-dependent osteostatin (OST) release from MSNs@PEI in PBS at pH 7.4, simulating the physiological fluids. Nanoparticles were loaded with OST and afterwards coated with PEI (OST-MSNs@PEI). Points to trace the curves are the means of three independent measurements per time period. Reproduced from Ref 13 with the permission from ACS.

The release data showed that MSNs loaded with osteostatin and coated with PEI (OST-MSNs@PEI) released osteostatin in a time-dependent manner, reaching values of 0.5476 micrograms of osteostatin per milligram of MSNs@PEI. Thus, despite PEI coating, which it is not acting as a physical barrier impeding the osteostatin release, the MSNs were able to release the cargo, confirming that MSNs@PEI could be used to transport and deliver osteostatin.

4.3 *In Vitro* Evaluation of OST-MSNs@PEI-SiRNA Synergy

After testing the osteostatin and siRNA release separately, both components were integrated into a multifunctional system capable of releasing both biomolecules inside cells. The next step was to evaluate the effect of the dual delivery inside cells regarding the expression of the silenced gene and the osteogenic markers, Runx2 and Alp. First, osteostatin was loaded into the mesopores as described above. Then, the PEI coating was accomplished, and siRNA was bound, leading to

the final system (OST-MSNs@PEI-siRNA). This platform was evaluated into MEF cells, which express SOST gene, as previously demonstrated in chapter 3. The MEF cells were seeded and after two weeks, the complete system (OST-MSNs@PEI-siRNA) was added to the cells following the same procedure described in the previous chapter. After 48 h, SOST, Runx2 and Alp mRNA expressions were measured to evaluate the effect of both biomolecules together compared to either of them independently (OST-MSNs@PEI and MSNs@PEI-siRNA). Figure 4.6 shows that SOST was effectively knocked down either by the SOST-siRNA release or the osteostatin release independently. It is worth mentioning that osteostatin produces an effect on wnt/β-catenin pathway as it was stated in the previous chapters. The silencing effect was even more noticeable by the delivery of both molecules at the same time, showing a potential additive effect.

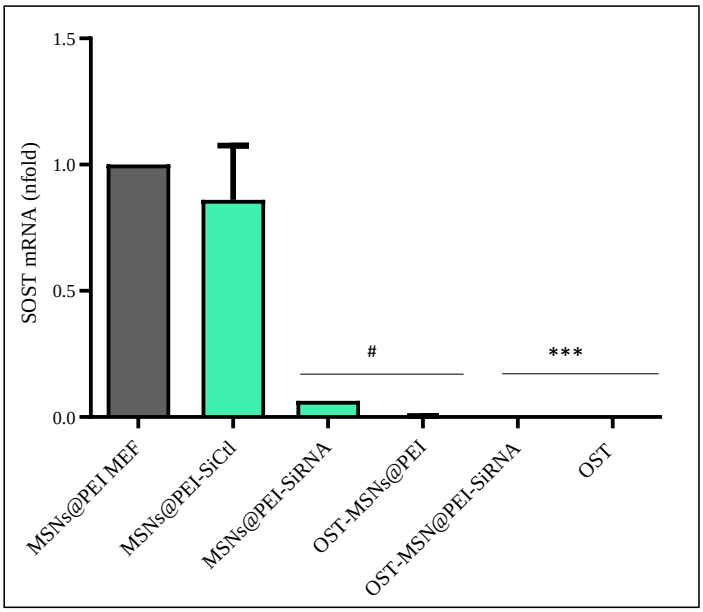

Figure 4.6 SOST gene expression with the application of siRNA-SOST bound to MSNs@PEI in mouse embryonic fibroblast (MEF) cells in the presence or absence of osteostatin (OST). SOST mRNA expression (measured by real-time qRT-PCR) in MEF cells after 14 days of cell culture. To optimize the experiment a negative control siRNA (SiCtl) ("non-targeting control", which targets a site that is absent in human, mouse, and rat genomes); MSNs@PEI nanoparticles were bound to SiCtl (MSNs@PEI-SiCtl). Data are mean ± SEM of three independent experiments performed in triplicate. Triple asterisks indicate $p < 0.001$ *vs* MSNs@PEI MEF; pound signs indicate $p < 0.05$ *vs* OST-MSNs@PEI and MSNs@PEI-SiRNA. Adapted from Ref 13 with the permission from ACS.

Taking into consideration the results obtained in SOST expression, osteostatin showed an effective silence effect, reducing the expression of SOST in a more effective manner even than the delivery of SOST-siRNA. It has been reported that both C- and N-terminal domains of PTHrP potently influenced in the activation of the wnt/β-catenin pathway, by reducing the oxidative stress responsible of a possible pathway inactivity.[45] It has been also reported that osteostatin specifically recovered wnt pathway activation in mice presenting a low activation of the canonical pathway with the consequent impairment of bone development.[46] Besides the osteostatin silencing

effect, the combination of SOST-siRNA and the osteogenic peptide increased the knockdown capability of the system, confirming the synergistic effect of both biomolecules regarding SOST expression.

In addition to the synergistic effect presented in the knockdown capability of both biomolecules, the evaluation of osteogenic markers expression was necessary to determine if the application of both molecules present an additive effect regarding osteogenic features. The results obtained with the administration of the nanocarrier loaded just with SOST siRNA (MSNs@PEI-siRNA) or only with osteostatin (OST-MSNs@PEI) were measured and compared with those obtained with the nanocarrier loaded with both biomolecules (Figure 4.7)

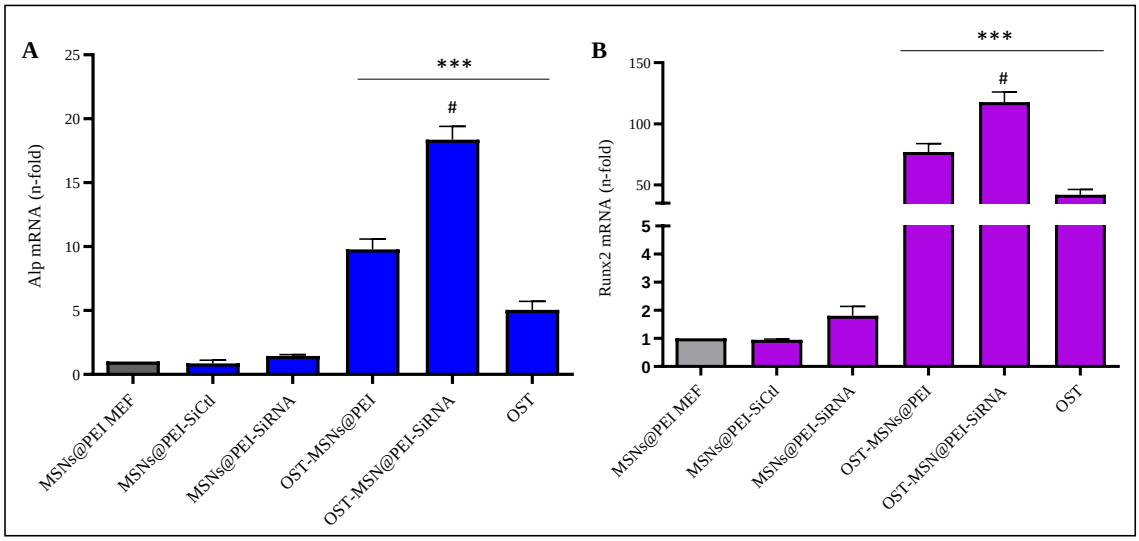

Figure 4.7 Alp and Runx2 bone osteogenic markers gene expression with SiRNA-SOST bound to MSNs@PEI in MEF cells in the presence or absence of osteostatin (OST). Alp (A) and Runx2 (B) mRNA expression (measured by real-time qRT-PCR) in MEF cells after 14 days of cell culture. To optimize the experiment, one control was used: a negative control siRNA (SiCtl) ("non-targeting control", which targets a site that is absent in human, mouse, and rat genomes); MSNs@PEI nanoparticles were bound to SiCtl (MSNs@PEI SiCtl). Data are mean ± SEM of three independent experiments performed in triplicate. Triple asterisks indicate $p < 0.001$ *vs* MSNs@PEI MEF; pound signs indicate $p < 0.05$ *vs* OST-MSNs@PEI and MSNs@PEI-SiRNA. Adapted from Ref 13 with the permission from ACS.

As it can be observed in Figure 4.7A, Alp expression rose up to 17-fold when OST-MSNs@PEI-siRNA were administrated. Besides, Runx2 expression notably increased up to 110-fold when osteostatin and SOST siRNA were released together by the nanoparticles (Figure 4.7B). The data showed that the coadministration of both biomolecules at the same time, compared with the administration of the biomolecules separately, increased the expression of both osteogenic markers to notably higher levels, being a combined effect between osteostatin and SOST siRNA. This fact confirms the synergy presented between osteostatin and SOST siRNA not only regarding SOST expression but also regarding osteogenic markers expression. Therefore, the presented synergy could be due to the reduction of sclerostin by the knockdown of the SOST gene, increasing the activation of wnt/β-catenin pathway and the consequent bone formation

stimulation, and the additive effect produced by the osteostatin regarding osteoblast stimulation and osteoclast inhibition by different mechanisms. It has been reported that osteostatin controls bone loss by inhibiting immune activation, pro-inflammatory cytokines, and osteoclastogenesis.[47] It was also measured the effect of one pulse of free osteostatin at the same concentration as the one achieved by the nanoparticles measured at the same time in a previous experiment (7×10^{-7} M). In both osteogenic markers (Runx2 and Alp), the gene expression levels rose up notably higher when the osteostatin was released from the nanoparticles (OST-MSNs@PEI) than when was added on its free form. This fact has been noticed before, producing higher effects in mineralization the continuous release of free osteostatin from a mesoporous biomaterial than one pulse of osteostatin at the beginning of the experiment.[35] The reasons that could support this finding could be that a controlled and sustained released of osteostatin for longer time is more effective than a punctual administration of higher doses of osteostatin. Additionally, it has also been reported that the mere presence of silica could increase the expression of different osteogenic markers as well as increase the proliferation of osteoblast.[34] In addition, the nanocarrier could also protect the peptide from degradation, being gradually released in perfect conditions. So, unlike just one pulse of osteostatin at the beginning of the experiment, which could be progressively degraded, the release from MSNs would keep a uniform concentration of active osteostatin for longer time, being the effect in this sense more noticeable. In any case, it has been demonstrated that the delivery of osteostatin from our MSNs system improves osteostatin effects in osteogenic markers expression, showing the benefits of using this type of nanocarriers for the potential treatment of osteoporosis.

Thanks to this *in vitro* experiment, we can conclude that co-administration of SOST siRNA and osteostatin from MSNs present a synergistic effect, increasing the expression of two osteogenic markers and silencing SOST gene effectively in MEF cells.

4.4 *In Vivo* Evaluation of OST-MSNs@PEI-SiRNA Knockdown Capability and Gene Expression Modulation Synergy

After the successful *in vitro* validation of the system, the next step was its *in vivo* evaluation in a reduced bone mass model. As described in chapter 3, we have employed ovariectomized C57/BL6 female mice with a decreased femoral bone mineral density compared to non-ovariectomized (62.98 ± 0.28 mg/cm^2 *versus* 66.56 ± 0.47 mg/cm^2; $p < 0.001$) as animal model.[48] First, 50 μL of the complete nanocarrier (OST-MSNs@PEI-siRNA) dispersion (0.8 mg/mL) were injected in the femur bone marrow of ovariectomized mice, as showed above in chapter 3. Higher concentrations of these nanoparticles have been widely used in different works without any toxic effects.[23,49,50] Therefore, we consider this concentration accurate for this experiment, being enough to observe several effects on gene expression modification. After 5 days of the injection, SOST, Runx2, and Alp mRNA were measured by qRT-PCR and the obtained results are displayed in Figures 4.8 and

4.9. First it should be mentioned that, because the injection of the nanoparticles was local, *i.e.*, the nanoparticles were already at the target tissue, the biodistribution of the nanoparticles in the animals was not evaluated. Figure 4.8 shows the expression of SOST in ovariectomized mice (OVX), which was increased compared to non-ovariectomized mice (control), as expected, and were statistically significant. This is in agreement with the previous results and reports, and validates our animal model for SOST silencing evaluation.

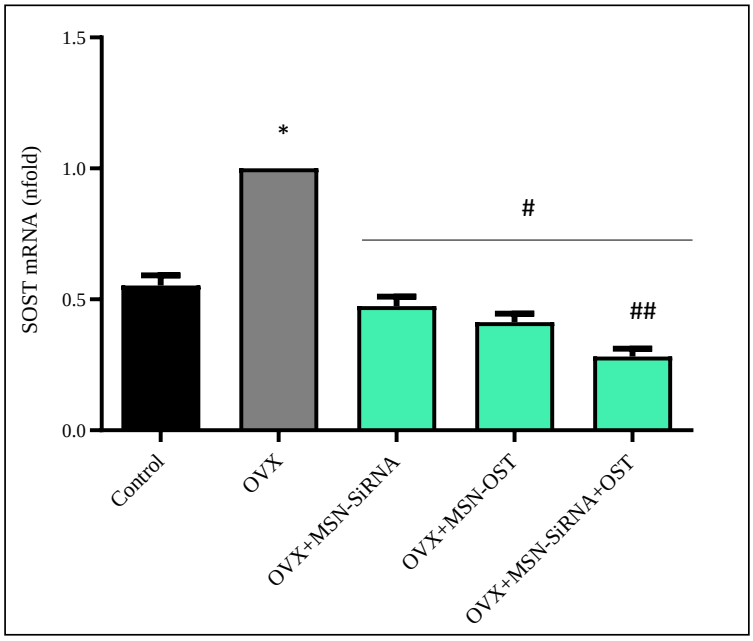

Figure 4.8 *In vivo* injection of OST-MSNs@PEI-siRNA. SOST gene expression in the presence of SiRNA-SOST bound to MSNs@PEI in ovariectomized mice (OVX) in the presence or absence of osteostatin. SOST mRNA expression (measured by real time qRT-PCR) in femur bone. To optimize the experiment, one control a negative control siRNA (SiCtl) was used ("non-targeting control", which targets an absent site in human, mouse, and rat genomes) bound to MSNs@PEI nanoparticles (MSNs@PEI-SiCtl). Data are mean ± SEM of three independent experiments performed in triplicate. Asterisk indicate $p < 0.0005$ *vs* OVX; pound signs indicate $p < 0.0001$ *vs* OVX and double pound indicate $p < 0.0001$ *vs* OVX+MSNs-siRNA and OVX+MSNs-OST. Adapted from Ref 13 with the permission from ACS.

The injection of the nanoparticles with SOST siRNA or osteostatin notably decreased the expression of SOST (*ca.* 50% and 60%, respectively). As it was mentioned before, osteostatin could effectively silence SOST, reducing the formation of sclerostin and therefore increasing the activity of the canonical wnt/β-catenin pathway. Although both molecules present a knockdown effect in SOST expression, the combination of the two therapeutic agents resulted in the greatest knockdown effect, ca. 75% of silencing. The activity of reducing SOST expression of both biomolecules by different mechanisms, led to an additive effect reflected in the results obtained. The co-delivery of SOST siRNA and osteostatin from our MSNs-based system generated a synergistic effect, being particularly effective silencing SOST gene. This fact reinforces the

results obtained in the *in vitro* experiment described above, confirming the additive effect obtained by the combination of these two biomolecules for the inhibition of sclerostin synthesis.

The osteogenic markers, Runx2 and Alp, decreased their expression in OVX compared to Control group as expected (Figure 4.9). The results also showed that Runx2 and Alp expression notably increased when osteostatin and SOST siRNA were released together by the complete system (up to 3 or 2.2 n-fold, respectively, compared with OVX), in total agreement with the previous *in vitro* results.

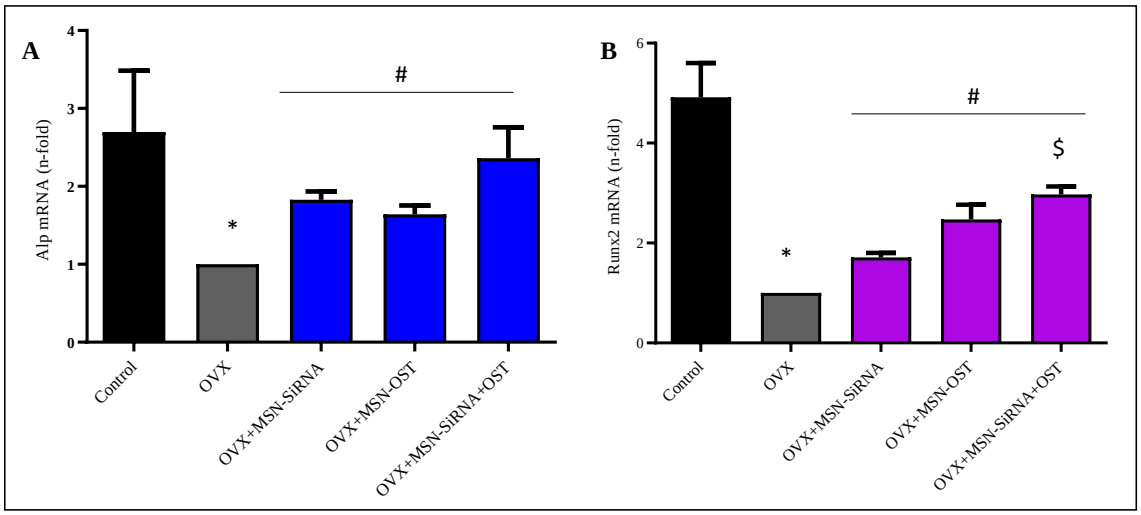

Figure 4.9 *In vivo* injection of OST-MSNs@PEI-siRNA. Alp, and Runx2 bone osteogenic markers gene expression with SiRNA-SOST bound to MSNs@PEI in ovariectomized mice (OVX) in the presence or absence of osteostatin. (A) Alp and (B) Runx2 mRNA expression (measured by real-time qRT-PCR) in femur bone. To optimize the experiment a negative control siRNA (SiCtl) was used ("non-targeting control", which targets an absent site in human, mouse, and rat genomes) bound to MSNs@PEI nanoparticles (MSNs@PEI-SiCtl). Data are mean ± SEM of three independent experiments performed in triplicate. Asterisk indicates $p < 0.0005$ *vs* OVX; triple asterisk indicates $p < 0.005$ *vs* OVX; pound signs indicates $p < 0.001$ *vs* OVX, and double pound indicates $p < 0.0001$ *vs* OVX+MSNs-siRNA and OVX+MSNs-OST. Adapted from Ref 13 with the permission from ACS.

The results obtained with the administration of the system loaded just with the SOST siRNA (OVX+MSNs-siRNA) or only with the osteostatin (OVX+MSNs-OST) were also measured. In this case, the administration of siRNA loaded in the nanoparticles increased the expression of Runx2 and Alp 1.5 n-fold and 1.8 n-fold respectively compared with OVX. Instead, the administration of osteostatin loaded inside the nanocarrier generated a more noticeable increased in the gene expression, being up to or 2.5 n-fold, for Runx2 and up to or 2.6 n-fold, for Alp, compared with OVX. Although both biomolecules separately produced and increase in bone osteogenic markers, the augmentation of the expression was slight.

The data obtained showed that the co-administration of both biomolecules at the same time compared with the administration of the biomolecules separately, increased the expression of both

osteogenic markers to notably higher levels and decreased the expression of SOST gene, being a combined effect between osteostatin and SOST-siRNA. The augmentation of the osteogenic markers expression would be related not only with the reduction of SOST expression but also with the osteogenic activity of the osteostatin. Both activities achieved by the different mechanisms proposed above end up in a synergistic effect as appreciated in the osteogenic markers expression. The design of the dual delivery nanosystem enhanced the expression of osteogenic markers and effectively knockdown SOST gene through the combined effect of osteostatin and SOST siRNA *in vivo*. This fact brings us to one step further in the osteoporosis remission path, being a synergy between these two molecules delivered by the MSNs-based nanocarrier in ovariectomized mice, increasing the expression of osteogenic related genes, which could be translate in an improvement of bone structure and reduction of bone fractures. This complete system could provide a potential alternative to the current treatment of osteoporosis, empowering cell differentiation by osteogenic features. In this way, we are approaching to the main objective of this doctoral thesis, developing a new promising treatment for osteoporosis disease.

4.5 Conclusions

Several treatments have been developed to overcome osteoporosis disease with different efficiency, but they still present important adverse effects which compromise their long-term use. Different approaches have been proposed to enhance the efficacy of the treatments reducing their side effects, such as new targets for osteoporosis treatment, further development in anabolic treatments and combination therapies looking for additive effects which could achieve better results in bone recovery.

Regarding the polytherapy, several combinations have been studied but still without solid results, therefore this field needs to be further studied. Our purpose was to co-deliver two therapeutic agents, SOST siRNA and osteostatin, at the same time inside cells. SOST siRNA would interrupt the inhibition by sclerostin (protein encoded by SOST) of the Wnt/β-catenin pathway, which is directly correlated with osteoblast activation and differentiation. On the other hand, osteostatin can inhibit osteoclastic bone resorption by affecting osteoclastic growth and/or differentiation and has also been found that osteostatin increase differentiation, proliferation and viability in osteoblastic cells *in vitro* and *in vivo*. Therefore, the co-delivery of both biomolecules could affect bone formation in an additive and synergistic way.

After evaluation of the effect of both biomolecules *in vitro* with promising results (high capacity of silencing SOST and notably higher levels of the osteogenic markers), the system was injected in the femoral bone marrow of ovariectomized mice, and the obtained results were in agreement with the *in vitro* experiments. However, mice treated with each biomolecule separately have

modified the expression of the three genes, (knocking down SOST and increasing the expression of Runx2 and Alp), the co-administration of both biomolecules yielded synergistic effects. Thus, it can be concluded that our system was able to transport, co-deliver, and transfect to cells SOST siRNA and osteostatin, maintaining its activity and achieving an effective silencing effect. The combination of SOST siRNA with the osteogenic peptide, promoted a synergistic effect, thus increasing the expression of early markers of osteogenic differentiation in ovariectomized mice. This system has demonstrated remarkable efficacy for an intra-bone marrow injection. In consequence, it will constitute a promising candidate as a platform for a polytherapy in osteoporosis treatment.

This proof-of-concept with the obtained promising results would lead us to further investigations to develop a systemic system able to obtain similar results but in this case by a systemic administration in order to target the different bones of the organism.

4.6 References

1. Khajuria, D. K., Razdan, R., Mahapatra, D. R. Drugs for the management of osteoporosis: A review. *Rev. Bras. Reumatol.* 51, 365–382 (**2011**).

2. Yoon, B. K. *et al.* Effects of Combination Therapy of Alendronate and Hormonal Therapy on Bone Mineral Density in Postmenopausal Korean Women: Multicenter, Randomized Controlled Clinical Trial. *J. Korean Med. Sci.* 32, 992–998 (**2017**).

3. Harris, S. T. *et al.* Effect of Combined Risedronate and Hormone Replacement Therapies on Bone Mineral Density in Postmenopausal Women1. *J. Clin. Endocrinol. Metab.* 86, 1890–1897 (**2001**).

4. Johnell, O. *et al.* Additive Effects of Raloxifene and Alendronate on Bone Density and Biochemical Markers of Bone Remodeling in Postmenopausal Women with Osteoporosis. *J. Clin. Endocrinol. Metab.* 87, 985–992 (**2002**).

5. Langdahl, B. L. Overview of treatment approaches to osteoporosis. *Br. J. Pharmacol.* 1, 1–16 (**2020**).

6. Gennari, L. *et al.* Emerging therapeutic targets for osteoporosis. *Expert Opin. Ther. Targets* 24, 115–130 (**2020**).

7. Black, D. M. *et al.* The Effects of Parathyroid Hormone and Alendronate Alone or in Combination in Postmenopausal Osteoporosis. *N. Engl. J. Med.* 349, 1207–1215 (**2003**).

8. Walker, M. D. *et al.* Combination therapy with risedronate and teriparatide in male osteoporosis. *Endocrine* 44, 237–246 (**2013**).

9. Cosman, F. *et al.* Effects of intravenous zoledronic acid plus subcutaneous teriparatide [rhPTH(1–34)] in postmenopausal osteoporosis. *J. Bone Miner. Res.* 26, 503–511 (**2011**).

10. Tsai, J. N. *et al.* Teriparatide and denosumab, alone or combined, in women with postmenopausal osteoporosis: the DATA study randomised trial. *Lancet* 382, 50–56 (**2013**).

11. Deal, C. *et al.* Combination Teriparatide and Raloxifene Therapy for Postmenopausal Osteoporosis: Results From a 6-Month Double-Blind Placebo-Controlled Trial. *J. Bone Miner. Res.* 20, 1905–1911 (**2005**).

12. Kelly, J. J., Garapati, S. S. Combination therapies in the treatment of osteoporosis. *Curr. Opin. Endocrinol. Diabetes. Obes.* 26, 291–295 (**2019**).

13. Sánchez-Salcedo, S. *et al.* Mesoporous core-shell silica nanoparticles with anti-fouling properties for ovarian cancer therapy. *Chem. Eng. J.* 340, 114–124 (**2018**).

14. Teo, P. Y., Cheng, W., Hedrick, J. L., Yang, Y. Y. Co-delivery of drugs and plasmid DNA for cancer therapy. *Adv. Drug Deliv. Rev.* 98, 41–63 (**2016**).

15. Li, Y. *et al.* Co-delivery of siRNA and hypericin into cancer cells by hyaluronic acid modified PLGA-PEI nanoparticles. *Drug Dev. Ind. Pharm.* 42, 737–746 (**2016**).

16. Song, B., Wu, C., Chang, J. Controllable delivery of hydrophilic and hydrophobic drugs from electrospun poly(lactic-*co*-glycolic acid)/mesoporous silica nanoparticles composite mats. *J. Biomed. Mater. Res. Part B Appl. Biomater.* 100B, 2178–2186 (**2012**).

17. Chen, A. M. *et al.* Co-delivery of Doxorubicin and Bcl-2 siRNA by Mesoporous Silica Nanoparticles Enhances the Efficacy of Chemotherapy in Multidrug-Resistant Cancer Cells. *Small* 5, 2673–2677 (**2009**).

18. Ma, X. *et al.* Redox-Responsive Mesoporous Silica Nanoparticles: A Physiologically Sensitive Codelivery Vehicle for siRNA and Doxorubicin. *Antioxid. Redox Signal.* 21, 707–722 (**2013**).

19. Zhao, S. *et al.* A redox-responsive strategy using mesoporous silica nanoparticles for co-delivery of siRNA and doxorubicin. *J. Mater. Chem. B* 5, 6908–6919 (**2017**).

20. Hanafi-Bojd, M. Y., Jaafari, M. R., Ramezanian, N., Malaekeh-Nikouei, K. A. Co-Delivery of Epirubicin and siRNA Using Functionalized Mesoporous Silica Nanoparticles Enhances *In vitro* and *In vivo* Drug Efficacy. *Current Drug Delivery.* 13, 1176–1182 (**2016**).

21. Ding, J. *et al.* Hyaluronidase-triggered anticancer drug and siRNA delivery from cascaded targeting nanoparticles for drug-resistant breast cancer therapy. *Nano Res.* 10, 690–703 (**2017**).

22. Meng, H. *et al.* Engineered Design of Mesoporous Silica Nanoparticles to Deliver Doxorubicin and P-Glycoprotein siRNA to Overcome Drug Resistance in a Cancer Cell Line. *ACS Nano* 4, 4539–4550 (**2010**).

23. Meng, H. *et al.* Codelivery of an Optimal Drug/siRNA Combination Using Mesoporous Silica Nanoparticles To Overcome Drug Resistance in Breast Cancer *in Vitro* and *in Vivo*. *ACS Nano* 7, 994–1005 (**2013**).

24. Wang, D. *et al.* Co-delivery of doxorubicin and MDR1-siRNA by mesoporous silica nanoparticles-polymerpolyethylenimine to improve oral squamous carcinoma treatment. *Int. J. Nanomedicine* 13, 187–198 (**2017**).

25. Wang, S. *et al.* Regulation of Ca^{2+} Signaling for Drug-Resistant Breast Cancer Therapy with Mesoporous Silica Nanocapsule Encapsulated Doxorubicin/siRNA Cocktail. *ACS Nano* 13, 274–283 (**2019**).

26. Taratula, O., Garbuzenko, O. B., Chen, A. M., Minko, T. Innovative strategy for treatment of lung cancer: targeted nanotechnology-based inhalation co-delivery of anticancer drugs and siRNA. *J. Drug Target.* 19, 900–914 (**2011**).

27. Bhattarai, P., Hameed, S., Dai, Z. Recent advances in anti-angiogenic nanomedicines for cancer therapy. *Nanoscale* 10, 5393–5423 (**2018**).

28. Paris, J. L., Villaverde, G., Gómez-Graña, S., Vallet-Regí, M. Nanoparticles for multimodal antivascular therapeutics: Dual drug release, photothermal and photodynamic therapy. *Acta Biomater.* 101, 459–468 (**2020**).

29. Zheng, G. *et al.* Co-delivery of sorafenib and siVEGF based on mesoporous silica nanoparticles for ASGPR mediated targeted HCC therapy. *Eur. J. Pharm. Sci.* 111, 492–502 (**2018**).

30. Han, L., Tang, C., Yin, C. Dual-targeting and pH/redox-responsive multi-layered nanocomplexes for smart co-delivery of doxorubicin and siRNA. *Biomaterials* 60, 42–52 (**2015**).

31. Zheng, G. *et al.* Dual-Targeting Multifuntional Mesoporous Silica Nanocarrier for Codelivery of siRNA and Ursolic Acid to Folate Receptor Overexpressing Cancer Cells. *J. Agric. Food Chem.* 65, 6904–6911 (**2017**).

32. Gan, Q. *et al.* A dual-delivery system of pH-responsive chitosan-functionalized mesoporous silica nanoparticles bearing BMP-2 and dexamethasone for enhanced bone regeneration. *J. Mater. Chem. B* 3, 2056–2066 (**2015**).

33. Trejo, C. G. *et al.* The osteoinductive properties of mesoporous silicate coated with osteostatin in a rabbit femur cavity defect model. *Biomaterials* 31, 8564–8573 (**2010**).

34. Lozano, D. *et al.* Osteostatin improves the osteogenic activity of fibroblast growth factor-2 immobilized in Si-doped hydroxyapatite in osteoblastic cells. *Acta Biomater.* 8, 2770–2777 (**2012**).

35. Lozano, D. *et al.* Osteostatin-loaded bioceramics stimulate osteoblastic growth and differentiation. *Acta Biomater.* 6, 797–803 (**2010**).

36. Lozano, D. *et al.* Osteostatin-loaded onto mesoporous ceramics improves the early phase of bone regeneration in a rabbit osteopenia model. *Acta Biomater.* 8, 2317–2323 (**2012**).

37. Cornish, J. *et al.* Stimulation of Osteoblast Proliferation by C-Terminal Fragments of Parathyroid Hormone – Related Protein. 14, 915–922 (**1999**).

38. Lozano, D. *et al.* The C-terminal fragment of parathyroid hormone-related peptide promotes bone formation in diabetic mice with low-turnover osteopaenia. *Br. J. Pharmacol.* 162, 1424–1438 (**2011**).

39. Fenton, A. J. *et al.* A Carboxyl-Terminal Peptide from the Parathyroid Hormone-Related Protein Inhibits Bone Resorption by Osteoclasts. *Endocrinology* 129, 1762–1768 (**1991**).

40. Lewinson, D., Rihani-Basharat, S. PTHrP (107 – 111) Inhibits *In Vivo* Resorption that was Stimulated by PTHrP (1 – 34) when Applied Intermittently to Neonatal Mice. *Calcif .Tissue Int.* 61, 426–428 (**1997**).

41. Lozano, D. *et al.* Parathyroid hormone-related protein (107-111) improves the bone regeneration potential of gelatin – glutaraldehyde biopolymer-coated hydroxyapatite. *Acta Biomater.* 10, 3307–3316 (**2014**).

42. Mora-Raimundo, P., Lozano, D., Manzano, M., Vallet-Regí, M. Nanoparticles to Knockdown Osteoporosis-Related Gene and Promote Osteogenic Marker Expression for Osteoporosis Treatment. *ACS Nano* 13, 5451–5464 (**2019**).

43. Ghisaidoobe, A. B. T., Chung, S. J. Intrinsic tryptophan fluorescence in the detection and analysis of proteins: a focus on Förster resonance energy transfer techniques. *Int. J. Mol. Sci.* 15, 22518–22538 (**2014**).

44. Paris, J. L., Cabañas, M. V., Manzano, M., Vallet-Regí, M. Polymer-Grafted Mesoporous Silica Nanoparticles as Ultrasound-Responsive Drug Carriers. *ACS Nano* 9, 11023–11033 (**2015**).

45. Portal-Núñez, S. *et al.* Parathyroid hormone-related protein exhibits antioxidant features in osteoblastic cells through its N-terminal and osteostatin domains. *Bone Joint Res.* 7, 58–68 (**2018**).

46. Rodríguez-de la Rosa, L. *et al.* Treatment with N- and C-Terminal Peptides of Parathyroid Hormone-Related Protein Partly Compensate the Skeletal Abnormalities in IGF-I Deficient Mice. *PLoS One* 9, e87536 (**2014**).

47. Nácher-Juan, J., Terencio, M. C., Alcaraz, M. J., Ferrándiz, M. L. Osteostatin Inhibits Collagen-Induced Arthritis by Regulation of Immune Activation, Pro-Inflammatory Cytokines, and Osteoclastogenesis. *Int. J. Mol. Sci.* 20, 3845 (**2019**).

48. de Castro, L. F. *et al.* Comparison of the skeletal effects induced by daily administration of PTHrP (1-36) and PTHrP (107-139) to ovariectomized mice. *J. Cell. Physiol.* 227, 1752–1760 (**2012**).

49. Dogra, P. *et al.* Establishing the Effects of Mesoporous Silica Nanoparticle Properties on *in Vivo* Disposition Using Imaging-Based Pharmacokinetics. *Nat. Commun.* 9, 1–14 (**2018**).

50. Wen, S., Zheng, F., Shen, M., Shi, X. Surface modification and PEGylation of branched polyethyleneimine for improved biocompatibility. *J. Appl. Polym. Sci.* 128, 3807–3813 (**2013**).

Chapter V: New Approach for Osteoporosis Systemic Treatment

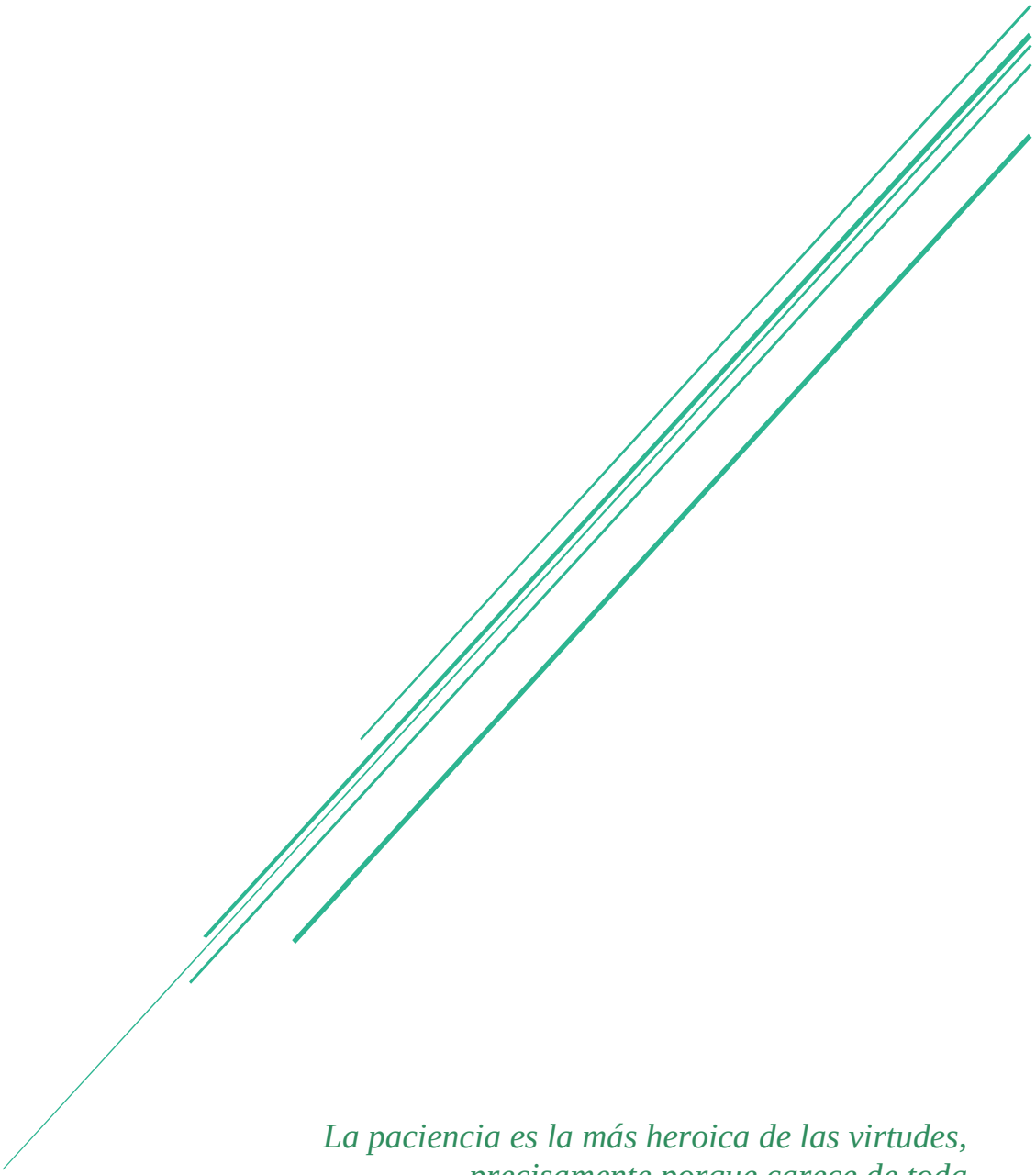

La paciencia es la más heroica de las virtudes,
precisamente porque carece de toda
apariencia de heroísmo
Giacomo Leopardi

5. New Approach for Osteoporosis Systemic Treatment

5.1 Introduction

Osteoporosis is a progressive silent disease with devastating clinical and economic consequences. Because of the systemic nature of osteoporosis, the associated increase in fracture risk affects virtually all skeletal sites. As population age, the prevalence of osteoporosis and its sequelae will increase substantially, becoming one of the largest global healthcare burdens.[1]

5.1.1 Osteoporosis: Systemic Disease

Osteoporosis, as systemic disorder, constitutes a major public health concern since the increase in bone fragility and susceptibility to fracture negatively impact the quality of life of the affected patients. Their direct and indirect effects on society are generally underestimated.

Although several approaches have been proposed for osteoporosis treatment as it has been mentioned in chapter 1, there is still not cure for this skeletal disorder. Local treatments have been studied as possible alternatives,[2] but since the disease affects systematically to the organism, systemic approaches have gained more importance.

Current osteoporosis treatments enclose orally administrated tablets or capsules such as some bisphosphonates, subcutaneous injections (teriparatide) or intravenous perfusions (zoledronate) among others. All these systemic treatments present several side effects due to their lack of specificity and, therefore, the off-target effects. To reduce the potential side effects produced by those conventional osteoporosis treatments, nanotechnology can offer protection and improvement in targeting through the use of nanocarriers to transport and deliver therapeutic agents.[3,4] In this sense, MSNs could play a key role in this field, considering their amazing properties for drug delivery, and therefore be used for the potential treatment of bone diseases, in particular osteoporosis.[5]

5.1.2 MSNs for Systemic Administration to Bone

Due to the systemic affection of osteoporosis, the treatment options should reach different bones around the body, and therefore should be administered systematically. For this reason, the chosen treatment options should be able to be injected in the circulatory system and there be able to stay for long periods of time preserving their stability, and also to be accumulated in the target tissue, in this case, the bone.

5.1.2.1 Bloodstream Half-Life

There are several properties required for any nanoparticle to be administrated through intravenous injection to reach bone tissue. First, the nanoparticles have to be stable in physiological media.

Otherwise, nanoparticle aggregation will lead to the obstruction of blood vessels and the subsequent clot that might compromise the patient´s life. In the case of osteoporosis treatment, the nanoparticles have to remain in the bloodstream long enough to accumulate in bones and there deliver the previously loaded cargo. Both chemical composition and surface charge play a pivotal role in the interaction with the physiological environment. Therefore, the challenges in designing MSNs are both to increase the blood circulation time and to enhance stability in physiological fluids in order to ensure their full functionality and efficacy along all their lifespan.

One key aspect to consider regarding nanoparticle circulation time is the opsonization of the nanoparticles.[6] When a pathogen or a foreign body arrives to the bloodstream, a type of proteins called opsonins surround it leading the phagocytic cells to indentify it and destroy it. This process is called opsonization. When nanoparticles without any surface modification might be dispersed in blood, they would be covered by a mixture of different proteins, the previously mentioned opsonins, leading to the formation of the protein corona.[7] The formation of this protein corona would dramatically accelerate the clearance of the nanoparticles from systemic circulation.

Different approaches for obtaining MSNs with long circulation half-life have been reported. The functionalization of the surface with PEG, the zwitterionization of the surface or the surface coating with phospholipid bilayers will be explain below (Figure 5.1).

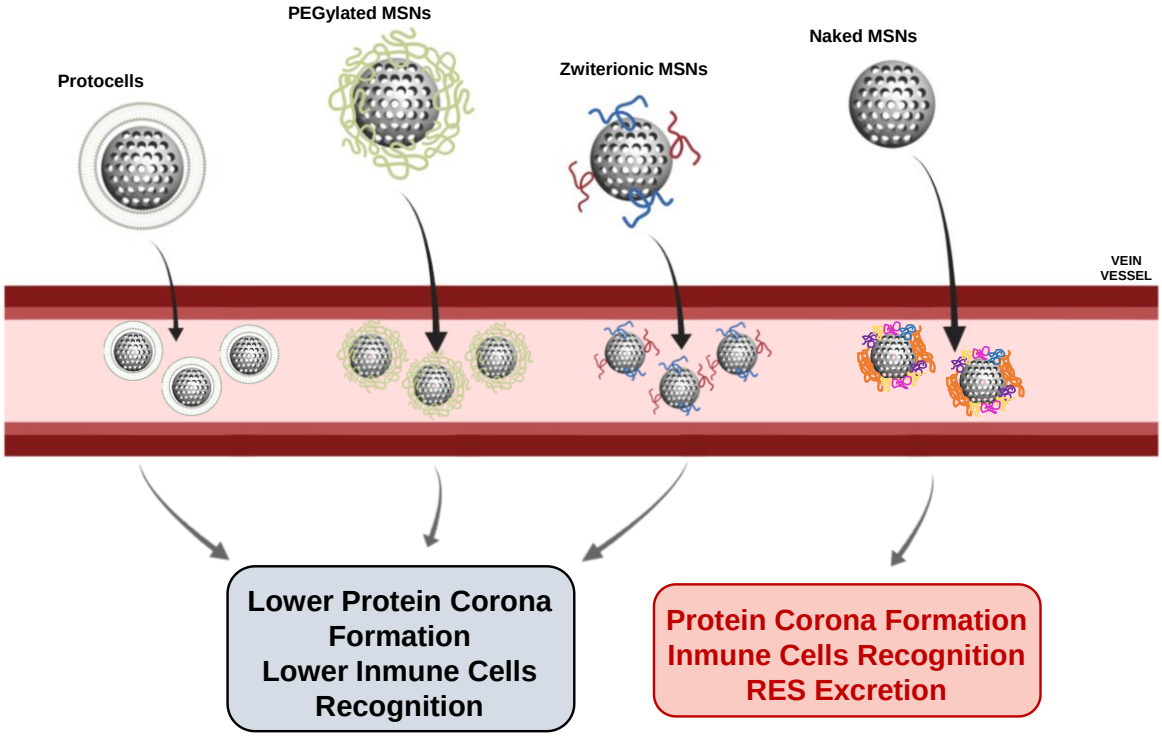

Figure 5.1 Different approaches for obtaining MSNs with long circulation time. Protocells, PEGylated MSNs and Zwiterionic MSNs would slow down the formation of the protein corona with the consequent reduction of opsonization. On the other hand, the naked nanoparticles would be surrounded by proteins and opsonins, being recognized by the immune system and rapidly eliminated by the reticuloendothelial system (RES)

One of the most common strategies to reduce the formation of the protein corona consists on modifying the nanoparticle surface with highly hydrophilic moieties that will hinder the protein adsorption. The presence of these moieties on the nanoparticles surface would produce the adhesion of water molecules forming a hydration layer. In this way, the proteins would not be able to attach to the nanoparticle surface. The most used molecule to achieve this is PEG.[8,9] The process of coating a nanoparticle with PEG has been called PEGylation. This process prevents the non-specific protein adsorption, which enhances the physiological stability and increases the blood circulation time.[6] *In vivo* studies have demonstrated that PEGylation of MSNs decreases their capture by liver, spleen and lung tissues, whereas it increases the blood circulation lifetime and decreases biodegradation.[10] However, the protein corona will eventually form (although more slowly), and the nanoparticles that have might not reached the targeted site will be removed from the circulation by the organs of the reticuloendothelial system (RES), mainly liver and spleen. The properties of PEGylated MSNs are strongly governed by the PEG size, density and conformation. However, the range of protein adsorption could also depend on the chemical strategy used to graft PEG to the MSNs surface. The covalently PEGylated MSNs achieve longer blood circulation times and lower protein adhesion than the PEGylated MSNs by electrostatic interactions.

Another strategy to reduce the formation of protein corona is the zwitterionization of the surfaces through covalent attachment of functional groups with both positive and negative charges. A zwitterion can be defined as a surface with the same number of positive and negative charges, which ensures their electrical neutrality.[11] Several strategies have been optimized to confer zwitterion properties to the MSNs surface.[11–14] One of the most employed approaches is the covalent grafting with zwitterion polymers that present positive and negative charged groups within their backbone.[13] However, such strategy can remarkably increase the hydrodynamic size of MSNs, which could represent a handicap for drug delivery applications. A different alternative could consist in attaching small zwitterionic moieties, such as 2-methacryloyloxyethyl phosphorylcholine,[12] or grafting two different organosilanes exhibiting functional groups with compensated positive and negative charges.[15]

Besides zwitterionization and PEGylation, an additional strategy for protecting the MSNs from the action of plasma proteins is the use of protocells. Briefly, protocells are lipid-coated mesoporous nanosystems. Coating the MSNs with a phospholipid bilayer avoids the possible adherence of opsonins. The protocells synergistically combine the advantages of liposomes (low inherent toxicity, immunogenicity and long circulation times) with those of mesoporous silica nanoparticles (stability and an enormous capacity for multiple cargos combinations). The presence of the outer phospholipid bilayer leads to a reduction in opsonization and therefore longer circulation times.[16]

Other aspects such as particle size, are also involved in the rapid clearance of nanoparticles from the organism. Renal clearance of nanoparticles is highly dependent on particle size, only nanoparticles smaller than 6 nm are going to be filtered by the kidneys.[17] Therefore, nanoparticles of higher diameter than 6 nm would persist in circulation for longer times. However, when the nanoparticles rise 100-150 nm, as they turn bigger, they suffer higher opsonization, therefore, bigger nanoparticles will be cleared more rapidly than 20-150 nm nanoparticles.[18]

In the case of osteoporosis, the most common strategy is the PEGylation. Several studies reported PEGylated MSNs for increasing the circulation half-time to achieve an effective bone delivery.[19,20]

5.1.2.2 Targeting

Another property that nanoparticles should achieve for an effective systemic administration is the capacity of being accumulated in the desired tissue to reduce the long-term adverse effects. This is known as targeting. Depending on how the targeting is achieved, it can be distinguished between two types of targeting, passive targeting and active targeting. Passive targeting is based on the presence of fenestrated vessels in tumor sites. In this sense, the fenestrations created in tumor veins are bigger than the healthy vessels. This fact and the ineffective tumoral lymphatic system, led to a passive accumulation of nanoparticles in the tumor area. Instead, active targeting is based on decorating the nanoparticle surface with molecules that would induce selective accumulation in the diseased tissue. Those moieties would be selected depending on the target tissue. Therefore, in the case of osteoporosis, the first step for providing the nanoparticles with the capacity of active targeting should be the evaluation of the bone composition to select the appropriated moieties with bone affinity.

The average human cortical bone matrix in adult is composed of mineralized tissue (67% of its overall mass) and 33% represents organic matter.[21] The inorganic phase of mineralized bone matrix consists mainly of HA which would represent a promising target for selective delivery. Due to their strong affinity to calcium from HA, BPs are still the major class of bone targeting moieties to deliver therapeutics to the skeleton.

On the other hand, the main component of the organic phase of the bone is type I collagen, which makes it highly interesting as potential target site. Collagen binding domains (CBDs) are abundant in collagenolytic proteases, which will recognize type I collagen.[22] These CBDs could be linked to the nanocarrier surface and used as targeting moiety. However, as collagen type I is ubiquitous within the body, *in vivo* therapeutic benefit from CBD-modified drugs or nanocarriers need to be carefully evaluated, particularly in light of a possible lack of targeting specificity.

Other targeting moieties have been proved to be effective. The natural concept of interactions between repeats of acidic amino acids of bone proteins with calcium within the mineralized tissue

has been recently translated into bone targeting purposes.[22] Small peptides composed of repetitive aspartate sequences have been proposed as a possible bone targeting moietie.[23]

5.1.3 Aims

Since osteoporosis is a systemic disease, all bone tissue would be affected. Therefore, a treatment able to be systemically administrated should be accomplished. Thus, the next step in the present approach and the main objective of this chapter was to achieve a systemic combination therapy by the modification of the previously evaluated system. The successful nanosystem developed in previous chapters was adapted for a systemic administration instead of local, aiming to reach different bone across the organism.

The main challenges that needed to be met were an increased circulation half-life of the nanoparticles and a specific bone tissue accumulation. Coating the nanoparticle surface with PEG should inhibit protein adsorption on the nanoparticle surface reducing its recognition by macrophages and increasing their circulation time in the bloodstream. On the other hand, in order to guide the nanoparticles to bone, it is important to find moieties with strong affinity to some of its compounds. It is known that bones are made of a mineralized matrix, being hydroxyapatite its principal component, so HA could be a promising target for selective delivery. Bisphosphonates, such as alendronate, have been used as bone targeting moieties due to their high affinity to HA and their capacity to bind at sites with osteoclastic activity as it was mentioned above (Figure 5.2). Therefore, the first objective of this chapter was to design an *alendronate modified PEG* (PA) to further functionalize the MSNs developed in previous chapters of the present work.

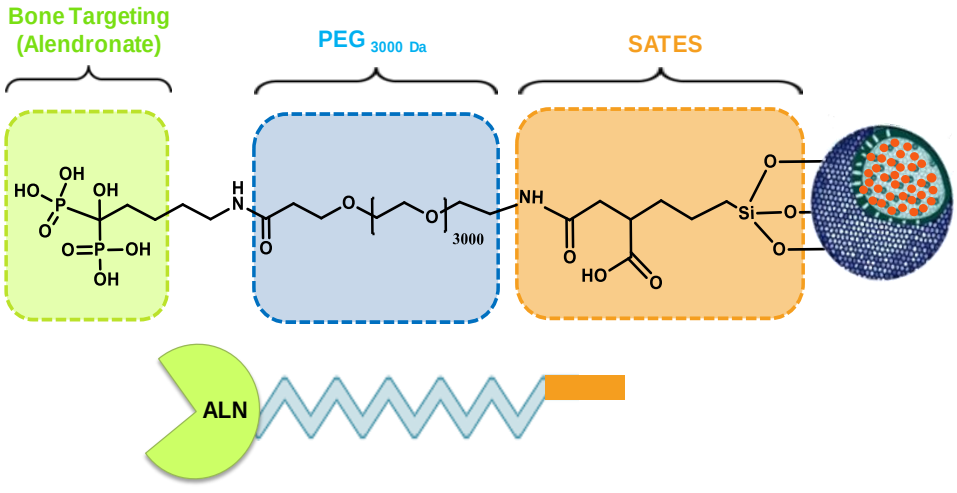

Figure 5.2 PEG-Alendronate moiety for MSNs functionalization.

Once the PA moiety was obtained, the next step was to functionalize the nanoparticles. Our main purpose was to obtain the targeting capacity for the nanocarrier, therefore, the PA needed to be exposed. Our first approximation was to functionalize the PEI with the PA ligand, but since we

were coating our nanoparticles with linear PEI there were not secondary amines to perform the functionalization. We decided to follow a different approach to evaluate its effectivity. We functionalized first the nanoparticle surface with the PA moiety, and after, we coated the nanoparticles with PEI (Figure 5.3). So, our next objective was to optimize the different coatings, regarding the toxicity of the nanoparticles and their capacity to load siRNA.

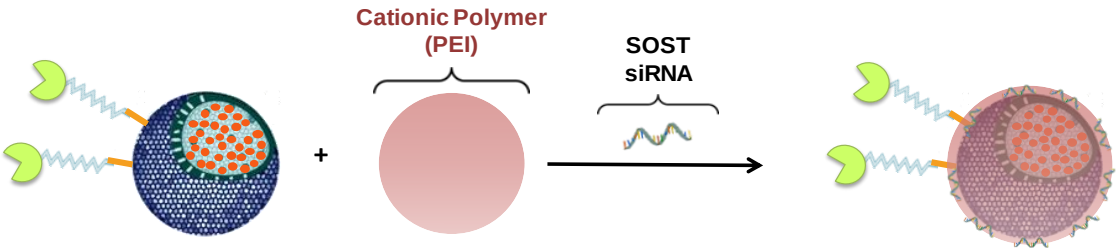

Figure 5.3 Schematic representation of the new system approach.

Since the PEI coating was after the PA functionalization, the first thing to evaluate was the targeting capacity of the particles, so it was necessary to determine if after coating them with the cationic polymer, the PA residue stayed exposed or covered. Also, for the systemic administration desired it was necessary to evaluate the colloidal stability of the new formulated nanoparticles. Before going forward, the capability of the new system of loading and releasing both biomolecules, siRNA and osteostatin, needed to be evaluated. Thus, our third objective was to verify that the diverse polymer coatings did not affect the osteostatin and siRNA load and release. With the system properly optimized and both drugs loaded, our last objective was to evaluate the effect of the systemic administration of the complete system after several injections during two or three weeks in ovariectomized mice. Those effects were evaluated regarding the gene expression modification and the bone quality, quantity and architecture.

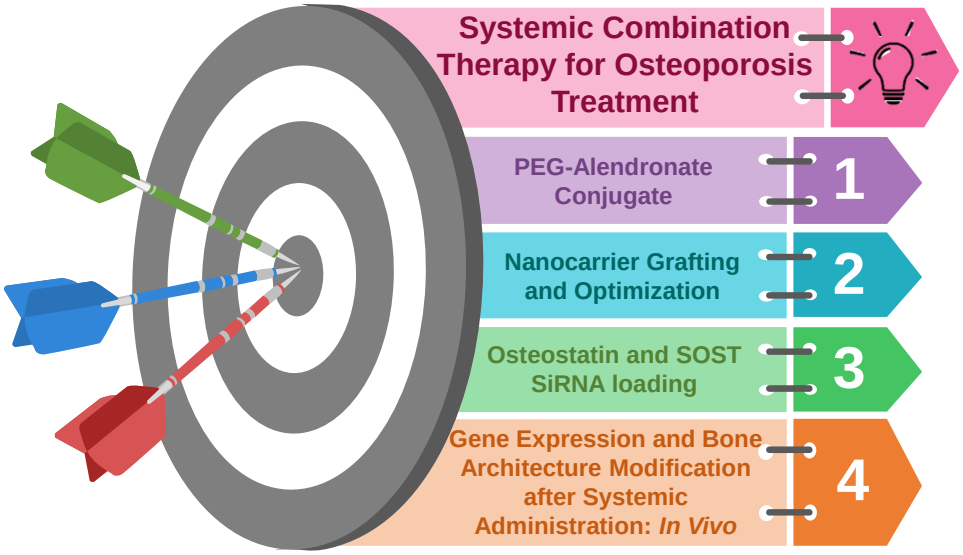

Figure 5.4 Schematic representation of Chapter V aims.

5.2 MSNs Surface Modifications for Systemic Administration

This last piece of research consisted in developing a systemic drug delivery system using mesoporous silica nanoparticles as carrier and functionalizing them with an alendronate modified PEG to achieve a longer blood circulation time and better bone targeting capacity. As mentioned in previous chapters, we have reported a system based on MSNs capable of transporting SOST siRNA and osteostatin for stimulating bone regeneration.[24] The translation of the produced nanomedicine to the clinic would require the systemic administration of the particles in order to potentially target all the osteoporotic bone tissue. Therefore, the present approach was to adapt the already cited nanocarrier to obtain the systemic administration desired.

The synthesis of the PEG-ALN conjugate was the first task to be accomplished. As it can be appreciated in the first step of the Scheme 5.1, alendronate was conjugated via carbodiimide chemistry to the carboxylic acid end of a bifunctional HO_2C-PEG-NH_2 (3500 Da), obtaining the desired targeting molecule (PA). The second step regards the obtention of PEG-NH_2. PEG was conjugated to a residue of glycine to achieve the amino end. The obtention of the final products were confirmed by ^{1}H-NMR as it can be observed in Chapter 2. When both conjugates were obtained, MSNs with diameter of *ca.* 150 nm and mesopores of 2 nm were synthesized following the modification of the Stöber method used in Chapter 3 (See Chapter 2 for MSNs synthesis, functionalization and characterization details). As it was done before, the external surface of the nanoparticles was functionalized with phosphonate groups, in order to have the proper negative surface charge to coat them at the end with the cationic polymer. Both conjugates, PEG-NH_2 and PA were then combined (50:50) and condensed to the MSNs surface for obtaining the two different abilities pursued. Both conjugates were linked to 3-triethoxysilylpropylsuccinic anhydride (SATES) by the reaction of the amino group presented in the PEG conjugates and the anhydride group of the silane. Then, the new sililated polymers were added to the nanoparticles for the condensation onto the surface. Finally, the hybrid nanoparticles functionalized with PA and PEG were collected by centrifugation and washed several times with water and ethanol. Scheme 5.1 summarizes all the process previously explained.

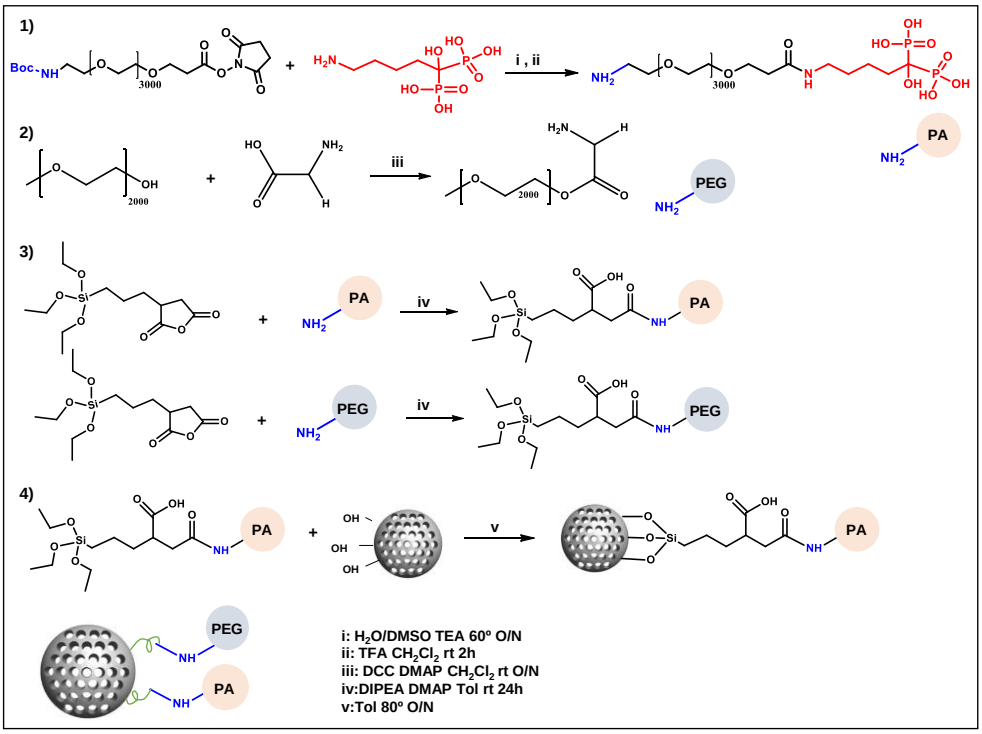

Scheme 5.1 Scheme of PA and PEG synthesis and nanoparticle functionalization. 1) Reaction between amino group of ALN and activated carboxylic acid of PEG. 2) Reaction between PEG and glycine to obtain amino functionalized PEG. 3) Reaction between both PEG conjugates with 3-triethoxysilylpropylsuccinic anhydride. 4) MSNs surface condensation with the sililated polymers.

After the PEGylation of the nanoparticles, they were grafted with PEI following the same protocol as described in Chapter 3. The correct functionalization of the nanoparticles was verified by different techniques. TGA assays confirmed and even quantified the amount of organic matter in the coated nanoparticles. It shows that after the functionalization with PA, a 5% of the weight was organic matter and after PEI grafting the amount increased until 15% of the weight, corresponding 10% to PEI matrix (Figure 5.5A).

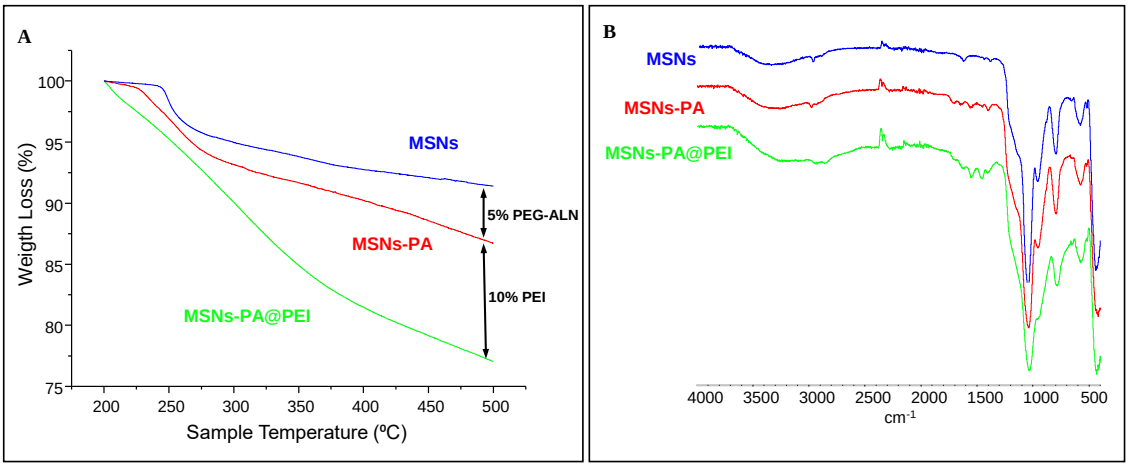

Figure 5.5 Physicochemical characterization of MSNs. The nanoparticles before (MSNs black) and after coating with PA (MSNs-PA red) and PEI (MSNs-PA@PEI blue) polymer were characterized by (A) thermogravimetric analysis (TGA), (B) Fourier Transform Infrared spectroscopy (FTIR).

In the FTIR spectra we can observe the presence of, silica and the different polymer coatings, PA and PEI. The presence of the typical vibration bands of silica (490-1090 cm^{-1} Si-O-Si) in the naked and coated nanoparticles confirmed the silica frame of the nanocarrier. After coating the MSNs with PA, the presence of the typical vibration bands of PEG (1400 cm^{-1} from the active methylene -CH_2-CH_2-CO- and 2900-2800 cm^{-1} from the C-H from CH_2 groups) could be appreciated. PEI grafting was confirmed through new vibration bands related with the presence of PEI appeared (3500 cm^{-1} stretching (δ) vibrations of -NH- groups; 2900-2800 cm^{-1} C-H from CH_2 and CH_3 groups; 1600-1400 cm^{-1} bending (ν) vibrations of -NH- groups) (Figure 5.5B).

Nitrogen absorption analyses confirmed the porous structure of the material as it can be appreciated in the isotherm plot (Figure 5.6A). The size of the mesopores was evaluated through the same technique, finding *ca.* 3.4 nm before coating, 3.2 nm and 2.6 after PA and PEI coating respectively. The slight reduction of the surface area, from 895 m^2/g in MSNs to 882 m^2/g in MSNs-PA verified the functionalization of the nanoparticles. However, since the reduction of surface are was not really appreciable, it could be due to the slight functionalization (5% weight) and/or due to the possible straight conformation (hairy conformation) of the polymer around the surface. On the other hand, after PEI coating, the surface are decrease until 210 m^2/g in MSNs-PA@PEI. This fact also confirmed the successful polymer coating of the nanoparticles, but in this case the reduction was more prominent, meaning that the coating with PEI developed a real polymeric matrix around the particle surface, preventing the access to the pores. The characteristic mesostructure of the MCM-41 type nanoparticles survived the functionalization process as revealed through low-angle XRD where the characteristic diffraction maxima of the 2D hexagonal symmetry were obtained (Figure 5.6B).

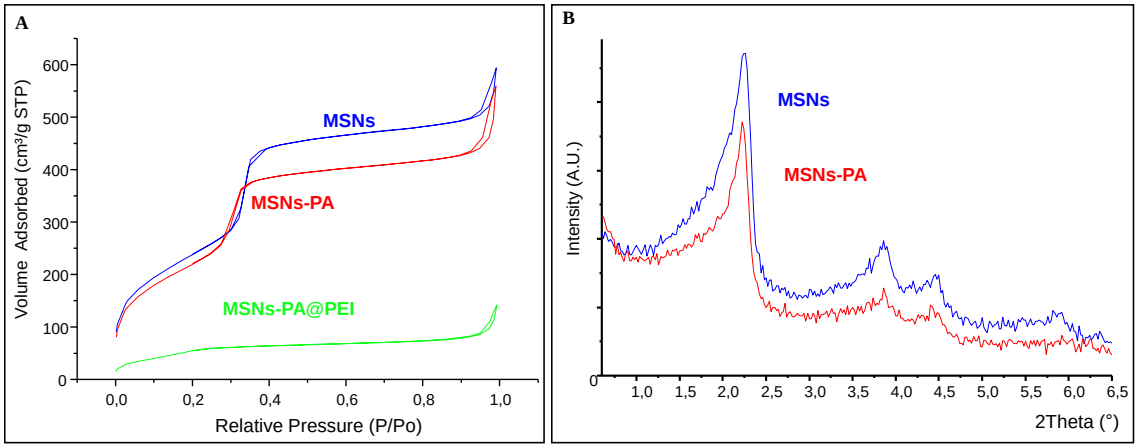

Figure 5.6 Physicochemical characterization of MSNs. The nanoparticles before (MSNs blue) and after coating with PA (MSNs-PA red) and PEI (MSNs-PA@PEI green) polymer were characterized by N_2 adsorption (A) and X-ray diffraction (XRD) (B).

The functionalization of the nanoparticles with PA and PEI was also confirmed through TEM, DLS and Z potential, as it can be observed in Figure 5.7.

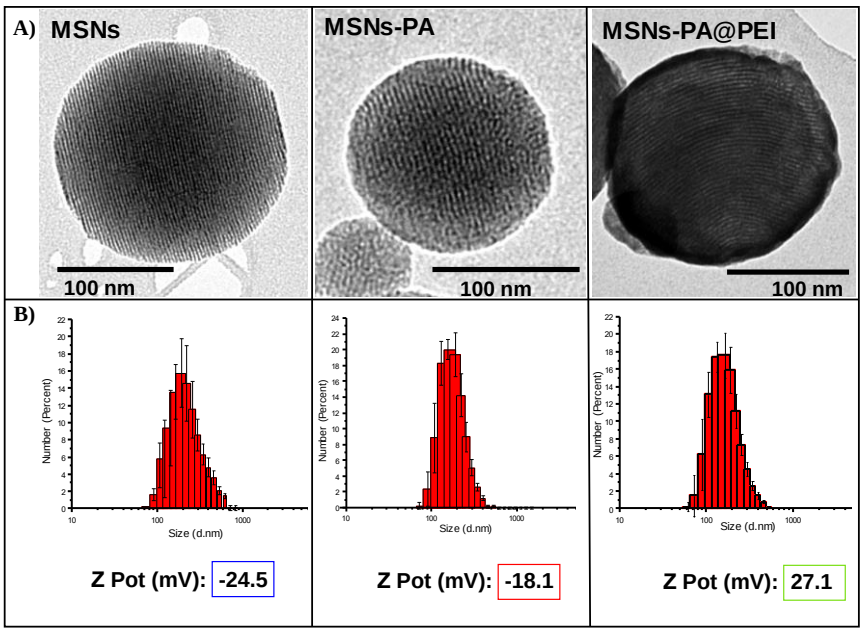

Figure 5.7 Polymer grafting to MSNs surface. TEM micrographs of the nanoparticles (A). Size distribution of the nanoparticles and Z potential of nanoparticles after grafting with the different polymers (PA and PEI) (B).

The nanoparticles were labeled with phosphotungstic acid to determine the correct grafting. Phosphotungstic acid is electron dense, *i.e.* opaque for electrons, and it links to organic matter. After PA grafting, a stained layer did not appear around the nanoparticles, meaning that the functionalization with the polymer was slight. On the other hand, the appearance of a stained layer in the MSNs-PA@PEI confirms the correct grafting with PEI as it can be appreciated in Figure 5.7A. These results were in accordance with the results obtained in N_2 absorption.

The size distribution of the different nanoparticles was also explored through DLS analysis. Figure 5.7B shows that the naked nanoparticles have a diameter of *ca.* 150 nm and were monodispersed. The size of the nanoparticles slightly increased after the different functionalization processes but, what it is more important, the monodispersity was unaffected by the successive reactions at their surface. Furthermore, it can be appreciated a change in the zeta potential in each modification of the surface (Figure 5.7B). Typical values of zeta potential for naked nanoparticles, -24 mV, were observed due to the presence of the silanol groups and phosphonate groups on the nanoparticle surface. After PA grafting, the zeta potential modestly increased up to -18 mV, due to the slight substitution of silanol groups by condensation with PEG, increasing the charge of the surface. Furthermore, after PEI coating, the zeta potential changed drastically. Since PEI is a cationic polymer and it was disposed as a polymer matrix, the surface charge of the nanoparticles changed to highly positive values rising to 27 mV. These data confirm that the external surface of the particles was successfully grafted with the different polymers.

5.3 System Optimization

5.3.1 PEI Grafting Optimization

After conferring the functionalization of MSNs with PA and PEI, the next step consisted on optimizing the amount of PEI grafted to the nanoparticles surface to obtain the proper siRNA biding capacity with the lowest possible cytotoxicity. The amount of PA grafted was kept constant and different ratios of PEI:MSNs-PA (1:2, 1:3, and 1:6) were evaluated to compare their biding capacity to siRNA *vs* their cell toxicity.

Figure 5.8 shows the *in vitro* cell viability of MSNs-PA@PEI of different ratios (1:2 green, 1:3 red, 1:6 yellow) which was evaluated by incubating different concentrations of nanoparticles (200, 100 and 50 µg/mL) with MC3T3 cells for 2 hours. The media was refreshed and after 48 hours of incubation the cell viability was measured.

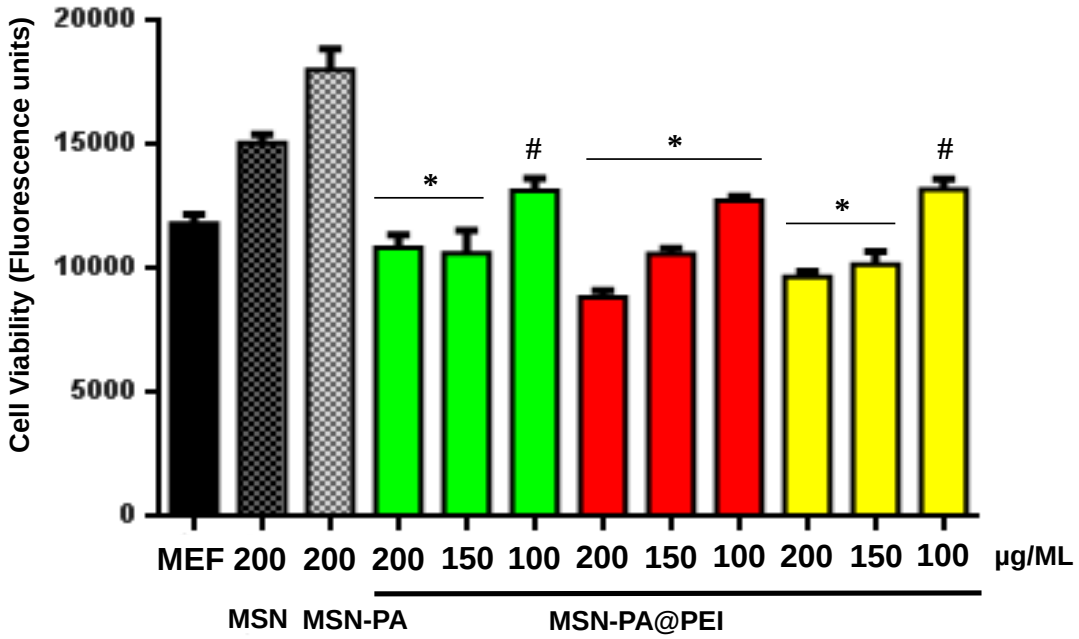

Figure 5.8 MSNs-PA@PEI cell viability in MC3T3-E1 cells. MC3T3-E1 cell viability (measured by Alamar Blue) in contact with different concentrations of MSNs-PA@PEI nanoparticles at 48 h of cell culture. Data are mean ± SEM of three independent experiments performed in triplicate. Asterix indicate $p < 0.01$ *vs* MSNs and hashtag sign indicates $p < 0.05$ *vs* MSNs.

As it can be appreciated in Figure 5.8, MSNs-PA@PEI of different ratios showed non-toxic effects at concentrations as high as 200 µg/mL as it was the case of naked MSNs. The concentration of 100 µg/mL was the best regarding cell viability in all ratios. In the case of 1:2 ratio, cell viability stayed unchanged even after administration of 200 µg/mL nanoparticles dispersion.

To evaluate the binding capacity of the polymeric coating towards the nucleic acid, the highest amount of siRNA that could be bound to MSNs-PA@PEI was determined by agarose gel electrophoresis (Figure 5.9).

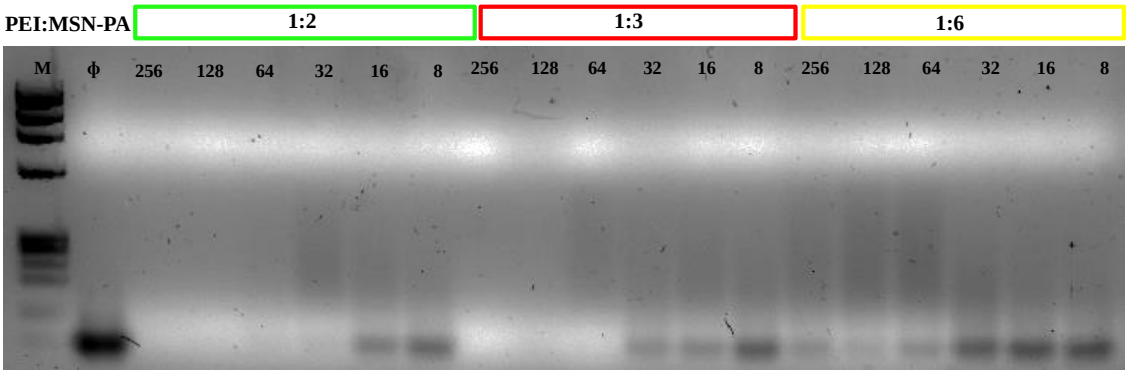

Figure 5.9 Effective SOST siRNA binding to MSNs-PA@PEI. Agarose gel electrophoresis of MSNs-PA@PEI (PEI:MSNs-PA ratio, 1:2 green, 1:3 red, 1:6 yellow) and complexed siRNA in different nanoparticle to nucleic acid (N/P) ratios. M: molecular weight marker. The ϕ lane contains only siRNA.

In particular, different amounts of MSNs-PA@PEI ranging from 0.8 to 25.6 μg (using different PEI:MSNs ratios; 1:2, 1:3 and 1:6) were dispersed together with 0.1 μg of siRNA in aqueous solution to obtain nanoparticle-to-nucleic acid ratios (N/P) of 8−256. N/P is a mass ratio in which N and P, respectively, correspond to the mass of positive (nitrogen (MSNs-PA@PEI)) and negative (phosphonate (siRNA)) charges respectively. One channel was filled just with siRNA as control (ϕ). Then, the dispersions with different nanoparticle to siRNA (N/P) ratios were electrophoresed.

Only uncomplexed siRNA was able to migrate to the positive electrode and, therefore, be observed on the gel. Thus, when the band generated by siRNA is no longer visible means that all the nucleic acid has been complexed with the added nanoparticles and that would be the optimal concentration of nanoparticles needed to complex all the siRNA presented.

The results observed in Figure 5.9 indicated that all siRNA was bound to the nanoparticles at a N/P ratio >32 for 1:2 ratio, and >64 for 1:3 ratio. Thus, 32 μg of MSNs-PA@PEI (1:2) and 64 μg of the MSNs-PA@PEI (1:3) were needed to load 1 μg of siRNA. Consequently, the siRNA loading capacity of the nanoparticles was found to be *ca*. 3 wt%, and 1.5 wt% for the 1:2 ratio and 1:3 ratio, respectively. On the other hand, the 1:6 ratio was unable to properly bind siRNA being visible the band of siRNA even after adding 25.6 μg of nanoparticles to 0.1 μg of siRNA. Therefore, the 1:6 ratio was directly dismissed for further investigations.

Taking into consideration that the amount of siRNA recommended by the manufacturer to achieve a proper knockdown effect was around 0.5 μM, it means that final concentration of siRNA should be *ca.* 6.65 μg/mL. Thus, taking into account the ratio obtained (32 N/P ratio), we can approximate

that the nanoparticle concentration should be *ca.* 200 µg/mL (32 µg of nanoparticles for each µg of siRNA), which was within the nontoxicity window for MSNs-PA@PEI (1:2 ratio) as appreciated in Figure 5.7. Then, although the loading capacity of the nanoparticles could be considered low, it was found to be good enough to transport the efficient amount of siRNA needed for an effective knockdown. Consequently, the MSNs-PA@PEI 1:2 ratio resulted on the better loading capacity with non-toxic effect. Based on these results, 1:2 was the ratio selected and further used for the next steps in our research. It is worth mentioning that the siRNA presence in the PEI mesh did not affect the cell viability as previously reported in the other system.

5.3.2 Bone targeting and Colloidal Stability

The aim of functionalizing the surface with PA was to achieve a bone targeting capacity, in order to increase the number of nanoparticles in the desired tissue. Additionally, decorating the nanoparticles with PEG aimed at the augmentation of the colloidal stability, avoiding the nanoparticle aggregation and the future blocking of blood vessels. Consequently, the evaluation of both capacities was the next task to accomplish in this work

5.3.2.1 Bone Targeting

A hydroxyapatite targeting assay was performed to evaluate the targeting capacity of the new system. The functionalized nanoparticles were exposed to a commercial HA tablet (ENGIPORE pre-formed bone substitute) and then the retention capacity was evaluated (Figure 5.10).

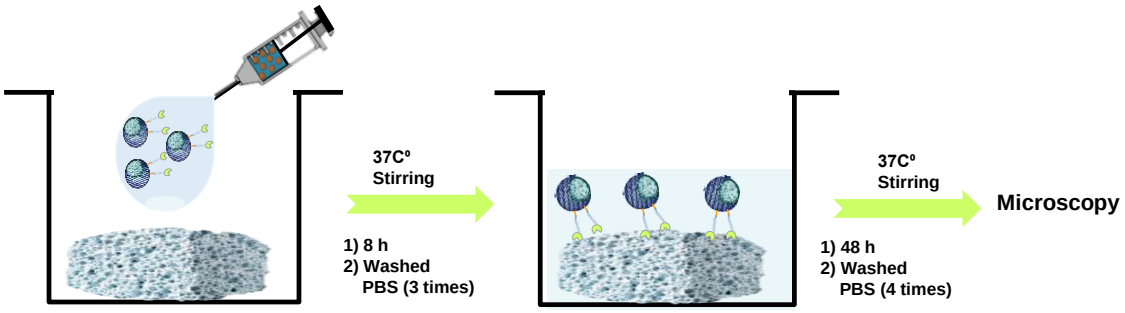

Figure 5.10 Hydroxyapatite targeting assay. The nanoparticles naked and functionalized with the different polymers were added to the HA tablets, incubated for 8 hours, and then washed. The HA tablets were after incubated with clean PBS and washed several times before the evaluation by fluorescence microscopy.

Different rhodamine-B-labeled nanoparticles, naked (MSNs), MSNs@PEI, MSNs-PEG, MSNs-PEG@PEI, MSNs-PA, MSNs-PA@PEI, were incubated for 8 hours with the HA tablet. Since the nanoparticles are functionalized with a PA conjugate, the ALN would be the targeting moiety of the nanoparticles. In this sense, ALN binds to HA, therefore the nanoparticles functionalized with the BP would be accumulated in the HA tablet. After the incubation time, the HA tablets were washed with fresh PBS and incubated for 48 hours in clean PBS to remove the possible

nanoparticles that could be adsorbed to the porous structure of the HA tablet. The HA tablets with different nanoparticles were compared by fluorescence microscopy (Figure 5.11).

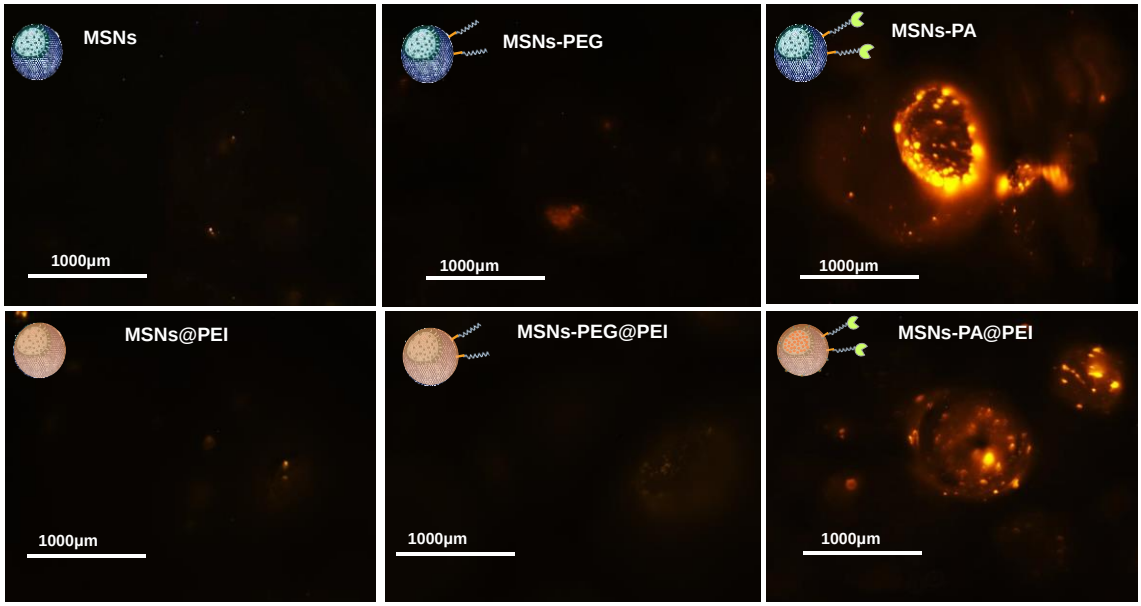

Figure 5.11 Hydroxyapatite targeting behavior of MSNs-PA@PEI. Representative microscopy images of HA tablets incubated for 8 hours with Rhodamine B-labeled MSNs, MSNs-PEG, MSNs-PA, MSNs@PEI, MSNs-PEG@PEI and MSNs-PA@PEI nanoparticles. Red fluorescence (nanoparticles).

The rhodamine-B-labeled nanoparticles were observed in red in the different tablets, revealing that the naked nanoparticles were not accumulated in the HA tablet, as well as the nanoparticles covered either with PEG or PEI, or with both of them. As it can be appreciated in the Figure 5.11, only when the ALN of the PA polymer was presented in the MSNs, a retention inside the HA matrix was achieved. This fact confirms the bone targeting capacity of this new system thanks to the presence of the BP in the PEG conjugate as initially hypothesized.

5.3.2.2 Colloidal Stability

As mentioned before, the nanoparticles must be stable in suspension while circulating in the blood, avoiding the obstruction of blood vessels, that could potentially compromise the patient´s life. In this case, in other to increase the colloidal stability, the nanoparticles were functionalized with PEG. This polymer would not only increase the dispersity of the nanoparticles, but also would reduce the opsonization of the nanoparticles in the blood. This fact would be critical in relation with the blood half-life of the nanocarriers. The stability of this new PEGylated nanoparticles (MSNs-PA) coated with PEI (MSNs-PA@PEI) was compared with our previously reported non-PEGylated nanoparticles (MSNs), using FITC-labeled MSNs (Figure 5.12).

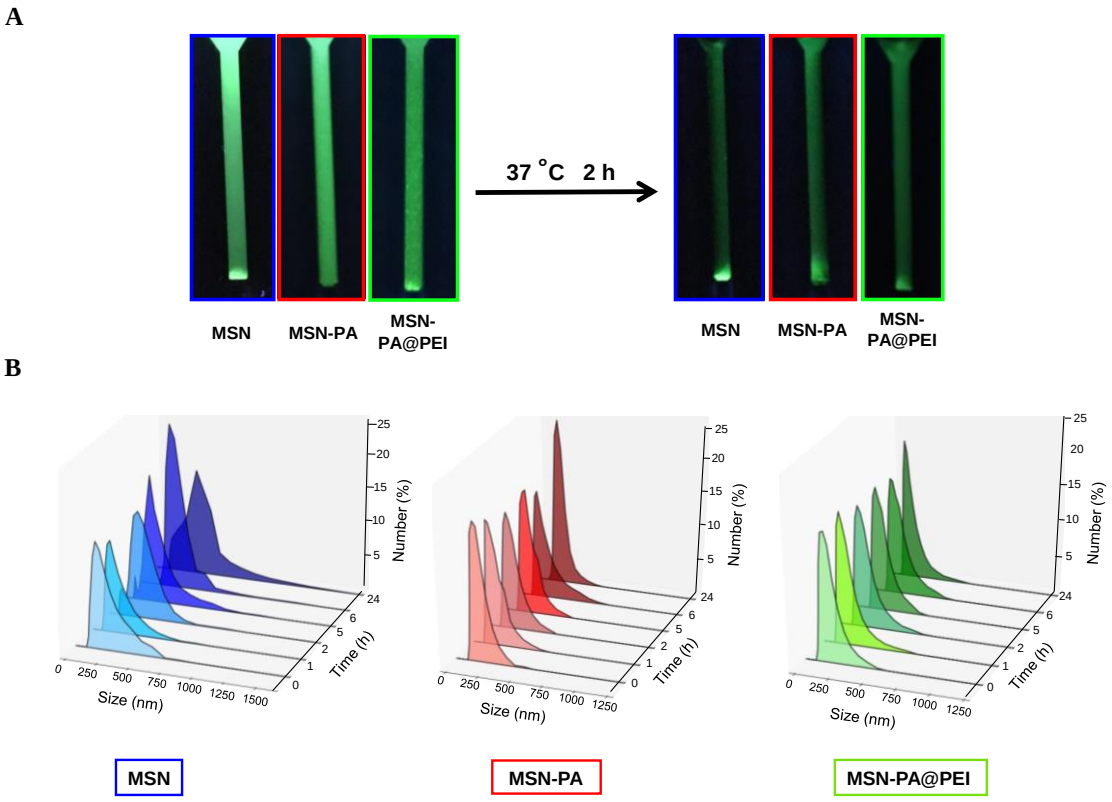

Figure 5.12 Colloidal stability of MSNs-PA@PEI nanoparticles. (**A**) Suspension stability of FITC-labeled MSNs (black), MSNs-PA (red), MSNs-PA@PEI (blue) nanoparticles. Photographs taken under ultraviolet light. (**B**) Hydrodynamic diameter of MSNs (black), MSNs-PA (red), MSNs-PA@PEI (blue) nanoparticles after 1, 2, 5, 6 and 24 hours.

The particles were dispersed in PBS (1 mg/mL of nanoparticles) and kept at 37°C for 1 h without stirring. After this time, they were evaluated under ultraviolet light. MSNs can be clearly observed at the bottom of the cuvette by the fluorescence of nanoparticles under UV light, while MSNs-PA or even MSNs-PA@PEI remained dispersed (Figure 5.12A).

This enhancement in nanoparticle suspension stability was further confirmed by evaluating the hydrodynamic diameter of the different nanoparticles after different periods of time in suspension in 1 mM PBS (Figure 5.12B). Non-PEGylated nanoparticles were aggregated after 2 hours in suspension, while the size and monodispersity of PEGylated nanoparticles remained unmodified for over 24 hours, meaning that nanoparticle aggregation was not taking place.

These results indicated that the stability of the nanoparticle suspension was greatly improved in the PEGylated systems, which was one of the main aims of our approach. Furthermore, after PEI coating the nanoparticles remained dispersed, therefore it should be remarked that the PEI coating did not affect to the stability of the nanoparticles.

5.3.3 Cellular Uptake

PEI was selected as grafting polymer for siRNA delivery due to its capability of enhancing the particle uptake into cells.[25] Although this fact was verified in the previous chapter, since the nanoparticle grafting has been changed, it was necessary to evaluate the cell penetration capability of the new system. In this case, the evaluation of the cellular uptake of the MSNs-PA@PEI through flow cytometry was performed in MC3T3-E1 cells (Figure 5.13).

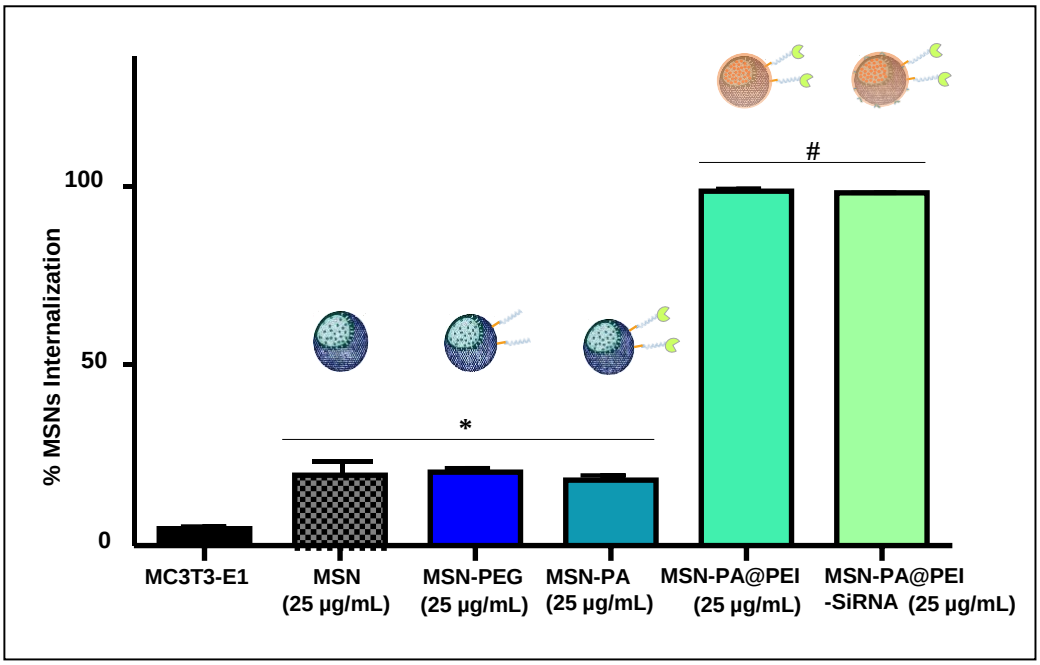

Figure 5.13 MSNs-PA@PEI-siRNA uptake by MC3T3 cells by flow cytometry. Cellular uptake of different fluorescein-labeled MSNs, MSNs@PEI, and MSNs@PEI-siRNA was measured by flow cytometry at 2 h of internalization in MC3T3-E1 cells. Data are mean ± SEM of three independent experiments performed in triplicate. Asterisks indicate $p < 0.05$ *vs* MC3T3-E1; hashtag indicate $p < 0.01$ *vs* MC3T3-E1, MSN, MSN-PEG and MSN-PA.

FITC-labeled MSNs, MSNs-PEG, MSNs-PA, MSNs-PA@PEI, MSNs-PA@PEI-siRNA nanoparticles were used. Figure 5.13 shows that after coating the MSNs-PA with PEI, the nanoparticle uptake significantly increased. This fact could be ascribed to the drastic change on the surface charge, from negative (MSNs-PA) to positive (MSNs-PA@PEI) being easier for the negatively charged cell membrane to wrap the positively charged nanoparticles.

5.3.4 Osteostatin Release

Since nanoparticles were functionalized with PEI and PA, it was necessary to test whether the PA functionalization could affect the osteostatin release from the MSNs. Osteostatin was loaded into the mesopores of the MSNs-PA by immersing the nanoparticles in a solution of osteostatin overnight. Then, the nanoparticles were first washed with PBS to eliminate the extra osteostatin and then coated with PEI. Afterwards, a release experiment was carried out, and the amount of osteostatin released was measured by fluorescence thanks to the presence of tryptophan (Trp) in

the pentapeptide of osteostatin (Thr-Arg-Ser-Ala-Trp). In this sense, the indole group of Trp is considered the dominant source of florescence, being excited at ~280 nm and emission at ~350 nm in proteins.[26]

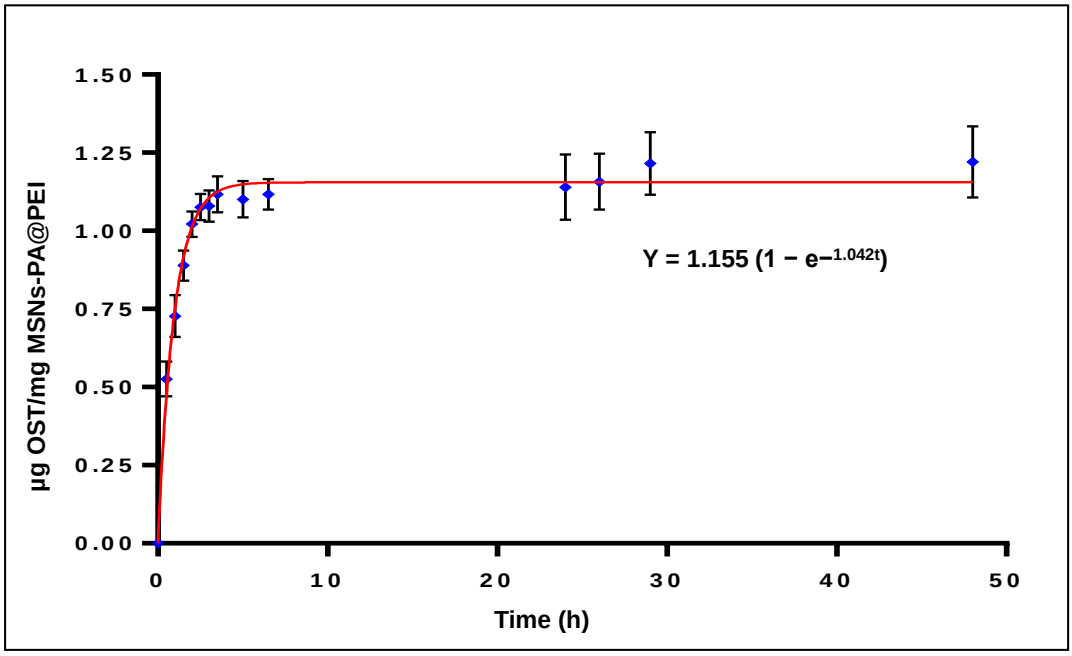

Figure 5.14 Time-dependent osteostatin (OST) release from MSNs-PA@PEI in PBS at pH 7.4, simulating the physiological fluids. MSNs-PA were loaded with OST and afterwards coated with PEI (OST-MSNs-PA@PEI). Points are the means of three independent measurements per time period.

The Osteostatin release kinetics (Figure 5.14) could be fitted to a first-order kinetic model, with a typical release profile from mesoporous materials (eq 5.1):

$$Y = A(1 - e^{-kt}) \qquad \text{eq 5.1}$$

The equation parameters could be described as Y being the amount of osteostatin released (micrograms of osteostatin per milligram of MSNs-PA@PEI) at time t (h), with A being the maximum amount of osteostatin released (in micrograms of osteostatin per milligram of MSNs-PA@PEI), and with k being the release rate constant.

The release data showed that MSNs loaded with osteostatin and coated with PEI (OST-MSNs-PA@PEI) released osteostatin in a time-dependent manner, reaching values of 1.155 micrograms of osteostatin per milligram of MSNs-PA@PEI. Thus, despite PA functionalization and PEI coating, which are not acting as a physical barrier impeding the osteostatin release, the MSNs were able to release the cargo. Therefore, MSNs-PA@PEI could be used to co-transport and co-deliver osteostatin and siRNA at the same time.

5.3.5 RNase Protection Assay

As explained before, one of the limitations of using naked siRNA for systemic treatment is its rapid degradation by enzymatic action. For this reason, we designed a system able to protect the siRNA from the action of these enzymes. Then, after evaluating the capacity of releasing both molecules from the nanosystem, it was necessary to evaluate the activity of the released siRNA demonstrating the protection capacity of the system from the RNase type I.

To evaluate the siRNA stability against RNase type I activity of the MSNs-PA@PEI-siRNA, free siRNA and MSNs-PA@PEI bound to siRNA were exposed to RNase. Free siRNA exposed to RNase type I would determine the activity of the enzyme, being siRNA degraded if the enzyme was active. Instead, siRNA loaded nanoparticles were exposed to RNase type I, in order to determine the protection capability of the nanoparticles. After the exposure of siRNA loaded nanoparticles to the enzyme for two hours, siRNA was released from the polymer coated nanoparticles by the addition of sodiumdodecylsulfate (SDS), which displaced the siRNA from the polymer due to its surfactant nature. This step was performed after inactivation of the enzyme with EDTA to determine the integrity of siRNA after enzyme activity. The samples were after electrophoresed by gel retardation assay to determine the integrity of siRNA (Figure 5.15). Only uncomplexed and intact siRNA would appear at end of the gel. Therefore, either when siRNA is complexed to nanoparticles or it has been degraded by RNases the band would be no longer visible. Instead, only when siRNA resist the action of RNase type I, a band would appear at the end of the gel.

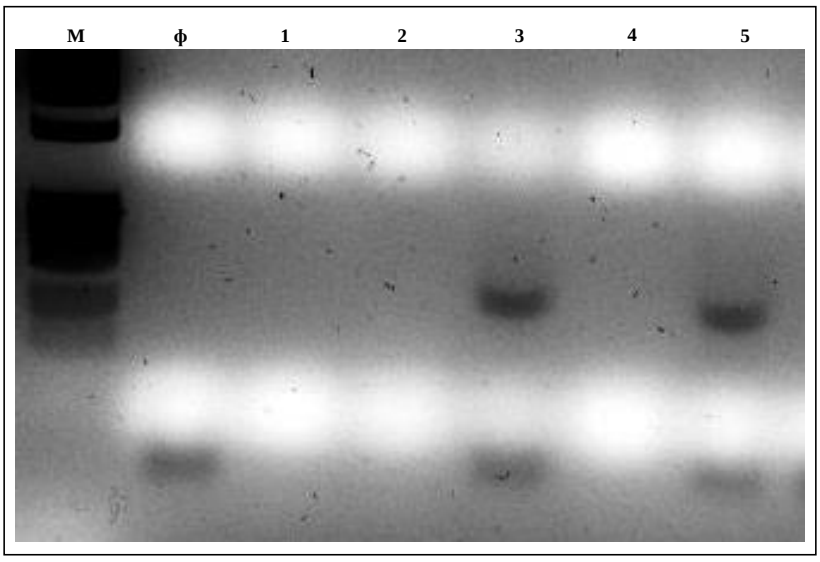

Figure 5.15 RNase type I stability assay. Agarose gel electrophoresis of MSNs-PA@PEI-siRNA exposed or not to RNase. M: molecular weight marker. Φ: free siRNA. 1: free siRNA incubated for 2 hours with RNase type I. 2: MSNs-PA@PEI bound with siRNA at 32 N/P . 3: MSNs-PA@PEI bound with siRNA and incubated with SDS for 15 minutes. 4: MSNs-PA@PEI bound with siRNA incubated with RNase type I for 2 hours. 5: MSNs-PA@PEI bound with siRNA incubated with RNase type I for 2 hours, then incubated with EDTA for enzyme inactivation, and finally mixed with SDS for the display of siRNA.

One channel was filled with siRNA as control (ϕ). The results showed that when free siRNA was exposed to RNase type I (channel 1) the siRNA band disappeared meaning that siRNA was degraded by the enzyme. MSNs bound to siRNA were charged in channel 2. After the electrophoresis, the band corresponding to the siRNA disappeared because all the siRNA was bound to the added nanoparticles. On the other hand, in channel 3, the nanoparticles were complexed with siRNA, and then SDS was added for releasing the siRNA from the nanoparticles. After electrophoresis the band related with siRNA appeared by the end of the gel. Therefore, after siRNA was bound to the nanoparticles and released by SDS it was possible to appreciate a band in the electrophoresis gel. In channel 4, nanoparticles loaded with siRNA were exposed to RNase type I for 2 hours. After electrophoresis, no band appeared at the end of the gel, meaning that the RNase type I did not generate any band. This fact would be important to take into consideration for the evaluation of channel 5. In this sense, the appearance of a band at the end of the gel would be only related with the presence of intact siRNA. Finally, in channel 5, MSNs bound to siRNA were incubated with RNase type I for 2 hours, and after inactivation of the enzyme, siRNA was released from the nanoparticles by the addition of SDS. In this case, a band appeared again by the end of the gel, meaning that siRNA resisted the action of RNase type I. Taking everything into consideration, only when siRNA was bound to the nanoparticles it would resist the enzyme activity being not degraded after 2 hours of contact with active RNase type I.

5.4 *In Vivo* Evaluation

After evaluating the effectiveness of SOST siRNA delivered from MSNs and confirming the synergistic effect between SOST siRNA and osteostatin both *in vivo* and *in vitro* by a local injection (inside femur bone marrow) (Chapters 3 and 4), the next step of this thesis was to evaluate the new systemic approach that has been optimized. This thesis is focused on the effect produced by the delivery of osteostatin and SOST siRNA from MSNs after several subcutaneous injections for 2 or 3 weeks. It was studied how this new system modified the expression of different osteogenic genes *in vivo* after a systemic treatment, and how this gene expression modification would affect bone formation in an osteoporotic scenario.

In this thesis the focus was on postmenopausal osteoporosis. The most popular model for postmenopausal osteoporosis is obtained by the ovariectomy of female animals.[27] Consequently, estrogen deficiency enhances bone resorption, being the main cause of this type of osteoporosis. The depletion of estrogen would produce significant bone loss after at least 14 days of surgery.[27] Therefore, for the evaluation of the treatment it has been used 12 weeks old ovariectomized C57/BL6 female mice, which surgery was performed 6 weeks before, with a decreased femoral bone mineral density compared to non-ovariectomized (49.814 ± 0.28 mg/cm^2 *versus* 46.67 ± 0.47 mg/cm^2; $p < 0.001$) in the beginning of the experiment.

They would be treated for 2 or 3 weeks with the MSNs loaded both with SOST siRNA and osteostatin. Nanoparticles were detectable inside mice for a limited period of time, which was determined to stablish the frequency of the injections to be performed in the animals. Therefore, 100 μL of a cyanine 7 (Cy7) labeled nanoparticles (MSNs-PA@PEI) dispersion (0.8 mg/mL) were injected subcutaneously (sc) in the left back (near by the leg) of the ovariectomized mice, and evaluated under fluorescence microscopy at different time points. In Figure 5.16 it could be observed that the nanoparticles remained in the organism after even 72 hours, so the injections of the nanoparticles would be performed every two days, to assure presence of nanoparticles at every moment.

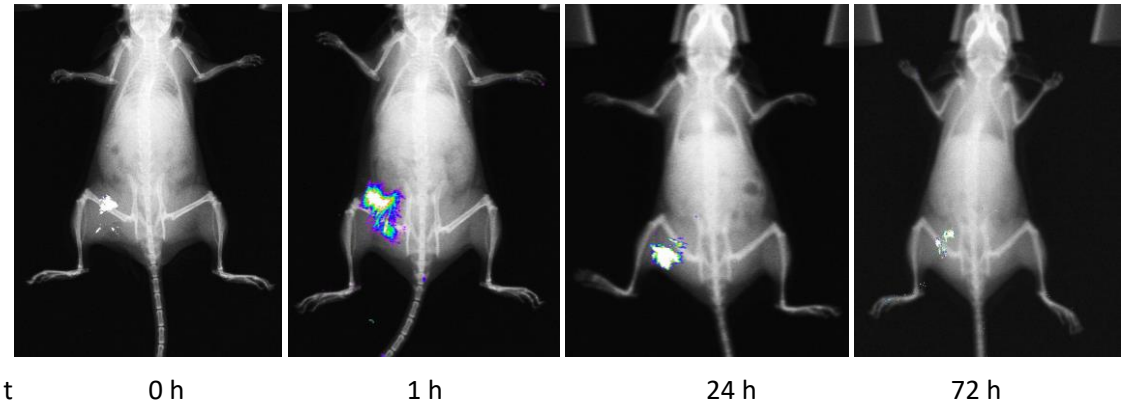

Figure 5.16 Subcutaneous injection in ovariectomized female mice of cyanine-7 labeled nanoparticles, distribution and accumulation at 0, 1, 24 and 72 hours.

According to the obtained results, the injections of the complete system (OST-MSNs-PA@PEI-siRNA) and each control (MSNs-PA@PEI and free PTH 100 μg/kg) were performed every 2 days for 2 and 3 weeks of treatment.

Animals were euthanized after 2 or 3 weeks of treatment, respectively. Femur and tibiae were removed and analyzed by different techniques to evaluate the systemic effect. The effect of the administrated system was evaluated through the expression of different osteoporotic genes such as, SOST, Runx2, Alp, osterix (OSX), and osteoprogeterin (OPG), and vascularization related genes such as vascular endothelial growth factor (VEGF). Figure 5.17 shows mRNAs measured by qRT-PCR after 2 (solid pattern) or 3 (line pattern) weeks of treatment (Figure 5.17).

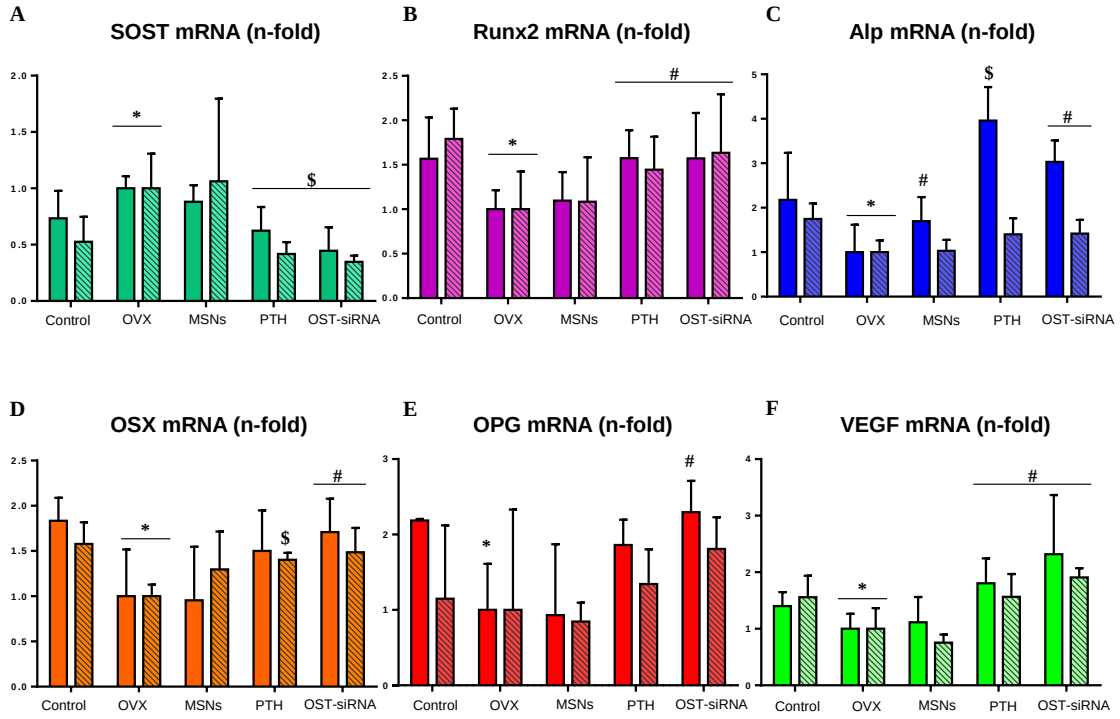

Figure 5.17 *In vivo* gene expression evaluation (measured by real-time PCR) in femur bone of healthy (Control) and ovarectomized (OVX) mice. SOST (A), Runx2 (B), Alp (C), OSX (D), OPG (E), VEGF (F) mRNA expression in presence of SOST-siRNA and osteostatin loaded in MSNs-PA@PEI nanoparticles (OST-siRNA). A gold stadart treatment control has been used (free PTH 100 μg/Kg every two days) (PTH), and free MSNs-PA@PEI nanoparticles were used as negative control (MSNs). Data are mean ± SEM of five independent mice. Asterisk indicate $p < 0.05$ *vs* Control; hastag signs indicate $p < 0.05$ *vs* OVX, and pound signs indicate $p<0.01$ *vs* OVX.

SOST gene is involved in different developmental processes, particularly, inhibits osteoblastic activity and differentiation being responsible of bone formation modulation. Therefore, its modification would affect bone status. In this study, the nanoparticles delivered SOST siRNA in order to reduce the expression of this gene and therefore increase bone formation. In Figure 5.16A it can be appreciated that the expression of SOST in ovariectomized mice (OVX) is higher compared to non-ovariectomized mice (Control) and was statistically significant. However, the injection of the nanoparticles with SOST siRNA and osteostatin (OST-siRNA) notably decreased the expression of SOST after 2 or 3 weeks of treatment (*ca.* 50% and 60%, respectively) (Figure 5.17A). The systemic administration of the osteostatin and siRNA loaded nanoparticles decreased the expression of the target tissue, verifying the knockdown activity of the injected system. Therefore, the synthesized nanoparticles were able to protect the siRNA and the peptide from the enzyme degradation, transporting the therapeutic agents to the target cells.

Besides the modification of SOST, we evaluated the expression of many other osteogenic markers to determine the osteogenic effect of our system. Since ovariectomy increases the bone resorption process, the expression of genes related with osteogenic features are expected to lessen. The osteogenic markers, Runx2 (Figure 5.17B), Alp (Figure 5.17C), OSX (Figure 5.17D) and OPG

(Figure 5.17E) decreased their expression in OVX compared to control group, as expected. In this case, being SOST a gene involved in cell differentiation inhibition, its knockdown was expected to increase the expression of osteogenic markers.[28–30] Therefore, after the application of the system with SOST siRNA and osteostatin, the results showed that Runx2, Alp, OSX and OPG expression notably increased being in total agreement with the previously reported *in vitro* and *in vivo* results.[24] The expression increment of the different genes was more noticeable after 2 weeks than after 3 weeks. Particularly, Alp and OPG presented a considerable difference between the results obtained at 2 and 3 weeks being 3 n-fold *vs* 1.4 in the case of Alp, and 2.15 n-fold *vs* 1.8 for OPG. Therefore, the relevant change in the gene expression occurred after 2 weeks. The delivery of osteostatin and SOST siRNA was traduced in an increment in osteogenic markers, confirming the osteogenic feature of SOST knockdown and osteostatin effect.

Furthermore, the expression of VEGF was evaluated, which could be ascribed to a bone formation process, since the new created bone would need vascularization. The expression of VEGF gene was also increased after the administration of OST-MSNs-PA@PEI-SOSTsiRNA (OST-siRNA) (Figure 5.17F). This fact would be in agreement with the hypothesis stated before. The increased VEGF expression could be correlated with the increment in bone formation, being necessary the production of blood vessels and therefore the increment in VEGF expression.

Unloaded nanoparticles were evaluated as control to discard any potential effect of the employed nanocarrier (negative control). The current gold standard treatment for osteoporosis, PTH was used to evaluate the better effectiveness of our nanosystem compared to an already approved treatment. Comparing the results obtained with the injection of free PTH and the injection of our system (OST-siRNA), it could be concluded that the administration of the co-loaded nanoparticles reached similar values of gene silencing and stimulation, being even slightly more effective our system in some particular cases such as OPG, VEGF, and OSX expression. Therefore, the here proposed system yielded better results than the gold standard osteoporosis treatment PTH, being considered as a potential alternative for osteoporosis treatment.

After the evaluation of the gene expression modification, the next step was to study the effect generated by the gene fluctuation in the bone microarchitecture. As mentioned in previous chapters, one of the main points for a successful osteoporosis treatment is not only to increase the BMD, but also to improve the bone architecture. The ability of a bone to resist fracture (or "whole bone strength") depends not only on the bone mass, but also on its spatial distribution (macro- and microarchitecture), and the intrinsic properties of the materials that constitute the bone. Quantitative assessment of macro- and microstructural bone features improves our ability to estimate bone strength. Thus, knowledge of bone microarchitecture is essential for understanding the pathophysiology of osteoporosis, determining the quality of bone, predicting fractures, and

evaluating the efficacy of a treatment.[31] The response of microarchitectural parameters to treatment should assess the real efficacy of anti-osteoporotic treatments, which are primarily expected to stop the progression of disease and prevent fractures. For this reason, the architecture of the treated and non-treated bones was evaluated by Micro-Computed Tomography (μCT) (Figure 5.18). Taking into consideration the fact that the most pronounced fluctuation of genes was after 2 weeks (see above) the architecture of the bone should be evaluated after 3 weeks of treatment. In this sense, we would be able to detect the consequences of the gene expression modifications after 2 weeks that would be appreciated in the bone microarchitecture 1 week after.

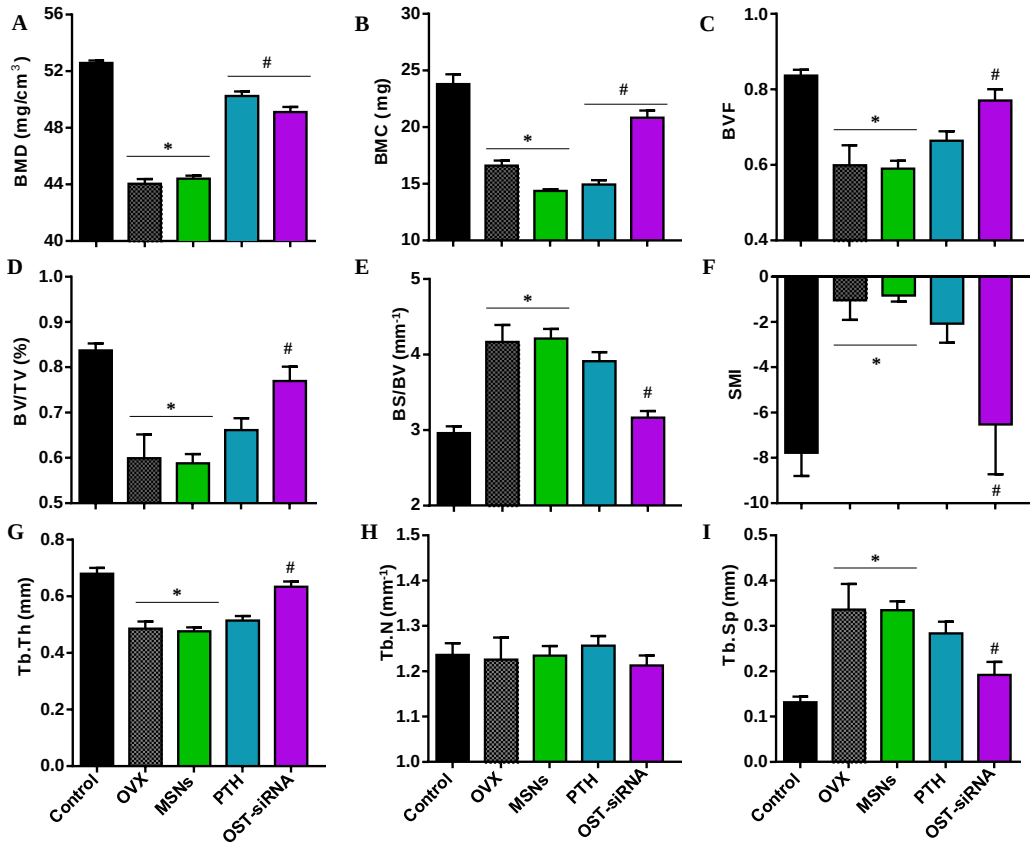

Figure 5.18 Representative parameters of trabecular morphology measured by μCT to evaluate the effect after 3 weeks of treatment. (A) Bone mineral density (BMD) (B) Bone mineral content (BMC) (C) Bone volume fraction (BVF) (D) trabecular bone volume per total volume (BV/TV) (E) Specific bone surface (BS/BV) (F) structure model index (SMI) (G) mean trabecular thickness (Tb.Th) (H) mean trabecular number (Tb.N) (I) Mean trabecular separation (Tb.Sp). Data are mean ± SEM of five independent mice. Asterisk indicate $p < 0.05$ *vs* Control and hashtag signs indicate $p < 0.05$ *vs* OVX.

There are several advantages of using μCT for the assessment of bone mass and morphology. First, it permits the direct 3D measurement of trabecular morphology, such as trabecular thickness and separation. Second, it also analyzes a large volume of bone, and third, the technique is non-destructive, so the same sample could be used for other evaluation.[31]

Different parameters have been considered for the evaluation of the different therapeutics effect. The bone mineral density is one of the most common used values to determine the quality of bone. It relates the amount of mineral (mainly HA) per volume of bone tissue. As appreciated in Figure 5.18A, in osteoporotic-like scenarios, BMD tent to decrease in comparison with healthy situation (control). In this case, BMD of healthy mice was around 53 mg/cm^3 (Control). Instead, ovariectomized mice (OVX) presented lower value of BMD, around 44 mg/cm^3. After 3 weeks of treatment, the values of BMD increased *ca.* 70% with PTH and *ca.* 60% with our system (OST-siRNA), approaching to a healthy mice situation (Figure 5.18A).

The bone mineral content (BMC) was also evaluated, which expresses the amount of mineral in a specific area of the bone tissue.[31] In this case, BMC also decreased after ovariectomy in agreement with the assumptions. After the loaded nanoparticles administration (OST-siRNA), BMC was recovered *ca.* 65%. In this case, our system presented better results than PTH treatment (Figure 5.18B).

The basic morphometric indices include the measurement of bone volume (BV) and the tissue volume (TV). The ratio of these two measures is the bone volume fraction (BV/TV or BVF). Figure 5.18C and D shows that ovariectomized mice presented lower values of bone volume fraction compared to healthy mice. After 3 weeks of several injections of free PTH or OST-MSNs-PA@PEI-siRNA (OST-siRNA), both values increased recovering around the 25% of the bone volume fraction in the case of PTH treatment and over 70% with the nanoparticle treatment.

Another basic measure is the bone surface (BS), which is necessary to obtain the specific bone surface or bone surface fraction (BS/BV). Figure 5.18E shows that BS/BV increased considerably in the ovariectomized group, reducing its value after PTH application (*ca.* 20%) or our system treatment (*ca.* 85%), reaching similar values to healthy mice.

An index called structure model index (SMI) was developed to estimate the trabecular bone structure. This index was designed to be 0 for perfect plates, 3 for perfect rods and 6 for perfect spheres. However, it might occur that values outside this range could be obtained in cases of very high or very low bone fraction. In healthy bones SMI is near to 0, therefore when SMI increases, it shows a worse bone structure, related with an osteoporotic scenario. In this case, after ovariectomy surgery in mice, the SMI increased from -8 to -1, and after treating mice with PTH or with our system, this value decreased again to values of -2 and -6 respectively (Figure 5.18F).

As noted earlier, μCT permits the evaluation of trabecular morphology by 3D measurements. Among them, it should be worth evaluate the mean trabecular thickness (Tb.Th) in mm. The Tb.Th tends to decrease after ovariectomy, leading to more breakable bones. Figure 5.18G showed that Tb.Th decreased in ovariectomized mice, as expected, being recovered *ca.* 15% with PTH treatment and *ca.* 75% by our nanosystem injections. The administration of the loaded

nanoparticles achieved better results than the gold standard treatment. The trabeculae thinkness increased after the delivery off both therapeutic agents by the nanocarrier obtaining stronger bones more resistant to fracture. Related with this value, other measures such as the mean trabecular separation (Tb.Sp), or the mean trabecular number (Tb.N) were also measured. The Tb.Sp is the mean distance between trabeculae, therefore, is inversely proportional to Tb.Th, so in this case the value is expected to increase in ovariectomized mice. In Figure 5.18I it could be appreciated how Tb.Sp triplicates in the case of OVX compared with Control group. After treatment either with PTH or with our nanoparticles the value decreased *ca.* 25% or 70% respectively, showing again the greater effectivity of the nanoparticles regarding the trabeculae structure. On the other hand, Tb.N, which is the average number of trabeculae per unit of length, did not present variations after either ovariectomy surgery or different treatments (Figure 5.18H). The number of trabeculae did not change even after ovariectomy, therefore osteoporosis led to a situation of thinner trabeculae but maintaining the same number. The application of the different treatments recovered the thickness lost during the disease progression.

In addition to the trabecular regions, some indices of the cortical region were also evaluated. The changes observed were not as noticeable as the ones obtained in the trabecular region, but this could be related to the osteoporotic model used. Ovariectomized mice present the greater reduction of bone in the trabecular regions instead of the cortical section after 14 days from the surgery.[27] Despite this fact, the cortical bone mineral density was *ca.* 60 mg/cm^2 in healthy mice, and after ovariectomy, this value decreased to *ca.* 48 mg/cm^2. After treatment either with PTH or with our system, this value increased to *ca.* 50 mg/cm^2 or 58 mg/cm^2, respectively.

Other parameter for cortical bone such as the cortical thickness (Ct. Th) has been measured. Here, the value also decreased after ovariectomy surgery, from 0.87 mm until 0.75 mm, and after treatment this value was recovered *ca.* 11% in the case of PTH application and *ca.* 60% after our system injections. The application of the co-loaded nanoparticles produced a greater effect compared with the golden osteoporosis treatment also in the cortical section.

Taking all the data into consideration, it can be appreciated that the treatment with our nanoparticles was effective, improving the microarchitecture of bones, approaching to healthy values. The results obtained also showed that the effect obtained by the administration of our system was higher than with the PTH injections. The designed system represents a potential alternative for the osteoporosis treatment obtaining promising results better than the current gold standard treatment for the disease. The development of this system could be one step further for osteoporosis remission.

5.5 Conclusions

Osteoporosis is considered the most prevalent systemic bone disease affecting all bone tissue with a progressive increasing number of patients both in developed and developing countries. Current clinical treatments are not able to offer a satisfying curative effect, so the development of more effective treatments is desired. In this sense, previous chapters proposed a local treatment involving nanoparticles with promising effects. However, since osteoporosis is a systemic disease, further research to achieve a systemic administration has been here carried out.

Here, we have proposed a modified mesoporous silica nanoparticle-based system able to transport and deliver SOST siRNA and osteostatin around the organism by systemic injection. MSNs have been modified with PEG and ALN to confer the nanoparticles (1) better colloidal stability, (2) increasing circulation time, and (3) bone targeting capacity, being accumulated around bone area to deliver the biomolecules more effectively in the target tissue.

After functionalization with the PEG-ALN conjugate, the PEI grafting for the siRNA loading was optimized considering the loading capacity and cell viability. Then, the targeting ability and the colloidal stability of the optimized system was validated. Furthermore, since the nanoparticles were going to be in blood circulation for a period of time, it was necessary to evaluate the stability against RNases. With the results obtained it could be concluded that the system was able to protect siRNA from RNases after being in contact with the enzyme for 2 hours.

After the system was completely optimized, the nanoparticles were loaded with osteostatin and siRNA. Then, the loaded MSNs were injected subcutaneously every two days for 2 and 3 weeks in ovariectomized mice. The gene expression modification was evaluated after the treatment periods. The results showed that SOST was effectively knocked-down, and osteogenic markers such as, Alp, Runx2, OPG and OSX and vascularization related gene, VEGF, were increased after the treatment. The application of the designed nanoparticles yielded a greater increase in the expression of osteogenic markers compare with the PTH injections. The here proposed system presented promising results regarding gene expression modification.

The microarchitecture of the bones was also measured by µCT. The results demonstrated that after 3 weeks of systemic treatment the microarchitecture of the bone was improved with increased values of BMD, BV/TV, Tr.Th, among others, revealing an improved bone architecture. The results obtained with our system injections were compared with one of the osteoporosis gold standard treatments, PTH, reaching better results with our nanoparticles injections than with the administration of the hormone. Therefore, the nanoparticles not only achieved a greater stimulation of osteogenic markers compared with the PTH administration, but also the gene

expression modification was traduced in a better bone architecture after the co-delivery of both therapeutic agents from the nanoparticles compared with the hormone treatment.

It can be concluded that our proposed system was effective in delivering SOST siRNA and osteostatin through systemic injection to bone tissue. The treatment with the nanoparticles produced an increase expression of several osteogenic related genes that produce an improvement in the microarchitecture of the bone. The treated ovariectomized mice almost recover values of healthy mice, meaning that the here proposed system could be consider a promising alternative for osteoporosis systemic treatment. The research here proposed showed the relevance of nanotechnology for the improvement in bone diseases treatment. It presented a new potential treatment for osteoporosis remission yielding better results than the current gold standard anabolic treatment, PTH.

5.6 References

1. Rachner, T. D., Khosla, S., Hofbauer, L. C. Osteoporosis: now and the future. *Lancet* 377, 1276–1287 (**2011**).

2. Kyllönen, L., D'Este, M., Alini, M., Eglin, D. Local drug delivery for enhancing fracture healing in osteoporotic bone. *Acta Biomater.* 11, 412–434 (**2015**).

3. Barry, M. *et al.* Advances in Nanotechnology for the Treatment of Osteoporosis. *Curr. Osteoporos. Rep.* 14, 87–94 (**2016**).

4. Shukla, A. *et al.* Nanotechnology towards prevention of anaemia and osteoporosis: from concept to market. *Biotechnol. Biotechnol. Equip.* 31, 863–879 (**2017**).

5. Gisbert-Garzarán, M., Manzano, M., Vallet-Regí, M. Mesoporous silica nanoparticles for the treatment of complex bone diseases: Bone cancer, bone infection and osteoporosis. *Pharmaceutics* 12, 83 (**2020**).

6. Wicki, A., Witzigmann, D., Balasubramanian, V., Huwyler, J. Nanomedicine in cancer therapy: Challenges, opportunities, and clinical applications. *J. Control. Release* 200, 138–157 (**2015**).

7. Clemments, A. M., Muniesa, C., Landry, C. C., Botella, P. Effect of surface properties in protein corona development on mesoporous silica nanoparticles. *RSC Adv.* 4, 29134–29138 (**2014**).

8. Cauda, V., Argyo, C., Bein, T. Impact of different PEGylation patterns on the long-term bio-stability of colloidal mesoporous silica nanoparticles. *J. Mater. Chem.* 20, 8693–8699 (**2010**).

9. Paris, J. L. *et al.* From proof-of-concept material to PEGylated and modularly targeted ultrasound-responsive mesoporous silica nanoparticles. *J. Mater. Chem. B* 6, 2785–2794 (**2018**).

10. He, Q. *et al.* The effect of PEGylation of mesoporous silica nanoparticles on non-specific binding of serum proteins and cellular responses. *Biomaterials* 31, 1085–1092 (**2010**).

11. Laschewsky, A., Rosenhahn, A. Molecular Design of Zwitterionic Polymer Interfaces: Searching for the Difference. *Langmuir* 35, 1056–1071 (**2019**).

12. Sánchez-Salcedo, S. *et al.* Mesoporous core-shell silica nanoparticles with anti-fouling properties for ovarian cancer therapy. *Chem. Eng. J.* 340, 114–124 (**2018**).

13. Chen, J. *et al.* Preparation of zwitterionic polymers functionalized fluorescent mesoporous silica nanoparticles through photoinduced surface initiated RAFT polymerization in the presence of oxygen. *J. Taiwan Inst. Chem. Eng.* 91, 570–577 (**2018**).

14. Liu, J. *et al.* PEGylation and zwitterionization: Pros and cons in the renal clearance and tumor targeting of near-IR-emitting gold nanoparticles. *Angew. Chemie - Int. Ed.* 52, 12572–12576 (**2013**).

15. Encinas, N. *et al.* Mixed-charge pseudo-zwitterionic mesoporous silica nanoparticles with low-fouling and reduced cell uptake properties. *Acta Biomater.* 84, 317–327 (**2019**).

16. Butler, K. S. *et al.* Protocells: Modular Mesoporous Silica Nanoparticle-Supported Lipid Bilayers for Drug Delivery. *Small* 12, 2173–2185 (**2016**).

17. Longmire, M., Choyke, P. L., Kobayashi, H. Clearance properties of nano-sized particles and molecules as imaging agents: considerations and caveats. *Nanomedicine* 3, 703–717 (**2008**).

18. Alexis, F., Pridgen, E., Molnar, L. K., Farokhzad, O. C. Factors affecting the clearance and biodistribution of polymeric nanoparticles. *Mol. Pharm.* 5, 505–515 (**2008**).

19. Narayanan, D., Anitha, A., Jayakumar, R., Chennazhi, K. P. In vitro and in vivo evaluation of osteoporosis therapeutic peptide PTH 1–34 loaded PEGylated chitosan nanoparticles. *Mol. Pharm.* 10, 4159–4167 (**2013**).

20. Fu, Y. C. *et al.* Aspartic acid-based modified PLGA-PEG nanoparticles for bone targeting: In vitro and in vivo evaluation. *Acta Biomater.* 10, 4583–4596 (**2014**).

21. Íñiguez-Ariza, N. M., Clarke, B. L. Bone biology, signaling pathways, and therapeutic targets for osteoporosis. *Maturitas* 82, 245–255 (**2015**).

22. Luhmann, T., Germershaus, O., Groll, J., Meinel, L. Bone targeting for the treatment of osteoporosis. *J. Control. Release* 161, 198–213 (**2012**).

23. Kasugai, S. *et al.* Selective Drug Delivery System to Bone: Small Peptide (Asp)6 Conjugation. *J. Bone Miner. Res.* 15, 936–943 (**2000**).

24. Mora-Raimundo, P., Lozano, D., Manzano, M., Vallet-Regí, M. Nanoparticles to Knockdown Osteoporosis-Related Gene and Promote Osteogenic Marker Expression for Osteoporosis Treatment. *ACS Nano* 13, 5451–5464 (**2019**).

25. Xia, T. *et al.* Polyethyleneimine coating enhances the cellular uptake of mesoporous silica nanoparticles and allows safe delivery of siRNA and DNA constructs. *ACS Nano* 3, 3273–3286 (**2009**).

26. Ghisaidoobe, A. B. T., Chung, S. J. Intrinsic tryptophan fluorescence in the detection and analysis of proteins: a focus on Förster resonance energy transfer techniques. *Int. J. Mol. Sci.* 15, 22518–22538 (**2014**).

27. Komori, T. Animal models for osteoporosis. *Eur. J. Pharmacol.* 759, 287–294 (**2015**).

28. Basha, G. *et al.* Lipid nanoparticle delivery of siRNA to osteocytes leads to effective silencing of SOST and inhibition of sclerostin in vivo. *Mol. Ther. Nucleic Acids* 5, 1–15 (**2016**).

29. Wang, Y. *et al.* Wnt and the Wnt signaling pathway in bone development and disease. *Front. Biosci.* 19, 379–407 (**2014**).

30. Canalis, E. Update in new anabolic therapies for osteoporosis. *J. Clin. Endocrinol. Metab.* 95, 1496–1504 (**2010**).

31. Bouxsein, M. L. *et al.* Guidelines for assessment of bone microstructure in rodents using micro–computed tomography. *J. Bone Miner. Res.* 25, 1468–1486 (**2010**).

Chapter VI:
Conclusions / Conclusiones

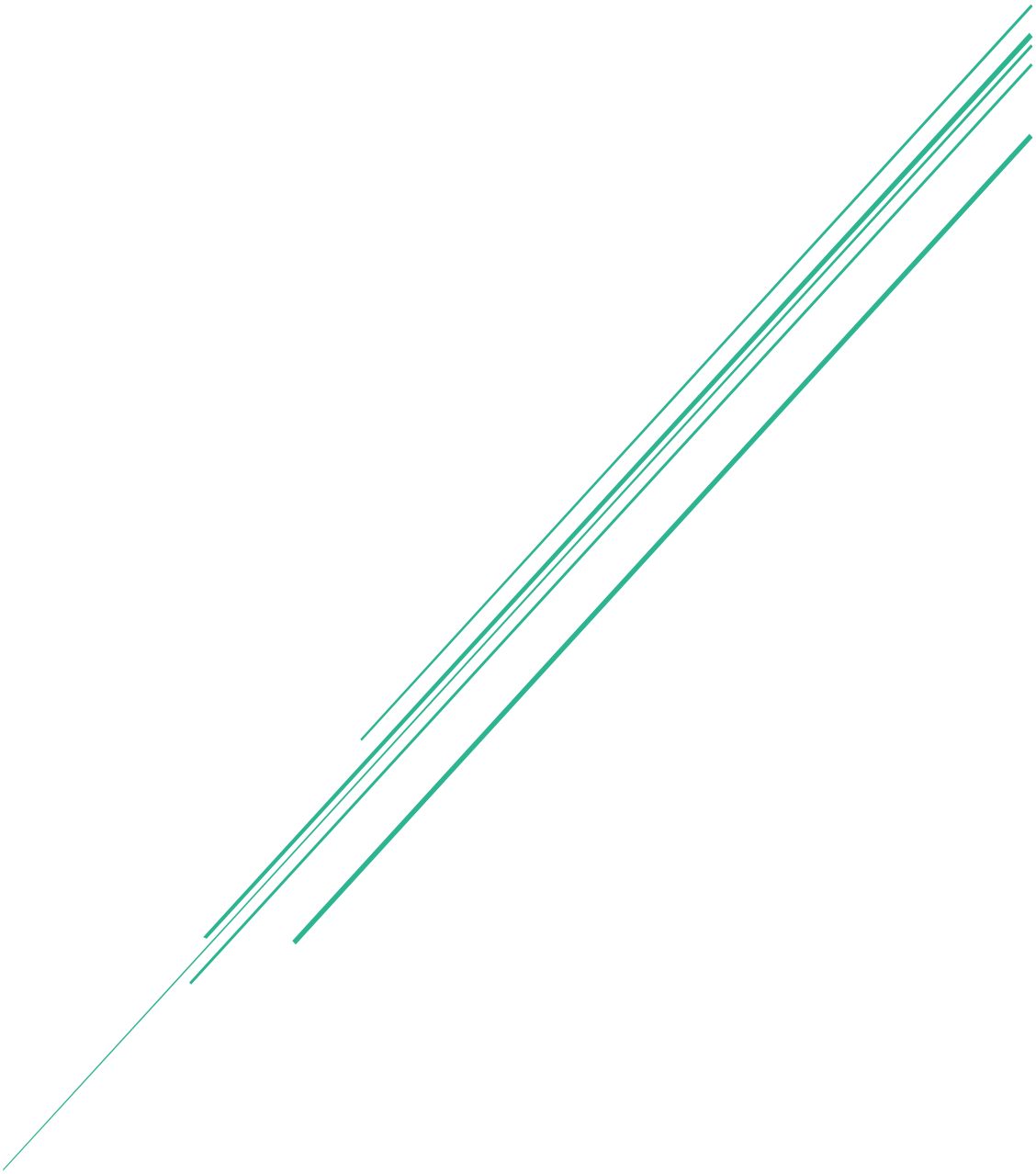

Aprendiz de todo, maestro de nada
Jorge Mora Bañó

6. Conclusions / Conclusiones

6.1 Conclusions

The overall objective of this doctoral thesis has consisted in the development and evaluation of mesoporous silica nanoparticles for the potential treatment of bone diseases, more specifically for osteoporosis. The general conclusions that can be extracted from the results here presented and discussed are described bellow.

During this doctoral thesis, the development of a nanocarrier able to transport and deliver siRNAs was successful. The particles were synthesized, yielding spherical and homogenous nanoparticles. The capacity of biding siRNA was achieved by coating a cationic polymer, PEI, to the particles. The proper molecular weight of PEI was optimized considering the capability of the nanoparticles of loading siRNA *versus* the cytotoxicity of the polymer. The designed nanocarrier was able to transfect SOST siRNA to cells, maintaining its activity and achieving an effective silencing effect. After evaluation of the effect *in vitro* with promising results (high capacity of silencing SOST and notably higher levels of the osteogenic markers), the system was injected in the femoral bone marrow of ovariectomized mice, and the obtained results were in agreement with the *in vitro* experiments. The knockdown of the gene SOST promoted the expression of osteogenic differentiation early markers in ovariectomized mice (Runx2 and Alp). Therefore, the system demonstrated remarkable efficacy for an intra-bone marrow injection, being a potential candidate for osteoporosis treatment since the augmentation of osteogenic markers expression would be related with bone formation.

The mesoporous structure of the nanoparticles empowered the application of the nanocarrier for the co-loading and co-delivering of two different biomolecules. In an attempt to increase of osteogenic markers expression, SOST siRNA was co-loaded with an osteogenic peptide (osteostatin) in the MSNs. SOST siRNA was bound to the polymer matrix linked to the surface, while osteostatin was loaded inside the mesopores. The *in vitro* effect of both biomolecules was evaluated with promising results, successful knockdown of SOST and an increased expression of osteogenic markers. The effect of each molecule separately modified the expression of the genes, SOST, Runx2 and Alp, but the dual administration of both molecules from the same nanoparticles yielded synergistic effects. Then, the system was injected in the femoral bone marrow of ovariectomized mice and the obtained results were in agreement with the *in vitro* experiments. Thus, it could be concluded that our system was able to transport, co-deliver, and transfect to cells SOST siRNA and osteostatin, maintaining its activity and achieving an effective silencing effect. The combination of SOST siRNA with the osteogenic peptide promoted a synergistic effect in ovariectomized mice, increasing the expression of osteogenic markers in an additive manner.

The last part of this thesis involved the modification of the system to achieve a systemic administration. MSNs were modified with PEG and ALN to confer the nanoparticles better colloidal stability than the non-functionalized nanoparticles and bone targeting capacity to deliver the biomolecules more effectively to the target tissue. The functionalized nanoparticles were coated with PEI to confer the positive charge to the nanoparticle surface needed for transporting siRNAs. The new proposed system was optimized using different ratios of PEI polymer to MSNs to obtain the highest siRNA loading capacity with the lowest cytotoxicity.

The modified nanoparticles were loaded with osteostatin and bound to siRNA and then administrated subcutaneously to ovariectomized mice every 2 days for 2 and 3 weeks, respectively. The expression of several genes related with osteogenic features, such as SOST, Alp, Runx2, OSX, and OPG, and with vascularization features, such as VEGF, were evaluated. The results showed that SOST was effectively knocked down, and the expression of osteogenic and vascularization related genes was increased after the treatment. It could be concluded that our proposed system was effective in delivering SOST siRNA and osteostatin to bone tissue through systemic injection, modifying the gene expression profile.

After the evaluation of the gene expression modification, the microarchitecture of the bones was also measured by μCT. The results demonstrated that after 3 weeks of treatment the microarchitecture of the bone was improved with increased values of BMD, BV/TV, Tr.Th, among others, revealing an improved bone architecture. The results obtained with our system injections were compared with one of the osteoporosis gold standard treatments, PTH. It could be concluded that the designed nanocarrier improved the structural and microarchitectural properties of bone after 3 weeks of treatment achieving better results than with the administration of PTH.

In summary, the work carried out during this doctoral thesis reinforces the suitability of using mesoporous nanocarriers as drug delivery systems, proving the capacity of delivering nucleic acids. In addition, the utility of mesoporous nanocarriers for combination therapy through the co-delivery of several biomolecules was verified. The treatment by the administration of SOST siRNA and osteostatin yielded a synergistic effect, showing promising results as a potential new alternative for osteoporosis treatment. Finally, this system will constitute a new candidate as a platform for a combination therapy in osteoporosis treatment, achieving better results compared with the PTH injections following the same treatment protocol. The MSNs-based system here presented could suppose one step forward for osteoporosis remission.

6.2 Conclusiones

El objetivo general de esta tesis doctoral ha consistido en el desarrollo y evaluación de nanopartículas mesoporosas funcionalizadas para el potencial tratamiento de enfermedades óseas, más específicamente de la osteoporosis. Las conclusiones generales que pueden derivarse de los resultados aquí presentados y discutidos son las siguientes.

Durante la presente tesis doctoral se ha desarrollado un nanotransportador capaz de transportar y liberar siRNAs de manera satisfactoria. Las partículas fueron sintetizadas usando el método sol-gel, obteniendo nanopartículas esféricas y homogéneas. La capacidad para cargar siRNAs sobre la superficie de las nanopartículas se obtuvo a través de el recubrimiento de las partículas con un polímero catiónico, PEI. El peso molecular apropiado del PEI fue seleccionado a través de la optimización del sistema teniendo en cuenta la capacidad de las nanopartículas de cargar siRNAs y la posible citotoxicidad del polímero.

El nanotransportador diseñado fue capaz de transfectar siRNAs contra el gen SOST, manteniendo su actividad y obteniendo un silenciamiento efectivo. El silenciamiento del gen SOST impulsó la expresión de marcadores osteogénicos de diferenciación temprana (Runx2 y Alp). Tras la evaluación del efecto *in vitro* con resultados prometedores (elevada capacidad de silenciamiento de SOST y un notable aumento de los niveles de expresión de marcadores osteogénicos), el sistema fue inyectado en la medula ósea femoral de ratonas ovarectomizadas. Los resultados obtenidos fueron acordes con los experimentos *in vitro*. De esta manera, se pudo concluir que el sistema demostró una eficacia considerable tras una inyección en medula ósea femoral, motivando así estudios posteriores.

La presencia de mesoporos en el interior de las nanopartículas permitió la aplicación del nanotransportador para la carga y liberación de dos biomoléculas diferentes. El siRNA de SOST se unió a la matriz polimérica presente en la superficie de las partículas y la osteostatina en cambio se cargó en el interior de los mesoporos. El efecto de ambas biomoléculas *in vitro* se evaluó presentando resultados prometedores, un silenciamiento de SOST exitoso y un aumento de la expresión de marcadores osteogénicos. Cada molécula por separado modificó la expresión de los genes, SOST, Runx2 y Alp, pero la administración de ambas moléculas en las mismas nanopartículas conllevó un efecto sinérgico. Más adelante, el sistema se inyectó en la medula ósea femoral de ratonas ovarectomizadas y los resultados obtenidos concordaban con los experimentos realizados *in vitro*. Por lo tanto, se puede concluir que nuestro sistema fue capaz de transportar, liberar y transfectar siRNAs y osteostatina, manteniendo su actividad y obteniendo un silenciamiento efectivo. La combinación de SOST siRNA y el péptido osteogénico, osteostatina, generó un efecto sinérgico en ratonas ovarectomizadas, aumentando la expresión de marcadores de diferenciación osteoblástica temprana.

La última parte de esta tesis engloba la modificación del sistema para conseguir una administración sistémica. Las MSNs se modificaron con PEG y ALN para conferir a las nanopartículas con una mayor estabilidad coloidal en comparación con las nanopartículas sin funcionalizar y la capacidad de vectorización a hueso liberando de esta manera las biomoléculas en el tejido diana. El nuevo sistema propuesto se optimizó utilizando diferentes ratios de PEI:MSNs para obtener la mayor carga de siRNA con la menor citotoxicidad posible.

Las nanopartículas modificadas se cargaron con osteostatina y se unieron a los siRNAs. Tras esto se administraron de manera subcutánea cada 2 días durante 2 y 3 semanas a ratonas ovarectomizadas. La expresión de diversos genes relacionados con (1) la osteogénesis como SOST, Alp, Runx2, OSX, y OPG, y con (2) la vascularización, como VEGF, fueron evaluados. Los resultados mostraron que SOST fue silenciado de manera efectiva y la expresión de los genes osteogénicos y de vascularización incrementó tras el tratamiento. Se puede concluir que nuestro sistema propuesto fue efectivo para el suministro de silenciadores génicos y osteostatina a hueso a través de una inyección sistémica, modificando el perfil de expresión génica.

Tras evaluar la modificación de la expresión génica, la microarquitctura de los huesos se midió por µCT. Los resultados obtenidos demostraron que tras 3 semanas de tratamiento, la microarquitectura del hueso mejoró, con mayores valores de BMD, BV/TV y Tr.Th, entre otros, mostrando una arquitectura ósea de mayor calidad. Los resultados obtenidos tras las inyecciones con nuestro sistema se compararon con los del tratamiento por excelencia de la osteoporosis, la PTH. Se puede concluir que el nanotransportador diseñado mejoró la estructura y las propiedades microarquitecturales del hueso tras 3 semanas de tratamiento de forma más efectiva que tras la administración de PTH.

En resumen, el trabajo realizado durante esta tesis doctoral refuerza la idoneidad del uso de nanotransportadores mesoporosos como sistemas de transporte de fármacos, demostrando su capacidad para transportar ácidos nucleicos. Además, se verificó la utilidad de las nanopartículas mesoporosas de sílice para una terapia combinada a través del transporte y liberación de dos biomoléculas al mismo tiempo. Finalmente, el sistema diseñado constituye un prometedor candidato como plataforma para la terapia combinada en el tratamiento de la osteoporosis. Con los estudios realizados en la presente tesis doctoral la investigación avanza en la batalla contra una de las enfermedades óseas más prevalentes, la osteoporosis, aportando nuevas alternativas para la posible remisión de la enfermedad.

Appendixes

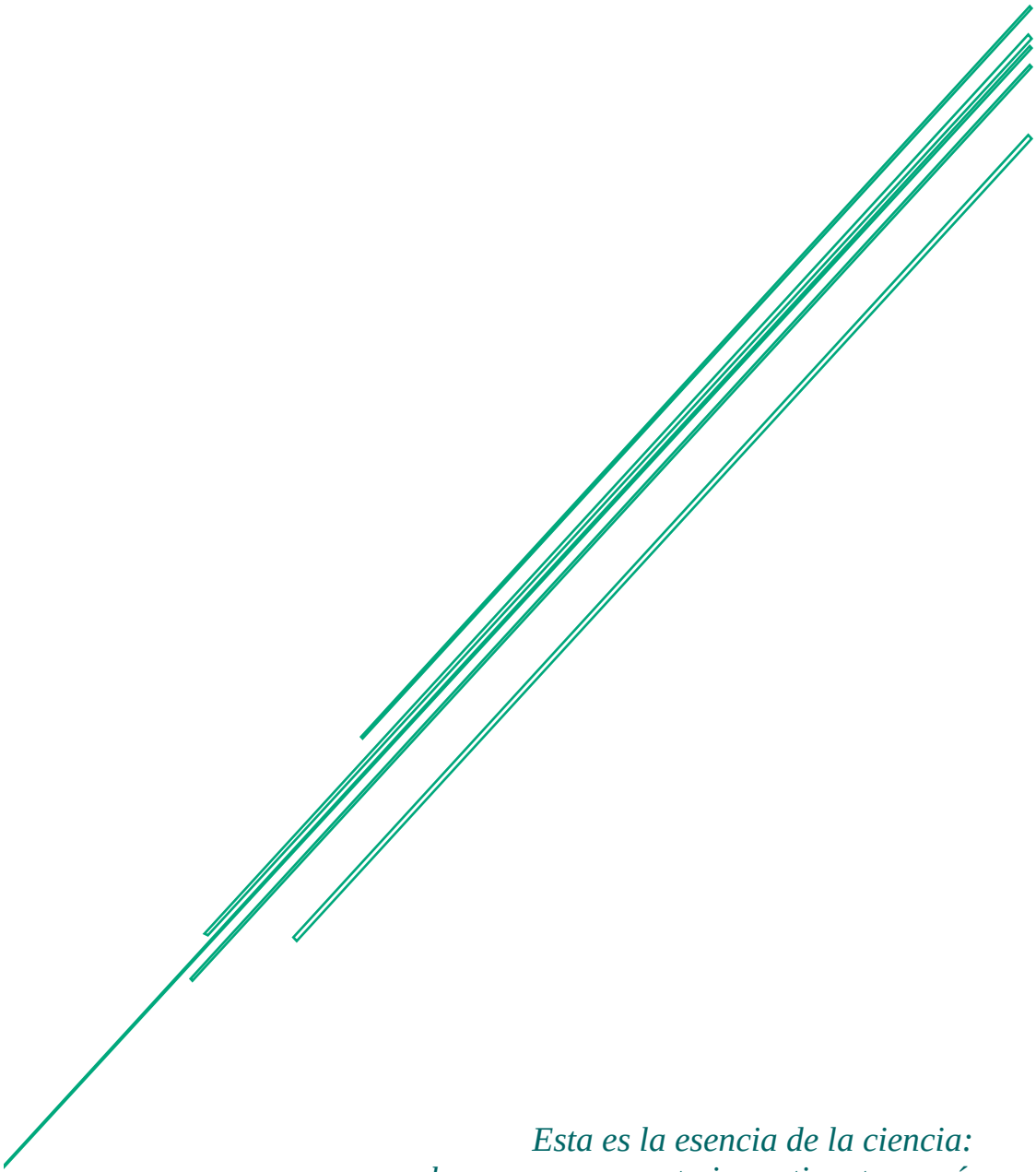

Esta es la esencia de la ciencia:
hacer una pregunta impertinente, y así,
estar en camino hacia la respuesta pertinente
Jacob Bronowski

Appendix I: Characterization techniques

The objective of this appendix is to provide a brief introduction to the different techniques employed to characterize the performance of the materials produced during this doctoral thesis. The information here presented is a summary of the instructions manuals as well as different online information from the different manufacturers. Table A1.1 summarizes the essential information provided by each technique.

Table A1.1 Summary of the techniques employed to characterize the performance of the materials here produced and the information that can be obtained from them.

Charaterization Technique	Information Obtained
Thermogravimetric Analysis (TGA)	Organic matter quantification
Fourier Transformed Infrared (FTIR) spectroscopy	Presence or absence of functional groups
X-Ray Diffraction (XRD)	Mesostructure periodicity
Nitrogen porosimetry	Textural properties
Transmission Electron Microscopy (TEM)	Morphology, porosity and size
Dynamic Light Scattering (DLS)	Colloidal stability and hydrodynamic size
Zeta potential	Surface charge
^{1}H-Nuclear Magnetic Resonance (1H-NMR)	Identification of ^{1}H atoms in an organic compound
Confocal microscopy	Qualitative cellular uptake of the particles
Flow cytometry	Quantitative cellular uptake of the particles
Real-time quantitative Reverse Transcription Polymerase Chain Reaction (qRT-PCR)	Gene expression quantification
Micro-Computed Tomography (μCT)	Structural bone properties
Dual-Energy X-Ray Absorptiometry (DXA)	Bone mineral density quantification

Thermogravimetric Analysis

This technique provides a quantitative analysis of the sample composition as a function of temperature. It allows to quantify the variations in the sample weight upon application of a heating ramp under a controlled atmosphere. In particular, this technique has been employed during this thesis to evaluate the correct surfactant removal and the amount of organic matter incorporated in the different mesoporous nanomatrices after each functionalization step.

Fourier Transformed Infrared spectroscopy

This technique allows the determination of the presence or absence of functional groups in a sample upon irradiation with infrared light (4,000-400 cm^{-1}). The irradiation of a sample provides a FTIR spectrum, which is composed of vibration bands that are unique for a particular sample. The origin of those bands is the various types of vibrations that can be detected for the different

bonds of the molecule upon infrared irradiation. FTIR spectroscopy finds wide application because it is possible to analyze liquids, gels, fibers, surfaces…In particular, this technique has been employed during this PhD to evaluate the proper surfactant elimination as well as the success of the different grafting steps.

X-Ray Diffraction

This technique provides information about the structural periodicity of a material upon irradiation with x-rays. The x-ray beams are elastically dispersed after interacting with the sample and, consequently, they preserve the initial wavelenght. The beams can only be dispersed in certain directions, which are characteristic of a particular periodic system and are determined by the Bragg law (Equation A1.1).

$$n\lambda = 2d_{hkl} \sin \Theta$$

Equation A1.1. The Bragg law provides the directions in which the x-ray beams are diffracted. n: diffraction order, λ: wavelength, d_{hkl}: distance between planes and Θ: irradiation angle.

In the case of the mesoporous materials here studied, the small angle XRD allows the determination of the periodicity of the corresponding mesostructure, although they are amorphous at the atomic scale.

Nitrogen porosimetry

This technique provides information about the textural properties of a sample based on the interaction between the nitrogen gas (adsorbate) and the solid to be analyzed (adsorbent). In general, adsorption processes can be classified either as chemisorption (existence of chemical bond between adsorbate and adsorbent) or physisorption (the interaction is labile and take place through Van der Waals interactions). The results of the nitrogen porosimetry, which is based on physisorption processes, are expressed as adsorption-desorption isotherms. These curves provide the volume of gas adsorbed by the surface as a function of the pressure conditions. The raw data obtained by the apparatus is treated using different mathematical models to provide the textural properties. In our case, the textural properties that have been measured are the specific surface area, the pore volume and the pore size:

- Specific surface area: It provides the surface of the solid per unit of mass. The value has been determined using the B.E.T. (Brunauer-Emmett-Teller) mathematical model.
- Pore volume: Nitrogen porosimetry provides the volume occupied by the adsorbate within the adsorbent at a p/p_0 close to 1. In this case, the value is the direct volume filled by the gas molecules and no mathematical models are employed.

- Pore size: This parameter can be elucidated using different mathematical models. The BJH (Barret-Joyner-Halenda) model, which allows to calculate the pore size in the range 2-50 nm, has been employed during this thesis.

This technique has been initially employed during this PhD thesis to determine the textural properties of the different as-produced mesoporous materials. In addition, the variations in the above-mentioned parameters after the different functionalization steps verify the success those synthetic steps.

Transmission Electron Microscopy

This technique allows the observation of materials, even at the atomic scale (HRTEM), when a high energy electron beam is focused on a thin sample. The beam interacts with the atoms of the sample and consequently, some electrons go directly through the sample while others are scattered. All electrons are then collected and a grayscale image is generated from the different degree of dispersion of the electrons. This technique provides information about the crystallinity of a material or whether it shows porosity, among others.

This electron microscopy technique has been employed during this thesis to evaluate the presence of porosity in the as-produced mesoporous samples. In addition, the presence of organic matter in the samples can be evaluated if materials are stained with phosphotungstic acid.

Dynamic Light Scattering

This technique allows the determination of the size distribution of particles or emulsions, among others. It is based on the Brownian motion of the particles or molecules present in the solution. As a consequence of this motion, light is dispersed showing different intensities, whose analysis permits the determination of the speed of the Brownian motion. In our case, that speed provides the size of the particles through the Stokes-Einstein equation (Equation A1.2).

$$D = k\mathrm{T} \div 3\pi\eta r$$

Equation A1.2. The Stokes-Einstein equations provides the diffusion coefficient D, which is related to the hydrodynamic size of the particle. k: Boltzmann constant, T: Temperature, η: liquid viscosity

In the case of the materials produced during this PhD thesis, this technique has been used to evaluate the correct synthesis of MSNs (indicated by the absence of large aggregates) as well as the colloidal stability of the particles after the different functionalization steps.

Zeta potential

This technique provides information about the surface charge of the particles through the application of an electric field between two electrodes. The magnitude of the zeta potential, which can be positive, negative or neutral, indicates the degree of electrostatic repulsion between adjacent as similarly charge particles in a dispersion. In particular, this technique has been employed during this thesis to evaluate the success of the different functionalization steps as a function of the variations in the surface charge of the particles.

^{1}H-Nuclear Magnetic Resonance

This technique is mainly used to elucidate molecular structures of organic compounds, although it can also be applied to thermodynamic and kinetic studies. ^{1}H has magnetic spin, which moves around a rotation axis as if it were a small magnet. The spins are randomly oriented in absence of magnetic field. However, the field is applied the nuclei can absorb the energy of the spins are promoted to a state of different energy. Nuclei emit signals when they go back to the ground state. That signal depends on the energy gap between the two spin states and can be detected by the apparatus. The magnetic field sensed by each atom and, consequently, the resonance frequency depends on the surrounding environment of each atom. This technique has been thoroughly applied during this doctoral thesis to evaluate the correct synthesis of the different organic molecules grafted to the mesoporous matrices.

Confocal microscopy

This technique allows the observation of discrete layers of a sample by using a pinhole that discards light that is out of focus. It is possible to generate 3D images from the stacking of individual layers. It is widely employed in biosciences because it allows the detection of light with different wavelengths. In this way, it is possible to stain different parts of the cells and the particles to observe them and to evaluate whether particles and cells are in the same plane, i.e., if particles are inside the cells. This technique has been employed during this PhD thesis to evaluate the effective internalization of the particles in different cellular models.

Flow cytometry

This technique provides qualitative information about the physical and chemical characteristics of a population of cell. The cells are suspended in a fluid and subsequently injected in the cytometer. Ideally, only one cell flow at a time through the laser beam and the scattered light is characteristic to the particular cell and its components. It allows the detection of fluorescent markers. This technique has been employed during this thesis to evaluate the amount of particles incorporated in the cells, providing a value of its ability to be internalized by different type of cells.

Quantitative Reverse Transcription Polymerase Chain Reaction

This technique is a major development of Polymerase Chain Reaction (PCR) technology which allows a reliable detection and measurement of products generated during each cycle of PCR process. In the case of quantitative reverse transcription PCR (RT-qPCR), the starting material is RNA. In this method, RNA is first transcribed into complementary DNA (cDNA) by reverse transcriptase from total RNA or messenger RNA (mRNA) (Figure A1.1). The cDNA is then used as the template for the qPCR reaction. PCR is a method where an enzyme, thermostable DNA polymerase, amplifies a short specific part of the DNA template (amplicon) in cycles. In every cycle, the number of short specific sections of DNA is doubled, leading to an exponential amplification of targets. Quantitative PCR is the reliable detection and measurement of products generated during each cycle of the PCR process. The amount of product produced is directly

proportional to the amount of template presented prior to the start of PCR. The detection of the products produce in every cycle would be through fluorescence.

The quantitative PCR assay used in our case is TaqMan®. The "TaqMan" probe has a fluorescent dye attached to the 5´end and a quencher dye at its 3´. If the target sequence is presented in the cDNA generated, the probe would link to the cDNA. While the probe is intact the fluorescence emission of the probe is absorbed by the quenching dye. When the DNA polymerase generates the new strand, the probe is cleavage and the fluorescence dye and the quencher are no longer together. The free fluorescence dye would increase the fluorescence intensity, being the amount of cDNA produce directly related with the fluorescence intensity.[1]

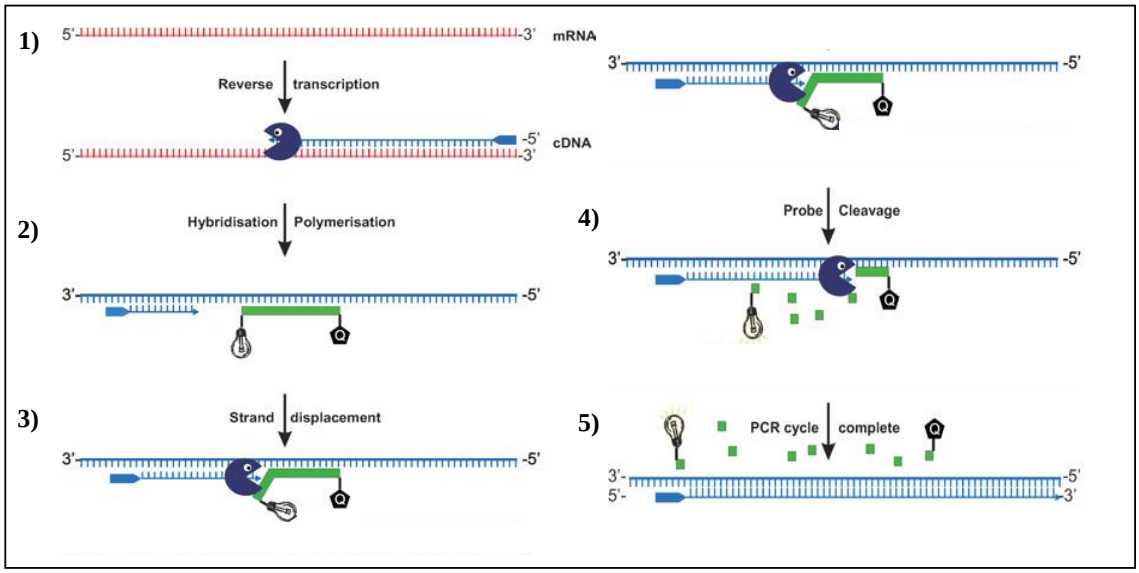

Figure A1.1 Quantitative Reverse Transcription Polymerase Chain Reaction phases. The mRNA is retro transcript to cDNA, the Taqman probe is hybridated with cDNA (the flourence is absorbed by the quenching dye), the DNA polymerase generates the new strand and clevage the probe from the initial cDNA strand (The quenching dye is no longer next to the flourescence dye), the flourescence intensity increase. Adapted from Ref 1 with the permission of Portland Press.

Micro Computed Tomography (µCT)

Microcomputed tomography (µCT) is a non-destructive imaging tool for the production of high resolution three-dimensional (3D) images composed of two-dimensional (2D) trans-axial projections of a target specimen. This technique is established as an essential tool for evaluating bone structure and quality. It has been used for the evaluation of metabolic bone diseases, such as osteoporosis, to evaluate preclinical models of disease and to test the efficacy of anti-resorptive or anabolic therapeutics.

The use of µCT imaging to assess trabecular and cortical bone morphology in animal and human specimens has grown immensely. The standard method of quantitatively describing bone architecture is the calculation of morphometric indices. The minimal set of variables that should be reported for trabecular regions includes bone volume fraction (BV/TV), trabecular thickness (Tb.Th), trabecular separation (Tb.Sp), and trabecular number (Tb.N) because these can be found

in most publications and also can be compared to some extent with classical histomorphometric variables. Depending on the research question, additional variables, such as the structure model index (SMI), and many others can be reported, but typically only variables that are critically discussed in the paper should be reported to avoid a long list of variables that are not put into perspective.[2]

Table A1.2 Definition and description of variables for trabecular bone microarchitecture. Adapted from Ref 2 with the permission of Wiley

Abbreviation	Variable	Description	Standard Unit
BMD	Bone Mineral Density	Amount of mineral (mainly calcium) per volume of bone tissue	mg/cm^3
BMC	Bone Mineral Content	Amount of mineral in a specific area of the bone tissue	mg
TV	Total Volume	Volume of the entire region of interest	mm^3
BV	Bone Volume	Volume of the region segmented as bone	mm^3
BS	Bone Surface	Surface of the region segmented as bone	mm^2
BV/TV	Bone Volumen Fraction	Ratio of the segmented bone volume to the total volume of the region of interest	%
BS/BV	Specific Bone Surface	Ratio of the segmented bone surface to the segmented bone volume	mm^2/mm^3
SMI	Structure Model Index	An indicator of the structure of trabeculae; SMI will be 0 for parallel plates and 3 for cylindrical rods	
Tb.N	Trabecular Number	Measure of the average number of trabeculae per unit length	1/mm
Tb.Th	Trabecular Thickness	Mean thickness of trabeculae, assessed using direct 3D methods	mm
Tb.Sp	Trabecular Separation	Mean distance between trabeculae, assessed using direct 3D methods	mm

For example, mean trabecular thickness (Tb.Th), mean trabecular separation (Tb.Sp), and mean trabecular number (Tb.N) all should be based on 3D calculations, namely, a spherefitting method, where for thickness measurement the spheres are fitted to the object and for separation the spheres are fitted to the background (Figure A1.2).

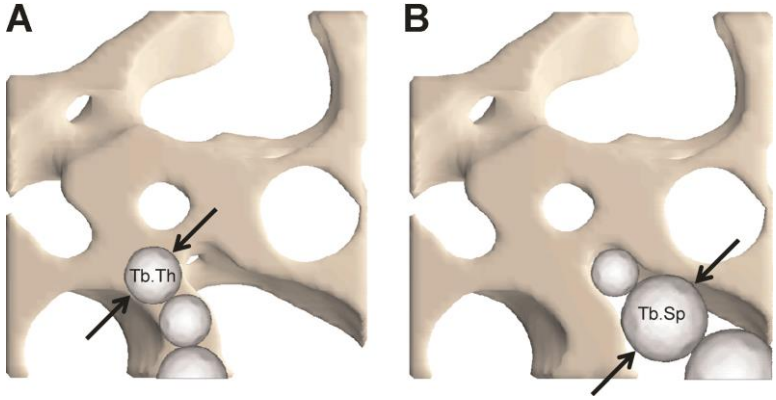

Figure A1.2 Schematic representation of algorithm used for direct 3D method for calculating trabecular thickness (A) and separation (B). Reproduced from Ref 2 with the permission of Wiley

References

1. Bustin, S. A., Mueller, R. Real-time reverse transcription PCR (qRT-PCR) and its potential use in clinical diagnosis. *Clin. Sci.* 109, 365–379 (**2005**).

2. Bouxsein, M. L. *et al.* Guidelines for assessment of bone microstructure in rodents using micro–computed tomography. *J. Bone Miner. Res.* 25, 1468–1486 (**2010**).

Appendix II: Publications

1) Mora-Raimundo, P., Manzano, M. & Vallet-Regí, M. Nanoparticles for the treatment of osteoporosis. *AIMS Bioeng.* **4**, 259–274 (2017)
   Cited by: 10; IF: 1.21
2) Mora-Raimundo, P., Lozano, D., Manzano, M. & Vallet-Regí, M. Nanoparticles to Knockdown Osteoporosis-Related Gene and Promote Osteogenic Marker Expression for Osteoporosis Treatment. *ACS Nano* **13**, 5451–5464 (2019).
   Cited by: 17; IF: 14.588
3) Mora-Raimundo, P., Lozano, D., Manzano, M. & Vallet-Regí, M. Using Targeted-Nanoparticles for Systemic Gene-Therapy Against Osteoporosis
   Under Preparation
4) Mora-Raimundo, P., Lozano, D., Manzano, M. & Vallet-Regí, M. Nanoparticles for the potential treatment of osteoporosis. *The NanoMed Zone Editorial. Pending of Publication*

This doctoral thesis is focused on the development and evaluation of mesoporous silica nanoparticles (MSNs) for the potential treatment of bone diseases, more specifically for osteoporosis. During this thesis it has been developed a system able to deliver small interfering RNAs (siRNAs) inside cells. The codelivery of an osteogenic peptide with SOST siRNA by MSNs has been evaluated as potential alternative for osteoporosis treatment through a local administration by an intra bone marrow injection. Furthermore, new modifications have been performed to obtain a new system able to transport both biomolecules via systemic administration, protecting and delivering them into the target tissue, with promising results. The results obtained during this research showed that the application of MSNs could be a new potential alternative for osteoporosis remission.

Esta tesis doctoral se centra en el desarrollo y evaluación de nanopartículas de sílice mesoporosa (MSNs) para el potencial tratamiento de enfermedades óseas, más específicamente para la osteoporosis. A lo largo de esta tesis se ha desarrollado un sistema capaz de transportar silenciadores génicos al interior de las células. La liberación combinada de un péptido osteogénico con SOST siRNA por parte de las MSNs ha sido evaluada como potencial alternativa para el tratamiento de la osteoporosis mediante una administración local a través de una inyección intramedular ósea. Se han llevado a cabo nuevas modificaciones para conseguir un sistema capaz de transportar ambas biomoléculas a través de una administración sistémica con resultados muy prometedores, protegiendo ambos agentes y haciéndolos llegar al tejido enfermo. Los resultados obtenidos a lo largo de esta investigación muestran que la aplicación de MSNs puede llegar a ser una nueva alternativa potencial para la remisión de la osteoporosis.